OPTIMIZATION OF MECHANICAL PROPERTIES AND MANUFACTURING TECHNIQUES TO ENABLE SHAPE-MEMORY POLYMER PROCESSING

A Dissertation
Presented to
The Academic Faculty

By

Walter Everett Voit

In Partial Fulfillment
Of the Requirements for the Degree
Doctor of Philosophy in Materials Science and Engineering

Georgia Institute of Technology
Atlanta, GA

December 2009

OPTIMIZATION OF MECHANICAL PROPERTIES AND MANUFACTURING TECHNIQUES TO ENABLE SHAPE-MEMORY POLYMER PROCESSING

Approved by:

Dr. Ken Gall, Advisor
Materials Science and Engineering
Mechanical Engineering
Georgia Institute of Technology

Dr. Karl Jacob
Polymers, Fibers, and Textile Engineering
Georgia Institute of Technology

Dr. Rina Tannenbaum
Materials Science and Engineering
Georgia Institute of Technology

Dr. Meisha Shofner
Polymers, Fibers, and Textile Engineering
Georgia Institute of Technology

Dr. David McDowell
Materials Science and Engineering
Mechanical Engineering
Georgia Institute of Technology

Dr. Kurt Jacobus
President and CEO
MedShape Solutions, Inc.

Date Approved: November 6, 2009

There once was a piece of plastic
When hot it became elastic
Its surface was slick
And it would not stick
Cause it lacked the proper mastic

Without shear toughness, at high cost
For moldable casts, all seemed lost
Then I did posit
Use a composite
And under e-beam it was tossed

Herein lies the basic science
Why? How? T_g and Compliance?
Of polymers new
Shape Memory too
Built on the shoulders of Giants

--Walter E. Voit

ACKNOWLEDGEMENTS

First and foremost, I would like to thank my mom and dad for all of their help and support. My mom's attitude has always been to help me focus on the big picture and find my place in the world and keep me focused not just on my work. My father has philosophized with me and given me great advice discussing taxing problems and helping orient my research to stand behind what I have done. In addition, my brothers, Richard and Benedict, and Felicity have been continual sources of support and inspiration, each to whom I am deeply indebted.

My thesis work is built upon the shoulders of giants and none tower higher than those of my advisor and mentor, Ken Gall. Ken's years of experience and ability to tell a story, to paint a picture of his research, that is both rigorous and engaging at the same time captivated me as a younger researcher and have driven me to paint my thesis as I have. If you like the flow and narrative style of my thesis, you can thank Ken. If you don't, I have obviously not come close to mastering his arts. Either way, my hope is that the good science stands on its own and the story woven around it can make it interesting.

My time at Georgia Tech both in the lab and out has been defined by the lasting bonds I have formed with my colleagues in the Advanced Materials Lab. I cannot thank Taylor enough for the valuable contributions he has made to my education and progress over the last three years. He has been a work horse in not only collecting data, but planning his own research, analyzing it and proposing new paths forward. The late night talks with Matthew ranging from foaming techniques to advanced constitutive modeling to anything military (nothing top secret of course) really helped me gain a broad understanding of materials science from his unique viewpoint. Dave, Kathryn and Scott have similarly been outstanding colleagues and friends in our quest for deeper understanding.

The slew of results and data I have collected in due in large part to the talented crop of undergraduates that have worked with me over the last three years. Taylor set the bar high, but I have had the privilege to work with outstanding students: to Paul, Lauren, Ainsley, Thomas, Melissa, Victor, Dustin, Liz, Karan, Parth, Nathan, Amy, Agatha, Stephanie and Sean I tip my hat for outstanding experimental techniques, great attitudes and a willingness to learn and go beyond the basic tests to derive hypotheses and theories that have stemmed from our joint work. In addition, thanks to Maya, Martha, Katie, Katy, Hillary, Michelle, Kathleen, Jessica, Vivas, Keith, Erica, Erin, Shannon and Roxanne for their help and presence to define the atmosphere in the Advanced Materials Lab.

Kurt Jacobus has also been instrumental in my graduate education. His emphasis on the practical and the applied side of my work has driven me to continually question and refine my research and techniques, to not be satisfied merely with something that works or something that could be published. I would also like to thank Heidi, Jack, Chris (both of you), Erin and Helen from MedShape Solutions who have guided and inspired me.

To the members of my committee, I am thankful for your years of wisdom and unique backgrounds that have helped shape and critique my research.

I am also thankful for a large number of professors and mentors here at Tech that have helped define my graduate experience. To Drs. Sanders, Thadani, Snyder, Boyan, Barlow, Bredas, Marder, Gokhale, Carter, Li, Kroeger, Temenoff, McDevitt, and Wang, I extend many thanks. In addition, the MSE staff is incredible—Jasmin, Susan, Teresa, Rusty, Jyoti, Renita, Tim, James and Nancy: thank you for being the face of the department. And I extend a special thanks to our department chair, who as well as anyone I know can cut through red bureaucratic tape to get things done and keep them running smoothly.

Although somewhat peripheral to my lab work, I would like to thank my TI:GER team of Brent, Justin and Rob for the efforts to turn Syzygy Memory Plastics from a drawing on the back of a napkin into a real company. I would also like to thank, Margi, Anne and Marie for their help and guidance throughout the course of the TI:GER program.

I would be remiss not to thank my friends from Dallas and Mt. Pleasant who have helped inspire me and get me where I am today. To Michael, Eric, Aidan, Chris, Rabea, Laura, Kim, Cheng, Nathan, Jonathan, Philip, Jimmy, Kenan, Jessica and Alyssa—thanks. I am indebted to the support network developed at UTD with my McDermott colleagues and with Charlie, Sherry, Molly, Reena, Ginny, Kristen, Colter and Kim.

Finally, my friends and roommates in the MSE department have been there for me through thick and thin, through holes in our roof to intramural championships. Thanks Jack, Chris, Brad, Kit, Gregg, Jake, Bryan, Yair, Schenck, Ken, Rachel, Jim, David, Jackie, Lex, Garritt and Ashley.

There are surely countless others without whom my quest would remain unfulfilled. To you I also offer my deepest thanks and regret for not including you by name.

Sincerely,
Walter

TABLE OF CONTENTS

ACKNOWLEDGEMENTS i
LIST OF TABLES iv
LIST OF FIGURES v
NOMENCLATURE vii
SUMMARY viii
Chapter 1 INTRODUCTION 1
Chapter 2 EXPERIMENTAL TECHNIQUES 24
Chapter 3 HIGH STRAIN SMPS 47
Chapter 4 MNEMOSYNATION 72
Chapter 5 RADIATION SENSITIZATION 98
Chapter 6 SMP COMPOSITES 120
Chapter 7 CONCLUSION 159
APPENDIX 165

LIST OF TABLES

Chapter 1

Table 1	Selected linear (meth)acrylate monomers	7
Table 2	Selected multi-functional (meth)acrylate monomers	8

Chapter 2

None

Chapter 3

Table 1	Shape-memory cycles of high strain thermosets	64

Chapter 4

Table 1	Radiation crosslinking parameters PMA and TMPTA	82
Table 2	High T_g linear builders for acrylate networks	85
Table 3	Max stresses and strains of 3 and 25 wt% TMPTA	88

Chapter 5

Table 1	Radiation crosslinking parameters of increasing PEGDA	104
Table 2	Radiation crosslinking parameters of mol% vs. wt% PEGDA	110

Chapter 6

Table 1	Max strains of polymer-impregnated fibers	131
Table 2	Toughness of polymer-impregnated fibers	131
Table 3	Changing T_g and Onset in fiber-reinforced SMPs	137
Table 4	Properties of SMP-Nylon Lycra composties	146

LIST OF FIGURES

Chapter 1

Figure 1	MMA	4
Figure 2	MA	4
Figure 3	IBoA	4
Figure 4	TMPTA	4
Figure 5	BA	12
Figure 6	tBA	12
Figure 7	DMPA	14
Figure 8	Dimethoxybenzyl radical	14
Figure 9	Benzoyl radical	14
Figure 10	PEGDMA	17
Figure 11	BPAEDA	17

Chapter 2

Figure 1	Stress-strain response of poly (MA-co-IBoA) systems	39
Figure 2	Measuring strain error in crosshead displacement	40

Chapter 3

Figure 1	Schematic of the shape memory cycle	49
Figure 2	DMPA, 44DMB and Xini	53
Figure 3	Gel fractions of poly (MA-co-IBoA) systems	54
Figure 4	DMA response of poly (MA-co-IBoA) systems	55
Figure 5a	Gel Fraction of Xini-based acrylate networks	56
Figure 5b	DMA response of Xini-based networks	57
Figure 5c	E_R comparisons of Xini and BPAEDA networks	58
Figure 5d	Comparative strains-to-failure	59
Figure 6a	Maximum strains of high-strain polymers	61
Figure 6b	Constrained strain recovery of high-strain polymers	62
Figure 6c	Free strain recovery of high-strain polymers	62
Figure 7	Head-to-head strain-to-failure comparisons	63

Chapter 4

Figure 1	Stress-temp, stress-strain and strain-temp (schematic)	76
Figure 2	Gel fraction as a function of radiation dose for PEGDA	79
Figure 3	Linear relationships between $s + s^{1/2}$ and 1/d for PEGDA	81
Figure 4	DMA response of PMA with PEGDA and irradiated	82
Figure 5	DMA response with increasing absorbed dose	84
Figure 6	Gel fractions as a function of absorbed dose	85

Figure 7 Linear relationships comparing mol% and wt% PEGDA 86
Figure 8 DMA response comparing mol% and wt% PEGDA 87
Figure 9 Dose response of modulus comparing mol% and wt% 88
Figure 10 Stress-temp, stress-strain and strain-temp (data) 89

Chapter 5

Figure 1 Stress-temp, stress-strain and strain-temp (schematic) 99
Figure 2 Gel fraction as a function of radiation dose for PEGDA 103
Figure 3 Linear relationships between $s + s^{1/2}$ and 1/d for PEGDA 103
Figure 4 DMA response of PMA with PEGDA and irradiated 105
Figure 5 DMA response with increasing absorbed dose 105
Figure 6 Gel fractions as a function of absorbed dose 107
Figure 7 Linear relationships comparing mol% and wt% PEGDA 108
Figure 8 DMA response comparing mol% and wt% PEGDA 109
Figure 9 Dose response of modulus comparing mol% and wt% 111
Figure 10 Stress-temp, stress-strain and strain-temp (data) 112

Chapter 6

Figure 1 Shape-memory cycle schematic of orthopedic cast 123
Figure 2 Cross-section of proposed orthopedic cast 124
Figure 3 Thermomechanical properties of tBA-PEDGA composites 129
Figure 4 Stress-strain and toughness endpoints for composites 132
Figure 5 Custom polyester fibers 133
Figure 6 Enhancing the strain capacity of composites 135
Figure 7 DMA response of poly(MA-co-IBoA) composites 136
Figure 8 Properties of poly(MA-co-MMA-co-BA) systems 138
Figure 9 Failure strain as a function of T_g 140
Figure 10 Properties of SMP-polyester composites 141
Figure 11 Stress-strain response of high performance fibers 143
Figure 12 Shifting T_g in SMP-Anteres Nylon Lycra composites 145
Figure 13 DMA response of orthopedic cast material candidates 147
Figure 14 Tensile response of orthopedic cast material candidates 148
Figure 15 SEM images of SMP-fiber interactions 150
Figure 16 DMA response of potential cast materials 151
Figure 17 DSC response of potential cast materials 152
Figure 18 Tensile response of hard inner layer of cast at room temp 153
Figure 19 Tensile response of soft outer layer of cast at room temp 153
Figure 20 Tensile response of hard, inner layer at deployment temp 154
Figure 21 Tensile response of soft, outer layer at deployment temp 154
Figure 22 Free strain recovery of hard inner layer with fiber 155

NOMENCLATURE

2,2-dimethoxy-2-phenylacetophenone	DMPA
Advanced Material Lab	AML
bisphenol A ethoxylate diacrylate	BPAEDA
bisphenol A ethoxylate dimethacrylate	BPAEDMA
crosslinker	XL
elastic modulus	E
glass transition temperature	T_g
isobornyl acrylate	IBoA
kiloGray	kGy
Matthew Di Prima	MDP
Mega Pascals	MPa
methyl acrylate	MA
methyl methacrylate	MMA
n-butyl acrylate	BA
photoinitiator	PI
poly ethylene glycol diacrylate	PEGDA
poly ethylene glycol	PEG
poly methyl acrylate	PMA
poly methyl methacrylate	PMMA
rubbery modulus	E_r
shape-memory polymer	SMP
strain-to-failure	E_f
tan delta	Tan(δ)
tert-butyl acrylate	tBA

SUMMARY

The research herein investigates the synthesis and manufacture of shape-memory polymer (SMP) systems for use in biomedical and commodity applications. The research centers on improving the mechanical properties of acrylate copolymers with memory properties at reasonable cost. Specifically, a multivariable optimization process is employed to synthesize and form new thermoset polymers. To improve mechanical properties without dramatically increasing costs, various design and manufacturing techniques are used and can be parsed into two major categories: *high-strain polymer synthesis* and *radiation crosslinking*. The combination of methods described in these two categories has unearthed a trove of challenging fundamental problems that can motivate a life's work in novel polymer synthesis, optimization, processing and characterization.

The research compares different combinations of linear monomers and a low density of crosslinker in acrylate systems to characterize the emerging mechanical properties of new functional materials. Within these new polymers, several mechanical properties are optimized: the glass transition temperature (T_g) is specifically tailored; the polymer is designed to show recurring shape recovery through an adjustment of the crosslinker density and thus the rubbery modulus (E_R); the polymer can be designed to be stiff and rigid below the naturally occurring set temperature (37 ºC for example) without being too brittle; and the drop in modulus at the T_g can be measured and controlled. Within the synthesis realm, several economic factors constrain decisions. The polymer processing technique must be relatively simple and cost-effective for rapid commercialization; thus the chosen polymers are off-the-shelf monomers and crosslinkers. Also, the polymerization process must be well-understood and repeatable; thus ultraviolet curing techniques, electron-beam curing and emulsion polymerizations are used as they can be readily scaled-up for large scale manufacturing processes.

Over the course of the research, the acrylates of choice changed to meet the changing demands that difficult technical problems posed. As a commercially available linear builder, *tert*-butyl acrylate (tBA) was the initial monomer-of-choice because poly(tBA) possesses a T_g near 60 ºC. Both methyl acrylate (MA) (T_g ~ 23 ºC) and methyl methacrylate (MMA) (T_g ~ 130 ºC) can also be photopolymerized using similar methods, and additional tests have validated these monomers as linear builders to make copolymers to target specific thermomechanical properties. However, poly(tBA) and poly methyl methacrylate (PMMA) were shown to behave less favorably than other acrylates during *radiation crosslinking* and gave way to other monomers for radiation crosslinking endeavors. The use of MMA gave way to another high T_g linear builder, isobornyl acrylate (IBoA) for a variety of processing reasons as the research moved forward. Beyond linear monomers, a wide variety of crosslinking (multi-functional) monomers was also screened. The fractional density of the crosslinker in the final polymer matrix dictates many of the new polymer's properties: when mixed in small fractions of 0.2 to 5.0 mole percent with the linear builders, vastly different mechanical properties emerge.

In parallel, the research examined different techniques to facilitate the scaling-up of production of the resulting devices from the test tube to a commercially viable solution. The two facets of research were codependent: to begin manufacturing explorations, the acrylate system exhibiting the best range of mechanical properties to optimize was selected; as better data and more comprehensive tests refined this "best system," manufacturing techniques began to reflect this change. A lack of complete characterization of these copolymer composite systems has limited their use in commercial device fields thus far, although (meth)acrylates have been used in devices and biomedical implants for decades. The aim of this research has been to understand the fundamental scientific drivers necessary to enable new devices mass-manufactured from acrylate copolymers and provide an assessment of emerging mechanical properties.

This work is divided into seven chapters. **Chapter 1 - Introduction**, presents a comprehensive overview of the existing literature, discussing current problems and solutions. **Chapter 2 - Experimental Techniques**, gives an overview of the instrumentation used and describes the characterization techniques that were necessary to gather experimental data and accomplish the research. **Chapter 3 - High Strain Shape SMPs** is an in-depth assessment of the thermomechanical properties of polymer with memory that possess very large fully recoverable strains. This chapter establishes the mole composition that separates a recoverable SMP thermoset from a thermoplastic polymer. The thermoplastic lacks the requisite crosslinker density to ensure full shape recovery for a specific acrylate system. The research pinpoints this regime across several systems and develops a specific heuristic to determine the crosslinker concentration that differentiates fully recoverable thermosets from thermoplastics for lightly-crosslinked acrylate copolymers. Furthermore, Chapter 3 presents a fully recoverable SMP with recoverable strains of up to 807%, more than twice the previously largest recoverable strain demonstrated. Chapter 3 also discusses the conception, synthesis, polymerization and characterization of a novel organic crosslinker and initiator nicknamed Xini. Xini is both photo-cleavable and forms a net point in a growing polymer chain allowing it to behave as both a crosslinker (X) and initiator (ini).

While Chapter 3 serves as an overview of thermomechanical properties and a discussion of some clever new techniques, **Chapter 4 - Mnemosynation** lays the groundwork for the enabling processes that allow the mass manufacture of thermoset acrylate shape-memory polymers—Chapter 4 describes in detail the *Mnemosynation* manufacturing technique. The driving concern pushing the development of *Mnemosynation* was the desire to create devices with thermoset shape-memory properties that could be mass-manufactured using traditional plastics processing techniques. In this capacity, this process was developed and refined; it combines chemical modification of thermoplastic acrylate systems to tailor T_g, the blending of a

crosslinking agent into the thermoplastic resin to tailor E_R, subsequent plastics processing (injection molding, blow molding, vacuum-assisted resin transfer molding), and post-crosslinking with ionizing radiation (e-beam or gamma). Chapter 4 lays the groundwork for a technique with considerable merit in the design and creation of next-generation shape-memory polymer devices. **Chapter 5 - Radiation Sensitization** continues to discuss radiation crosslinking of acrylates specifically focusing on the radiation sensitization of the blended crosslinking agent. The Chapter clarifies the effects of measuring the crosslinking agent concentration in mole and weight ratios and assesses the effect of crosslinker length during the radiation crosslinking method. Chapters 4 and 5 together form the core knowledge to mass produce thermoset acrylates with very specific shape-memory properties. Chapters 3, 4 and 5 present the core contributions to fundamental scientific knowledge that drive this work.

Chapter 6 - SMP Composites describes application-driven future work, outlines a potential SMP casting device and utilizes the knowledge developed in Chapters 3, 4 and 5 to pose challenging problems in diverse fields. The initial work presented in Chapters 6 should be viewed as a roadmap that has unearthed a host of engaging technical problems and some limited posturing of potential solutions and explanations. Chapter 6 presents this first application-driven discussion of *Mnemosynation*, the use of this process to create flexible moldable shape-memory polymer compression sleeves and shape-memory polymer orthopedic casts. The sections of Chapter 6 discuss various technical hurdles that must be overcome to design a working SMP orthopedic cast, including developing fiber-reinforced SMP composites to help meet the criteria for a functioning SMP orthopedic cast. The idea was to choose a fiber that would be impregnated with a high T_g SMP and coated with a low T_g SMP that will serves as a rigid stable inner layer and a soft flexible outer layer.

Fundamental breakthroughs in the underlying science are enabling new cost-effective advances in applied engineering. **Chapter 7 - Conclusion** summarizes results from across the

work and discusses several new ideas and techniques to be explored in future studies. Finally the **Appendix** contains additional figures and descriptions which would have distracted from the flow the presented work but nonetheless were invaluable to reaching the stated conclusions. The Appendix also contains selected segments of written code that have helped with the volumes of raw data processing that enabled the results in this work.

CHAPTER 1

INTRODUCTION

1.1 Motivation

> "I just want to say one word to you—just one word. Are you listening? Plastics. There's a great future in plastics. Think about it. Will you think about it? Enough said."
>
> --Mr. McGuire, *The Graduate* (1967)

Forty-two years later, market research predicts world demand for "engineered plastics" to be $17.5 billion by 2015, due to their widespread application in every sector of the global economy*[1]*, while demand for foamed plastics is expected to reach $27 billion*[2]*. Large global markets in myriad niche "plastics" areas such as these drive continued innovation in many plastics fields. However, one particular plastics niche that has not seen widespread acceptance in mass markets is the field of thermoset shape memory polymers (SMPs). Shape-memory polymers are self-adjusting smart materials that undergo a change in stiffness at a defined temperature and exhibit viscoelastic behavior at or above room temperature. Devices made from SMPs can be synthesized, heated and deformed into in a metastable state, and cooled. Energy, and a temporary shape, is stored in this metastable state. Upon reheating, devices can be deployed and the resulting actuation can be used to perform work to solve a specific mechanical or spatial problem.

The study of shape-memory polymers can be loosely classified into three broad categories: processing, thermomechanical testing, and deployment. To better understand the existing literature surrounding each of these three domains, an intertwined history of advances in polymer science and the molecular physics of the shape-memory effect will be examined relying on the mathematics behind thermomechanical testing to validate theories and results. Then a description of the role of kinetics in polymerization, the shape memory effect and thermo-mechanical stress-strain behavior can be placed within a larger framework, to foster big-picture

understanding of the myriad processes that govern the mechanics and thus the resulting properties of thermoset polymers with memory properties.

1.2 The Shape-Memory Effect

The shape memory effect is an entropy-driven phenomenon that causes materials to "remember" their original shape and in thermoset polymers arises as follows: Polymer segments between crosslinks undergo rapid molecular motion above the glass transition temperature (T_g) of the polymer resulting in mechanical deformation when a stress is applied *[3]*. To achieve the shape-memory effect, this stress must be applied above a critical temperature facilitating an unwinding of the chains of the crosslinked polymer and allowing initial deformation. As the material cools, stereochemistry dictates new intermolecular interactions and locks the material into a new shape *[4]*. When the material returns to a state above or near the critical temperature, entropy springs drive chain recoiling, shepherding the material back to its unstressed, minimum free energy shape.

The temperature-induced shape-memory effect is also present in thermoplastic polymers—materials with physical entanglements, rather than covalent chemical crosslinks—but often results in materials without fully recoverable strains and reduced shape fixity. One class of thermoplastic polymers relies on differing energy states and conformations with 'hard' and 'soft' regions to demonstrate shape-memory properties. The 'hard' regions form semi-crystalline sections connected by strong periodic secondary bonds that simulate the function of covalent crosslinks, while the 'soft' amorphous regions are free to rotate at each single covalent bond in the backbone and act like a spring under applied forces when the temperature exceeds T_g *[5]*. This allows for shape stability and shape recovery.

Shape memory polymers (SMPs) offer advantages over shape memory alloys like nickel titanium (NiTiNOL), the material in which the shape memory effect was first discovered. SMPs

can recover strains on the order of 50 to 800 percent, enabling them to experience relatively large on-demand shape changes in severely restricted environments*[6]*. Other polymers can experience large strains without full recovery: according to Lendlein, multi-block copolymers can be elongated up to 1000% before they break *[7]*. For comparison, NiTiNOL can recover strains of around 8% and experiences failure strains near 30% *[8]*. Other factors beyond peak strain, such as biocompatibility, leachability and bio-toxicity must be studied to gain FDA approval for implantable devices and are thus necessary characterizations for acrylate systems tailored for applications in the biomedical device realm *[9]*. Thus far, thermoset SMP applications have centered on biomedical devices. The difficulty in mass-manufacturing thermosets has pushed exploration in markets where individual devices can be sold at a premium to cover manufacturing costs.

Advances in materials science and engineering have often come when scientists and researchers attempt to duplicate both simple and complex structures from nature and mimic natural functions to then improve upon them: synthetic shape memory polymers (SMPs) are no exception. By providing structural components to interface with the human body, one class of SMPs is already proving useful in reconstructive orthopedic surgeries *[4]* and also shows promise in cardiovascular applications *[10]*. According to Langer, et al. in Nature (2004), one of three directions shaping the future of biomaterials science is focusing on synthesizing materials using synthetic building blocks for specific medical and biological applications *[11]*. The ability to tailor the specific mechanical properties of SMPs is driving further innovation in the biomedical device field *[7]*.

A variety of polymer systems have been explored in emerging biomedical device fields, including acrylate copolymers. Small changes in fractional compositions when polymerizing

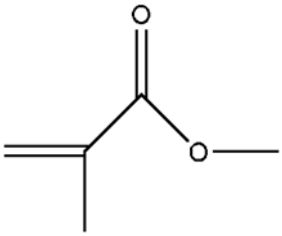

Figure 1. Linear builder methyl methacrylate (MMA)

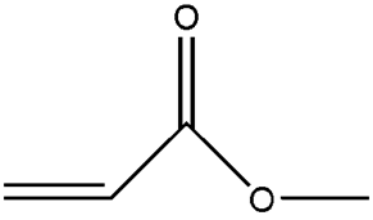

Figure 2. Linear builder methyl acrylate (MA)

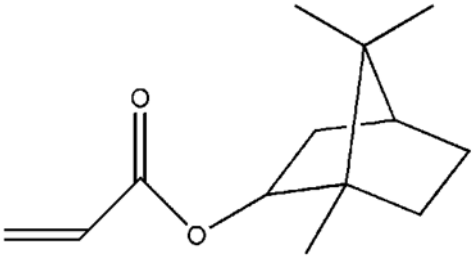

Figure 3. Linear builder isoborynl acrylate (IBoA)

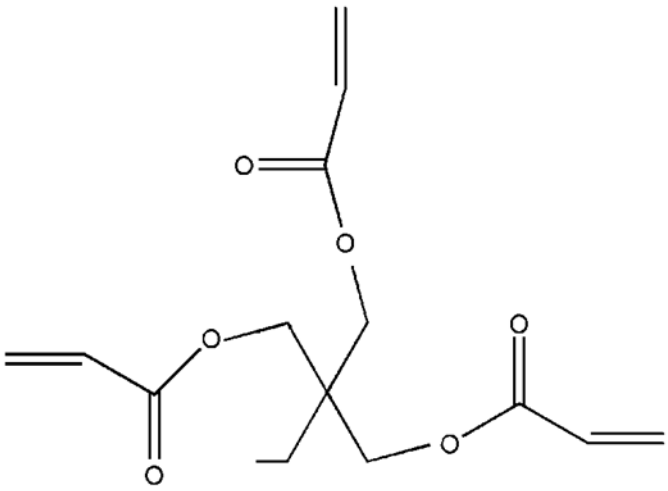

Figure 4. Trifunctional crosslinking agent trimethylolpropane triacrylate (TMPTA)

different combinations of acrylate monomers can dramatically affect properties such as the elastic modulus, deformability peak, glass transition temperature, brittleness at ambient temperatures and percent deformation in the rubbery regime *[12]*. Combining different linear building acrylates (mono-functional monomers) and cross-linking acrylates (multi-functional monomers) in varying ratios yields new SMPs with different material properties that can be optimized for very specific biomedical applications. Single component methyl methacrylate systems have been studied *[13]* and a random assortment of AB copolymers with methyl methacrylate (MMA) (**Figure 1**) as a component have been observed *[14]*, but specifically tailored copolymers of methyl acrylate (MA) (**Figure 2**) and isobornyl acrylate (IBoA) (**Figure 3**) and trimethylolpropane triacrylate (TMPTA) (**Figure 4**) have not been characterized in the literature. Thus before complex biomedical devices or optimized commodity devices can be designed using these acrylate copolymers, their behavior of under many conditions must be understood.

1.3. A Brief History of Polymers and 'Memory'

Polymers consist of a large class of both natural and synthetic materials with diverse applications in many areas including biomedical devices. From their role in cellulose derivatives to their behavior in the vulcanization of rubber, polymers began to be engineered into pseudo-synthetic materials until 1909, when Bakelite *[15]*, the first fully man-made polymer, was synthesized. Since then, the development of polymer science has moved in tandem with advances in physics and chemistry during the early 20th century, as physicists struggled to elucidate the structure and role of atoms and bonding. Meanwhile, metallurgists, ceramists and experimentalists began to derive theories of diffusion and heat transfer that would be extended and expanded to model polymer networks *[16]*.

In the early 1960's Nickel-Titanium alloys were discovered to have curious properties when exposed to stresses at different temperatures *[17]*. The shape-memory effect in NiTi was

discovered to be a martensitic transformation from a close-packed B2 (BCC like) lattice into an open B19' structure that is strain-rate dependent *[18]*. The original shape memory application in polymers emerged in the form of heat-shrink tubing which first began appearing in US patents in 1970 *[19]*. The original heat shrink tubing was a polyurethane-based thermoplastic invented by Raychem Corp., which is now a part of Tyco[1]. The shape-memory effect is observed in polymers with various chemistries and operates on a much different principle: unlike a martensitic transformation which is a first-order, military, virtually diffusionless, deviatoric lattice distortion between crystal structures, the shape memory effect in polymer networks stems from configurational changes in the long polymer chains. Both structural changes are controlled by the need to minimize free energy with the available activation energy *[20]*. In polymers it is an entropic difference between a cooled, stressed metastable equilibrium and the stress-free, global, free-energy minimum that "remembers" the original shape of the polymer. Similarly, in shape memory alloys, the B19' phase has the minimum enthalpy compared to the B2 phase, but the symmetric B2 phase allows more randomness and thus higher entropy and is thus favored at higher temperature. Entropy is thus important to both shape memory alloys and shape memory polymers and as a consequence, the behavior of both materials is strongly dependent on thermo-mechanical history. As a framework for describing the natural world on the submicron scale came into place, a greater understanding of the mechanisms behind polymer synthesis and the applications of shape memory polymers arose. Today entire textbooks cover topics from photo-initiated polymerization *[21]* to polymer physics *[22]*.

[1]Raychem used their knowledge on developing shape memory polymer's for heat shrink tubing to develop the first application of NiTiNOL, shrink fit pipe couplings for Navy aircraft. The successful launch of this application drove Raychem away from shape memory polymers and their attention focused on shape memory alloys. Therefore, although there has been a recent surge of interest in shape memory polymer in biomedicine and other fields driven by advances in polymer science, the first application of shape memory polymers precluded that of shape memory alloys.

Table 1. Selected linear (meth)acrylate monomers are copolymerized into shape-memory polymers using UV polymerization. Purchase prices were calculated from list prices at Sigma Aldrich in Dec. 2008

Linear Builders - Monomers	$/mL
Butyl acrylate	0.01
Methyl Methacrylate	0.0107
Methyl Acrylate	0.0108
2-Ethylhexyl methacrylate	0.0228
Isodecyl acrylate	0.0512
tert-Butyl Acrylate	0.0578
2-Ethoxyethyl methacrylate	0.0755
Isobornyl methacrylate	0.0991
Benzyl methacrylate	0.101
PEG phenyl ether acrylate (324)	0.2028
PEG phenyl ether acrylate (280)	0.2032
PEG phenyl ether acrylate (236)	0.2032
Poly propylene glycol acrylate	0.208
tert-Butyl Methacrylate	0.2908

A certain class of polymers, acrylate assemblages, provides a stable polymer backbone and the ability to incorporate chemical crosslinks into a polymer matrix. A swath of acrylate monomers, based on commercial availability from Sigma-Aldrich is pictured in **Table 1**. When combined with difunctional or multifunctional monomers, shape-memory networks with tunable recoverable force can be created. **Table 2** shows a list of potential crosslinkers along with their calculated glass transition temperatures (T_g) as determined by Safranski et al. *[23]*. The data in Table 2 represents an average T_g (chosen as the peak of the tan delta curve *[24]*) over multiple

Table 2. Selected multi-functional (meth)acrylate monomers and their experimental glass transition temperatures as measured from pure polymerized samples. Starred T_g indicates a broader transition.

Crosslinkers: multi-functional monomers	**Avg. Exp. T_g**
Bisphenol A ethoxylate dimethacrylate (1700)	-21
Bisphenol A ethoxylate dimethacrylate (540)	75
Bisphenol A ethoxylate diacrylate (468)	65
Bisphenol A ethoxylate diacrylate (512)	66
Bisphenol A ethoxylate diacrylate (688)	33
Trimethylolpropane ethoxylate triacrylate (428)	88
Trimethylolpropane ethoxylate triacrylate (604)	41
Trimethylolpropane ethoxylate triacrylate (912)	-2
Trimethylolpropane propoxylate triacrylate	35

experiments as determined on the Q800 Dimensional Mechanical Analyzer (DMA) in 5 °C per minute temperature ramp tensile tests measuring stiffness as a function of temperature.

Controlling the synthesis is an important first step toward optimizing the mechanical properties of acrylate systems. Shape memory polymers exist in three temperature-dependent regions which greatly influence the behavior of the polymer at the given temperature *[25]*. The *glassy state* is the region of low deformability where steric hindrance and chain entanglement limit the ability of individual polymer chains to uncoil and move relative to one another. There are few (assumed no) internal stresses in the polymer *[26]* although it is difficult to reach true equilibrium in the glassy state.

As the material heats up it enters into a *linear viscoelastic transition* represented under ideal conditions by the Maxwell model which is a Hookean solid and a Newtonian liquid in series *[22]*. Within this region, the T_g represents the temperature at which amorphous materials

(polymers in their glassy state) begin to soften and exhibit pseudo-elastic properties *[27]*. In DMA curves plotting the elastic modulus as a function of temperature, the T_g can be observed in the orders-of-magnitude drop in the elastic modulus or the spike in the *tan delta* curve. The tan delta is a complex component of polymers that represents the ratio of the *loss modulus* to the *storage (elastic) modulus*. The stiffness is also a rate-dependent function because in the viscoelastic region, strain creeps with time *[26]*. At more elevated temperatures, the polymer enters into the rubbery regime. In a thermoset polymer, the flat region on the right of the elastic modulus as a function of temperature curve represents the *rubbery modulus* (E_R). This metric conveys the stiffness at high temperatures; from this stiffness metric, the crosslinker density can be inferred. The hypothesis based on rubber elasticity theory is that the resulting elastic modulus (the measure of stiffness), *G*, is proportional to both temperature and cross-link density through the following relationship:

$$G = nKBT = rRT/M_c$$

where n is the number density of network chains, *r* is the mass density, *R* is the universal gas constant, and M_c is the molecular weight between crosslinks *[28]*. The experimental elastic modulus and tan delta can be used to extrapolate information about the acrylate system. In 2002, Cao, et al discussed the temperature dependence of storage modulus and tan delta on a specific poly (ethylene glycol) system *[29]* and how theses parameters define shape-memory. Another important metric, *shape recoverability*, measures how much of the original shape is regained after a deformation and shape recovery. This calculation allows for work output to be determined which in turn can illuminate more about the energy state of the deformed material. Gall et al have drawn several conclusions and experimentally confirmed several hypotheses about the T_g and failure strain of acrylate polymer systems *[12]*:

- T_g does not change appreciably with heating rates in 1-10 ºC/min range
- Higher crosslinker density → higher rubbery modulus
- Increased testing frequencies → higher T_g
- Higher temp greater than T_g → lower failure strain
- Increased crosslinking → lower failure strain

Although simple correlations have been made, according to Liu and Gall details regarding the thermomechanical couplings between the pre-deformation, storage, recovery and corresponding thermal conditions are still not well-understood *[26]*. Measuring unconstrained vs. constrained recovery, Liu and Gall examined the effect of heating and cooling rates on stress strain curves in SMPs. Because the thermal mass of the specimens are small, the heat conduction rate is quick compared with the slow heating/cooling rate. The systems remain close to a quasi-equilibrium thermal state *[26]*. Thus thermo-mechanical behavior is dependent on both time and temperature and the following additional observations can be made from Liu and Gall's work *[26, 30]*:

1. At fixed strain, stress relaxes as a function of time.
2. Lower cooling rate → more time spent at high temp → peak recoverability.
3. Peak recovery stress is the greatest possible stress generated by a shape recovery. This occurs at a low cooling (packaging) rate.
4. Once the material is packaged properly (at a fast enough cooling rate), the stresses are quenched into the material and stored as entropy. If however, the material is packaged at a slow rate, stresses which remain internal cannot be recovered because some of them relax out of the material. Those converted to entropy are recovered.
5. As the material is heated, the modulus drops. A slower heating rate yields more recoverable force for deployment.
6. Larger applied strain → larger recovery stress.

7. Higher cooling rates during packaging→ lower temp for shape fixity → higher peak recoverable stress.
8. Lower heating rates during recovery → lower onset for recovery → higher peak recoverable stress.

To monitor and fully characterize the shape memory effect for a specific biomedical application or commodity application, other mechanical properties must also be considered and more qualitative relationships must be determined. In addition to SMPs alone, Gall et al. have further designed nanocomposites by micro-casting SiC particles into a polymer matrix *[31]* to alter the mechanical properties of the matrix. Strength, toughness, biocompatibility, and deformability all must be understood if not controlled in device design, whether in SMPs or SMP-composites. For these metrics to fit into a larger framework, a more complete understanding of the chemistry of the different acrylate monomers, and the polymerization methods of synthesizing acrylates, is necessary.

1.3. Polymerization Methods

Polymerization is the chemical process of reacting monomers together to form of polymer chains. Polymerization usually occurs through one of two different broad processes: chain growth or step growth. Within these two large categories, competing polymerization methods each have their own sets of advantages and drawbacks: a step-growth block copolymer approach gives the material designer complete control over the growing polymer chain and which monomers or blocks will be added next, but significantly narrows the choices of polymers by imposing solubility constraints on the chosen polymers; a chain-growth polymer blend method allows for a pre-polymerization mixture of any soluble polymers, whose final properties will be an average of the combined polymers based on their functional percentages as they randomly

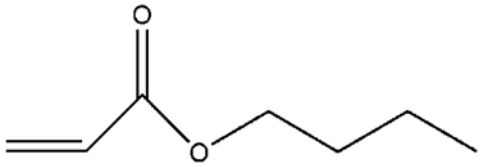

Figure 5. Linear builder n-butyl acrylate (BA)

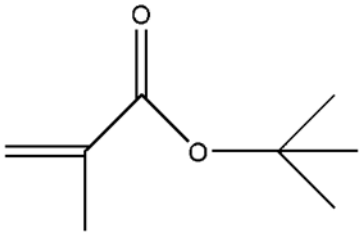

Figure 6. Linear builder *tert*-butyl acrylate (tBA)

polymerize onto the growing backbone; and a mechanical combination of a shredded, shaped or insoluble polymers into a solution creates an interpenetrating network with both the elastic properties of the matrix and the stiffness of the shred. Acrylate systems in this research are polymerized through the chain growth mechanism. This process can be understood through a discussion of acrylate chemistry.

1.3.1. Acrylate Chemistry

An acrylate is a vinyl ester. A vinyl group is an alkene, a carbon-carbon double bond with two hydrogen atoms on the first carbon and two side groups on the other carbon *[32]*. In acrylate chemistry, one side group bonded to the second carbon is an ester and the second side group is a hydrogen or CH_3 (in methacrylate chemistries). The ester group is essentially a carbon, pi bonded to one oxygen atom and sigma bonded to another oxygen atom.

In acrylates, the ester is carbon bonded to the remaining spot on the second vinyl carbon. The sigma-bonded oxygen has another free bond to which the carboalkoxy group is attached. The carboalkoxy group leads to the naming convention of acrylates: methyl acrylate (Figure 3) has a methyl group (CH_3) as the carboalkoxy group; *n*-butyl acrylate (BA) (**Figure 5**) is of similar chemical structure to *tert*-butyl acrylate (*t*BA) (**Figure 6**) which has a *tert*-butyl group (C_4H_9) in this spot; the standard naming convention is similarly straightforward for other acrylates as well.

1.3.2. Kinetics and the Effects of Polymerization

Several methods of observation and analysis exist to validate the final microstructures of the polymerized acrylates. Miller, et al. have used Real-time Fourier-Transform Infrared Spectroscopy (RTFTIR) to analyze polymerized formulations and compare the amorphous microstructure to their predictions *[33]*. This data is consistent with the Photo-DSC data they received. Decker developed and used infrared spectroscopy to monitor the real-time disappearance of each of the monomers undergoing polymerization and created a plot of monomer conversion vs. time *[34]*. The purpose of his study was to study the effect of light-induced crosslinking polymerization of monomer blends and the kinetic aspects of these reactions *[34]*. Other possible methods of observation include:

- XRS: x-ray scattering
- TRAS: time resolved absorption spectroscopy
- TLS: thermal lens spectroscopy
- PAS: photo acoustic spectroscopy
- CW Photolysis: continuous wave photolysis
- CIDNP: Chemically Induced Dynamic Nuclear Polarization
- ESR: Electron Spin Resonance Spectroscopy or EPR (paramagnetic)

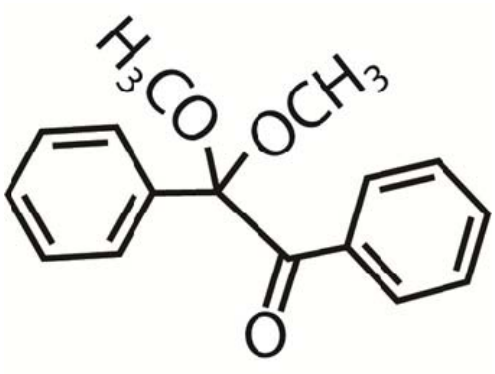

Figure 7. Photoinitiator 2,2-dimethoxy-2-phenylacetopehnone (DMPA)

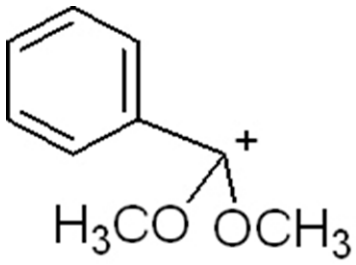

Figure 8. Dimethoxybenzyl free-radical

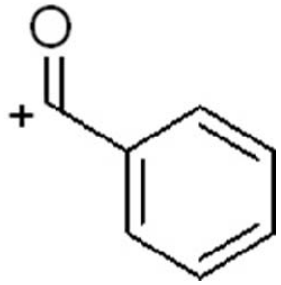

Figure 9. Benzoyl radical

Allonas, et al. developed an analysis technique based on TLS and PAS to determine the rate constant and the enthalpy of an addition reaction or a radical onto a monomer unit *[35]*. Lendlein, Schmidt and Langer studied an AB-polymer network showing shape-memory properties : poly(ε-caprolactone) and *n*-butyl acrylate and also found that the degree of functionalization of the oligo(ε-caprolactone) diols with methacrylate end groups through ^{1}H NMR spectroscopy *[36]*. Although the means of analysis has some affect on the observed results, it is the kinetics of the various polymerization processes that determines the microstructure of the polymer network. Different kinds of photo-polymerization include cationic, anionic and free-radical polymerizations *[21]*. Cavitt et al. have explored different photo-initiation methods for acrylate systems in particular *[37]*.

A common photo-initiator to begin the acrylate chain reactions is 2,2-dimethoxy-2-phenylacetopehnone pictured in **Figure 7**. Direct cleavage of 2,2-dimethoxy-2-phenylacetopehnone can undergo a Norrish type I cleavage into a dimethoxybenzyl radical (**Figure 8**) and a benzoyl radical (**Figure 9**). Thus:

$$R^{\bullet} + M \rightarrow k_i \rightarrow R\text{-}M^{\bullet} \quad \Delta H_r$$

Where ΔH_r is the enthalpy accompanying the reaction and k_i is the rate constant of initiation *[35]*. Thus according to Allonas, the heat released as function of time can be further represented by the following relationship:

$$H(t) = h\nu - \Phi_{rad} \cdot E_{rad} - \Phi_{rad} \cdot \Delta H_r \cdot (1\text{-}exp(-t/\tau))$$

$\Phi_{rad} \cdot E_{rad}$ is the energy stored in the radicals before the addition of the monomer; τ is the lifetime of the initiating radical $R^{\bullet}$ *[35]*. In comparison to other photo-initiators, relatively low rate

constants have been determined for the benzoyl radical *[38]* and the dimethoxybenzyl radical *[39]* through detailed observations using the indirect laser method *[40]*, although 12 other less common possible products can result from the interaction of high-intensity UV light with 2,2-dimethoxy-2-phenylacetopehnone *[39]*.

A wide variety of models have evolved to describe photo polymerization as applicable to acrylate systems, but none of the models fully describes the kinetic profiles *[41]*. These models include bi-molecular termination combined with reaction diffusion control, mono-molecular termination in the glassy region, primary radical termination, chain length dependent termination, random walk for heterogeneity and primary stylization *[41]*. Furthermore, Jansen, et al. show that systems in which acrylates undergo hydrogen bonding, a kind of pre-organization spatially forces the acrylate double bonds closer to each other, thereby enhancing the rate of polymerization *[41]*. Although ester acrylates, the primary focus of the proposed research, and carbonate acrylates are not capable of forming hydrogen bonds, secondary bonding clearly plays a role in determining the kinetics of polymerization.

To begin the acrylate chain reaction polymerization, UV radiation cleaves the central carbon-carbon bond of the selected photo-initiator, 2,2-dimethoxy-2-phenylacetophenone, see Figure 7. In the most-likely case, the cleavage forms two radicals: a benzoyl radical and a dimethoxybenzyl radical *[39]*. Each of these charged radicals attacks a vinyl double bond on one of the acrylate monomers. The free radical bonds to the monomer by opening the monomer's vinyl bond, attaching to the monomer and creating a new free radical. This new radical, on the former vinyl pi bond that is now a sigma bond, attacks another vinyl pi bond on a neighboring monomer. This anaerobic process continues until the growing polymer chain runs into an oxygen-laden free surface, coils back upon itself so as to spatially preclude the tailing radical from polymerizing further, or couples with another free radical *[21]*.

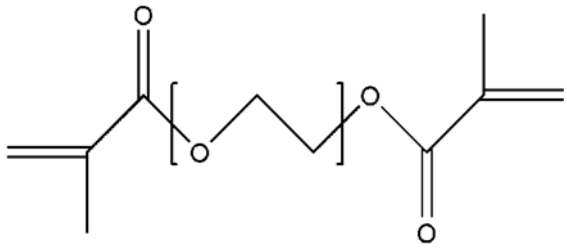

Figure 10. Crosslinker poly(ethylene glycol) dimethacrylate (PEGDMA)

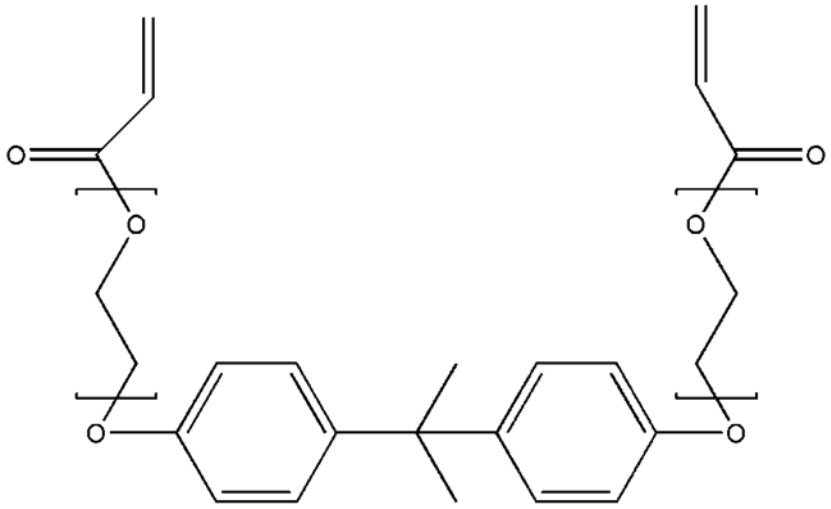

Figure 11. Crosslinker bisphenol A ethoxylate diacrylate (BPAEDA)

Kinetics and its driving thermodynamic mechanisms play a vital role in the characterization of shape memory polymers in the processing of acrylate systems, the deployment of biomedical devices (based on the shape memory effect) and the theory behind thermal-mechanical testing. The kinetics of polymer processing strongly affects the resulting mechanical properties that are composition and process dependant. Furthermore, changing the composition of the linear monomers and crosslinkers is a proven method for tailoring the mechanical properties of acrylate systems *[4]*. For instance crosslinkers such as poly(ethylene glycol) dimethacrylate seen in **Figure 10** help reduce the T_g of many acrylate copolymers because of the inherent flexibility of the crosslinking chain while other crosslinkers such as bisphenol A ethoxylate diacrylate seen in **Figure 11** may help increase the copolymer's T_g.

A new shape can be attained from the tailored polymers by increasing the temperature above the T_g and applying a force. Lendlein et al. have also explored alternate methods of activation and deployment: light-activated shape memory polymers *[42]* where light rather than temperature drives the shape memory effect. Furthermore, Behl and Lendlein have observed indirect actuation of shape memory polymers with an infrared light and remote actuation of the thermally-induced shape memory effect in an alternating magnetic field in SMP composites embedded with magnetic nanoparticles *[43]*.

1.4 Overview of Results

An understanding of the problems faced drives what information is incorporated into the upcoming Chapters and dictates the flow of information and analysis throughout this work. General problems addressed whose approaches and results comprise the remainder of the work include:

1. Understanding of toughness as a function of temperature for tailored thermoset acrylate copolymer systems, through experimentation and extrapolation using Gordon-Taylor analyses and a failure envelope
2. Assessing the effect of small changes in crosslinker density to pinpoint the transition from a thermoplastic to a lightly-crosslinked thermoset copolymer
3. Determining the deformability curves (and maximum strain-to-failure peaks) as a function of temperature to compare with the T_g for each acrylate copolymer system
4. Finding cost-effective ways to manufacture thermoset acrylate systems.
5. Building composites with low-cost high toughness fibers
    a. Optimizing the crosslinker in the composite systems
    b. Optimizing the volume fraction of fiber to polymer
    c. Choosing the optimal weave and weave direction
    d. Choosing the best fibers to interface with a given polymer system
6. Optimizing crosslinker density to reduce the fraction of crosslinker
7. Optimizing the photo-initiator concentration
8. Exploring electron beam curing vs. ultraviolet curing
9. Optimizing post-processing methods such as e-beam crosslinking to crosslink thermoplastic polymer systems and impart shape memory

More broadly, the objective of the research centers on gaining a better fundamental understanding of the emerging mechanical properties of low-cost thermoset acrylate copolymers, comprised of linear monomers and a low density of crosslinker. Finding ways to synthesize different combinations of acrylate mers and ways to effectively crosslink them is enabling a new generation of shape-memory materials that may be durable enough for commoditization. Techniques toward this end involve the addition of monomers with different activation functionalities with dependences on various temperatures and on time. Other techniques involve mixing mono-functional monomers with small fractional compositions of multi-functional crosslinkers. Finding other non-synthesis-driven methods to crosslink acrylates is a post-processing task of the research. Determining how to synthesize SMPs has been a challenge in and of itself: balancing the crosslinker concentration within the concentration of linear acrylate monomers affects the brittleness of the material and the speed and deformation temperature. Overall objectives of this research spread across the remaining chapters are as follows:

(1) **Understand** strain capacity as a function of temperature and composition for various acrylate copolymers;

(2) **Assess** the effect of small changes in crosslinker density on a polymerized polymer matrix of each acrylate system;

(3) **Correlate** the T_g to the deformability peaks to give further insight into the behavior and properties of acrylate systems;

(4) **Find** cost-effective ways to manufacture thermoset acrylate systems; and

(5) **Expand** upon the knowledge gained in objectives (1)-(4) to address emerging gaps in understanding surrounding thermoset acrylate copolymer systems.

Rudimentary understanding of objectives (1)-(3) had existed. The research presented improves upon this base of knowledge and relates each topic toward the ends of objectives (4) and (5). Chapter 2 presents the experimental techniques that enable this research. Chapter 3

details processes to describe phenomena related to tasks 1-3. It explores large strain SMPs with a specific focus on recoverable strain. Chapter 4 describes a new paradigm in SMP manufacturing by describing a process called *Mnemosynation*. It enables the mass-manufacture of thermoset acrylate SMPs with very specific thermomechanical properties. Chapter 5 discusses an optimization within the *Mnemosynation* manufacturing process, namely adjusting the amount, length and ratio of crosslinking agent to linear monomer. The effects of this adjustment on the thermomechanical properties of the underlying acrylate copolymers are explored. Chapter 6 outlines future continuing work toward which vast strides have already been made. It describes how coupling *Mnemosynation* with an understanding of large strain SMP syntheses enables a biomedical engineering exploration into creating a self-adjusting shape-memory polymer orthopedic cast. Numerous fundamental scientific problems are unearthed as this SMP-fiber composite roadmap seeks to establish a new paradigm in fiber-reinforced polymers: namely, using composites to achieve large strains and moderate stresses instead of large stresses through extreme stiffness. Chapter 6 presents preliminary SMP-fiber composites research and exposes problems to be addressed in greater detail in upcoming studies. Chapter 7 succinctly summarizes the scientific contributions of the presented work.

1.6 References

[1] L. Wood, Reuters: Business Wire, **2009**.
[2] C. Eyre, in *European Plastics News*, **2009**.
[3] B. Sillion, *Actualite Chimique* **2002**, 182.
[4] K. Gall, C. M. Yakacki, Y. Liu, R. Shandas, N. Willett, K. S. Anseth, *Journal of Biomedical Materials Research, Part A* **2005**, *73A*, 339.
[5] F. Rodriguez, C. Choen, C. K. Ober, L. A. Archer, *Principles of Polymer Physics*, Taylor & Francis Group, Ithica, NY **2003**.
[6] *W. Voit*, *T. Ware*, *R. R. Dasari*, *P. Smith*, *L. Danz*, *D. Simon*, *S. Barlow*, *S. R. Marder*, *K. Gall*, *Advanced Functional Materials* **2009**, *accepted*.
[7] A. Lendlein, R. Langer, *Science* **2002**, *296*, 1673.
[8] F. E. Feninat, G. Laroche, M. Fiset, and D. Mantovani, *Advanced Engineering Materials* **2002**, *4*, 91.
[9] K. Smith, *Research Notes and Preliminary Results* **2007**.
[10] C. M. Yakacki, R. Shandas, C. Lanning, B. Rech, A. Eckstein, K. Gall, *Biomaterials* **2007**, *28*, 2255.
[11] R. Langer, D. A. Tirrell, *Nature* **2004**, *428*, 487.
[12] K. Gall, C. M. Yakacki, S. Willis, C. Luders, *Submitted to the Journal of Biomedical Materials Research, 2007* **2007**.
[13] Y. Grohens, M. Brogly, C. Labbe, M. O. David, J. Schultz, *Langmuir* **1998**, *14*, 2929.
[14] E. Penzel, J. Rieger, H. A. Schneider, *Polymer* **1997**, *38*, 325.
[15] Baekeland, *942809*, **1907**.
[16] P. J. Flory, *Principles of Polymer Chemistry* Cornell University Press, Ithica, NY **1953**.
[17] G. B. Kauffman, I. Mayo, *The Chemical Educator* **1997**, *2*, 1.
[18] H. Tobushi, Y. Shimeno, T. Hachisuka, K. Tanaka, *Mechanics of Materials* **1998**, *30*, 141.
[19] J. A. Forss, *3512643*, **1970**.
[20] N. Thadani, Georgia Institute of Technology, Atlanta, GA **2007**.
[21] K. D. Belfield, J. V. Crivello, *Photoinitiated Polymerization*, Vol. 1, American Chemical Socitey, Washington D.C. **2003**.
[22] M. Rubinstein, R. H. Colby, *Polymer Physics*, Oxford University Press, Oxford **2003**.
[23] D. Safranski, W. Voit, Georgia Institute of Technology, Atlanta, GA **2007**.
[24] N. F. L. M. C. F. L. Averous, in *Journal of Applied Polymer Science*, Vol. 76, **2000**, 1117.
[25] I. M. Ward, J. Sweeney, *The Mechanical Properties of Solid Polymers*, John Wiley and Sons, Ltd., West Sussex, England **2004**.
[26] Y. Liu, G. Ken, L. D. Martin, M. Patrick, *Smart Materials and Structures* **2003**, 947.
[27] I. Bellin, Kelch,S., Langer,R., and A. Lendlein, *PNAS* **2006**, *103*, 18043.
[28] C. Liu, Qin,H., and P. T. Mather, *Journal of Materials Chemistry* **2007**, *17*, 1543.
[29] Y. Cao, Ying Guan, Juan Du, Juan Luo, Yuxing Peng, C. W. Yip and, A. S. C. Chan, *Journal of Materials Chemistry* **2002**, *12*, 2957.
[30] Y. Liu, K. Gall, M. L. Dunn, A. R. Greenberg, J. Diani, *International Journal of Plasticity* **2006**, *22*, 279.
[31] K. Gall, M. L. Dunn, Y. Liu, D. Finch, M. Lake, N. A. Munshi, *Acta Materialia* **2002**, *50*, 5115.
[32] J. L.G. Wade, *Organic Chemistry*, Prentice Hall, Upper Saddle River, NJ **1999**.

[33] C. W. Miller, C. E. Hoyle, S. Jonsson, C. Nason, T. Y. Lee, W. F. Kuang, K. Viswanathan, in *Advances in Photoinitiated Polymerization*, American Chemical Society, Chicago, Illinois **2001**.
[34] C. Decker, in *Advances in Photoinitiated Polymerization*, American Chemical Society, Chicago, Illinois **2001**.
[35] X. Allonas, J. Lalevee, J.-P. Fouassier, in *Advanced Photoinitiated Polymerizations*, American Chemical Society, Chicago, Illinois **2001**.
[36] A. Lendlein, A. M. Schmidt, R. Langer, *PNAS* **2001**, *98*, 842.
[37] T. B. Cavitt, B. Phillips, C. E. Hoyle, C. K. Nguyen, V. Kalyanaraman, S. Jonsson, in *Advanced in Photoinitiated Polymerization*, American Chemical Society, Chicago, Illinois **2001**.
[38] W. Schnabel, *In Lasers in Polymer Science and Technology: Applications*, Vol. 2, CRC Press, Boca Raton **1991**.
[39] H. Fischer, R. Baer, R. Hany, I. Verhoolen, M. Walbiner, *J. Chem. Soc., Perkin Trans. 2,* **1990**, 787
[40] S. Jockusch, N. J. Turro, *J. Am. Chem. Soc* **1999**, *121*, 3921.
[41] J. F. G. A. Jansen, A. A. Dias, M. Dorschu, B. Coussens, in *Advances in Photoinitated Polymerizations*, American Chemical Society, Chicago, Illinois **2001**.
[42] A. Lendlein, H. Jiang, O. Junger, R. Langer, *Nature* **2005**, *434*, 879.
[43] M. Behl, A. Lendlein, *Soft Matter* **2007**, *3*, 10.

CHAPTER 2

EXPERIMENTAL METHODS

2.1 Instrumentation

Various tools and characterization methods are necessary to carry out the research described herein. This Chapter discusses the instruments and techniques necessary to collect and process experimental data to enable the conclusions put forth.

2.1.1 Dynamic Mechanical Analysis (DMA)

With the TA Instruments Q800 Dynamic Mechanical Analyzer (DMA), a series of tension or compression tests can be run on a material between two grips or platens in a furnace. Under a steady temperature ramp, the 18 Newton load cell applies a sinusoidal mechanical force on the material as the temperature changes. To calculate the material properties, the DMA requires a host of inputs: a desired maximum applied strain (0.2 % is standard), a preload force (.01 N for instance), a Force Track (150%) and the specific dimensions of the sample to be tested.

The testing equipment, applies an oscillatory stress at the same frequency as the strain, but out of phase with the strain, to reach the specified input maximum *[1]*. Back-calculating the force required to meet the given strain criterion through iteration, the DMA can output the modulus of the tested materials as a function of temperature. This elastic modulus is determined through computation using the user-measured and inputted cross-sectional area of the material and the machine-calculated applied force to calculate the instantaneous modulus as a function of temperature as measured by the thermocouple positioned within the furnace. The linear response of acrylate systems is measured, because the polymers are assumed to behave as viscoelastic materials at the small applied strains.

The Q800 DMA is coupled with an attachable Gas Cooling Accessory (GCA) that holds liquid nitrogen. The Q800 has a temperature range from that of liquid nitrogen (minus 196 ºC) to 600 ºC. Typical testing temperatures for acrylate systems are in the minus 75 ºC to 250 ºC range. The DMA is also used to run free-strain response curves, which yield insights about the shape of several parameters during a shape-memory cycle. Samples are measured and placed into the chamber. The material is heated to a temperature above T_g and strained (say to 50%). The drive shaft is locked and the material is cooled to a temperature below the onset of T_g. The drive is unlocked (set to float) and the materials may contact yielding the shape fixity measurement. Upon reheating, the material will contract as the load cell maintains a zero load upon the frame. The amount of residual strain after one, or several cycles is measured.

2.1.2 Differential Scanning Calorimeter

The Differential Scanning Calorimeter (DSC) is a thermoanalytical device that measures the relative heat flow through a material relative to the heat flow though air (or any other substance placed into the reference pan) and tracks the difference in temperature needed to heat the sample as a function of temperature. The DSC consists of two sealed pans: a sample pan and the reference pan which is usually empty. The polymers to be tested are either polymerized directly into the sample pan, or placed into the pan after small polymerized samples are cut to size. The final plot is a graph of differential heat flow as a function of temperature. This result, known as a heating or cooling curve for the given acrylate system, can be used to calculate the enthalpies of transitions *[2]*. The TA Instruments Q100 DSC contains an attachable refrigerant cooling system (RCS). The Q100 has a temperature range of about minus 80 ºC to 600 ºC. A computerized mechanical arm facilitates loading and unloading of up to 50 samples and five reference pans for more comprehensive tests beyond single comparisons. The TA software is

used to set up between one and fifty experiments at once. The robotic arm facilitates the automatic loading and unloading of sample pans.

2.1.3 MTS Insight 2

The Insight is a thermo-analytical device used to measure an array of mechanical properties. Manufactured by MTS Systems, the Insight 2 has swappable 2 kN, 100 N, and 10 N load cells to stretch and compress material samples. Samples are cut into a standard dog-bone shape, the ASTM D 638-03 Type IV (half scaled), to minimize interference of the grips on the test sample and eliminate the buildup of stress concentrations within the thinner central testing region. The Insight 2 has a vertical testing space of 750 mm (29.5 in.) though which the crosshead can move *[3]*. The results and plots from the Insight 2 vary depending on the test administered. Most common for the research presented herein are measurements of a tensile specimen loaded at a fixed strain rate until the strain-to-failure point is reached as a function of applied stress at a specific temperature. TestWorks 4 software was used to collect and process raw data.

2.1.4 Bluehill Instron

Thermomechanical tensile tests were also performed with an Instron 5567 load frame equipped with a variable thermal chamber. The Instron is screw-driven and has swappable load cells of 100N, 5 kN and 30 kN. Bluehill2 software is used to write test methods, track tests in progress and collect raw experimental data. The Instron has an attachable video extensometer that was had limited use due its limited field of view when assessing the stress-strain response of high strain SMPs.

2.1.5 Brabender PlastiCorder

Thermoplastic pellets were blended with various crosslinking agents of various molecular weights in a Brabender PlastiCorder. 35 g batches were fed into the mixer and heated to 150 ˚C.

Depending on blend concentration, varying amounts of the liquid crosslinking agent were poured directly into the mixing head. Unless otherwise stated, samples were mixed for 7 minutes at which point the torque had leveled off to near 10 Nm.

2.2 Technical Approach

2.2.1 Materials Systems

Thin sheets (~0.89 mm thick) of acrylate polymers with varying crosslinker densities were polymerized between 2" by 3" glass slides under a UV lamp that has an intensity of 10 *milliwatts* per square *centimeter*. The polymers contain some combination of the linear monomers discussed in Chapter 1 and other materials with similar structural properties as mentioned in the remainder of this document. Specifically crosslinker densities of between 0.25 to 50% were ultimately studied although the most frequently synthesized concentrations were 1 wt%, 2 wt%, 5 wt% and 10 wt% crosslinker.

Except in unique cases where noted (i.e. Xini-based materials), the samples were mixed with 0.1 wt% to 0.5 wt% of photo-initiator, usually DMPA while still in solution form. The solution was thoroughly mixed either with a magnetic stir bar or through physical agitation or a Sonicator until the DMPA was fully dissolved in the polymer solution. The polymer solution was typically agitated in a 25 *mL* glass test tube that is 80 *mm* tall with a circular base diameter of 20 *mm*. The tube was labeled and dated. Using a pipette, a volume of liquid is deposited between two glass slides that are clamped apart about 0.89 *mm*. As preparation, glass slides were cut into ¼ inch strips that serve as the structural framework to keep glass slides apart this distance and ensure uniform sample thickness.

The samples were typically irradiated under a Mercury UV lamp for a time period of at least 5 minutes and not exceeding 240 minutes (except in rare cases) , depending on the chemistry of the ingredients of the acrylate solution. Upon removal from the UV chamber, the polymerized

acrylates were removed from between the glass slides, deposited into specimen bags, which were labeled and dated, to await mechanical testing. Over the course of the research, sample Teflon molds were cut at the Georgia Tech machine shop and where noted, samples were polymerized into these molds. The mold was cut with a fill hole and an air oulet hole and open on top. A glass slide of the appropriate size was placed on top of the mold and clamped down. The mold was filled with the copolymer solution and polymerized as described above.

2.2.2 Techniques for Targeting Mechanical Properties

Several methods exist, to infer the T_g of polymer solutions composed of known monomers in specific molar concentrations: an inverse method, a linear interpolation, and a logarithmic approximation. The molar concentrations must be converted to fractional weight percent concentrations and two of the T_gs must be known to calculate the third. The inverse method is:

$$T_g^{\,1} = X_1 / ((T_g^{\,tot})^{-1} - (X_2 / (T_g^{\,2}))$$

Where $T_g^{\,1}$ and $T_g^{\,2}$ are the glass transition of the two components, X_1 and X_2 are the fractional weight percent of the two components and $T_g^{\,tot}$ is the final glass transition temperature. The three methods are averaged to arrive at a hypothetical glass transition temperature for each new polymer concoction. These methods based on Gordon and Taylor's empirical observations have been known since the 1950s *[4, 5]*. The rule of mixture for polymer blends or polymers mixed with a plasticizer has been slightly modified to include volume elements and is know now as the Fox Equation*[6]* Initial tests confirm these empirical relationships in most cases.

2.2.3 Characterization of samples

Polymerized samples will be tested primarily on the three pieces of equipment discussed in the Instrumentation portion of this Chapter. The DSC Q100 is typically first used on the samples to get a rough approximation for the glass transition temperature and the melt temperature for thermoplastics based on the heating curves. After DSC Q100 analysis, DMA Q800 thermomechanical analysis will refine the T_g and also shown time and temperature dependent modulus information. The third leg of testing on the Insight 2, will give full stress-strain curves and show strain-to-failure points at different temperatures. While the proposed project is not solely focused on the heat flow of acrylate systems as they polymerize, characterization of the micro-structure (esp. the distribution of cross-links) is a key part of the proposed research and is heavily influenced by the concentration of photo-initiator and the rate of UV curing. The kinetics of the shape memory effect plays a strong role in the thermo-mechanical properties that are being characterized in this project and the shape memory effect and greatly affects the polymerization of acrylate systems. A realizable goal of the research is to tailor the microstructure of an acrylate for specific applications in the biomedical device realm to engineer better materials with reproducible properties.

2.2.4. Mechanical Testing and Modeling

The DSC, DMA and Insight are complex testing apparatuses used to characterize polymerized acrylates. Through different mechanisms, each piece of testing equipment strictly controls temperature to plot its functional dependence against a variety of other metrics. Both Differential Scanning Calorimetry (DSC) and Dynamic Mechanical Analysis (DMA) are testing methods that are being used to determine the glass transition temperature and other mechanical properties *[7, 8]*. The tests also gage the shape recoverability, shape stability and the temperature dependency of the various mechanical properties. The DSC measures the heat flow through the

sample as a function of temperature. The acrylates undergo a structural change at the glass transition temperature, which appears as a jog in the plot of heat flow per mass vs. temperature. The DMA ties thermal and mechanical properties together beyond the capabilities of the DSC and details how the kinetics of the acrylate system can affect mechanical properties. The Insight yields stress-strain curves that help characterize the different regions of the polymer, from which a rudimentary strength measure can be extrapolated. From similar experimental data on polyurethane shape memory materials, Tobushi et al. have constructed constitutive models based on linear viscoelastic theory modified through the addition of a slip mechanism due to internal friction and by considering thermal expansion *[9]*. Similarly Liu and Gall have developed constitutive models for shape memory polymer systems with an emphasis on stress and strain recovery *[8]*. Monkman *[10]* has explored a combination of models such as the parallel combination of the Prandl (thixotropic) and the Maxwell (rheopectic) models as suggested by Tobushi. Textbooks outline much of the theoretical foundation and the first principles upon which these models are built *[11-14]*. Experimentation and mechanical analysis validate these models, help categorize SMPs based on their mechanical properties and aid in the task of designing an appropriate biomaterial for a specific application.

2.3 Thermomechanical Properties

The *Instrumentation* and *Technical Approach* sections are prologues for collecting data to make predictions as to the behavior of specific polymer systems. Several material properties and phenomena are explored. Beyond those parameters described above such as stress, strain, modulus as a function of temperature and heat flow through a material, several other parameters, inputs and limitations deserve extra attention.

2.3.1 Toughness

Toughness is an indication of the energy that a polymer can absorb before breaking. To determine toughness at a given temperature, the integrated area under the stress-strain curve is used *[15]*. Toughness has the units of *joules per cubic meter* (or alternatively in *MJ* m^{-3}) with stress in *pascals* (or alternatively *MPa*) and strain in *meters per meter* (or *mm* per *mm*) and may be stored elastically or dissipated as heat through crystalline deformation. Since materials usually fail at a defect or a stress concentration, reported values must be regarded as average distributions *[6]*. The Izod Test and Charpy Test *[6]* are two methods that can be used to measure impact strength or the energy needed to rupture a material, which is another definition of toughness. However, these tests can only be performed on glassy or crystalline materials, as most rubbers or materials that experience very large strains will not fracture in these setups. Smith developed the concept of a failure envelope *[16]* to characterize ruptures for rubbery materials which can also be used in the viscoelastic regime. Using the Gordon-Taylor analyses *[17]* to target the correct Tg for a given copolymer, toughness vs. temperature plots can be derived from failure envelopes in the correct temperature ranges for characterization of the desired biomedical applications *[18]*.

Toughness data does not exist in the open literature for the Methyl Acrylate-Methyl Methacrylate co polymer systems with a low density of crosslinker. In addition, there is no simple experiment for measuring the toughness of such a polymer network as a function of temperature. Instead a calculation must be performed at each temperature based on data from the experimental stress-strain curve. No theoretical method exists in the literature to extrapolate this information based on the mole fraction of the components in the copolymer and their known mechanical properties.

2.3.2. Crosslinker Concentrations

Shape-memory polymers possess high recoverable strain levels (100% to 800%) *[19]* which are innately tied to crosslinker density. Despite the significance of large strain deformations in a useful shape memory effect, systematic work has not been performed to understand the strain limits in shape memory polymer networks as a function of network structure or relevant deformation parameters *[20]*. An open problem in the literature is gaining insight into how small fractional changes in crosslinker density alter maximum strain, toughness and shape recoverability. For each specific copolymer acrylate system, the transition between a thermoplastic and a thermoset, and ultimately the viability of a material for a targeted application, has not been determined. There exists some critical composition that defines the line between a highly recoverable thermoset SMP and a thermoplastic polymer, for each acrylate system, that is a function of the cross-linker density. According to Gall et al., a lack of understanding of deformation limits makes it difficult to systematically adjust polymer structure or deformation temperature to obtain optimal strain recovery characteristics *[20]*. No systematic study has been performed in the open literature examining the effects of small changes in crosslinker density below 5% for acrylate co-polymer systems.

2.3.3. Deformability Peak

The failure strain in polymer networks demonstrates a strong maximum, denoted as the "deformability peak" close to the onset of glass transition. Failure strains outside of the deformability peak, well into the glassy and rubbery regimes, are considerably smaller than the achievable strain while the material is viscoelastic *[20]*. Verifying that this correlation holds for different copolymer acrylate systems, systematically assessing peak strain as a function of temperature and relating these findings to the experimental and theoretical glass transition temperatures is necessary to determine the optimum packaging temperature for a biomedical

device. Liu, et al. examined the recoverability of shape memory polymers that undergo large strains *[21]*. Liu pinpoints a peak recoverability stress, which occurs near the T_g. Although these tests were performed in a three-point bend setup yielding non-uniform stresses and strain, Liu claims the trends in results are broadly applicable to stresses and strains in SMPs *[21]*. Despite the advantages enabled by large strain deformation, prior studies have not examined the effect of key processing and structural variables on the failure strain of shape memory polymers *[20]*. The deformability peaks have not been evaluated as a function of temperature for low crosslinking density, acrylate co-polymer systems in the open literature.

2.3.4. Manufacturing

An ongoing problem in the development of new polymers with optimal properties is scaling up production of a material from the test tube to a process that is commercially feasible. Once the acrylate system has been chosen through a non-linear optimization process involving multiple mechanical properties, many new tests must be undertaken to determine how to polymerize, process, shape and package this specific material in bulk quantities. What may work well between glass slides in an anaerobic environment under an intense UV lamp may differ substantially from the final bulk polymerization process. Other methods of crosslinking exist for large-scale industrial applications *[22-28]*. As the research progresses, more emphasis will be shifted to this area of exploration. No attempt has been made in the open literature to explain the efficacy of such approaches for acrylate co-polymer systems in the open literature.

2.3.5. Approach for Assessing Toughness

The first task of the proposed research was to construct a toughness curve as a function of temperature for a specific acrylate copolymer system. To establish a baseline, a ply(MA-co-MMA) systems were chosen for characterization. Following the procedures outlined in this

Chapter, 192 ASTM D 638-03 Type IV (half-scaled) dogbone tensile samples were created. Each dozen identical samples were strained to failure at 12 discrete temperature values (0, 20, 30, 35, 40, 45, 50, 55, 60, 65, 80, 100 degrees Celsius) on the Insight 2. 16 different chemical compositions were chosen at which to repeat this experiment. The variability in composition targets two critical glass transition temperatures for biomedical applications, 37 degrees and 57 degrees Celsius and allows for controls. Designing the copolymer with the correct mole fractions of MMA and MA to be near each of these target glass transition temperatures is the first step based on theory. Then four different percentages of crosslinker (0%, 1%, 5%, 10%) of Poly (ethylene glycol) dimethacrylate (Mw ~550) were added into the pre-polymerized solution to physically crosslink the material upon polymerization. This had a slight effect on T_g which was accounted for in the final analysis. Finally two control studies of pure MMA and pure MA have were also synthesized and then combined with crosslinkers in each of the four percentages.

The outcome of this experiment was a representation of toughness for two MMA-MA copolymer systems as a function of temperature. With a large number of acrylate systems to characterize, this was tedious at best and involved very many samples of the same material at each composition to achieve a complete materials characterization. The results in uncoming sections show that a better method exists to gather or infer toughness data from a material. As part of the research, further heuristics were developed to compare the relative toughness of different acrylate concoctions based on their underlying chemistries and fractional compositions. These heuristics were coupled with known procedures for optimizing other mechanical properties in this non-linear optimization problem.

2.3.6. Approach for Analyzing Crosslinker Densities

The second task during initial research phases of the research was rheological in nature. The task was to pinpoint the line that separates a very lightly crosslinked thermoset from a

thermoplastic for the two co-polymer systems and forms the legwork for the results presented in *Chapter 3*. Li et al. have gathered extensive data on heavily crosslinked ethylene–vinyl acetate copolymers *[29]* to demonstrate a high recovery force. The preliminary research sought to understand the other extreme where shape recovery forces are small but total percent strain deformation is very large.

The method was to polymerize 40 samples of MMA-co-MA with varying crosslinker densities below 2wt% at each 0.2% weight percent increment. Three identical samples were tested at each point to control errors that may arise from improper mixing or separation of the polymer solution. The samples were strained to 80% of their failure peaks as determined by the failure peak of the first sample that will be strained until failure. The first attempt at this experiment was to only test the materials at their expected T_g. A follow-up experiment verified this metric (the crosslinker density that separates a thermoplastic from a thermoset) as a function of temperature for the given acrylate system. Completing this analysis left a number of open problems for future research and future researchers.

2.3.7 Approach for Determining Deformability Peaks

The third objective of the initial phases of research wass to verify the location of deformability peaks as a function temperature against the glass transition temperature for the two acrylate co-polymer systems. The task to complete this objective did not involve any additional mechanical testing, but rather a different analysis of the data gathered in the tasks described above. The hypothesis based on related results *[18, 20, 21]* was that the deformability peak will move in tandem with glass transition temperature. This was confirmed and is seen in various Figures in the results sections in *Chapters 3* and *4*. The results of this analysis are a more complete understanding of the aforementioned copolymer systems and a validation of these predictions about the behavior of deformability peaks from the literature.

2.3.8 Approach for Improving Manufacturing Techniques

The final objective of the initial phases of research forms the core of this dissertation. The tasks required to meet this objective were multifold:

- to explore alternate methods for synthetically crosslinking acrylate copolymers after polymerization using a variety of high-energy techniques
- to explore alternate methods of UV induced free-radical polymerization to attain different geometries for shape-memory thermoset acrylates
- to explore machining and manufacturing techniques for cost-effective post processing of shape memory thermoset acrylates.

The results of this task are described in great details in Chapters 4 and 5 and are the underlying science behind the *Mnemosynation* manufacturing process.

2.4. Experimental Methods for High Strain Shape-Memory Polymers

The results from *Chapter 3* were obtained by following a strict set of experimental techniques listed in this section.

Materials: Methyl methacrylate (MMA), methyl acrylate (MA), isobornyl acrylate (IBoA), *tert*-Butyl Acrylate, *n*-Butyl acrylate, poly(ethylene glycol) dimethacrylate (PEGDMA) with $M_n \sim 750$, bisphenol A ethoxylate dimethacrylate with $M_n \sim 1700$, bisphenol A ethoxylate diacrylate with $M_n \sim 468$ and photoinitiators 2,2-dimethoxy-2-phenylacetophenone (DMPA) and 4,4'-dimethoxybenzil (44DMB) were all used as received from Sigma Aldrich, unless otherwise noted.

Synthesis of Xini: The first step was modified from a previously reported procedure [31]. A 500 mL 3-neck flask charged with 4,4'-dimethoxybenzil (Figure 3b), (8.0 g, 29 mmol), 50 mL of 48% aqueous HBr, 50 mL of a 33% solutions of HBr in acetic acid, and 80 mL of glacial acetic

acid and heated at reflux for 12 hours. The solution was poured into water precipitating a fine gray powder. The precipitate was collected through filtration, washed with water and air dried to yield 5.6 g (79%) of 4,4'-dihydroxybenzil, the ^{1}H NMR spectrum of which was consistent with that reported in the literature [31].

A 25 mL flask was charged with 4,4'-dihydroxy benzil (0.3 g, 1.24 mmol) and tetrahydrofuron solvent (2 mL) under a nitrogen atmosphere and then cooled in an ice bath. To the cooled solution, triethylamine (0.25 mL, 3.1 mmol) was added and the resulting mixture was stirred for 5 minutes. Then acryloyl chloride (0.43 mL, 3.1 mmol) was added dropwise and the contents were stirred between 0 $^{\circ}$C and room temperature for 4 hours. The reaction mixture was diluted with 10 mL of THF solvent and filtered through Celite. The precipitate was washed with THF solvent (20 mL) and the solvent was removed from the filtrate under reduced pressure to yield a yellow-colored solid. Purification was achieved by column chromatography on silicagel with 40:60 (v/v) ethylacetate / hexane solvent mixture and afforded a yellow solid. The second step of the synthesis yielded: 0.28 g 4,4'-di(acryloyloxy)benzil (Xini), 65%. ^{1}H NMR ($CDCl_3$, 300 MHz): δ 8.02 (d, J = 6.9 Hz, 4H), 7.30 (d, J = 6.9 Hz, 4H), 6.63 (dd, J = 17.1, 1.2 Hz, 2H), 6.28 (dd, J = 10.4, 8 Hz, 2H), 6.06 (dd, J = 10.5, 1.2 Hz, 2H). ^{13}C{^{1}H} NMR ($CDCl_3$, 100 MHz): δ 192.7, 163.5, 155.6, 133.6, 131.5, 130.3, 127.2, 122.2. GC/MS (*m/z*): 350 (M^+). Anal Calcd. For $C_{20}H_{14}O_6$: C, 68.57; H, 4.03, Found C, 68.26; H, 4.35.

Synthesis of Polymer Networks: MA-co-MMA-co-PEGDMA and MA-co-IBoA-co-BPAED(M)A networks were synthesized by free radical polymerization using 0.001 to 10.00 wt% DMPA or 44DMB. MA-co-IBoA-co-Xini networks were synthesized by free radical polymerization using 0.10 to 100 wt% Xini. Mixtures of monomers mixed with photoinitiator were injected between glass slides separated using 1 mm glass spacers or onto precut Teflon molds and covered with glass slides. Sample molds were clamped with binder clips. Polymerization was performed using a Translinker crosslinking chamber with five overhead 365

nm UV bulbs (UVP). Materials were cured for different lengths depending on the Xini or photoinitiator concentration ranging from 5 minutes to 300 minutes. Polymer networks were synthesized with BPAEDMA compositions of below 2.50 wt% for the bulk high strain tests. Material compositions were subsequently converted to mole% to facilitate comparisons across samples with different components.

Dynamic Mechanical Analysis: Dynamic mechanical analysis (DMA) in tensile loading was used to determine the T_g, onset of T_g and rubbery modulus of the networks using a TA Q800 DMA. Rectangular samples with dimensions of approx. 1 × 5 × 25 mm^3 were cut and tested. The samples were thermally equilibrated at T_{low} for 2 minutes and then heated to T_{high} at a rate of 2 ˚C per minute at 1 Hz. Testing was performed in cyclic strain control at 0.200% strain. A preload force of 0.001N and a force track setting of 125% were used. T_g was defined at the peak of tan delta. Samples were run in triplicate, and variations in T_g were within one standard deviation of 3–5 ˚C. The onset was calculated by the intersecting line method. The rubbery modulus was taken at T_g +25 ˚C or T_g +33 ˚C and noted as such in the representative figures.

High Strain Tests: Mechanical tensile tests were performed with a Bluehill Instron unless otherwise denoted. The Xini tests in **Figure 1** were performed on the MTS Insight 2. Both mechanical testing fixtures were equipped with variable thermal chambers. Samples were initially cut to ASTM dogbone Type IV samples. Equipment limitations regarding the height of the thermal chamber mandated a new design. DMA sized rectangular pieces (20 mm × 4 mm ×1 mm) were used to verify the stress-strain response of Xini at onset and T_g in Figure 1. However, stress concentrators at the grips caused premature failure and crosshead displacement proved to be an inaccurate measure of actual strain. A new dog bone shape was created with a shorter 5 mm gage section and large grip areas. Duct Tape was placed on the grips and samples were colored with black felt-tip markers outside of the gage section. All tests were conducted at a strain rate of 10 mm/min. A Sony HD video camera was set up outside of the thermal chamber window as the

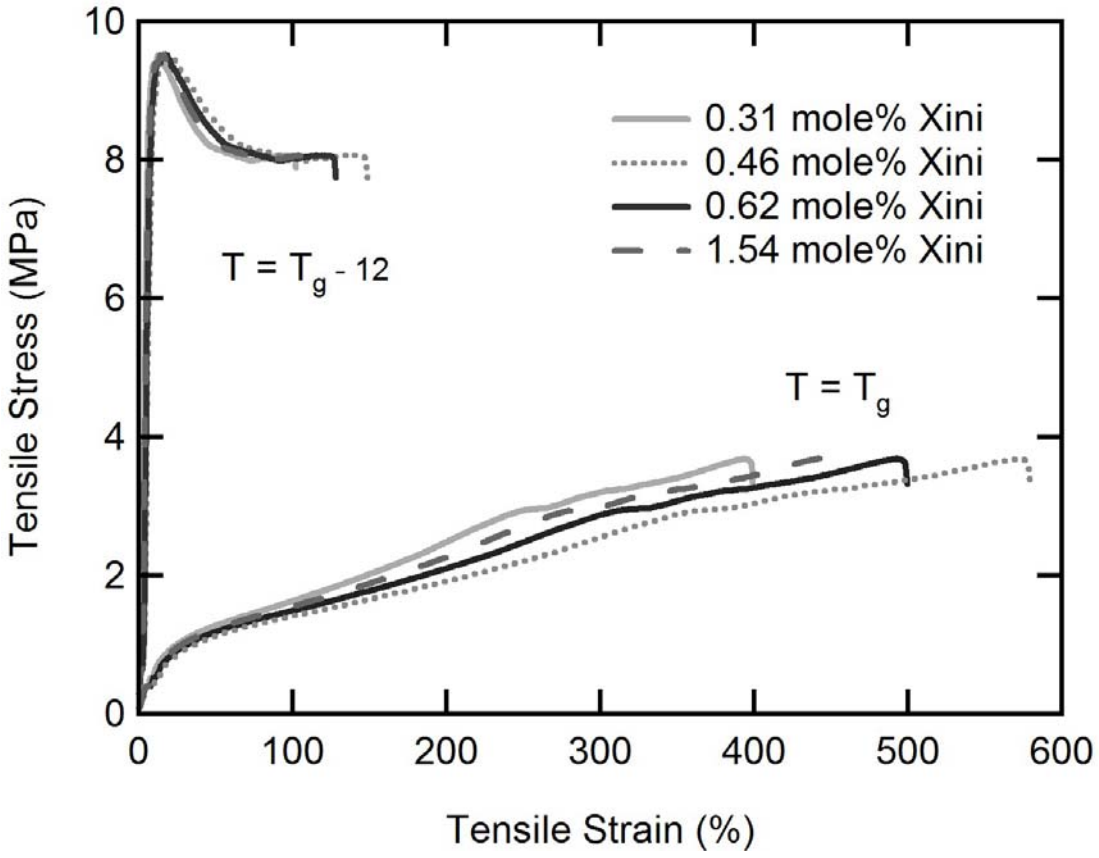

Figure 1. Stress-strain responses of 2:1 wt% MA-co-IBoA based polymers initiated and crosslinked with varying amounts of Xini at the onset of T_g and at T_g.

field of view on the video extensometer and laser extensometer were not large enough to monitor the actual strains. A ruler was placed vertically into the thermal chamber along the same vertical plane at which the sample was being pulled. This eliminated any perspective problems with using the video. The video was necessary to ensure accurate measurements of strain. **Figure 2** plots crosshead displacement vs. displacement gleaned from the video. Using a gage section of 5 mm, strains of over 3000% were recorded by the crosshead when actual local strains were near 800% or 900%. Figure 2 also shows several selected time points of images captured with the HD video. Adobe Photoshop CS4 and Adobe Premiere CS4 were used to analyze still frames captures from the video at critical time points (e.g. the frame before failure) and measure the gage length. Large grip contributions of the high strain material were minimized with this method.

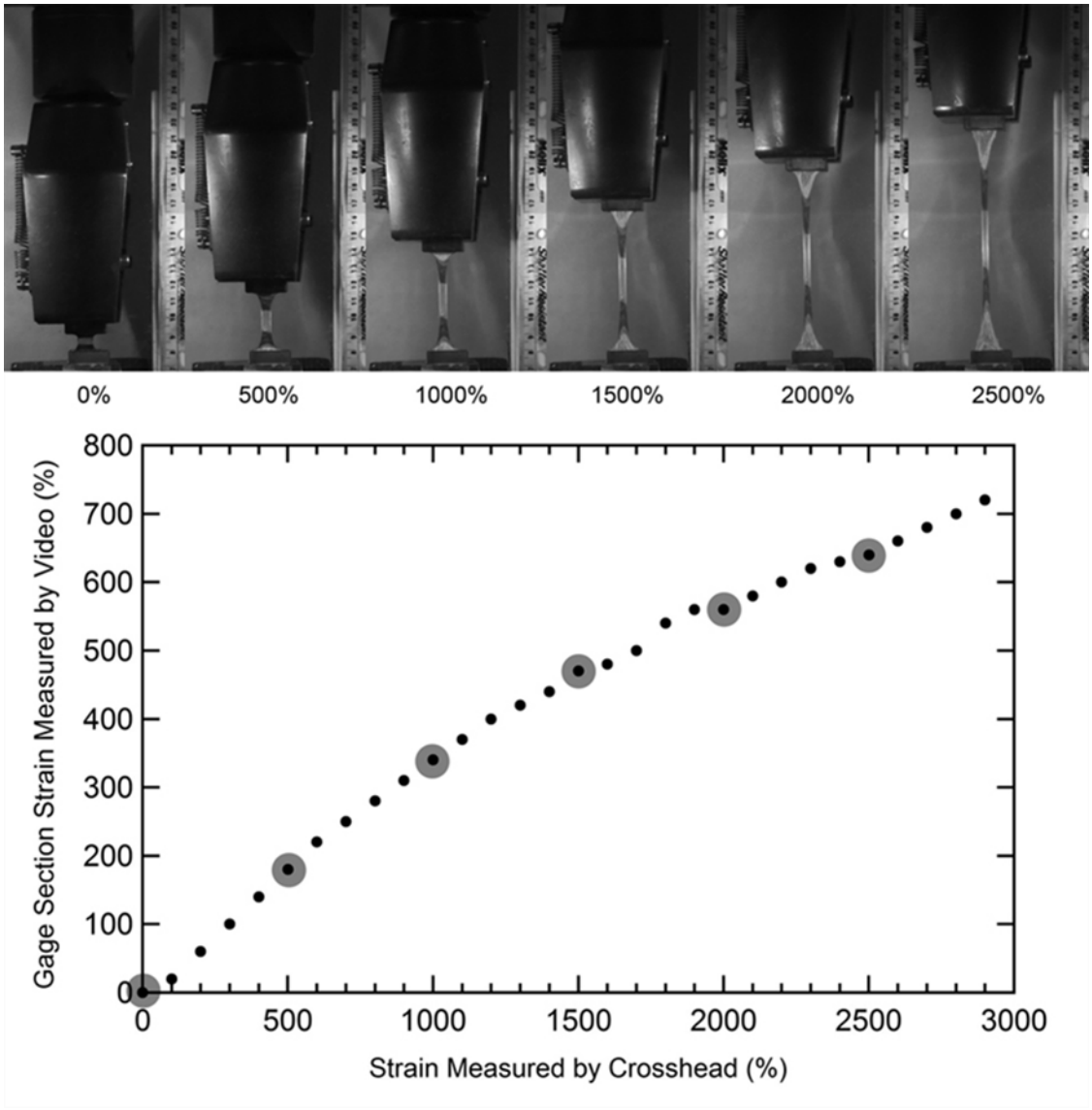

Figure 2. Strain-to-failure as measured by crosshead displacement was inaccurate due to strain contributions from the grip sections. A new method was developed that delineated gage section edges with black felt-tip markers and tracked strain in real time with an HD video camera. Video strain is correlated with crosshead displacement and pictures are shown every 500% strain increment as measured through crosshead displacement.

Gel Fraction Tests: Vials were prepared with approximately 20 mL of acetone placed in each. Three samples of each polymer weighing between 80 mg and 110 mg were weighed and then placed in a separate vial. The vials were allowed to soak for 7 days to allow all non-crosslinked material to be removed from the network polymer. The polymer was then removed

from the acetone and placed on pre-weighed weigh paper. The paper and polymer were then placed into a vacuum oven at 40 °C and 0.33 atmospheres for 24 hours to drive off the remaining solvent. The polymers and paper equilibrated to standard conditions in the ambient lab environment for 24 hours. The samples were then weighed on the paper. The final polymer weight was determined by subtracting the weigh papers' original weight from the total weight.

2.5. Experimental Methods for Mnemosynation

The results from *Chapter 4* were obtained by following a strict set of experimental techniques listed in this section.

Materials: Methyl acrylate (MA), isobornyl acrylate (IBoA), Triallylisocyanurate (TAIC®), Trimethylolpropane triacrylate (TMPTA), *n*-isoproyl acrylamide (NiPAAm), Acryloyl morpholine (AMO), 4-*tert*-Butylcyclohexyl acrylate (tBCHA), 2-Carboxyethyl acrylate oligomers (Mn ~ 170) (CXEA) and photoinitiator 2,2-dimethoxy-2-phenylacetophenone (DMPA) were all ordered from Sigma Aldrich, unless otherwise noted and used in their as received conditions without further purification.

Synthesis of Polymer Networks: Copolymers were synthesized by free radical polymerization using 0.1 wt% DMPA. For networks formed solely through free radical polymerization: 3 g mixtures of the monomers mixed with the photoinitiator were injected between glass slides separated using 1 mm glass spacers. For thermoplastics that would be subsequently be irradiated: 35 g mixtures of linear builders and DMPA were poured into 100 mL polyethylene containers. Polymerization was performed using a crosslinking chamber with five overhead 365 nm UV bulbs (Cole-Parmer). Materials were cured for 1 hour. Samples were either cut for testing or pelletized for further processing.

Crosslinker Blending: Samples were blended with unreacted crosslinker (TMPTA or TAIC®) in a Brabender PlastiCorder. 35 g thermoplastic copolymer batches were pelletized and

fed into the mixer and heated to between 150 ˚C and 220 ˚C. The liquid crosslinking agent was dripped into the mixing chamber. Samples were mixed for 7 minutes at which point the torque had leveled off to near 10 Newton-meters.

Radiation Crosslinking: Samples blended with unreacted crosslinker (TMPTA or TAIC®) were injection molded or heated and pressed with a 12-Tonne Carver Press into their desired shapes. Samples were packaged in air into sealed polyethylene specimen bags and sent to Sterigenics' Electron Beam facility in San Diego CA. Samples were exposed to either 5, 10, 20, 33, 50, 66, 100, 200 or 300 KGy as denoted. Samples were tested as received from Sterigenics.

Dynamic Mechanical Analysis: Dynamic mechanical analysis (DMA) in tensile loading was used to determine the T_g, onset of T_g and rubbery modulus of the networks using a TA Q800 DMA. Rectangular samples with dimensions of approx. 1 x 5 x 25 mm^3 were cut and tested. The samples were thermally equilibrated at T_{low} for 2 minutes and then heated to T_{high} at a rate of 2˚C per minute at 1 Hz. Testing was performed in cyclic strain control at 0.2% strain. A preload force of 0.001N and a force track setting of 125% were used. T_g was defined at the peak of tan delta. Samples were run in triplicate, and variations in T_g were within one standard deviation of 3–5 ˚C. The onset was calculated by the intersecting line method. The rubbery modulus was observed between T_g + 24˚C or T_g +50˚C and noted as such in the representative figures.

Differential Scanning Calorimeter: The Q100 DSC from TA Instruments with an RCA cooling accessory was used to confirm shifts in T_g. Hermitic Aluminum pans were filled with polymer samples weighing between 3 and 15 mg. Nitrogen was used as the purge gas. Polymers were subjected to a Heat-Cool-Heat cycle to erase thermal memory. Samples were heated from ambient to 150 ˚C at 5 ˚C per min, then cooled to -25 ˚C at 10 ˚C per minute and heated at 5 ˚C per min to combustion near 320 ˚C. The intersecting line method was used to determine T_g.

Uniaxial Tensile Tests: Mechanical tensile tests were performed with the MTS Insight 2. Samples were cut to ASTM dogbone Type IV samples. Materials were strained isothermally at 10

mm per min using a 100N Load Cell in a variable temperature Thermal Chamber at the temperature specified. Grips were hand-tightened and the chamber was allowed to equilibrate for 10 minutes at the specified testing temperature. For samples tested above T_g, grip were often re-tightened after an initial heating above T_g to minimize slippage. Testing limitations regarding the size of the thermal chamber and slippage due to high strains led to lower bounds on max strain and max stress for samples of PMA-co-IBoA blended with 3 wt% TMPTA and subsequently irradiated with an electron beam.

Gel Fraction Tests: Vials were prepared with approximately 20mL of acetone placed in each. Three samples of each polymer weighing between 80mg and 110mg were weighed and then placed in a separate vial. The vials were allowed to soak for 7 days to allow all non crosslinked material to be removed from the network polymer. The polymer was then removed from the acetone and placed on pre-weighed weigh paper. The paper and polymer were then placed into a vacuum oven at 40°C and 0.33 atmospheres for 24 hours to drive off the remaining solvent. The polymers and paper equilibrated to standard conditions in the ambient lab environment for 24 hours. The samples were then weighed on the paper. The final polymer weight was determined by subtracting the weigh papers' original weight from the total weight.

2.6 Experimental Methods for Adjusting Radiation Sensitizer

The results from *Chapter 5* were obtained by following a strict set of experimental techniques listed in this section.

Materials: Methyl acrylate (MA), poly(ethylene glycol)diacrylate M_n~258 (PEGDA 258), poly(ethylene glycol)diacrylate M_n~575 (PEGDA 575), poly(ethylene glycol)diacrylate M_n~700 (PEGDA 700) and photoinitiator 2,2-dimethoxy-2-phenylacetophenone (DMPA) were all ordered from Sigma Aldrich, unless otherwise noted and used in their as received conditions

without further purification. All composition and blend ratios are presented in mole% unless otherwise denoted.

Synthesis of Polymer Networks: PMA was synthesized by free radical polymerization using 0.10 wt% DMPA. For thermoplastics that would be subsequently blended and irradiated: 35 g mixtures of monofunctional acrylates and DMPA were poured into 100 mL polyethylene containers. Polymerization was performed using a crosslinking chamber with five overhead 365 nm UV bulbs (Cole-Parmer). Materials were polymerized for 1 hour. Samples were then pelletized for further processing.

Blending: Thermoplastic pellets were blended with PEGDA of various molecular weights in a Brabender PlastiCorder. 35 g thermoplastic pelletized PMA batches were fed into the mixer and heated to 150 ˚C. Depending on blend concentration, varying amounts of the liquid PEGDA were poured directly into the mixing head. Samples were mixed for 7 minutes at which point the torque had leveled off to near 10 Nm.

Radiation Crosslinking: Blends of PMA and PEGDA were heated and pressed with a 12-Tonne Carver Press into ~1 mm thick sheets. Samples were packaged in air into sealed polyethylene specimen bags and sent to Sterigenics' Electron Beam facility in San Diego, CA. Samples were exposed to 5, 10, 20, 33, 50, 66, 100, 200 or 300 KGy as denoted. Samples were tested as received from Sterigenics.

Dynamic Mechanical Analysis: Dynamic mechanical analysis (DMA) in tensile loading was used to determine the modulus over a temperature range from 0 °C to 95 °C of the networks using a TA Instruments Q800 DMA. Rectangular samples with dimensions of approx. 1 mm × 5 mm × 25 mm were cut and tested. The samples were thermally equilibrated at 0 °C for 2 minutes and then heated to 95 °C at a rate of 2 ˚C per minute at 1 Hz. Testing was performed in cyclic strain control at 0.100% strain. A preload force of 0.001N and a force track setting of 125% were

used. The rubbery modulus is defined as the storage modulus at 90 °C. T_g is determined as the peak of tan δ.

Gel Fraction Tests: Vials were filled with approximately 20mL of acetone. Three samples of each polymer weighing between 80mg and 110mg were massed and then placed in separate vials. The samples were allowed to soak for one week to allow material not incorporated in the network to be removed from the sample. The polymer was then placed into a vacuum oven at 40 °C and 0.33 atmospheres for 24 hours to drive off the remaining solvent. The samples equilibrated to standard conditions in the ambient lab environment for 24 hours. The samples were then massed again. The gel fraction was calculated by Equation 3:

$$\text{Gel Fraction} = \frac{m_f}{m_o} \tag{3}$$

In Equation 3, m_f is the residue that remains after the test and m_o is the initial weight of the polymer. The gel fraction reported is an average of the three tests. Standard deviations are reported in Table A1 in Appendix A.

Shape-Memory Tests: The dynamic mechanical analyzer was used in strain-rate control. Rectangular samples with dimensions of approx. 1 mm × 5 mm × 25 mm were cut and tested. Tests were performed on samples irradiated at 50 kGy. Samples were thermally equilibrated at 60 °C and strained to 50.00% at 15.00% per minute. Samples were then allowed to equilibrate for 3 minutes and then cooled at 5 °C per minute to 0 °C. The samples equilibrated for 3 minutes at 0 °C and were subsequently unloaded. The samples were then heated at 5 °C per minute to 110 °C.

2.7 References

[1] M. Rubinstein, R. H. Colby, *Polymer Physics*, Oxford University Press, Oxford **2003**.

[2] D. A. Skoog, F. J. Holler, T. Nieman, *Principles of Instrumental Analysis*, New York **1998**.

[3] M. Systems, *MTS Insight™ Electromechanical Testing Systems Stat Sheet*, **2007**.

[4] M. Behl, E. Hattemer, M. Brehmer, R. Zentel, *Macromolecular Chemistry and Physics* **2002**, *203*, 503.

[5] M. M. Feldstein, *Polymer* **2001**, *42*, 7719.

[6] F. Rodriguez, C. Choen, C. K. Ober, L. A. Archer, *Principles of Polymer Physics*, Taylor & Francis Group, Ithica, NY **2003**.

[7] J. H. Yang, B. C. Chun, Y.-C. Chung, J. H. Cho, *Polymer* **2003**, *44*, 3251.

[8] Y. Liu, K. Gall, M. L. Dunn, A. R. Greenberg, J. Diani, *International Journal of Plasticity* **2006**, *22*, 279.

[9] H. Tobushi, K. Okumura, S. Hayashi, N. Ito, *Mechanics of Materials* **2001**, *33*, 545.

[10] G. J. Monkman, *Mechatronics* **2000**, *10*, 489.

[11] I. W. Hamley, *Introduction to Soft Matter: Polymers, Colloids, Amphiphiles and Liquid Crystals*, John Wiley and Sons, Ltd., Chichester **2000**.

[12] R. A. L. Jones, *Soft Condensed Matter*, Oxford University Press, Oxford **2002**.

[13] R. S. Stein, J. Powers, *Topics in Polymer Physics*, Imperial College Press, London **2006**.

[14] M. F. Ashby, *Materials Selection in Mechanical Design*, Butterwirth-Heinemann, Oxford **2003**.

[15] L. E. Nielson, R. F. Landel, *Mechanical Properties of Polymers and Composites*, Marcel Dekker, Columbus, OH **1994**.

[16] L. S. Thor, *Journal of Polymer Science Part A: General Papers* **1963**, *1*, 3597.

[17] H. A. Schneider, *Die Makromolekulare Chemie* **1988**, *189*, 1941.

[18] K. Gall, C. M. Yakacki, Y. Liu, R. Shandas, N. Willett, K. S. Anseth, *Journal of Biomedical Materials Research, Part A* **2005**, *73A*, 339.

[19] K. Gall, P. Kreiner, D. Turner, M. Hulse, *Microelectromechanical Systems, Journal of* **2004**, *13*, 472.

[20] K. Gall, C. M. Yakacki, S. Willis, C. Luders, *Submitted to the Journal of Biomedical Materials Research, 2007* **2007**.

[21] Y. Liu, K. Gall, M. L. Dunn, P. McCluskey, *Smart Materials and Structures* **2003**, 947.

[22] A. Bhattacharya, *Prog. Polym. Sci.* **2000**, *25*, 371.

[23] A. Charlesby, *Nature* **1953**, *4343*, 167.

[24] S. Cheng, and David R. Kerluke, *Annual Technical Conference Of The Society Of Plastic Engineering (ANTEC)* **2003**.

[25] M. R. Cleland, and Lewis A. Parks, *Nucl. Instr. and Meth. in Phys. Res. B* **2003**, *8*, 74.

[26] R. L. Clough, *Nuclear Instruments and Methods in Physics Research B* **2001**, *185*, 8.

[27] R. K. Graham, *Journal of Polymer Science* **1959**, *XXXVII*, 441.

[28] R. K. Graham, *Journal of Polymer Science* **1959**, *XXXVIII*, 209.

[29] F. Li, W. Zhu, X. Zhang, C. Zhao, M. Xu, *Journal of Applied Polymer Science* **1999**, *71*, 1063.

CHAPTER 3

HIGH STRAIN SHAPE MEMORY POLYMERS

3.1 Problem

Shape-memory polymers (SMPs) are self-adjusting, smart materials qin which both shape changes and changes in stiffness can be accurately controlled at specific, tailored temperatures. In this study, the glass transition temperature (T_g) is adjusted between 28 ˚C and 55 ˚C through synthesis of copolymers of methyl acrylate (MA), methyl methacrylate (MMA) and isobornyl acrylate (IBoA). Acrylate compositions with both crosslinker densities and photoinitiator concentrations optimized at fractions of a mole percent, demonstrate fully recoverable strains at 807% for a T_g of 28 ˚C, at 663% for a T_g of 37 ˚C and at 553% for a T_g of 55 ˚C. A new compound, 4,4'-di(acryloyloxy)benzil (referred to hereafter as Xini) in which both polymerizable and initiating functionalities are incorporated in the same molecule, was synthesized and polymerized into acrylate shape-memory polymers and thermomechanically characterized yielding fully recoverable strains above 500%. The materials synthesized in this work were compared to an industry standard thermoplastic SMP, Mitsubishi's MM5510, which showed failure strains of similar magnitude but without full shape recovery: residual strain after a single shape-memory cycle caused large-scale disfiguration. The materials in this study are intended to enable future applications where both recoverable high strain capacity and the ability to accurately and independently position T_g are required.

3.2. Background

Shape-memory polymers (SMPs) with high strain capacities are important for a variety of advanced applications in ergonomic products and biomedical devices. In fact, synthesizing materials using synthetic building blocks for specific medical and biological applications with

specific properties is one of three key directions shaping the future of biomaterials science.[1] Often advanced applications require material systems that offer trade-offs among strength, toughness and strain capacity. Some SMP applications require high-strength structural components to interface with the human body for reconstructive orthopedic surgeries[2] or cardiovascular applications.[3] Other applications require enhanced toughness.[4-7] Yet other SMP applications in the biomedical device field require high strains to enable large on-demand shape changes.[8-12] Enabling large-strain applications of SMPs are of particular interest in this study.

Large strains have been shown in a number of materials. SMPs have previously been reported to have recoverable strains of up to 400%.[13] Other studies on thermoplastic SMPs have shown large strains dominated by plastic deformation with limited shape recovery. For example, Lendlein and Langer showed multi-block copolymers can be elongated up to 1500% but recover only 400%.[8] For comparison, NiTi shape-memory alloys, which have been coupled with SMPs in novel composites demanding high strength,[14] can recover strains of roughly 8%.[15] The creation of fully recoverable high-strain SMPs may facilitate further innovation into smart next-generation devices with extreme, but specific thermomechanical needs, and could be coupled with advances in other soft materials.[16]

Figure 1 demonstrates the shape-memory cycle in a) stress-temperature, b) stress-strain and c) strain-temperature pairings. The cycle consists of four distinct steps:

1. Loading at T_{high} at constant temperature above the T_g
2. Shape fixing at a constant strain by decreasing temperature below T_g
3. Unloading at T_{low} at constant temperature below T_g and measuring shape fixity
4. Heating and measuring shape recovery

Polymer segments undergo conformational motion above T_g causing mechanical deformation when a stress is applied[17] as seen in *Step 1*. To optimize recovery in the shape memory cycle, this stress is typically applied above T_g facilitating low-stress unwinding of the

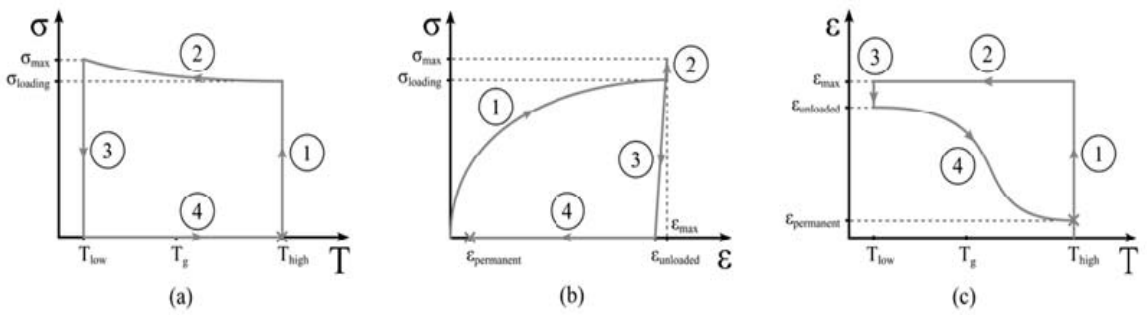

Figure 1. Demonstration of the shape-memory cycle in a) stress-temperature, b) stress-strain and c) strain-temperature regimes. Step 1 is isothermal loading. Step 2 is cooling at constant load. Step 3 is isothermal unloading. Step 4 is shape recovery upon heating.

chains. As the material cools during *Step 2*, new intermolecular interactions created upon reorientation of entangled chains lock the material into its new fixed shape. Applied stresses can be released with minimal impact on this trained shape as shown in *Step 3* and shape fixity measurements[14] can be obtained. When the material is heated towards a state near T_g during *Step 4*, requisite activation energy enables chain mobility of locally deformed chain segments and returns the polymer to its initial shape, minimizing free energy through an increase in entropy. In previous studies, the maximum strain applied during the shape memory cycle, ε_{max}, has been reported well above 1000%, but to the authors' knowledge, values of the quantity ε_{max} minus $\varepsilon_{permanent}$, a measure of the recoverable strain, have not been reported to exceed 400%.

The shape-memory effect can occur in both physically crosslinked thermoplastic polymers and in chemically crosslinked thermoset network polymers. Thermoplastic polymers do not have chemical (covalent) crosslinks connecting individual polymer chains, and thus they rely on physical crosslinks such as chain entanglements or local regions of crystallinity.[18] As thermoplastics approach melt temperatures, they can be stretched virtually indefinitely but with limited shape recovery. In contrast, since thermosets are chemically crosslinked, they do not melt and typically possess fully recoverable strains at all temperatures between T_g and combustion. Analogous to traditional engineering applications involving polymers, tradeoffs exist between the use of shape memory polymers with thermoset versus thermoplastic structures.

Thermoplastic SMPs have the ability to be remolded into different "permanent" shapes, but their recovery behavior is highly dependent on the degree of crystallization and more susceptible to stress relaxation and creep.[19] In polyurethanes for example, hard crystalline regions in the polymer behave as net points that anchor shape recovery while soft segments lend chain mobility.[20, 21] This allows for shape stability and limited shape recovery. Full shape recovery at high strains however, particularly under cyclic loading, does not occur in thermoplastics, resulting in residual strains that may blunt or destroy the "permanent" shapes of devices. In other words, thermoplastic SMPs often possess high strain capacities, but when complete shape memory (i.e. fully recoverable high strain) is important, such materials can constitute a relatively poor choice. For example, a commercial thermoplastic SMP is Mitsubishi's MM 5510 polyurethane[22] that elongates as much as 600% but possesses large residual strains upon recovery.[23]

Thermoset SMPs utilize covalent crosslinks to fix the relative positions of polymer chains to one another forming an insoluble network with infinite molecular weight. These crosslinks serve as net points and will not break under nominal stresses until combustion temperatures are reached. The recoverable force of a thermoset SMP is directly related to its crosslinker density, which may or may not scale linearly with crosslinker concentration, depending on the polymerization reaction kinetics.[24] In addition, researchers have shown that failure-strain is inversely related to crosslinker density, and test temperatures near or slightly below T_g maximize strain-to-failure in lightly crosslinked SMPs.[25] Although thermoset shape memory polymers typically recover all of their applied strain, they often have lower failure strains than thermoplastics. In terms of high strain capacity, the ideal material may exist at the boundary of a thermoset and thermoplastic that has light enough crosslinking to facilitate large strain-to-failure with full recoverability.

Acrylate polymers represent an ideal system to assess the strain capacity of shape memory polymers, and have various potential applications. Acrylate polymers have highly tunable thermomechanical properties and can be tailored specifically for recoverable strain capacity. When co-polymerizing different acrylate monomers, small compositional changes have a large effect on mechanical properties including elastic modulus, strain-to-failure, T_g, brittleness at ambient temperatures and percentage deformation in the rubbery regime.[26, 27] Copolymerizing linear acrylates (mono-functional monomers) with crosslinking acrylates (multi-functional monomers) yields SMPs with tunable properties that can be optimized for very specific applications. Single component MMA polymers[28] and random AB MMA copolymers[29] have been examined. Studies combining MMA with various crosslinkers have also been undertaken,[5] but researchers typically consider copolymers with greater than 1 mole% crosslinker, which have somewhat limited strain capacity.

The overarching objective of this work is to fundamentally understand the transition of tunable acrylate-based materials from thermoplastics to thermosets and thus maximize the recoverable strain capacity of such materials when functioning as SMPs. The authors have proposed several methods to understand this crosslinking transition and maximize the recoverable strain capacity of acrylic SMPs without introducing permanent strain. The approach consists of: Minimizing photoinitiator concentration, without hindering polymerization, to lengthen the distance between chain "ends" so that lower crosslinker concentrations will still yield fully-formed networks;

- Minimizing crosslinker concentration to form looser networks with fewer net points without resulting in thermoplastic behavior; and
- Maximizing crosslinker length without adversely affecting reaction kinetics to increase the theoretical extent of polymer coiling between net points.

- The results of the work form a basic understanding of the polymerization parameters necessary to form a loosely crosslinked SMP network that can experience and recover large strains.

3.3. Results

This study assesses acrylate copolymers containing one or several linear monomers including methyl acrylate(MA), methyl methacrylate (MMA) and isobornyl acrylate (IBoA) combined with less than 0.25 mole% of a crosslinker such as poly(ethylene glycol) dimethacrylate (PEGDMA) or bisphenol A ethoxylate di(meth)acrylate (BPAEDMA or BPAEDA). These polymers can be synthesized under UV light through free radical polymerization[30] using a photoinitiator such as 2,2-dimethoxy-2-phenylacetophenone (DMPA, **Figure 2a**). In addition, a new organic molecule that serves as both a crosslinker and photoinitiator was synthesized and characterized. The starting material for the synthesis, 4,4'-dimethoxybenzil (44DMB), is pictured in **Figure 2b**, while the final material, 4,4'-(diacryloyloxy)benzil, named Xini for its role as both a crosslinker (X) and initiator (ini), is shown in **Figure 2c**. Comparisons between Xini and traditionally crosslinked acrylates are undertaken through gel fraction measurements, dynamic mechanical analyses and ultimately tensile stress-strain tests to measure maximum recoverable strains. In this capacity, the strain-to-failure of polyacrylates crosslinked with less than 0.25 mole% of PEGDMA or BPAED(M)A were characterized against polyacrylates crosslinked with Xini and then compared with an industry standard SMP, Mitsubishi's 5510 MM thermoplastic.

3.3.1 Optimization of Initiator and Crosslinker

The first of the competing approaches to achieve high strain SMPs was to independently optimize both crosslinker concentration and photoinitiator concentration. Average gel fraction

a)

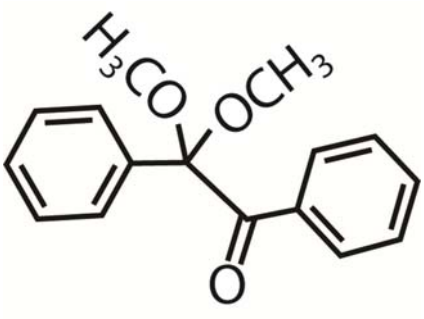

b)

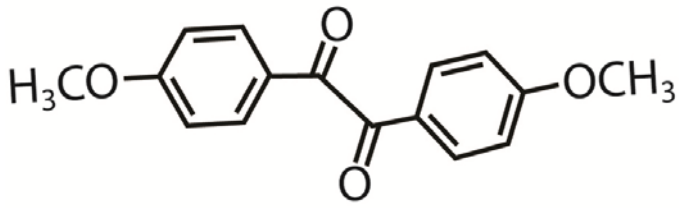

c)

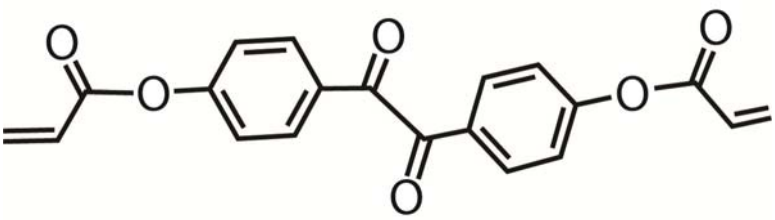

Figure 2. a) 2,2 dimethoxy-2-phenylacetophenone (DMPA), b) 4,4'-dimethoxybenzil (44DMB) and c) 4,4'-diacrylicbenzil (Xini) are photoinitiators that catalyze free radical polymerizations to form solid polymers with acrylate monomers under 365 nm UV light.

measurements (from 3 samples), shown in **Figure 3**, were used to define the extent of network formation across a broad range of crosslinker concentrations and photoinitiator concentrations. Figures 3a and 3b fix the concentration of crosslinker poly (ethylene glycol) dimethacrylate, M_n ~ 750, (PEGDMA 750) at 1.00 wt% (0.115 mole%) and display the effects of varying initiator (DMPA) concentrations in poly(MA-co-PEGDMA). Gel fractions peak between 0.01 and 0.033 mole% DMPA. Figure 3c shows the effect of increasing the concentration of PEGDMA 750 while maintaining a constant photoinitiator concentration at 0.18 mole% when polymerized with linear monomers MA and MMA. Gel fractions begin to level near 0.10 mole% PEGDMA 750 and are greater than 95% above 0.20 mole% PEGDMA 750. Similar studies were duplicated using two linear *acrylate* monomers, MA and IBoA (instead of the *methacrylate,* MMA), moving

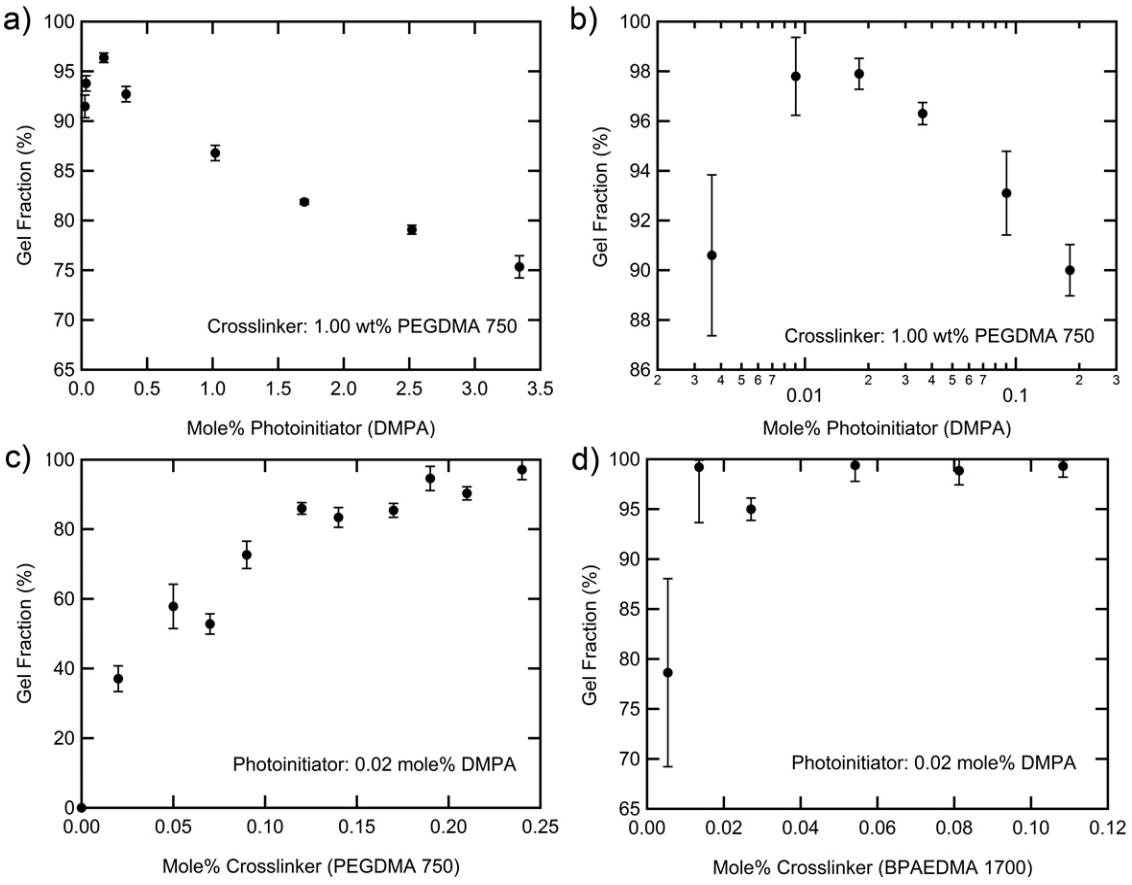

Figure 3. Gel fractions (n=3) for an 87:13 wt% MA-co-MMA base system with increasing crosslinker density and constant photoinitiator are shown on a) a coarse scale of increasing DMPA and b) at optimized concentrations near 0.02 mole% DMPA. Gel fractions (n=3) are shown for c) a PMA base system with 1.00wt% PEGDMA 750 crosslinker with varying concentrations of DMPA, and d) a 95:5 wt% MA-co-IBoA base system with 0.02 mole% DMPA and increasing amounts of BPAEDMA 1700 crosslinker.

to a linear base that is entirely acrylate instead of acrylate and methacrylate. A longer crosslinking agent, bisphenol A ethoxylate dimethacrylate, $M_n \sim 1700$ (BPAEDMA 1700), was also used. This system, shown in Figure 3d, yields gel fraction results near 100% from 1.00 wt% (0.06 mole%) BPAEDMA 1700 onward. The use of gel fraction measurements to establish compositions that may yield high-strain materials is not well-established. However, this gel fraction data is used a guide to target specific materials to obtain their dynamical mechanical responses over a temperature range. Then high-strain predictions can be made based on rubbery modulus and confirmed with uniaxial tensile tests.

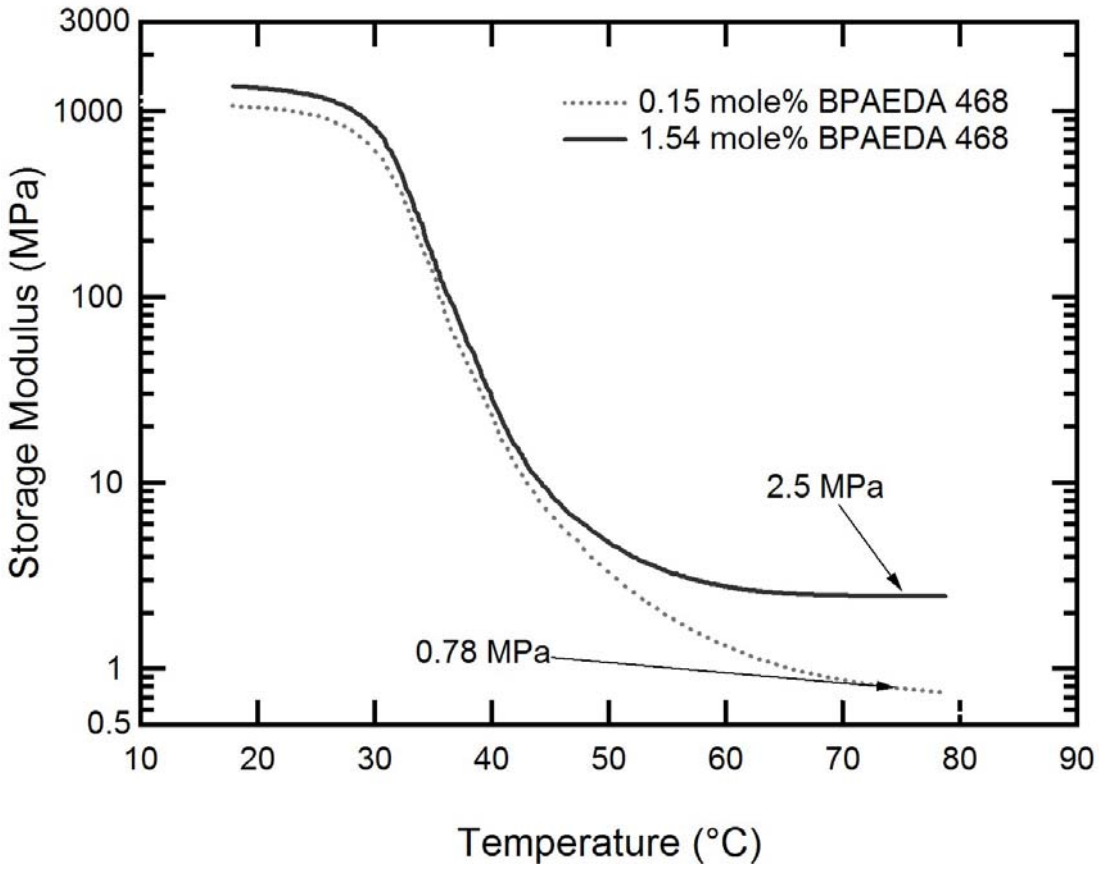

Figure 4. The dynamic mechanical response of 2:1 wt% MA:IBoA polymer systems with different amounts of BPAEDA 468. The rubbery modulus change is significant at increasing crosslinking concentrations.

Figure 4 shows these dynamic mechanical responses of two representative poly(MA-co-IBoA) materials crosslinked with varying amounts of BPAEDMA 468 (0.15 mole% and 1.54 mole%) both containing 0.02 mole% DMPA. This graph shows the bounds on rubbery modulus of these lightly crosslinked systems to be 0.78 and 2.50 MPa. From the gel fraction results in Figure 3, a material designed with 0.05 wt% (0.02mole %) DMPA and 0.25 wt% (0.01 mole %) BPAEDMA 1700 was identified as a high strain candidate with chemical crosslinks.

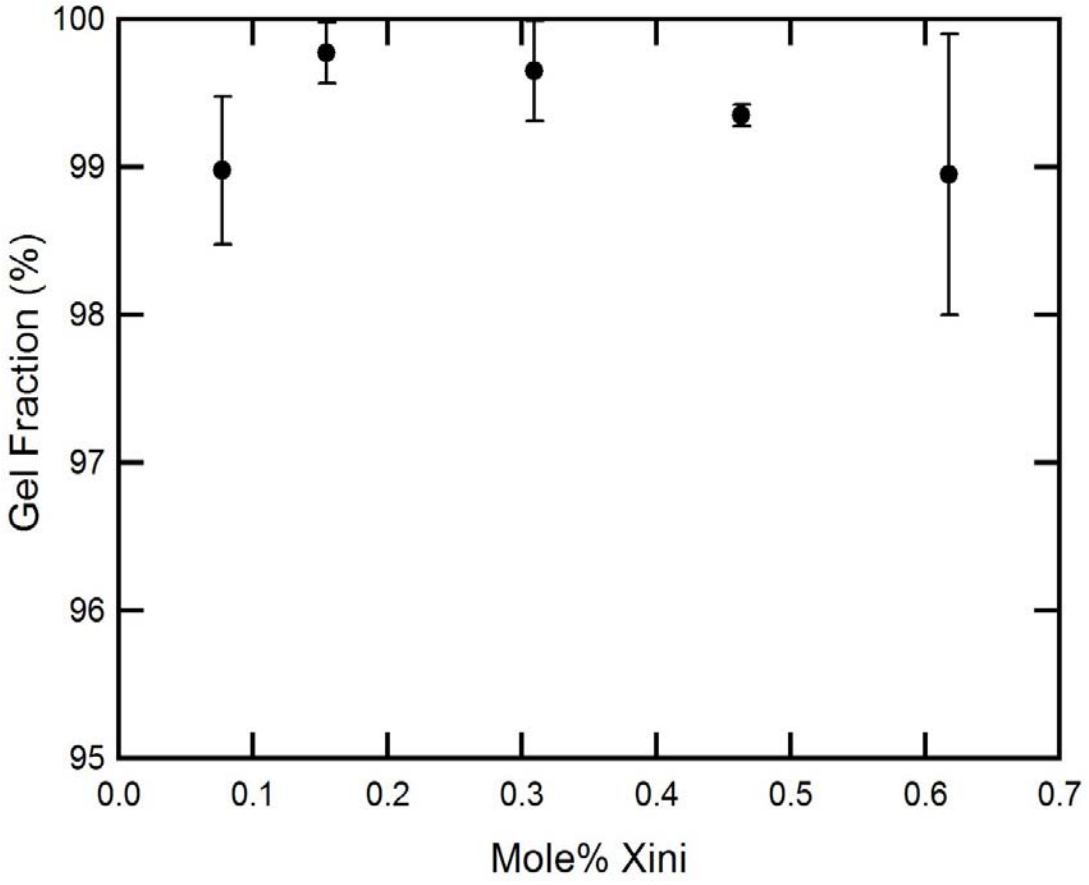

Figure 5a. The gel fraction of PMA with Xini in acetone is above 98% at all concentrations from 0.10 to 0.60 mole%.

3.3.2 Use of a Crosslinking Initiator, Xini

A second competing approach to achieve large recoverable strains was to use a molecule that can serve as both a crosslinker and photoinitiator. In this capacity, an acrylate-functionalized benzil molecule, 4,4'-di(acryloyloxy)benzil, Xini (Figure2c) was synthesized: 44DMB was converted to the corresponding 4,4-dihydroxybenzil using an adaptation of a literature procedure[31, 32], which was then esterified using acryloyl chloride in the presence of triethylamine. Xini is a yellow powder at room temperature; Elemental Analysis, mass spectrometry, and ^{1}H NMR and ^{13}C NMR spectroscopy were used to confirm its chemical structure. Thermomechanical and sol-gel tests confirmed its efficacy as both a crosslinker (X) and

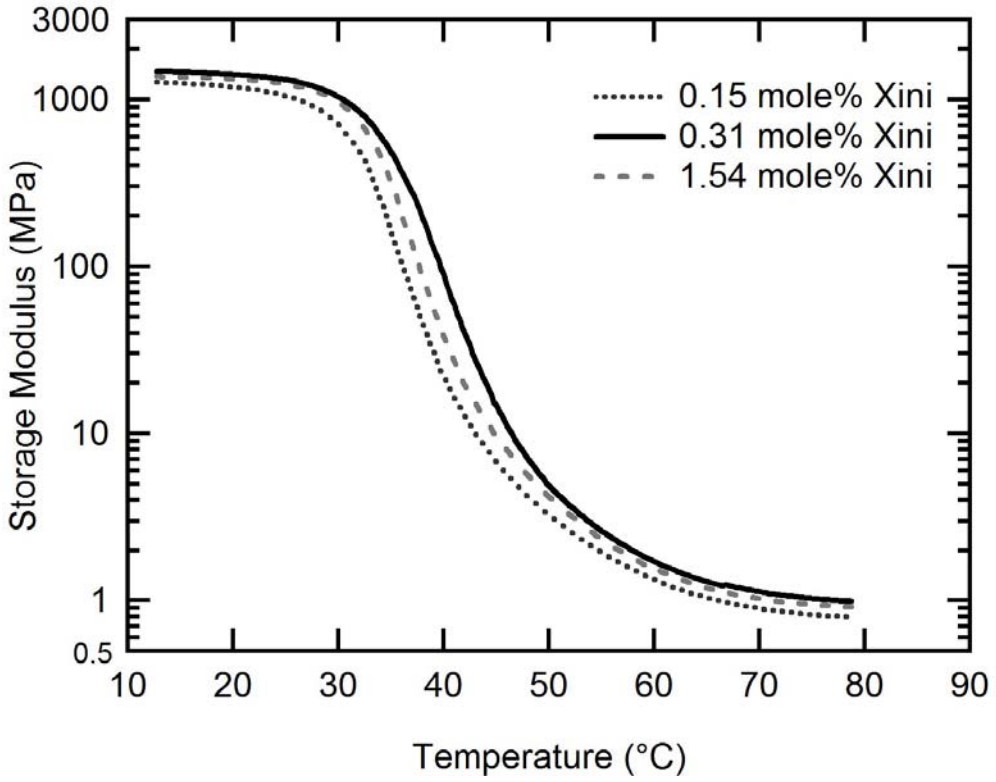

Figure 5b. The dynamic mechanical response of 2:1 wt% MA:IBoA polymer systems with different amounts of Xini. The rubbery modulus change is much smaller than in traditionally crosslinked polymer systems (as in Figure 4) and does not scale linearly with increasing crosslinker concentration.

initiator (ini). Xini was combined with a variety of linear acrylate monomers (including MA, MMA, IBoA, *tert*-Butyl Acrylate and *n*-Butyl Acrylate) in a variety of ratios. **Figure 5a** shows the gel fraction of poly(MA) crosslinked and initiated with Xini over a range of compositions. **Figure 5b** shows the dynamic mechanical response of an average of three runs each of three different compositions: a 2:1 wt% solution of MA and IBoA respectively, with 0.15 mole% (0.50 wt%), 0.31 mole% (1.00 wt%) and 1.54 mole% (5.00 wt%) Xini. The T_g of this base system was set to be near 42 ˚C so that the onset of T_g as measured by the Dynamic Mechanical Analyzer (DMA) would occur several degrees below body temperature and the polymers would be glassy at room temperature. Each of three different runs was decomposed into 0.25 ˚C intervals and the average across all three runs of these points is shown in Figure 5b.

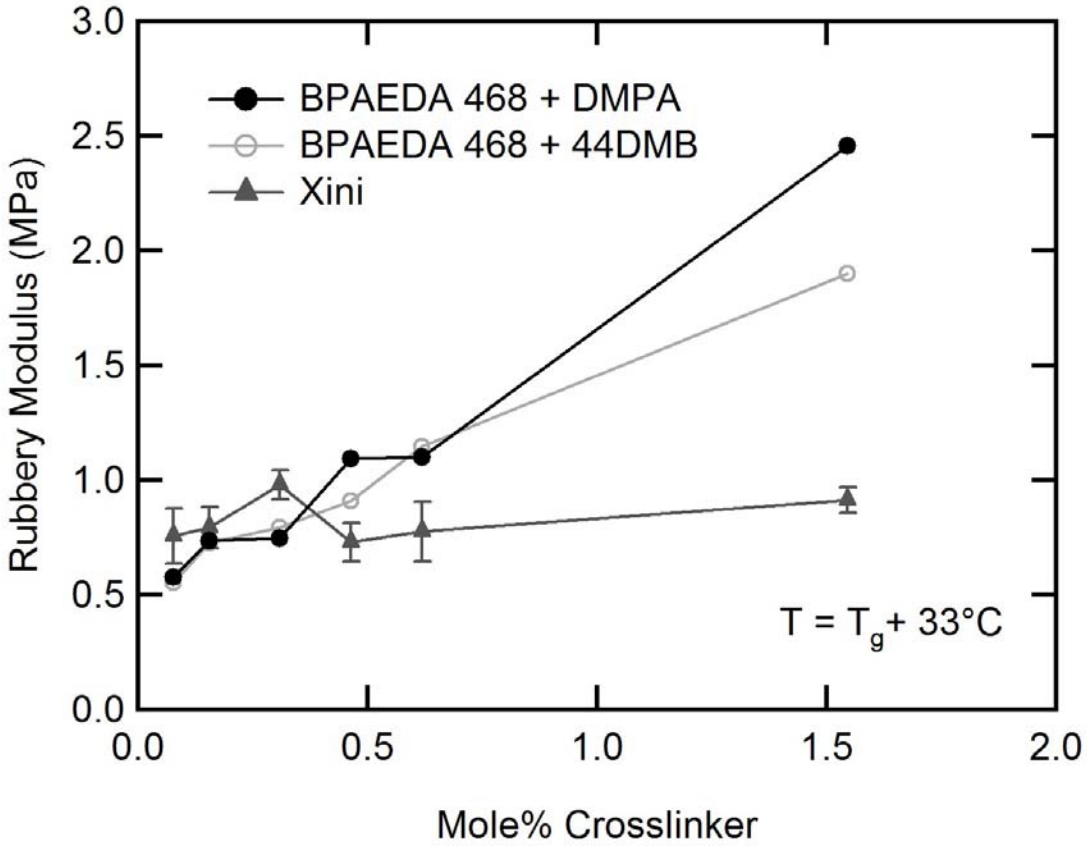

Figure 5c. Rubbery moduli in 2:1 wt% MA-co-IBoA based polymers as a function of mole% crosslinker (Xini and BPAEDA 468) at $T = T_g + 33^{\circ}C$.

Xini was tested in this MA-co-IBoA base polymer system at increasing concentrations: 0.10, 0.25, 0.50, 1.00, 1.05, 2.00, 2.50, 5.00, 10.00, 25.00 and 100.00wt% Xini. Samples below 0.08 mole% (0.50 wt%) Xini were slow to polymerize (2-5 hours) in a 2:1 MA-co-IBoA base and mechanical properties were similar to that of the thermoplastic control sample that contained no Xini. Samples above 1.54 mole% (5.00 wt%) Xini showed a sharp degradation in mechanical properties that included curling at the edges, clumping and very soft spots that tore easily and made thermomechanical testing increasingly difficult. 0.31 mole% (1.00 wt%) Xini yielded more robust mechanical properties showing a maximum rubbery modulus above 1 MPa as seen in Figure 5b, while 0.46 mole% (1.50 wt%) Xini showed a lesser rubbery modulus but had sufficient mechanical properties to strain above 500%.

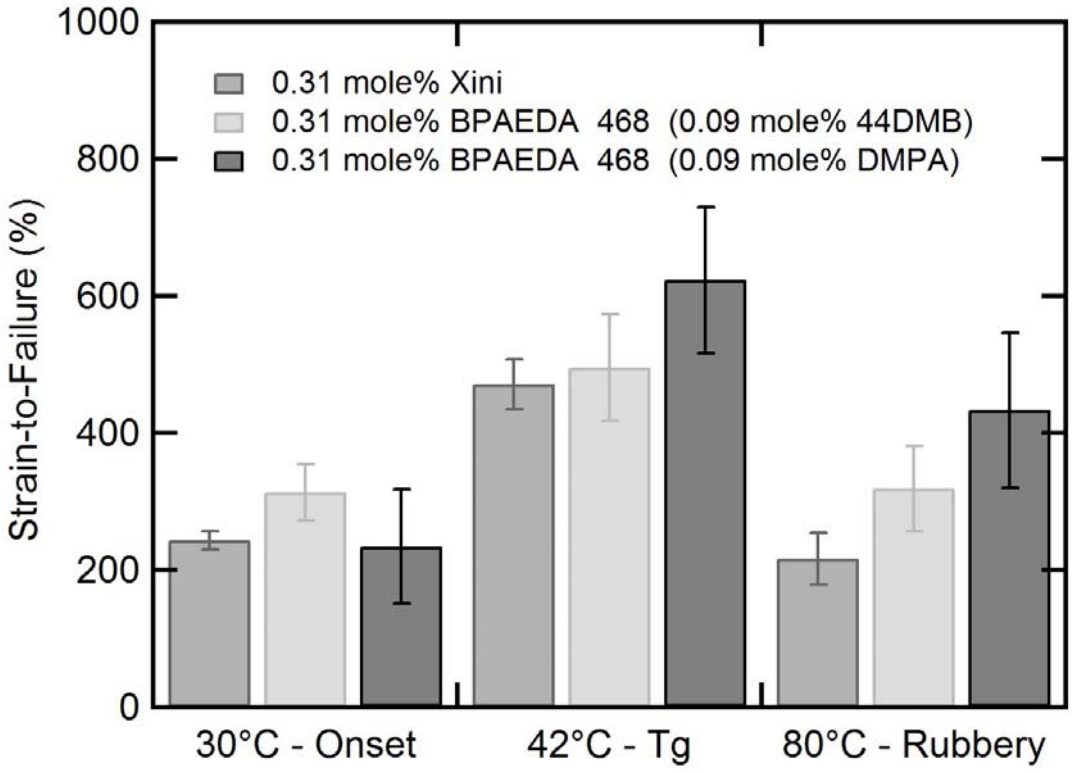

Figure 5d. Strain-to-failure values for 2:1 wt% MA-co-IBoA based polymers with 0.31 mole% Xini, and 0.31 mole% BPAEDA 468 with either 0.09 mole% DMPA or 0.09 mole% 44DMB at onset, T_g and in the rubbery regime.

3.3.3 High Strain Comparisons

In comparing the high strain capacity of the materials, it is important to do so in light of the rubbery modulus of the material since it is an indicator of average crosslink density and is expected to partially dictate strain-to-failure. **Figure 5c** compares the rubbery modulus values at T_g + 33 ˚C (~75 ˚C) of Xini-based samples to those crosslinked with traditional photoinitiators. A 2:1 wt% mixture of MA:IBoA was synthesized with Xini at increasing concentrations and compared to samples synthesized with the same base mixture with traditionally crosslinked DMPA and BPAEDA 468 at increasing concentrations. These samples were also compared with the same base material synthesized with 44DMB and BPAEDA 468 at increasing concentrations. At concentrations above 0.50 mole%, Xini-based SMPs showed lower rubbery moduli than

traditionally crosslinked materials, which showed the characteristic increase in rubbery modulus with increasing crosslinker concentration.

Figure 5d compares Xini-based systems with traditionally crosslinked SMPs using DMPA and 44DMB as photoinitiators and BPAEDA 468 as the crosslinker, such that all samples would have equivalent rubbery moduli of 1 MPa as determined by the DMA. This comparison was made not yet to maximize strains but rather to compare the strain-to-failure performance of Xini-based systems to more traditionally crosslinked systems at equivalent rubbery modulus. Figure 5d shows the strain-to-failure (n=3) of each of these three systems at the onset of T_g, at T_g, and above T_g in the rubbery regime. At all three temperature comparisons, Xini-based systems show the smallest strain-to-failure values. The three differently initiated samples, when tested at T_g, showed strain-to-failure values of 471% (Xini), 495% (44DMB) and 624% (DMPA).

Since difunctional (meth)acrylate-crosslinked samples outperformed Xini-based systems, the information gleaned from Figures 3a, 3b, 3c and 3d were combined to create a series of high strain materials with increasing crosslinker concentrations consisting of a 19:1 wt% MA-co-IBoA base polymer with BPAEDMA 1700 as crosslinker and 0.05wt% DMPA. Maximum strains for each different crosslinker concentration are shown in **Figure 6a**. Although strains-to-failure exceeded 900% for the most lightly crosslinked samples, the two most lightly crosslinked samples did not show full strain recovery after a single shape-memory cycle. Thus for fully recoverable high-strain SMPs, the sample with 0.05 mole% BPAEDMA 1700 and 0.02 mole% DMPA was the optimized *fully recoverable* high-strain SMP denoted HSP I-28. **Figure 6b** presents data from four representative samples, ranging between 0.01 mole% and 0.11 mole% BPAEDMA 1700, characterized in Figure 6a and demonstrates how the normalized maximum stresses at 400% strain for each of the samples drop off as a function of the number of applied shape memory cycles. The materials with higher crosslinking density demonstrate more stable behavior with cycling. **Figure 6c** shows one shape-memory cycle to 200% for HSP I-28. Shape

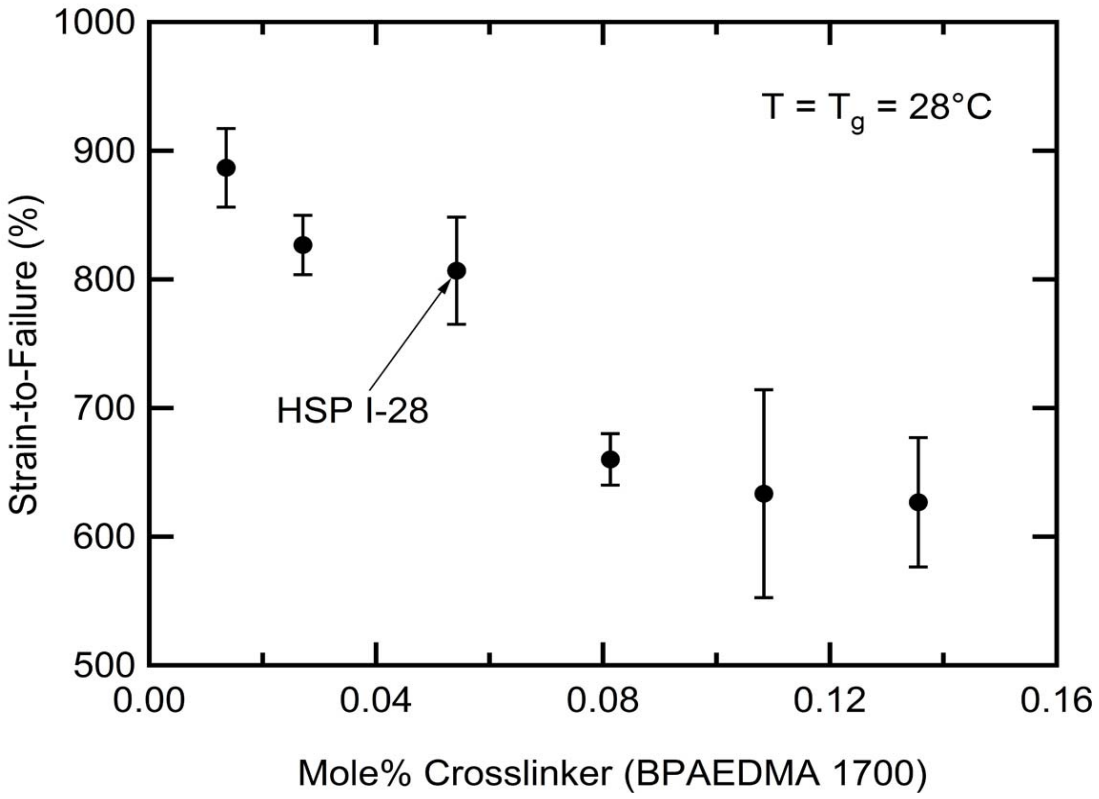

Figure 6a. Maximum strains as a function of crosslinker density at T_g in 19:1 wt% MA-co-IBoA based polymers at constant 0.02 mole% DMPA. HSP I-28 was the most lightly crosslinked sample that showed complete strain recovery under a shape-memory cycle.

fixity is near 100% while residual strain is initially less than 3% of the applied strain during the test at 100 °C at a ramp rate of 5 °C per minute. The residual strain disappears when the sample is removed from the testing fixture, stored above T_g for 30 additional minutes and measured again at room temperature. Once the high strain material optimization was complete, data was collected to construct a head-to-head comparison of high strain polymers with identical optimized amounts of DMPA and crosslinker but with different linear builders to adjust the T_g between 28 ˚C and 55 ˚C (**Figure 7**). The high strain polymer (HSP) in **Table 1** and Figure 7 with the largest strain-to-failure had a T_g at 28 ˚C and recovered strains of 800%. All synthesized HSPs and Xini-based materials in Table 1 and Figure 7 showed full shape recovery (no residual strain) after a single shape memory cycle when strained to one standard deviation below failure. In the three of five

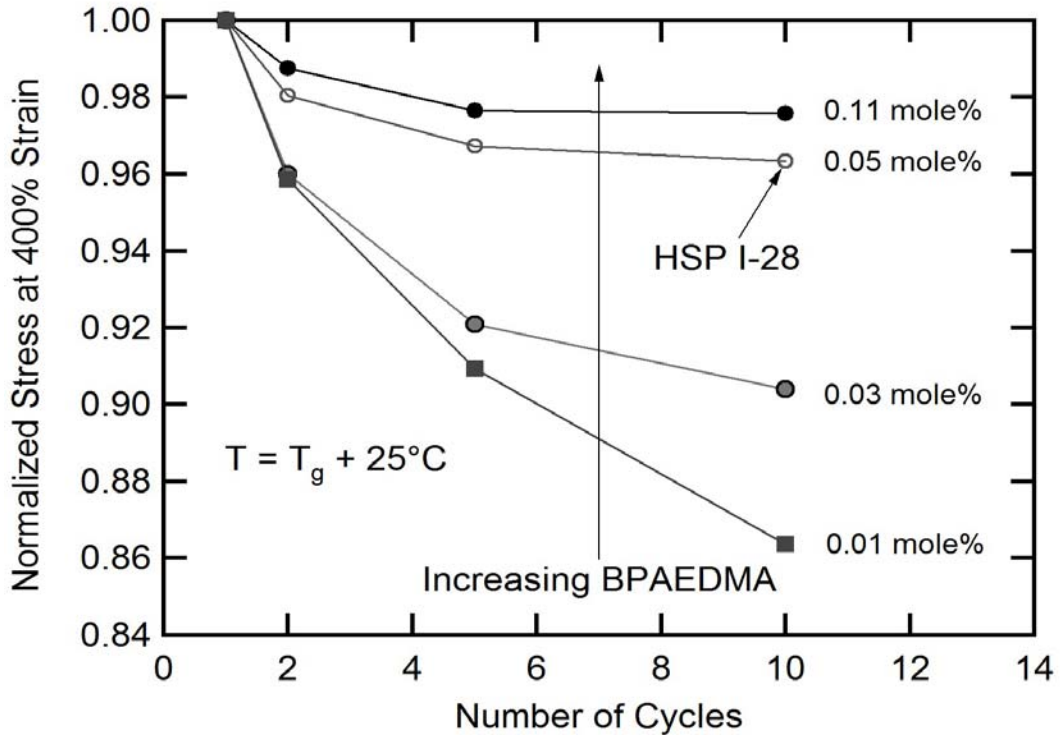

Figure 6b. Constrained strain recovery tests monitor stress relaxation over multiple cycles to 400% strain in several samples from Figure 6a.

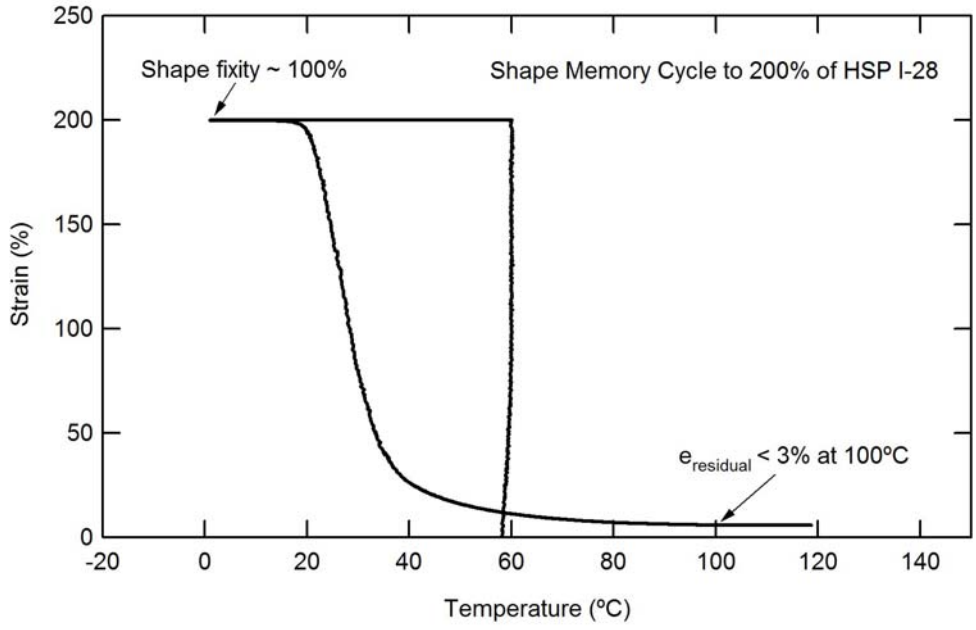

Figure 6c. Free strain recovery tests monitor shape fixity and residual strain in a shape-memory cycle to 200% strain in HSP I-28. HSP I-28 fully recovers over a longer time period, 30 additional minutes above T_g, past the test time frame.

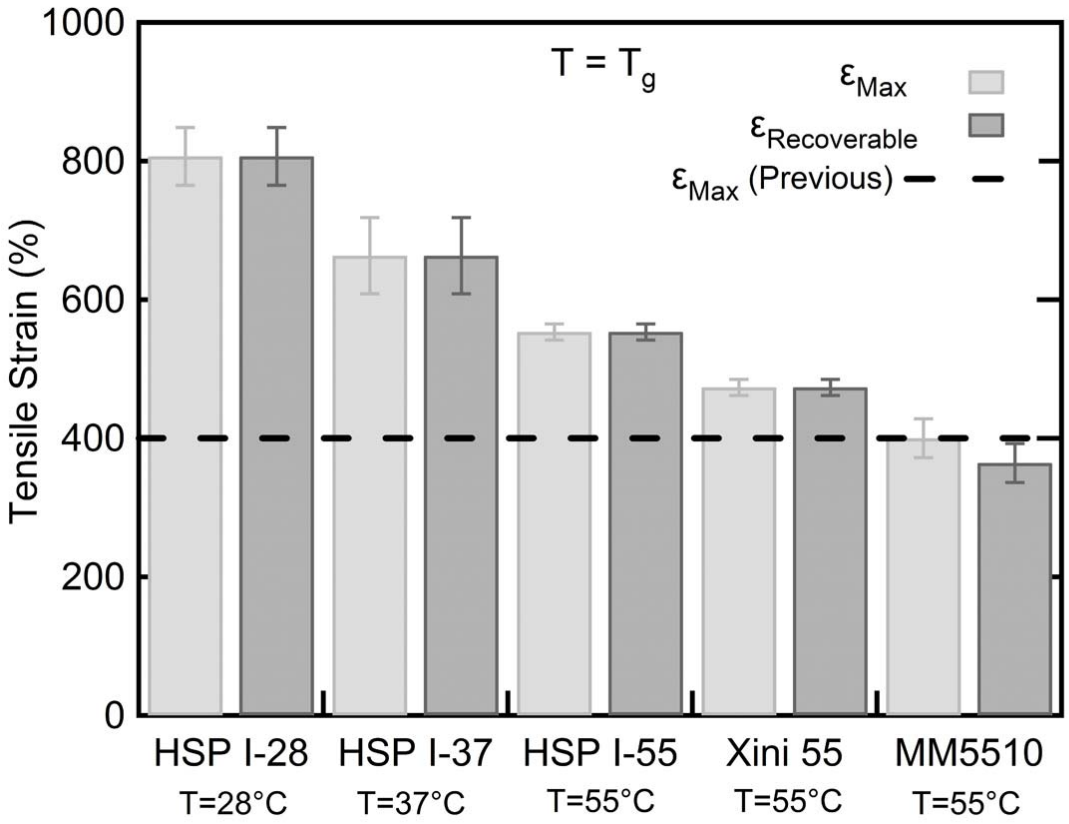

Figure 7. Head-to-head comparisons of the strain-to-failure of optimized high strain samples at 28 ˚C, 37 ˚C and 55 ˚C. Samples are compared with the industry standard Mitsubishi MM 5510 thermoplastic SMP. Not only do the HSP and Xini samples show larger strains when tested at T_g, but these strains are fully recoverable whereas MM5510 shows considerable deformation (36% on average) under a shape-memory cycle.

samples that strained without failure to 400%, the Mitsubishi thermoplastic showed an average (n=3) of 36% residual strain undergoing one shape-memory cycle. All materials were strained at their respective T_g. Ultimately, the HSP I-28 which contains 0.02 mole% DMPA and 0.05 mole% BPAEDMA 1700, and linear monomers MA and IBoA in a 19:1 wt% ratio, showed fully recoverable strains of 807% over one shape memory cycle. With differing ratios of linear monomers MA and IBoA, HSP I-37 and HSP I-55 showed fully recoverable strains of 663% and 553% respectively when strained at T_g. The shape-memory cycle was thus demonstrated with larger strains just below failure for HSP I-28, HSP I-37 and HSP I-55. HSP-I28 strained to an

Table 1. The shape-memory cycles of high strain thermosets

SMP	T_g	e_{Max}	Shape Fixity	$e_{Residual}$
HSP I-28	28	807% ± 42%	>99%	0%
HSP I-37	37	663% ± 55%	>99%	0%
HSP I-55	55	553% ± 12%	>99%	0%
Xini 55	55	473% ± 12%	>99%	0%

average of 807%, was 100% fixed and fully recovered. HSP I-37 strained to an average of 663%, was 100% fixed and fully recovered. HSP I-55 strained to an average of 553%, was 100% fixed and fully recovered.

3.4. Discussion

SMPs have been proposed for a wide range of applications from advanced automotive parts to custom biomedical devices. For many commercial applications, high-strength or high toughness coupled with tailorable shape-memory properties is desirable. In addition, there are commercial opportunities for lower strength, very high strain SMPs with fully recoverable strains that do not suffer from non-recoverable deformation during the shape memory cycle. The goal of this study is to maximize *the fully recoverable* strain capacity of shape-memory materials to enable future shape-memory applications.

The detailed kinetics of acrylate chain interactions has received attention in the literature through descriptions of the reaction diffusion mechanism and the development of rate constants for different polymerization environments.[24] This study attempts to minimize changes in polymerization kinetics across sample comparisons while maximizing strains. Two methods are proposed to achieve this, and both methods yield materials with fully recoverable strains of more than 400%. The first method optimizes photoinitiator concentration, crosslinker concentration and

the type of crosslinker. The second method makes use of a new organic molecule containing both initiator and crosslinking functionalities (Xini) to achieve fully recoverable high strains.

3.4.1 Optimization of Initiator and Crosslinker

Figures 3a and 3b present the effect of varying DMPA photoinitiator on the gel fraction of SMP networks. At very low DMPA concentrations, free radicals are scarce and the polymer networks do not fully form, while above 0.50 mole% DMPA the abundance of free radicals limits chain growth through termination and leads to decreases in network formation.[30] Figure 3b presents results showing the observed peak in gel fraction at 0.02 mole% DMPA. Figure 3c defines an order of magnitude range for crosslinker density in which high strain material candidates can be designed and synthesized. However, Figure 3d is a better representation of accurate gel fractions as the underlying linear monomer chemistry is solely acrylate. Methacrylates take longer to polymerize by free radical means and this can result in unreacted monomer that is not incorporated into the network in addition to free oligomer-sized chains. In Figure 3d, beyond 0.01 mole% crosslinker, all samples showed repeatable gel fractions above 90% while above 0.05 mole% crosslinker, all samples showed repeatable gel fractions above 96%. Figure 4 shows the expected trend of increasing rubbery modulus as a function of crosslinker concentration, while T_g is shifted by less by than 3 ˚C between the samples. Note that BPAEDA 468 was used in Figures 4, 5c and 5d while BPAEDMA 1700 was used in Figure 3d, 6a, 6b and 7. The BPAEDA 468 was chosen for Figures 4, 5c and 5d because its M_n of 468 is closer to that of Xini (M_n ~ 350) and it provided a better metric by which to compare traditionally crosslinked samples to Xini-based samples. Ultimately however, the longer BPAEDMA 1700 crosslinker was chosen to synthesize the fully recoverable HSP I-28, HSP I-37 and HSP I-55 network polymers due to its greater chain length between functional ends.

Further efforts could be made to optimize across different photoinitiators, at different wavelengths of UV light, or by using different polymerization techniques, but these optimizations were beyond the scope of this study. However, the data presented suggests that the key factor for achieving fully recoverable strain capacity is ensuring a fully crosslinked network with crosslink spacing that is large and evenly distributed.

3.4.2 Design and Properties of Xini

The reasoning behind the anticipated effectiveness of Xini as a high strain SMP candidate is as follows. Xini, pictured in Figure 2c, cleaves under 365 nm UV light into an acrylate-substituted dimethoxybenzyl radical and an acrylated benzoyl radical. These radicals begin the free radical polymerization process that forms the network polymer. At some later point in time during the polymerization, a growing linear chain opens and incorporates through the acrylate bond on these Xini components. In essence each of the two radicals would form a 1.5 functional crosslinker, meaning they would create a branch in the linear chain and allow future chain growth in multiple directions. Thus the length of crosslinker molecule would not be determinate but rather proportional to the crosslinker spacing along the main chains. Xini was found to deliver large recoverable strains. Gel fractions near 100% for all compositions of Xini, as seen in Figure 5a, show the efficacy of Xini as a crosslinker.

Ultimately the materials crosslinked with Xini did not outperform traditionally crosslinked materials. Although recoverable strains above 400% were recorded, Xini did not demonstrate larger recoverable strains than networks synthesized with traditional crosslinking methods. Several possible explanations exist that may relate to polymerization kinetics, including a looping mechanism whereby the initiated radical chain grows to incorporate the acrylate group covalently attached to the initiator, not crosslinking the material at all but yielding a chain termination in a loop. The proximity of the growing chain to the backside acrylate bond may

foster this morphological structure, but more advanced characterization techniques would be necessary to confirm the extent to which looping occurs. A second explanation centers on the free-radical polymerization parameters. While DMPA, Figure 2a, has an absorption peak near 365 nm, 44DMB's absorption peak is lower. Thus Xini may not cleave and initiate as well as DMPA under the given test conditions. Complete understanding of this phenomenon of Xini polymerization kinetics is beyond the scope of this paper.

Instead the resulting thermomechanical properties are studied in detail. Three averaged DMA curves of increasing concentrations of Xini form each of the plotted lines shown in Figure 5b. It should be noted that optimum properties can be observed in the 0.31 mole% (1.00 wt%) Xini sample which yields the highest rubbery modulus and the largest increase in T_g. Figure 5c served as the basis by which additional samples were synthesized to generate the results in Figure 5d. Figure 5c confirms the trends in maximum strain from Figures 4 and 5b. The 0.31 mole% Xini sample showed the highest rubbery modulus and similarly the lowest strain-to-failure while the 0.46 mole% sample showed a much lower rubbery modulus and therefore a higher strain. While the trends for rubbery modulus values as pulled from DMA curves at T_g + 33 ˚C were expected for the traditionally crosslinked samples (i.e. increasing crosslinker yields higher rubbery modulus), the peak in Xini behavior was unexpected. These tests were repeated three times independently with similar results. This rubbery behavior of Xini between 0.50 MPa and 1.00 MPa, regardless of the concentration may be explained by the competing phenomena that arise when polymerizing with Xini. As the concentration of Xini is increased, not only does the crosslinking density rise—so too does the amount of initiator. Thus in the ranges presented, although higher concentrations of Xini may lead to greater chain branching, they are coupled with increasing chain termination events from the initiating ends of Xini.

3.4.3 High Strain Comparisons

To construct Figure 5d, samples with similar rubbery modulus were chosen based on the DMA curves of Xini, BPAEDA 468 with 44DMB and BPAEDA 468 with DMPA. Attempts were made to use both 44DMB and DMPA controls. However, it can be seen in Figure 5d that with identical linear monomer compositions and XL densities, DMPA–based materials out-strained 44DMB materials at T_g and in the rubbery regime. The material initiated with DMPA demonstrated the highest strain-to-failure when tested at T_g and in the rubbery regime. Materials polymerized with Xini strained less than traditionally crosslinked samples with similar rubbery moduli. As a consequence, a matrix of lightly crosslinked samples with acrylate linear monomers in a 19:1 wt% MA-co-IBoA base polymer and a long crosslinker, BPAEDMA 1700 were synthesized in an attempt to maximize recoverable strains.

At 0.100 wt% or 0.005 mole% BPAEDMA 1700, the samples were thermoplastic in nature, and showed limited recoverability—it was difficult to obtain consistent high strain measurements. These samples are not pictured in Figure 6a and due to the small fraction of crosslinker, precision in sample preparation was increased by one significant figure. The BPAEDMA 1700 samples containing 0.014 mole% and 0.027 mole% crosslinker both strained repeatedly above 800%, but upon navigation through a single shape-memory cycle showed residual strains of 8% and 5% respectively. The sample with 0.054 mole% BPAEDMA 1700 strained to failure at 807% with a standard deviation of 41.63%. This sample is labeled HSP I-28 in Figure 6a. In three separate tensile loadings of this polymer composition, different samples strained to 840%, 820% and 760% before failing. Additionally, two samples of this composition that did not fail at 800%, showed 100% recoverable strains of 800% with no permanent deformation or residual strain upon unloading and recovery at T_{high} as pictured in Figure 1.

Figure 6b is a normalized stress plot that shows the results of straining four selected samples from Figure 6a to 400% ten times while measuring the stress relaxation over these

cycles. As the amount of BPAEDMA 1700 increased, the stress relaxations dropped off to less than 2% over ten cycles. This provides some measure of the permanent damage in the material during cyclic loading although it does not provide an accurate metric by which to predict residual strain over multiple cycles. The sample that showed full recovery over one cycle, HSP I-28, began to plateau above 96% normalized stress after 10 cycles. Figure 6c is presented to demonstrate the strain-temperature response in HSP I-28 that undergoes one shape-memory cycle. Data is collected on the DMA as materials strain to 200% and are cooled, fixed and reheated. Shape-memory cycles were conducted on each material in Table 1 and Figure 7 to their fully recoverable strain limits using a universal testing machine. Strain-temperature could not be continuously collected with this method. Testing limitations (stroke length limit on the DMA) precluded collecting strain-temperature data at high strains on the DMA. Thus data points from various stages in the high-strain shape memory cycle are collected from video monitoring of deformation induced by the universal testing machine and presented in Table 1 and Figure 7, while a full strain-temperature shape memory cycle to 200% strain is presented in Figure 6c.

HSP I-28 was designed with a T_g of 28 ˚C. In the final comparison, additional samples were synthesized by altering the ratio of MA to IBoA in the underlying polymer while maintaining crosslinker and photoinitiator concentrations. This variation was performed to impart shape fixity properties at room temperature by raising the T_g. Maximum strains-to-failure dropped off as T_g increased. An explanation for this decrease could be the bulky nature of the IBoA side group and the increased steric hindrance that drives the T_g upward. Chains may have a difficult time fully disentangling themselves from one another as the spatial volume of the side groups increases. Nonetheless, strain-to-failure metrics are consistently above 400% for all samples in Figure 7. Mitsubishi's MM 5510 was also strained at its T_g using the same method resulting in strains of 400% but yielding large-scale sample deformation after one shape-memory cycle. Published elongation values for this material are >600%, which are likely achieved closer

to melt temperature for the thermoplastic and may result in considerable non-recoverable strain.[23] Averaging three tensile loadings at 55 ˚C, deformation for the MM5510 was 36% (residual strain in the gage section) while all other samples showed no measurable residual strain.

3.5. Conclusions

Tailored shape-memory polymer networks can be photopolymerized from methyl acrylate and isobornyl acrylate (or methyl methacrylate) with an optimized amount of crosslinker such as bisphenol A ethoxylate di(meth)acrylate. Linear monomers can be combined in the appropriate ratios to tailor the base glass transition temperature, and photoinitiator and crosslinker are minimized while still ensuring a fully crosslinked network with fully recoverable strains. Recoverable strains of above 800%, twice the previously published value, can be obtained for materials with a T_g of 28 ˚C, while fully recoverable strains above 550% can be achieved for materials with a T_g of 55 ˚C. Although Xini-based systems do not stretch as far as traditionally crosslinked, optimized systems, Xini may be used as both a crosslinker and initiator combined into a single molecule.

3.7 References

[1] R. Langer, D. A. Tirrell, *Nature* **2004**, *428*, 487.

[2] K. Gall, C. M. Yakacki, Y. Liu, R. Shandas, N. Willett, K. S. Anseth, *J. Biomed. Mat. Res. A* **2005**, *73A*, 339.

[3] C. M. Yakacki, R. Shandas, C. Lanning, B. Rech, A. Eckstein, K. Gall, *Biomaterials* **2007**, *28*, 2255.

[4] K. E. Smith, J. S. Temenoff, K. Gall, *J. Appl. Polym. Sci.* **2009**, *In Press.* .

[5] C. M. Yakacki, R. Shandas, D. Safranski, A. M. Ortega, K. Sassaman, K. Gall, *Adv. Funct. Mater.* **2008**, *18*, 1.

[6] Y. Tanaka, J. Gong, Y. Osada, *Prog. Polym. Sci.* **2005**, *30*, 1.

[7] Myung D, Koh WU, Ko JM, Hu Y, Carrasco M, Noolandi J, Ta CN, F. CW, *Polymer* **2007**, *48*, 5376.

[8] A. Lendlein, R. Langer, *Science* **2002**, *296*, 1673.

[9] P. R. Buckley, G. H. McKinley, T. S. Wilson, W. Small, W. J. Benett, J. P. Bearinger, M. W. McElfresh, D. J. Maitland, *Biomed. Eng., IEEE Transactions on* **2006**, *53*, 2075.

[10] T. S. Wilson, W. S. IV, W. J. Benett, J. P. Bearinger, D. J. Maitland, "Shape memory polymer therapeutic devices for stroke", **2005**.

[11] M. Cabanlit, D. Maitland, T. Wilson, S. Simon, T. Wun, M. E. Gershwin, J. V. d. Water, *Macromol. Biosci.* **2007**, *7*, 48.

[12] I. A. Rousseau, P. T. Mather, *J. Am. Chem. Soc.* **2003**, *125*, 15300.

[13] K. Gall, P. Kreiner, D. Turner, M. Hulse, J. *Microelectromechanical Sys.* **2004**, *13*, 472.

[14] H. Tobushi, S. Hayashi, K. Hoshio, Y. Makino, N. Miwa, *J. Intell. Mater. Sys. Struct.* **2006**, *17*, 1075.

[15] F. E. Feninat, G. Laroche, M. Fiset, and D. Mantovani, *Adv. Eng. Mater.* **2002**, *4*, 91.

[16] P. T. Mather, *Nat. Mater.* **2007**, *6*, 93.

[17] B. Sillion, *Actualite Chimique* **2002**, 182.

[18] C. Liu, Qin,H., and P. T. Mather, *J. Mater. Chem.* **2007**, *17*, 1543.

[19] A. Lendlein, S. Kelch, *Angew. Chem., Int. Ed.* **2002**, *41*, 2034.

[20] R. N. Haward, G. Thackray, Proc. Royal Soc. London. Series A, Math. Phys. Sci. **1968**, 302, 453.

[21] H. M. Jeong, S. Y. Lee, B. K. Kim, *J. Mater. Sci.* **2000**, *35*, 1579.

[22] G. Baer, T. Wilson, D. Matthews, D. Maitland, *J. Appl. Polym. Sci.* **2007**, *103*, 3882.

[23] H. Tobushi, H. Hara, E. Yamada, S. Hayashi, *Smart Mater. Struct.* **1996**, *5*, 483.

[24] K. S. Anseth, C. M. Wang, C. N. Bowman, *Macromolecules* **1994**, *27*, 650.

[25] D. L. Safranski, K. Gall, *Polymer* **2008**, *49*, 4446.

[26] A. M. Ortega, S. Kasprzak, C. M. Yakacki, J. Diani, A. R. Greenberg, K. Gall, *J. Appl. Polym. Sci.* **2008**.

[27] K. Gall, C. M. Yakacki, S. Willis, C. Luders, *J. Biomed. Mater. Res.* **2007**.

[28] Y. Grohens, M. Brogly, C. Labbe, M. O. David, J. Schultz, *Langmuir* **1998**, *14*, 2929.

[29] E. Penzel, J. Rieger, H. A. Schneider, *Polymer* **1997**, *38*, 325.

[30] H. Fischer, R. Baer, R. Hany, I. Verhoolen, M. Walbiner, *J. Chem. Soc., Perkin Trans. 2,* **1990**, 787

[31] C. Giansante, P. Ceroni, V. Balzani, M. Maestri, S.-K. Leeb, F. Voegtle, *New J. Chem.* **2007**, *31*, 1250.

CHAPTER 4

MNEMOSYNATION

4.1. Problem

Shape-memory polymers (SMPs) are active smart materials with tunable stiffness changes at specific, tailored temperatures and exhibit viscoelastic properties at or above room temperature. Thermoplastic SMPs lose “memory” properties near melt temperatures and possess large residual strains, while network (thermoset) SMPs are chemically crosslinked and do not show large residual strains. The use of thermoset SMPs has been limited in mass-manufacture and commodity applications because a variety of common low-cost plastics processing techniques are not possible with network polymers. In this study of thermoset SMPs, beyond adjusting the glass transition temperature (Tg) between 10 and 70 °C and tuning the recoverable force between 0.5 and 13 MPa, a novel manufacturing process, Mnemosynation, is described. The customizable mechanical properties of traditional SMPs are coupled with traditional plastic processing techniques to enable a new generation of mass producible plastic products with thermosetting shape-memory properties: low residual strains, tunable recoverable force and adjustable Tg. Specifically, this study assesses a model poly(methyl acrylate-co-isobornyl acrylate) (MA-co-IBoA) polymer system blended separately with both triallyl isocyanurate (TAIC®) and trimethylolpropane triacrylate (TMPTA) in varying concentrations. These blended systems are subsequently exposed to electron beam (e-beam) radiation at doses ranging from 5 to 300 kilogray (kGy) and mechanically evaluated. Gel fraction, Tg, rubbery modulus, toughness, and stress-strain responses of TAIC® or TMPTA blended into MA-co-IBoA systems are determined. MA-co-IBoA systems blended with at least 3 wt% TMPTA and exposed to e-beam radiation display high gel fractions (above 90%) across all doses above 10 kGy while 3 wt% blended TAIC® systems require at least 100 kGy to be 85% crosslinked. The results of this study

are intended to enable future advanced applications where mass manufacturing, the ability to accurately and independently position T_g and the ability to tune recoverable force in SMPs are required.

4.2. Background

Nearly 2,000 years ago in his *Discourses*, Epictetus said that materials themselves affect us little; it is the way we use them which influences our lives*[1]*. Thermoset shape memory polymers (SMPs) are self-adjusting smart materials with variable activations*[2]* and low residual strains*[3]* but their *use* and thus *influence* in mass-market applications has been limited due to manufacturing and scale-up difficulties. Covalent crosslinks preclude thermosets from being melted and reshaped after initial polymerization. Techniques such as injection molding*[4, 5]*, blow molding*[6]* and vacuum-assisted resin transfer molding*[7]* were developed to enable cheap mass production of thermoplastic polymers, but cannot reshape network polymers. Today, injection molding is widely used for manufacturing a variety of parts, from small custom plastic components to entire car body panels*[8]*. Reaction injection molding was developed to cure thermoset polymers into complex shapes but necessitates curing polymers directly into a mold*[9]*. This technique puts constraints on design, limits polymer composition and initiation choices, and suffers from shrinkage problems limiting precision control of final mechanical properties as specific additives are incorporated to manage this shrinkage*[10, 11]*.

Vulcanization, named after the Roman god of Fire, utilizes sulfur and heat to crosslink natural rubber (polyisoprene)*[12]* and has enabled mass manufacture of natural rubber with enhanced network properties. This process overcomes limitations by molding thermoplastic polyisoprene and subsequently crosslinking it with sulfur. Other methods to subsequently crosslink thermoplastics after polymerization and remolding also exist. Targeted irradiation of thermoplastic precursors such as polyethylene can lead to grafting and the creation of a network

polymer which resembles chemical crosslinking*[13]*. Controlled irradiation of myriad polymer systems has provided cost effective methods to bestow enhanced properties upon polymers for industrial applications*[14, 15]*. Much progress in this area has been driven by needs in the oil and automotive industries for tougher, more durable or heat resistant plastics. One such method that has gained widespread acceptance is electron beam (e-beam) irradiation*[14, 16-21]*. That process today is very clean, operates at ambient temperatures, permits greater processing speed and requires less energy than methods in which crosslinking occurs during polymerization*[21]*.

Numerous studies have been undertaken to enhance the effectiveness and minimize the dose required for crosslinking. To minimize the amount of chain scission versus crosslinking as determined by the modified Charlesby-Pinner equation*[22]*, various polyfunctional monomers can be blended into the thermoplastic networks to enhance crosslinking. Polymer irradiation has been successfully used to impart shape-memory on natural rubber*[16, 23]*, polyethylene *[24]* and poly(ε-caprolactone) *[25, 26]*. The crosslinking effects of ionizing radiation on synthetic polymers is defined by the classical Charlesby-Pinner equation shown in Equation 1 *[27]*.

$$s + s^{1/2} = \frac{p_0}{q_0} + \frac{1}{q_0 \mu_1 d} \qquad (1)$$

In the classical Charlesby-Pinner equation, *s* is sol fraction, p_0 is degradation density, q_0 is crosslinking density, μ_1 is initial weight, average degree of polymerization and *d* is radiation dose. A linear data set is generated when $s+s^{1/2}$ is plotted vs. *1/d*. A linear fit yields intercepts at *1/d* equals zero and $s+s^{1/2}$ equals two. The *1/d* equals zero intercept represents the ratio of scission to crosslinking (p_o/q_o). The $s+s^{1/2}$ equals two intercept represents the minimum dose of gelation (d_o).

The use of multifunctional monomers, such as trimethylol propane triacrylate (TMPTA) to crosslink acrylic polymer chains can be achieved at reduced dose levels and yield optimum

properties without deterioration of the base polymer*[28]*. Thus far, the effect of e-beam radiation has been investigated on synthetic acrylic elastomers*[16]* and acrylic rubbers*[21]* but no systematic modification and curing of an acrylate system demonstrating *useful* and tunable shape-memory properties has been investigated. In particular, the authors are not aware of any published work that has demonstrated a controllable shape-memory effect in radiation crosslinked acrylic polymers by simultaneously optimizing recoverable force, glass transition temperature and polymer toughness.

The shape-memory effect is observed in both thermoplastic and thermosetting polymers with various chemistries. The fundamental distinction is that the memory in thermoplastics can be erased over multiple cycles, especially over large applied strains. One class of thermoplastic shape memory polymers relies on block co-polymers with alternating hard (crystallized) and soft (amorphous) segments*[29, 30]*. The hard segments act as net points while the soft segments can unwind, uncoil and provide strain capacity. However, even at ambient temperatures, physical crosslinks can often break down with applied strain, hold time, or exposure to humidity, rendering the material incapable of remembering its fixed shape resulting in an effective loss of memory. Thermosets have seen a rise in importance through their benefit to custom biomedical devices*[31]*. Several recent studies have proposed novel devices fabricated from SMPs*[32-36]*, which have been shown to potentially impact minimally invasive surgery and implants. Compared to other shape-memory materials such as nickel titanium shape-memory alloys, which recover strains on the order of 10 percent, SMPs can recover strains on the order of 50 to 800 percent, enabling them to experience relatively large on-demand shape changes in severely restricted environments*[33, 37, 38]*.

Figure 1 schematically demonstrates the shape memory cycle in a polymer. A polymeric device is first synthesized into a permanent shape by standard polymer processing techniques (previously, custom machining was used to sculpt complex geometries). Subsequently, the

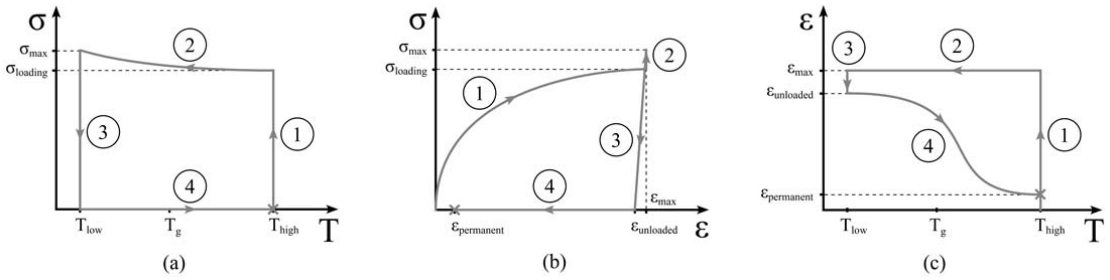

Figure 1. Demonstration of the shape-memory cycle in a) stress-temperature, b) stress-strain and c) strain-temperature regimes. Step 1 is isothermal loading. Step 2 is cooling at constant load. Step 3 is isothermal unloading. Step 4 is shape recovery upon heating.

polymer is heated above a critical temperature, such as the glass transition temperature (T_g), and thermo-mechanically deformed into a temporary shape, a process known as shape storage (Figure 1). The polymer remains in the stored shape until it is heated in the vicinity of its T_g, upon which it will experience controlled shape recovery. Control of T_g enables the underlying polymer to be targeted for a specific application where shape change can be programmed at a specific temperature. Control of rubbery modulus, through varying crosslinker density, enables the underlying copolymer to be targeted for a specific application where specific recoverable force is necessary. Conversely, if recoverable strain if more important than recoverable force, the copolymer can be similarly optimized to demonstrate a large difference between the maximum achievable strain, e_{max}, during deformation and permanent plastic strain after recovery, e_p*[39]*.

Although materials may possess a useful shape-memory effect, they may not be important in engineering applications due to manufacturing limitations. The goal of this work is to demonstrate a *cost-effective* manufacturing technique to enable shape-memory polymers with *useful* properties for a wide variety of applications. In this work, we propose such a manufacturing technique, *Mnemosynation*, and examine the resultant shape-memory polymers and their relevant thermomechanical properties.

4.3. Results

Mnemosynation is a five-step polymer manufacturing process developed to enable mass production of acrylic thermoset SMP devices, which would otherwise be cost-prohibitive using traditional thermoset polymerization techniques. Named for the Greek goddess of memory, Mnemosyne*[40]*, this manufacturing process is the controlled imparting of memory on an amorphous thermoplastic material utilizing radiation-induced covalent crosslinking, much like *Vulcanization* of rubber is the controlled imparting of recoverable elastomeric behavior on a rubber using sulfur crosslinks. *Mnemosynation* combines advances in radiation grafting and advances in simultaneously tuning the mechanical properties of acrylic SMPs to enable traditional plastics processing (blow molding, injection molding, etc.) and allows thermoset shape memory properties in complex geometries. An overview of the five necessary steps of M*nemosynation* in acrylate systems are as follows:

1. Combine selected linear acrylic monomers and photo-initiator in optimum ratios to tailor T_g, and M_w (thus melt viscosity) of the thermoplastic precursor
2. Cure with ultraviolet (UV) light based on the photoinitiator used (e.g. long wave UV at 365nm for 2,2 dimethoxy-2-phenylacetophenone) for a specified time and intensity (both polymer system dependent)
3. Melt the thermoplastic precursor and blend in an optimized amount of crosslinking agent (e.g. TMPTA) at an optimized temperature (polymer system dependent)
4. Injection mold (or otherwise shape) a device in a custom mold using the polymer system resulting from *Step 3*
5. Cure molded part with e-beam radiation at a specified dose (polymer system dependent) to covalently crosslink and obtain desired thermo-mechanical properties

The novelty in this process lies in the ability to finely tune the thermo-mechanical properties through modifications at each step in the process. The process enables mass manufacture of thermoset acrylates and allows independent control of T_g and the rubbery modulus, E_R. The correct ratio and type of linear monomers must be combined with the proper ratio of photo-initiator to tailor the thermoplastic precursor. The correct ratio of crosslinking agent blend must be mixed in at the correct temperature to facilitate homogeneity in the mixing process and ensure proper dispersion of the agent throughout the polymer. The blended system must be exposed to the proper dose of high-energy radiation to target specific crosslink densities and ensure control of the end thermo-mechanical properties. Preliminary results presented in this work describe the optimizations made within the *Mnemosynation* process to enable materials with tuned thermomechanical and shape-memory properties.

4.3.1 Altering Dose

Thermoplastic PMA polymerized with 0.10 wt% of the photoinitiator 2,2-dimethoxy-2-phenylacetophenone (DMPA) was pelletized and blended with 0.00, 1.00, 3.00, and 5.00 wt% of radiation sensitizers TAIC and TMPTA. Samples were pressed or molded into flat sheets and subsequently exposed to increasing doses of e-beam radiation of 5, 10, 25, 33, 66, 100, 200 and 300 kGys. After radiation crosslinking, samples were soaked for one week in acetone. **Figures 2a** and **2b** show the effects of network formation (gel fraction) as a function of radiation dose across the four composition ranges of each radiation sensitizer. Unblended PMA (0% TAIC or TMPTA) does not begin to crosslink until exposed to at least 25 kGy. Samples with increasing TAIC show a gradual increase in crosslinking which mimics the shape of the pure PMA curve while samples radiation-sensitized with TMPTA at 3.00 and 5.00 wt% begin to crosslink below 5 kGy. Charlesby-Pinner analyses confirm these trends. **Figures 3a** and **3b** show a decrease in slope with increasing radiation sensitizer and predict a decrease in the minimum dose for gelation

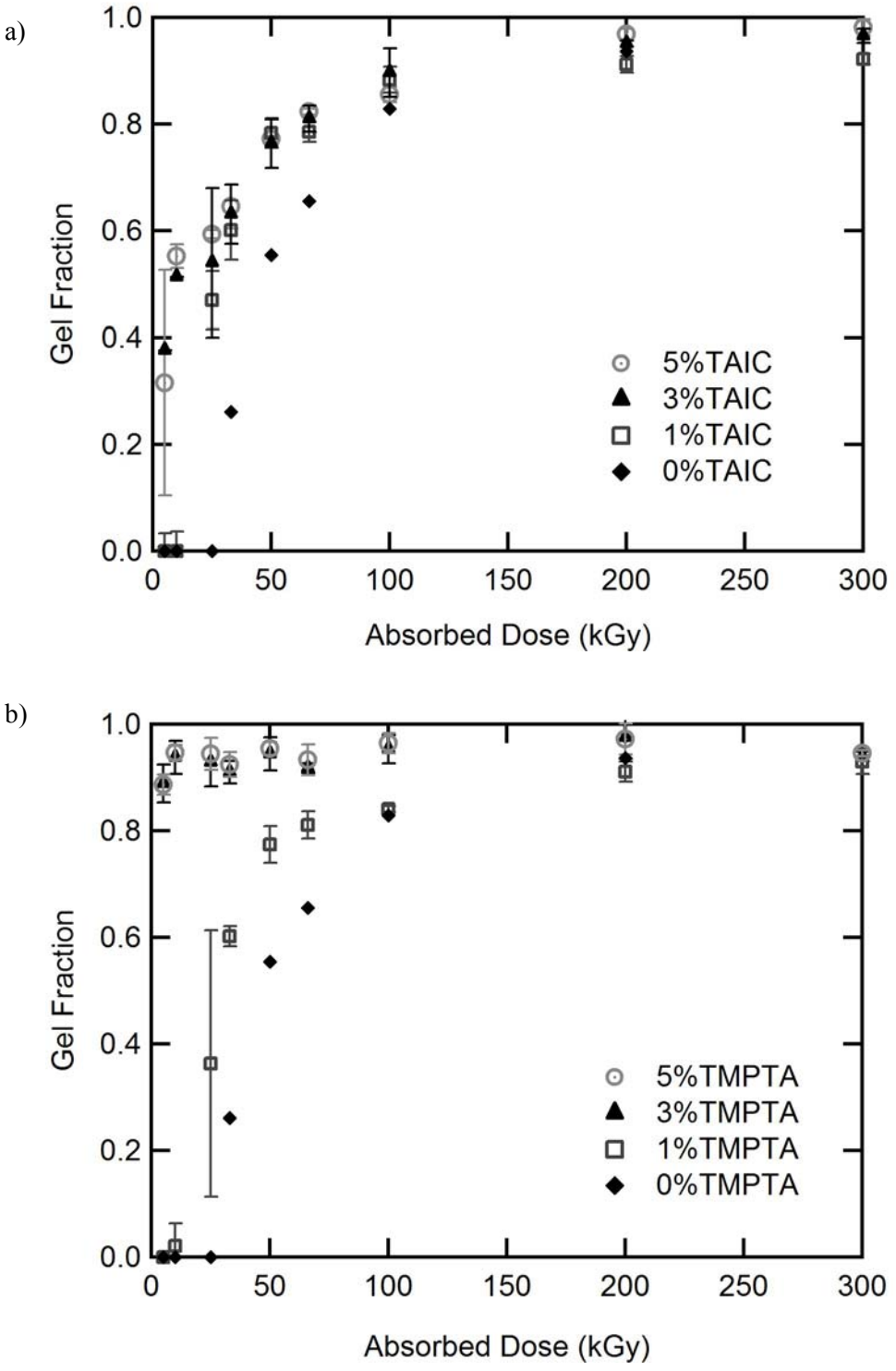

Figure 2. Gel fraction (n=3) as a function of radiation dose for PMA blended with increasing concentrations of a) TAIC® and b) TMPTA.

as shown in **Table 1**. This minimum dose for gelation can be found by extrapolating the linear fit to assess the value of radiation dose (*d)* when the graphed function of sol fraction ($s+s^{1/2}$) is equal to 2. Additionally, Table 1 shows R^2 values for all blended TAIC samples and for the 1.00 wt% TMPTA sample to be above 0.9, but a breakdown in fit to Charlesby-Pinner analyses is observed in the 3.00 and 5.00 wt% TMPTA samples.

The MA-co-IBoA polymer systems blended with TMPTA or TAIC® were characterized by running dynamic mechanical analysis (DMA) on a broad range of compositions varying both the amount of crosslinking agent and the exposure to high energy e-beam radiation. **Figure 4** shows the increase in rubbery modulus of PMA sensitized with 5.00 wt% TMPTA with increasing radiation dose. Only the rubbery regime is displayed to accentuate differences in the range of rubbery moduli between 0.5 and 1.8 MPa. T_g for these samples did not vary by more than 3 °C from 28 °C.

a)

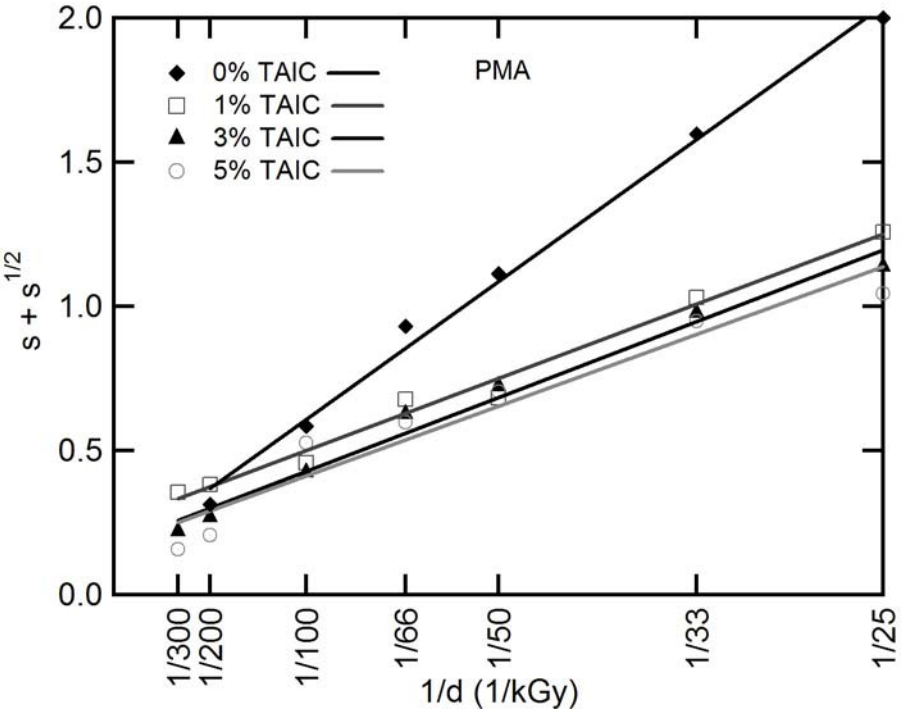

b)

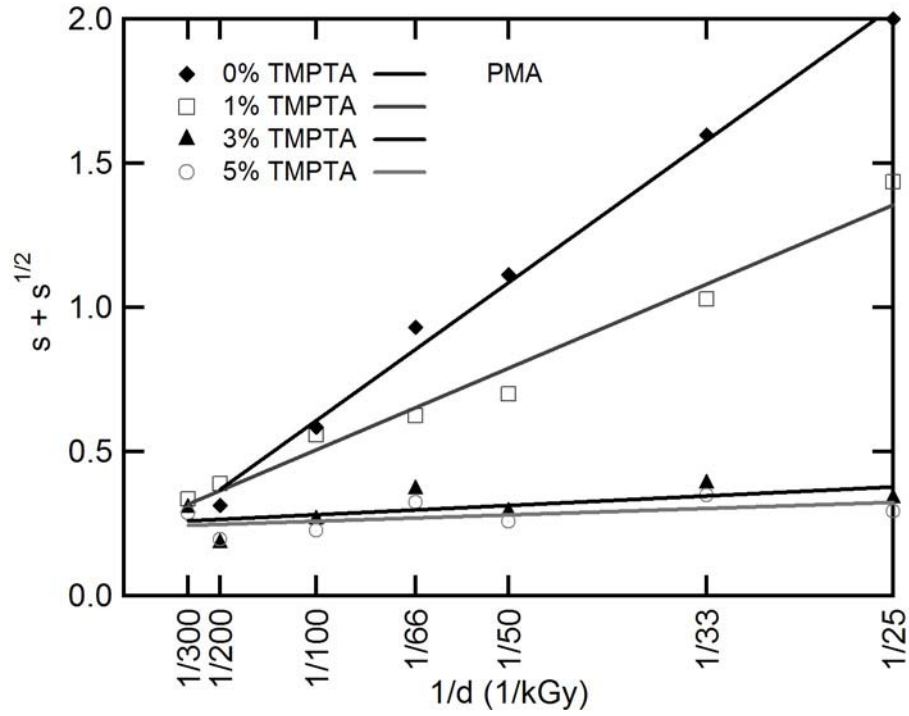

Figure 3. Relationship of $s + s^{1/2}$ and 1/d for PMA blended with a) TAIC® and b) TMPTA and subsequently irradiated.

Table 1. Radiation crosslinking parameters of PMA-crosslinker blends

Crosslinker	p_o/q_o	d_o (kGy)	R^2
0%	.129	25.57	.993
1% TAIC	.248	14.30	.985
3% TAIC	.173	14.00	.982
5% TAIC	.170	13.21	.934
1% TMPTA	.223	15.94	.976
3% TMPTA	.248	1.836	.383
5% TMPTA	.237	1.240	.300

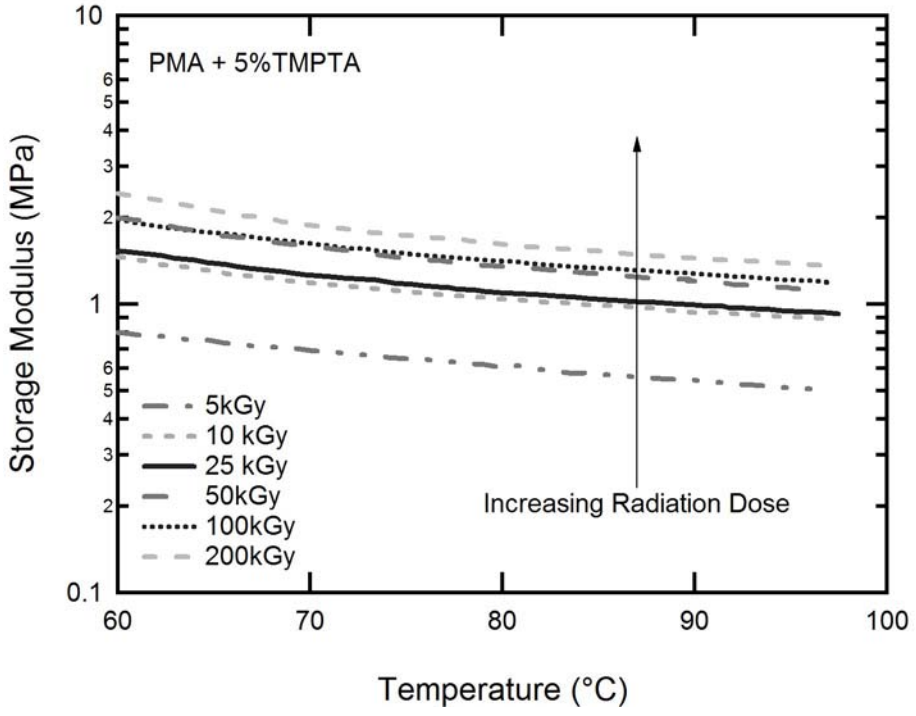

Figure 4. The dynamic mechanical response in the rubbery regime of PMA blended with 5 wt% TMPTA at increasing radiation dosages.

4.3.2 Altering Crosslinker Concentration

Figures 5a and **5b** highlight the differences between materials crosslinked during polymerization and materials crosslinked through irradiation at 50 kGy. At similar concentrations of TMPTA first as a crosslinker during polymerization and then as a radiation sensitizer, the rubbery modulus drops from 3.25 MPa to below 1 MPa for the radiation sensitized samples. This difference is also coupled with a 10 °C increase in T_g for radiation crosslinked samples for the 5.00 wt% TMPTA blends as compared to samples crosslinked during polymerization. Figure 5b additionally includes PMA blended with 9.00 wt% TMPTA to demonstrate the fact that rubbery modulus can additionally be increased with increasing sensitizer concentration.

4.3.3 Manipulating Glass Transition

T_g can be manipulated independently by altering the ratio of linear builders in radiation crosslinked SMP systems. **Table 2** shows the T_g and rubbery modulus (E_R) of PMA copolymers polymerized with 30.0 wt% of other listed monomers and subsequently blended with 9.00 wt% TMPTA and radiation crosslinked at 5, 50 and 300 kGy. Each sample showed the highest T_g at 50 kGy while the peak in E_R varied among samples. Across samples, the T_g is shifted by more than 30 °C without significantly affecting E_R. **Figure 6** assesses the gel fraction of three particular copolymers blended with 9.00 wt% TMPTA. CXEA oligomers blended with 9.00 wt% TMPTA demonstrate a higher gel fraction at all radiation doses than sensitized PMA while copolymers of PMA and 4-*tert*-Butylcyclohexyl acrylate (tBCHA) show significantly less formed network structures. **Figure 7** compares the storage modulus of 94:6 MA:IBoA copolymers and 70:30 MA:IBoA copolymers each sensitized with 9.00 wt% TMPTA and subsequently irradiated at 50 kGy. The T_g is shifted by nearly 20 °C while the rubbery modulus does not move by more than 0.5 MPa.

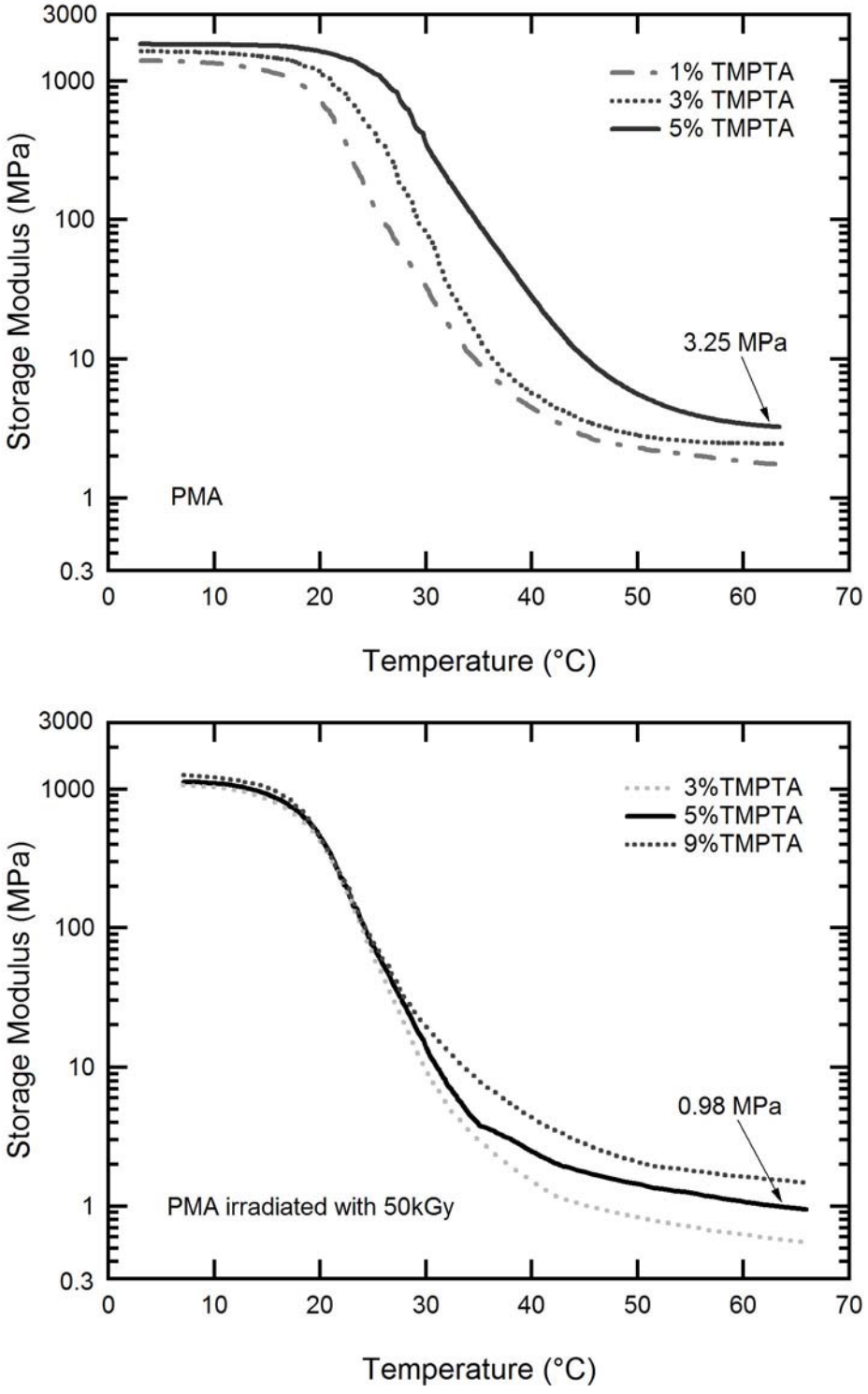

Figure 5. The dynamic mechanical response of PMA with increasing TMPTA a) crosslinked during UV polymerization and b) crosslinked during electron beam radiation at 50 kGy.

Table 2. The thermomechanical effects of irradiation on a 70:30 wt% MA:linear builder copolymer system blended with an additional 9 wt% TMPTA

Linear Builder	T_g (˚C) 5 kGy	T_g (˚C) 50 kGy	T_g (˚C) 300 kGy	E_R (MPa) 5 kGy	E_R (MPa) 50 kGy	E_R (MP 300 kG
IboA	52.2	55.6	52.2	0.79	0.82	1.1
TbCHA	47.0	59.8	51.4	0.46	0.98	0.47
NiPAAM	61.3	69.2	67.2	0.57	0.68	0.97
AMO	61.6	68.6	61.2	1.0	3.2	1.2
CXEA	32.1	34.7	30.1	0.92	2.1	2.1

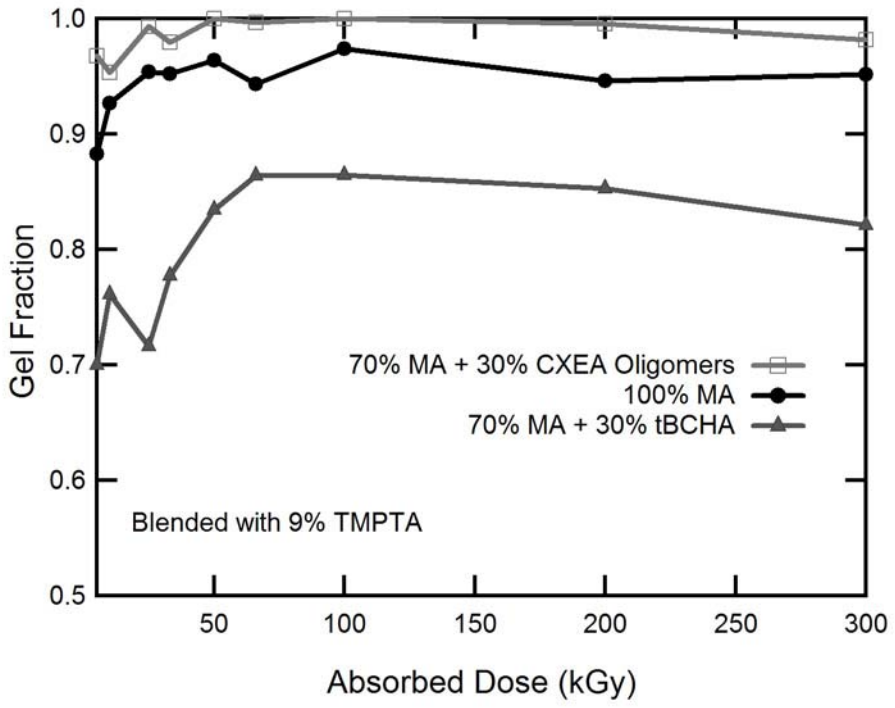

Figure 6. Gel fraction as a function of radiation dose for selected copolymers from Table 2 compared with a control of PMA, each blended with 9 wt% TMPTA.

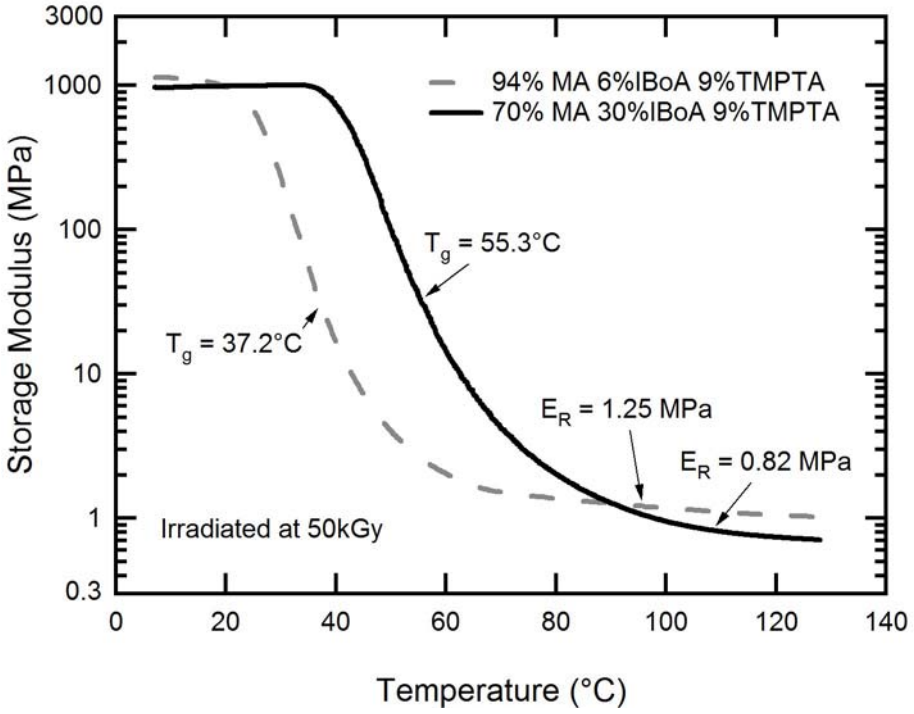

Figure 7. The effect on rubbery modulus and T_g of changing the composition of linear builders from 94:6 to 70:30 wt% MA:IBoA when blended with 9 wt% TMPTA and irradiated at 50 kGy.

4.3.4 Tuning Mechanical Properties

Large scale tunability of rubbery modulus is demonstrated in **Figure 8**. 94:6 MA:IBoA copolymers are blended with increasing concentrations of radiation sensitizer from 6.25 wt% TMPTA and 25.0 wt% TMPTA. A greater than order of magnitude increase in rubbery modulus from 1.09 to 13.13 MPa is observed in samples irradiated at 50 kGy. **Figure 9** shows the difference in thermo-mechanical behavior of the 94:6 MA:IBoA copolymer system sensitized with 25.0 wt% TMPTA and subsequently irradiated at 50 kGy. This copolymer exhibits the highest toughness at the onset of T_g, the highest total strain-to-failure at T_g and the lowest stresses when elongated in the rubbery regime. **Table 3** presents maximum stress and strain data for poly(MA-co-IBoA) sensitized with either 3.00 wt% TMPTA or 25.0 wt% TMPTA. At 3.00 wt%

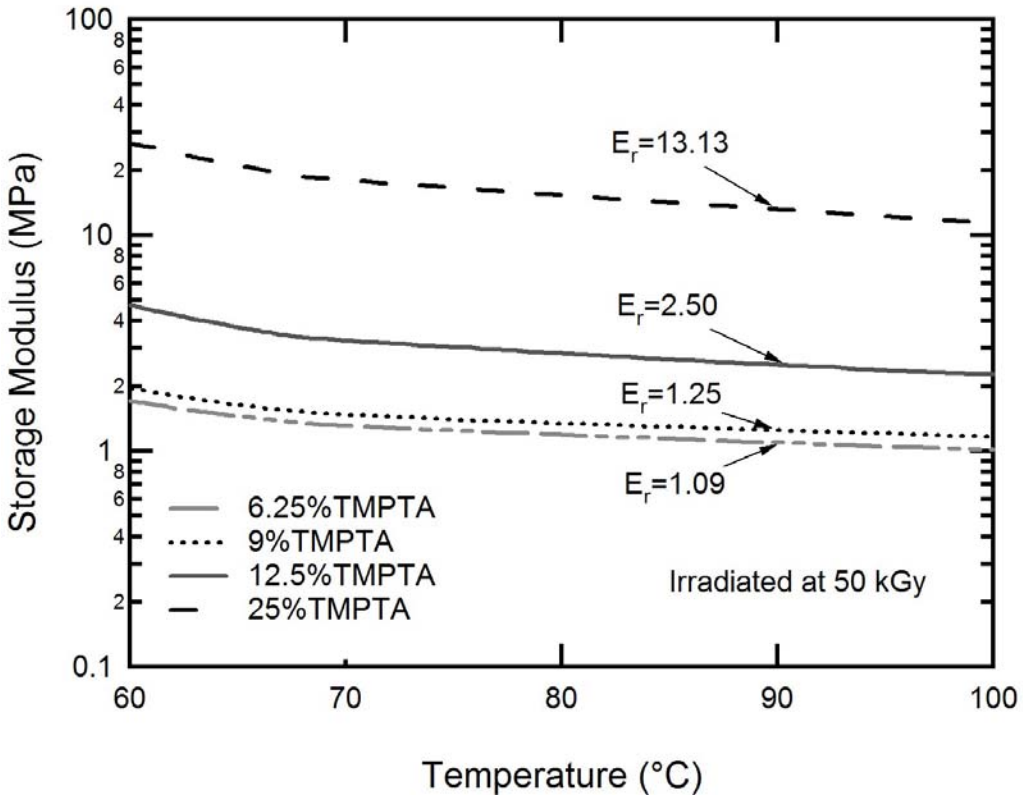

Figure 8. The effect on rubbery modulus of changing the blend concentration of TMPTA in 94:6 MA:IBoA copolymers, irradiated at 50 kGy.

TMPTA maximum strains were measured by crosshead displacement to be above 700% for samples strained in the rubbery regime and above 1000% for samples strained at T_g and at onset. Testing limitations prevented accurate large strain measurements of the deformation of these samples, but the given metrics present comparative order of magnitude bounds on maximum strains. The stresses obtained at the given strains present lower bounds of the maximum stress each material can withstand. This metric is highest at onset of T_g. In comparison, samples blended with 25.0 wt% TMPTA strain an order of magnitude less than the samples sensitized with 3.00 wt% TMPTA but demonstrate stresses roughly four times larger.

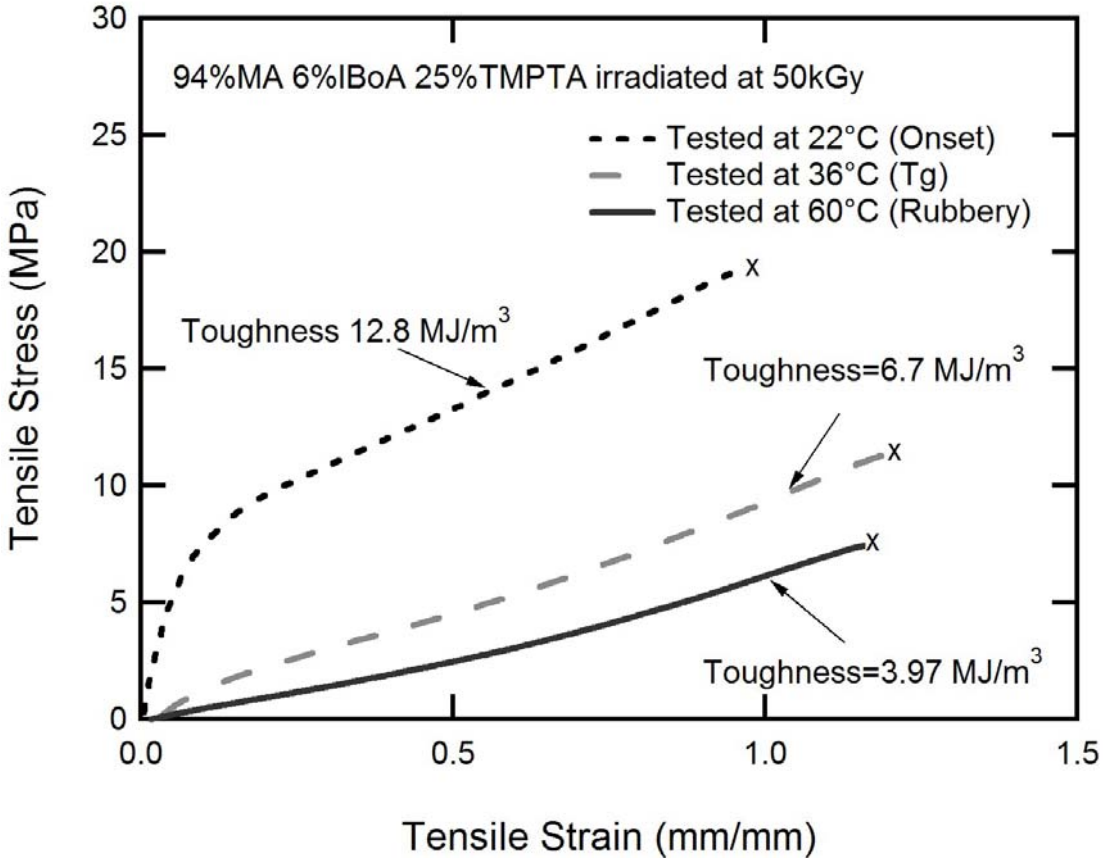

Figure 9. The stress-strain responses and toughnesses of 94:6 MA:IBoA copolymers blended with 25 wt% TMPTA and irradiated at 50 kGy. Test were performed at onset (22 ˚C), T_g (36 ˚C) and in the rubbery regime (60 ˚C).

Table 3. The max strains and stress at max strain of 94:6 MA:IBoA blended with 3 and 25 wt% TMPTA at onset, Tg and in the rubbery regime

	Max. Strains (mm/mm)			**Stress at Max Strain (MPa)**		
Crosslinker	T_g – 12 ˚C	T_g	T_g + 24 ˚C	T_g – 12 ˚C	T_g	T_g + 24 ˚C
3% TMPTA	> 10 *	> 10 *	> 7 *	> 4.8 *	> 2.9 *	> 1.7 *
25% TMPTA	.835 ± .13	1.14 ± .06	1.09 ± .10	19.9 ± 3.5	13.8 ± 3.6	6.67 ± 2.0

* Minimum bounds on strain-to-failure, max stress

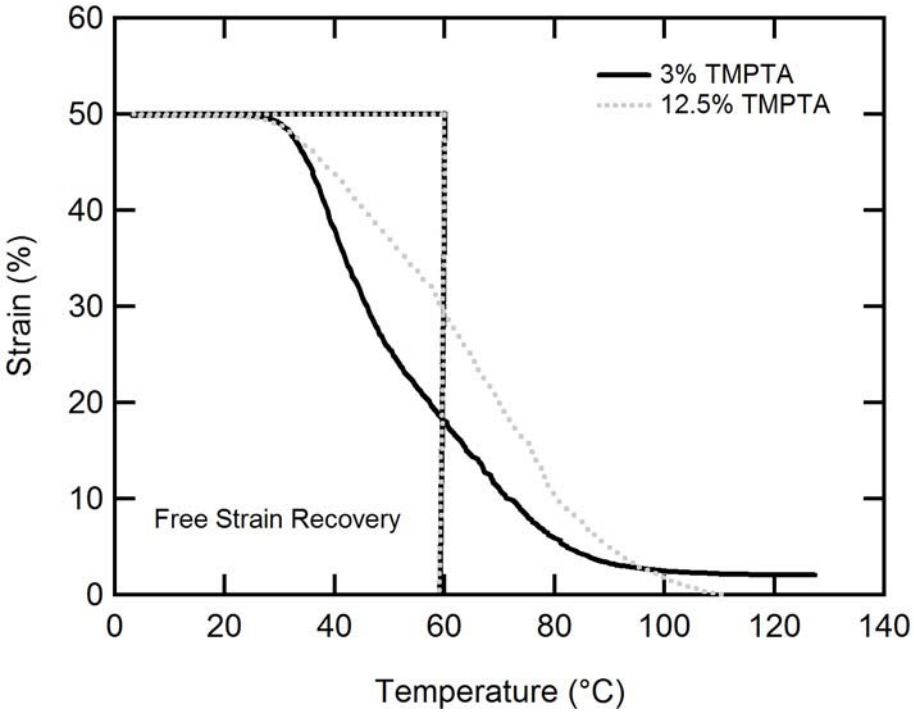

Figure 10. Free strain recovery of 94:6 MA:IBoA blened with 3 and 12.5% TMPTA strained at 60 ˚C to 50%, cooled to 0 ˚C, unloaded and heated to 120 ˚C at 5 ˚C per minute.

Figure 10 demonstrates the shape memory cycle on both MA-IBoA copolymers blended with 3.00 wt% and 12.5 wt% TMPTA. When strained to 50%, the 3.00 wt% TMPTA samples shows residual strains of 3.00% while the 12.5 wt% sample fully recovers.

4.4. Discussion

Mnemosynation enables exploration into shape-memory polymer systems and emergent properties that have not traditionally been studied because the resultant devices would have been cost prohibitive. These new devices can now be manufactured through traditional plastics processing techniques and still possess end thermomechanical properties of thermoset shape-memory polymers. We believe that this manufacturing technique opens the door to a swath of new commercial products that could benefit from tunable thermoset shape-memory properties and are, for the first time, able to be produced in a low cost manner and able target these specific thermomechanical properties: T_g and E_R.

4.4.1 Altering Dose

TAIC and TMPTA have both been proposed as radiation sensitizers, but in the acrylate systems assessed, the performance of TMPTA as a radiation sensitizer was far superior to that of TAIC. The efficacy of each is shown in Figures 2 and 3 and Table 1. The behavior of the TAIC-sensitized systems at doses from 0.00 to 5.00 wt% follows the Charlesby-Pinner model well, which describes random crosslinking. This indicates the relative ineffectiveness of TAIC in promoting additional crosslinking. Deviation from the line of fit of the 5.00 wt% TAIC blend as seen in one minus the R^2 value is .066. This means the TAIC blends when irradiated do not dramatically alter the crosslinking of the underlying polymers. This is further evidenced by a decrease in minimum dose for gelation from 25.57 kGy to only 13.21 kGy.

The TMPTA, however, is very effective a sensitizing radiation crosslinking. R^2 values below .400 indicate that the Charlesby-Pinner equation does not predict the experimental sol-gel values well and that TMPTA is effective in inducing additional crosslinks when irradiated. This trend is also noticeable in 3.00 and 5.00 wt% TMPTA blends in Figure 2b, which show gel fractions above 90% across all doses from 5 kGy onward. As further evidence, the minimum dose

for gelation is below 2 kGy for both the 3.00 wt% and 5.00 wt% TMPTA blends, indicating the relative ease with which crosslinks can be induced even at low radiation doses. Thus TMPTA blended into PMA systems sensitizes crosslinking much more effectively than does TAIC.

Several factors combine to dictate the value of the scission to crosslinking ratio, $p_0/q_{0.}$, which is determined by extrapolating the linear fit of *1/d* vs. $s+s^{1/2}$ onto the y axis, where *1/d* would be equal to zero. The ratio is lowest with no blended sensitizer. As reactive as the sensitizers are, some amount of sensitizer will not incorporate into the network and wash out during the gel analysis, which in turn will appear as if there is less crosslinking relative to scission. Thus increasing the amount of sensitizer in general increases the apparent ratio. This seems counter-intuitive, but although there are more crosslinking events at higher sensitizer concentrations, the ratio does in fact increase to a point. Once enough sensitizer is incorporated, such as at 5.00 wt%, the ratio begins to taper off again, representing that the amount of unincorporated material is heavily outweighed by the increases in crosslinking and the relatively higher number of total events.

The ability to move E_R is primarily shown in Figure 8 through an increase in the concentration of the TMPTA blend. However, Figure 4 presents an alternative way to increase E_R by changing the radiation dose to which the polymer is exposed. Figure 4 demonstrates the ability to move rubbery modulus with altering the dose alone, but the magnitude of this change is dwarfed by the control of E_R seen in Figure 8 by altering the amount of blended sensitizer TMPTA. It is important to note in Figure 4 however, the positive effect that increasing dose has on increasing E_R.

4.4.2 Altering Crosslinker Concentration

Figure 5 compares materials crosslinked during polymerization to materials in which crosslinking was induced by radiation sensitization through the *Mnemosynation* process. Increasing the amount of tri-functional crosslinker in systems crosslinked during polymerization

from 1.00 to 5.00 wt% has a large effect on the E_R, nearly doubling it from 1.72 to 3.25 MPa. In *Mnenmosynated* systems such as those pictured in Figure 5b, the incremental effect of increasing blend composition has a much smaller effect on both T_g and E_R. Increasing the blend concentration from 3.00 wt% TMPTA to 9.00 wt% TMPTA, E_R increases from 0.55 MPa to 1.55 MPa while the T_g remains constant.

4.4.3 Manipulating Glass Transition

The most challenging aspect of this work was to devise a system that showed true independent control of the T_g and E_R. In traditional systems this can be accomplished by copolymerizing various linear monomers with different side groups that dictate the end chain mobility and thus T_g of the polymer on the macro scale. Often this is accomplished by copolymerizing acrylates with methacrylates. The additional methyl group opposite the ester group off the main polymer chain after polymerization, creates a backbone ternary carbon, leading to increased steric hinderance, that impedes molecular motion and thus raises the T_g. So although methacrylates are often used to raise the T_g in SMP systems, their effect in radiation crosslinked systems is undesirable. The ternary carbon is a target for chain scission, which drives the scission to crosslinking ratio over 1 and leads to poor mechanical properties. Thus a fundamental challenge exists to raise the T_g while avoiding chemical structures that typically move T_g upward such as backbone ternary carbons. A search of a variety of copolymer candidates was condensed into five candidates in Table 2: isobornyl acrylate (IBoA), 4-*tert*-Butylcyclohexyl acrylate (TbCHA), n-isopropyl acrylamide (NiPAAm), 4-Acryloylmorpholine (AMO) and 2-carboxyethyl acrylate oligomers (CXEA). Isobornyl acrylate was selected due to the large increase in T_g exhibited by MA-IBoA copolymers .

There is uncertainty concerning the specific targets of radiation crosslinking of acrylates as to which bonds from the thermoplastic polymer chains act as active sites when exposed to radiation. One theory has proposed that hydrogen atoms connected to main chain carbons are

potential sites for crosslinking*[21]*. Another theory predicts that α-hydrogen atoms, bound to the carbon atom which is in turn bound to the ester in the acrylate side chain, are the most likely targets, in turn generating a free radical which becomes a site for crosslinking*[41, 42]*. Data from Figure 6 support the latter hypothesis. tBCHA only contains two α-hydrogen atoms while MA contains three α-hydrogen atoms and the CXEA oligomers contain four α-hydrogen atoms. Increased gel fraction is observed in copolymer systems irradiated at the same dose with additional α-hydrogen atoms. While other variables may be at play, the authors believe that the number of α-hydrogen atoms is directly related to crosslinking efficacy in systems crosslinked by electron beams.

Although IBoA only has two α-hydrogens (compared to more in alternative lower Tg choices), it was chosen as a candidate to copolymerize with MA that would raise the T_g in place of a methacrylate. The bulky nature of the large side group increases steric hindrances and moves the T_g considerably as seen in Table 2. Figure 7 additionally demonstrates the ability to shift T_g using MA-IBoA copolymers. By increasing the concentration of IBoA relative to MA from 6.00 wt% to 30.0 wt%, T_g is moved upward by nearly 20 ˚C without adversely affecting the rubbery modulus by more than 0.5 MPa.

4.4.4 Tuning Mechanical Properties

Figure 8 demonstrates the ability to alter E_R by more than an order of magnitude by increasing the amount of radiation sensitizer blended into the given copolymers. The extent of crosslinking is primarily governed by the amount of sensitizer blended into the copolymer while the T_g is primarily driven by the main chain interactions of the specific concentration of linear copolymers selected. Thus independent control of E_R and T_g has been established, and this allows specific polymer systems to be designed for specific applications with specific thermomechanical needs. *Mnemosynation* yields the added benefit of enabling mass-market scale up of devices

though the ability to perform traditional plastics processing steps on the material to shape it into complex geometries before it is radiation crosslinked at very low costs.

Figure 9 is noteworthy in that it demonstrates predicted shape-memory stress-strain properties of blended copolymers when tested at the onset of T_g, at T_g and in the rubbery regime. As in traditional lightly crosslinked shape memory polymer systems, the strain-to-failure is highest at T_g while the toughness is the greatest at the onset of T_g. Table 3 tabulates the stress-strain response for samples crosslinked with 3.00 wt% TMPTA and 25.0 wt% TMPTA. Maximum strains for the lightly crosslinked samples exceed 700% while stresses at these large strains are relatively low. High strains of SMPs measured by crosshead displacement are not accurate due to slippage in and contribution from the grip sections as the polymer elongates. High strain measurements were taken in similar polymers systems with accurate video measurement of the strains which corresponded to roughly 40% of the strain measured by crosshead displacement alone*[43]*. High strain metrics were tabulated here to demonstrate the large difference in strain between the heavily crosslinked samples and the lightly crosslinked samples rather than to show precise large strain endpoints. In more heavily crosslinked samples such as the 25.0 wt% TMPTA blend, maximum strains are observed near 100% while the maximum stresses are nearly 4 times greater than those in the lightly crosslinked samples. As the blend concentration increases the residual strain after a shape-memory cycle decreases. Figure 10 depicts the shape-memory cycle in a strain-temperature plane. When at least 12.5 wt% TMPTA is blended into the copolymer, no permanent strain is evident after one cycle while in the selected MA-IBoA copolymer blended with 3.00 wt% TMPTA, 3% strain remains in the sample after undergoing a shape-memory cycle in which the material was strained to 50%. Thus residual strain of 6% of the induced strain remains in the material after a single cycle.

4.5. Conclusions

A new method has been proposed and validated for accurately tuning the thermomechanical properties of network acrylates with shape-memory properties. Adjustment of rubbery modulus in the range from below 1 MPa to above 13 MPa was demonstrated. Rubbery moduli were tailored by varying both radiation dose between 5 and 300 kGy and crosslinker concentration between 1.00 and 25.0 wt%. T_g manipulation was independently shown between 23 ˚C and 70 ˚C in copolymers of MA and various other linear acrylates and acrylamides. Shape memory behavior was demonstrated by free strain recovery tests with recovered strains above 90% for all samples. The proposed method, *Mnemosynation*, could enable low cost mass-manufactured devices in complex shapes with tunable thermomechanical and shape-memory properties.

4.7 References

[1] Epictetus, *Discourses, Book Chapter 5*, Athens, Greece **50 A.D.** .
[2] A. Lendlein, H. Jiang, O. Junger, R. Langer, *Nature* **2005**, *434*, 879.
[3] C. M. Yakacki, S. Willis, C. Luders, K. Gall, *Advanced Engineering Materials* **2008**, *10*, 112.
[4] M. Kamal, S. Kenig, Polymer Engineering and Science **1972** 12 294
[5] M. Kamal, S. Kenig, *Polymer Engineering & Science* **1972**, *12*.
[6] D. Rosato, A. Alberghini, *Blow Molding Handbook*, Hanser, Munich **1989**.
[7] C. Williams, J. Summerscales, S. Grove, *Composites Part A: Applied Science and Manufacturing* **1996**, *27*, 517.
[8] G. Marsh, *Materials Today* **2003**, *6*, 36.
[9] C. Macosko, RIM, fundamentals of **reaction injection molding**, Hanser, Munich **1989**.
[10] W. K. Neo, M. B. Chan-Park, *Macromolecular Rapid Communications* **2005**, *26*, 1008.
[11] H. G. Kia, in *Sheet molding compounds: science and technology*, (Ed: K. E. Atkins), Hanser Verlag, **1993**, 257.
[12] C. Goodyear, **1853**.
[13] A. Charlesby, *Nature* **1953**, *4343*, 167.
[14] J. Hu, G. Pompe, U. Schulze, J. Pionteck, *Polymers for Advanced Technologies* **1998**, *9*, 746.
[15] G. G. A. Böhm, M. Detrano, D. S. Pearson, D. R. Carter, *Journal of Applied Polymer Science* **1977**, *21*, 3193.
[16] I. Banik, A. K. Bhowmick, *Radiation Physics and Chemistry* **2000**, *58*, 293.
[17] F. Benard, B. Mailhot, J. Mallegol, J. L. Gardette, *Polymer Degradation and Stability* **2008**, *93*, 1122.
[18] M. R. Cleland, and Lewis A. Parks, *Nucl. Instr. and Meth. in Phys. Res. B* **2003**, *8*, 74.
[19] V. J. Lopata, C. B. Saunders, A. Singh, C. J. Janke, G. E. Wrenn, S. J. Havens, *Radiation Physics and Chemistry* **1999**, *56*, 405.
[20] V. K. Sharma, J. Mahajan, and P. K. Bhattacharyyali, *Radiat. Phys. Chem.* **1995**, *45*, 695 701.
[21] V. Vijayabaskar, S. Bhattacharya, V. K. Tikku, A. K. Bhowmick, *Radiation Physics and Chemistry* **2004**, *71*, 1045.
[22] J. Olejniczak, J. Rosiak, A. Charlesby, International Journal of Radiation Applications and Instrumentation. Part C. Radiation Physics and Chemistry **1991**, 37, 499.
[23] M. E. Haque, N. C. Dafader, F. Akhtar, and M. U. Ahmad, *Radiat. Phys. Chem.* **1996**, *48*, 505.
[24] S. M. Kurtz, O. K. Muratoglu, M. Evans, A. A. Edidin, *Biomaterials* **1999**, *20*, 1659.
[25] G. Zhu, G. Liang, Q. Xu, Q. Yu, *Journal of Applied Polymer Science* **2003**, *90*, 1589.
[26] G. Zhu, Shuogui Xu, Jinhua Wang, and Longbin Zhang, *Radiation Physics and Chemistry* **2006**, *75*, 443.
[27] A. Charlesby, S. H. Pinner, Proceedings of the Royal Society of London. Series A, Mathematical and Physical Sciences **1959**, 249, 367.
[28] P. A. Dworjanyn, J. A. Garner, M. A. Khan, X. Y. Maojun, M. G. Ring, C. Y. Nho, *Radiation Physics and Chemistry* **1993**, *42*, 31.
[29] R. N. Haward, G. Thackray, Proceedings of the Royal Society of London. Series A, Mathematical and Physical Sciences **1968**, 302, 453.
[30] H. M. Jeong, S. Y. Lee, B. K. Kim, *Journal of Materials Science* **2000**, *35*, 1579.
[31] R. Langer, D. A. Tirrell, *Nature* **2004**, *428*, 487.
[32] I. Bellin, Kelch,S., Langer,R., and A. Lendlein, *PNAS* **2006**, *103*, 18043.

[33] K. Gall, C. M. Yakacki, Y. Liu, R. Shandas, N. Willett, K. S. Anseth, *Journal of Biomedical Materials Research, Part A* **2005**, *73A*, 339.
[34] D. Ratna, J. Karger-Kocsis, *Journal of Materials Science* **2008**, *43*, 254.
[35] C. M. Yakacki, R. Shandas, C. Lanning, B. Rech, A. Eckstein, K. Gall, *Biomaterials* **2007**, *28*, 2255.
[36] C. M. Yakacki, R. Shandas, D. Safranski, A. M. Ortega, K. Sassaman, K. Gall, *Advanced Functional Materials* **2008**, *9999*, NA.
[37] Y. Liu, K. Gall, M. L. Dunn, A. R. Greenberg, J. Diani, *International Journal of Plasticity* **2006**, *22*, 279.
[38] Y. Liu, G. Ken, L. D. Martin, M. Patrick, *Smart Materials and Structures* **2003**, 947.
[39] H. Zuidema, G. W. M. Peters, H. E. H. Meijer, *Macromolecular Theory and Simulations* **2001**, *10*, 447.
[40] Hesiod, *Theogony*, **700 B.C**.
[41] A. R. Shultz, *Journal of Polymer Science:* **1959**, *XXXV*, 369.
[42] A. R. Shultz, and Frank A. Bovey, *Journal of Polymer Science* **1956**, *XXII*, 485.
[43] W. Voit, T. Ware, R. R. Dasari, P. Smith, L. Danz, D. Simon, S. Barlow, S. R. Marder, K. Gall, Advanced Functional Materials **2009**.

CHAPTER 5

RADIATION SENSITIZATION

5.1 Problem

Shape-memory polymers (SMPs) are smart materials that can be designed to retain a metastable state and upon activation, recover a preprogrammed shape. In this study, poly(methyl acrylate) (PMA) is blended with poly(ethylene glycol) diacrylate (PEGDA) of several molecular weights in various concentrations and subsequently exposed to ionizing radiation. PEGDA sensitizes the radiation crosslinking of PMA, lowering the minimum dose for gelation and increasing the rubbery modulus, after crosslinking. Minimum dose for gelation, as determined by the Charlesby-Pinner equation, decreases from 25.57 kGy for unblended PMA to 2.06 kGy for PMA blended with 10.00 mole% PEGDA. Moreover, increasing the blend concentration of PEGDA increases the crosslinking density of the resulting networks. Sensitizer length, namely the M_n of PEGDA, also affects crosslinking and final mechanical properties. Increasing the length of the PEGDA molecule at a constant *molar* ratio increases the efficacy of the molecule as a radiation sensitizer as determined by the increase in gel fraction and rubbery modulus across doses. However, at a constant *weight* ratio of PEGDA to PMA, shorter PEGDA chains sensitize more crosslinking because they have more reactive ends per weight fraction. Sensitized samples of PMA with PEGDA were tested for shape-memory properties and showed shape fixity of greater than 99%. Samples had a glass transition temperature near 28 °C and recovered between 97% and 99% of the induced strain when strained to 50%.

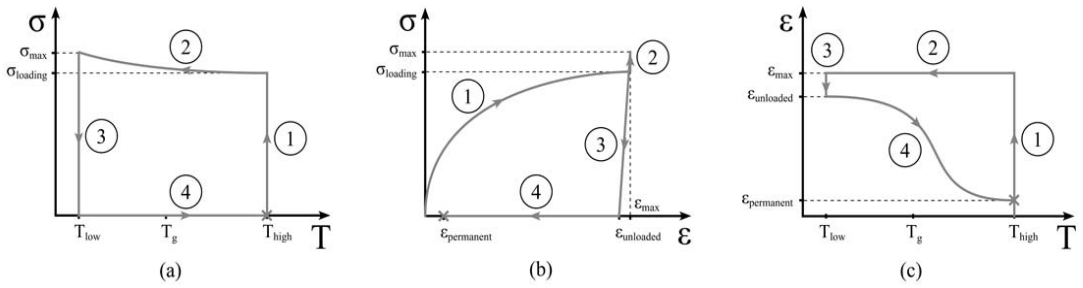

Figure 1. Demonstration of the shape-memory cycle in a) stress-temperature, b) stress-strain and c) strain-temperature regimes. Step 1 is isothermal loading. Step 2 is cooling at constant load. Step 3 is isothermal unloading. Step 4 is shape recovery upon heating.

5.2. Background

The shape-memory effect has been demonstrated in metals, ceramics and polymers (Gall et al. 2004). In polymers, this effect was first utilized in heat-shrink tubing comprised of radiation crosslinked polyethylene (Liu 2007). SMPs have since been proposed for various components that require complete, large-strain shape recovery at low stress. Such components, for example, include implantable biomedical devices as well as parts for specialized industrial applications (Feninat 2002; Langer and Tirrell 2004). **Figure 1** demonstrates the shape-memory cycle in the a) stress-temperature, b) stress-strain and c) strain-temperature planes. The cycle consists of four distinct steps:

1. Straining at T_{high} at constant temperature above the T_g
2. Shape fixing at a constant strain by cooling below T_g
3. Unloading at T_{low} below T_g and measuring shape fixity
4. Heating and measuring shape recovery

In *Step 1,* polymer chains disentangle and uncoil at temperatures above the glass-transition temperature (T_g) causing deformation under applied stresses (Liu et al. 2006). This deformation is fixed by cooling to below T_g while maintaining an applied strain, as seen in *Step 2*. This shape fixing can be attributed to the lack of activation energy necessary for large-scale chain segment movement at low temperatures. The lack of chain mobility allows the polymer to remain in a metastable, strained state. *Step 3* is isothermal unloading. This unloading minimally affects the metastable state and shape fixity can be measured. In *Step 4*, the device is heated to above T_g: the activation energy necessary for chain motion is surpassed, allowing entropy to drive polymer chains to recoil and return the polymer to its original shape as dictated by physical or chemical crosslinks (Bellin 2006; Lendlein and Langer 2002; Tobushi et al. 1996). Through this cycle, SMPs have been shown to fully recover strains of up to 800% (Voit et al. 2009).

Radiation crosslinking has been successfully used to facilitate the shape-memory effect on polyethylene (Kurtz et al. 1999), poly(ε-caprolactone) (Zhu et al. 2003; Zhu 2006) and natural rubber(Banik and Bhowmick 2000; Haque 1996). Radiation crosslinking, in particular by electron beam (e-beam), could enable the production of thermoset, shape-memory devices in complex shapes at low costs, which could lead to an expansion of the use of SMPs in certain commodity devices.

The random nature of radiation crosslinking is defined by the classical Charlesby-Pinner equation shown in Equation 1 (Charlesby and Pinner 1959).

$$s + s^{1/2} = \frac{p_0}{q_0} + \frac{1}{q_0 \mu_1 d} \quad (1)$$

In Equation 1, s is sol fraction, p_0 is degradation density, q_0 is crosslinking density, μ_1 is initial weight, average degree of polymerization and d is radiation dose. Random radiation crosslinking generates a linear data set when $s+s^{1/2}$ is plotted against $1/d$. A linear fit yields intercepts at $1/d$ equals zero and $s+s^{1/2}$ equals two. The intercept at $1/d$ equals zero represents the ratio of scission to crosslinking (p_o/q_o). The intercept of $s+s^{1/2}$ equals two represents the minimum dose of gelation (d_o).

Beyond random crosslinking induced by radiation alone, the use of radiation sensitizers has also been effective in promoting covalent crosslinking in polymers. Radiation sensitizers such as trimethylol propane tri(meth)acrylate, triallyl isocyanurate and polymethylvinylsiloxane all have multiple vinyl bonds which help form network structure by free radicals generated through irradiation (Sharma 1995; Vijayabaskar et al. 2004; Zhu 2006). Increasing the number of unreacted vinyl bonds in the polymer-radiation sensitizer blend has been shown to increase the extent of crosslinking after irradiation (Dworjanyn et al. 1993; Voit et al. 2009b; Zhu 2006). An increase in the molecular weight of the thermoplastic polymer has also been shown to increase the efficiency of crosslinking (Burlant et al. 1964). To the authors' knowledge, other factors such as the length of the sensitizer, have not been systematically varied with a focus on the resultant thermomechanical properties, such as rubbery modulus (E_r) which dictates the recovery force in SMPs (Yakacki et al. 2007) and also scales with the strain capacity in these materials (Safranski and Gall 2008). According to the elastic theory of rubber, E_r is inversely proportional to the molecular weight between crosslinks (James and Guth 1943). In Equation 2, E is elastic modulus, ρ is material density, R is the ideal gas constant, T is temperature and M_c is molecular weight between crosslinks.

$$E=\frac{3\rho RT}{M_c} \quad (2)$$

Control of rubbery modulus has been demonstrated in poly-n-alkyl acrylates which have been successfully crosslinked when blended with several radiation sensitizers (Burlant et al. 1964; Shultz 1959). Control of rubbery modulus has also been demonstrated using PEGDA and poly(ethylene glycol) di(meth)acrylate of various molecular weights (M_n) as a crosslinker in the free radical photo-polymerization of acrylate shape-memory polymer networks (Gall et al. 2005; Safranski and Gall 2008; Yakacki et al. 2008). The authors propose blending and irradiating a system of poly(methyl acrylate) PMA and poly(ethylene glycol) diacrylate (PEGDA) in various ratios to assess the ability of PEGDA to sensitize the radiation crosslinking of PMA and also assess the effects of changing PEGDA length and concentration. Irradiated blends will be evaluated based on the gel fraction, Charlesby-Pinner analyses, resultant crosslinking density and the ability to fix and recover strain.

5.3. Results

5.3.1 Increasing Concentration of PEGDA 258

Each formed network polymer was characterized thermomechanically with the DMA and also by determining the gel fraction, using the Charlesby-Pinner equation to determine the nature of the crosslinking. In **Figure 2**, the gel fractions of PMA blended with between 0.00% and 10.00 mole% PEGDA 258 and irradiated at nine doses between 5 and 300 kGy are shown. Blends with an increased amount of PEGDA 258 show higher

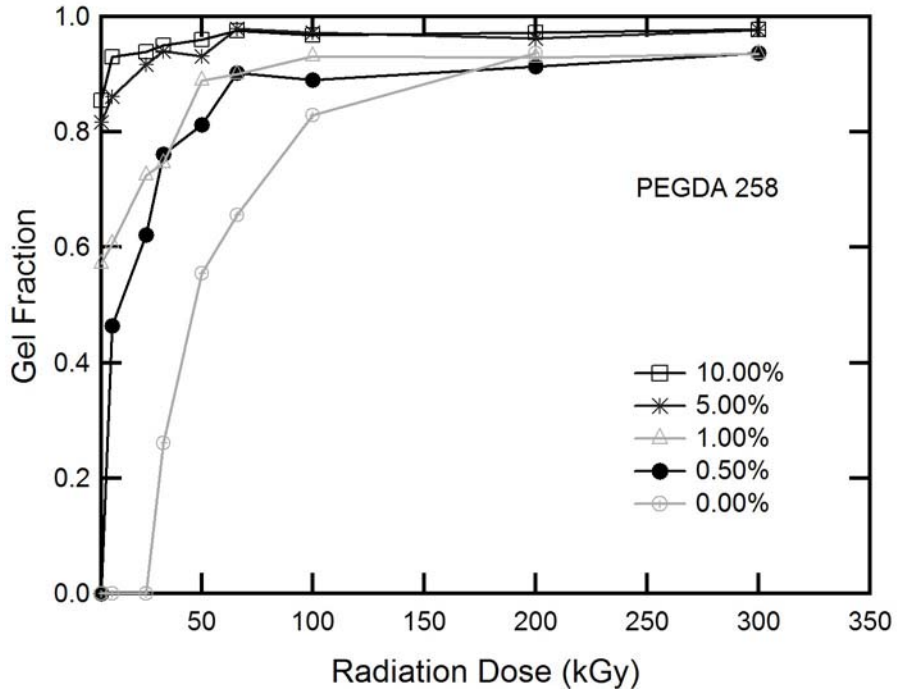

Figure 2. Gel Fraction of irradiated blends of PMA with PEGDA 258.

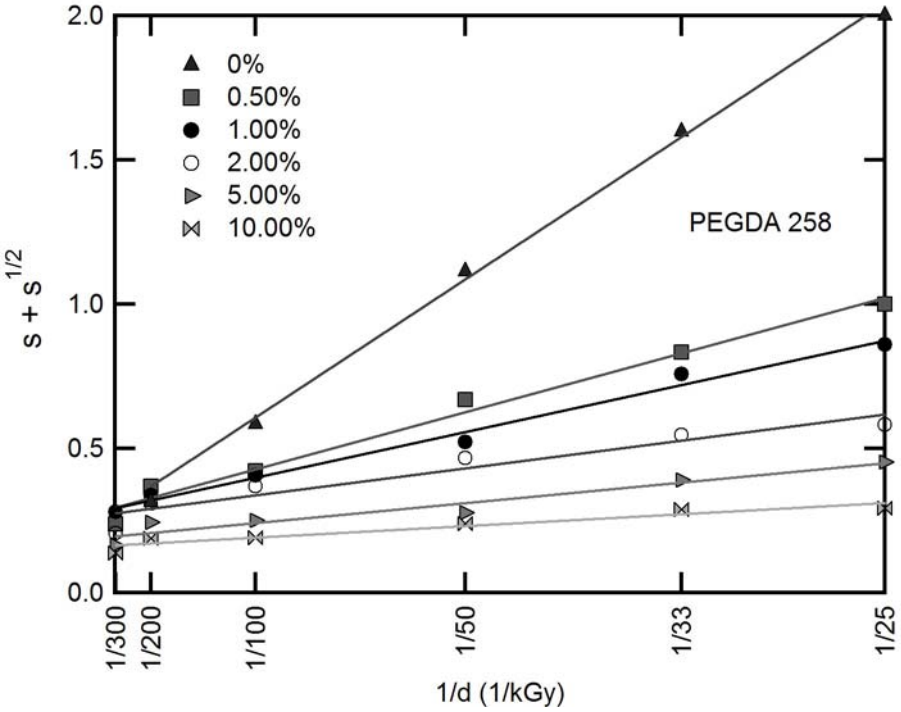

Figure 3. Relationship of $s + s^{1/2}$ and the 1/d for blends of PMA with PEGDA 258.

Table 1. Radiation crosslinking parameters for blends of PMA with PEGDA 258

PEGDA 258	p_o/q_o	d_o (kGy)	R^2
0%	.129	25.57	.993
0.5%	.228	11.19	.985
1%	.243	8.97	.988
2%	.253	5.26	.905
5%	.223	3.92	.885
10%	.163	2.06	.778

gel fractions across doses below 200 kGy, while at 300 kGy increases in concentration made little difference in gel fraction. In **Figure 3**, $s+s^{1/2}$ is plotted against $1/d$. A linear fit for each material was determined yielding d_o and p_o/q_o which are shown in **Table 1**. A measurement of the variance from the determined linear fit, R^2, is also given for each blend in Table 1. It should be noted that at higher concentrations of PEGDA 258 the minimum dose for gelation (d_0) decreases and the deviance from linear fit increases. The ratio of scission to crosslinking (p_o/q_o) increases from 0.00% until 2.00% PEGDA 258, but decreases between 2.00% and 10.00% PEGDA 258.

Figure 4 plots storage modulus as a function of temperature, above T_g, for blends of PMA and PEGDA 258 between 0.50% and 10.00%, irradiated at 50kGy. There is an increase in the rubbery modulus associated with an increase in the amount of blended PEGDA 258. **Figure 5** plots storage modulus as a function of temperature between 10 °C and 95 °C for samples blended with 2.00 mole% PEGDA 258 and irradiated at 5, 50, and 300 kGy. Over this range, the rubbery modulus increases with irradiation dose from 0.77 MPa to 1.02 MPa. These curves are representative of the dynamic mechanical responses of all the blends and the T_g is within 5 degrees of 28 °C for all characterized samples.

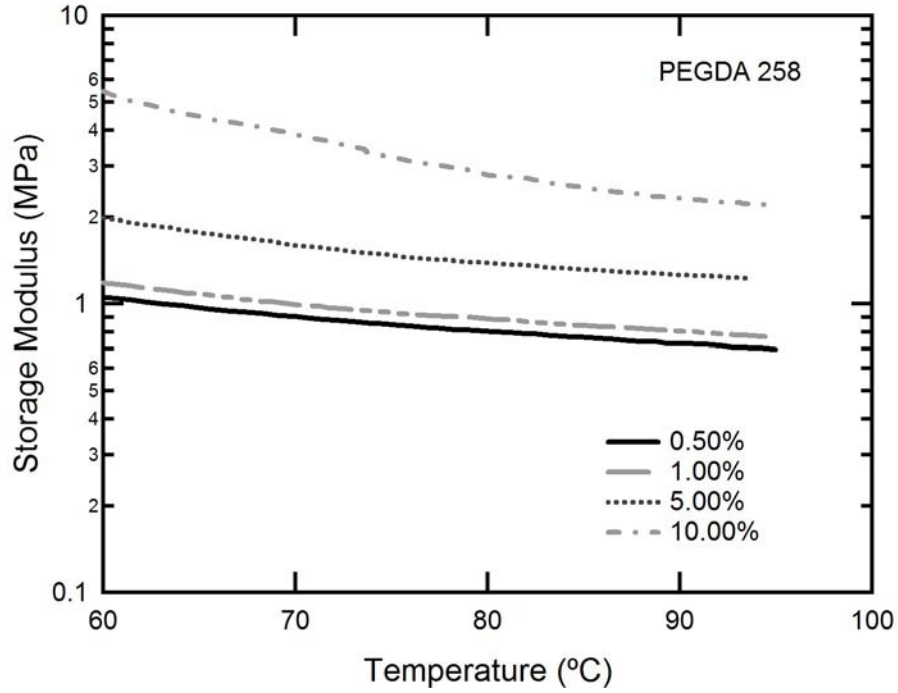

Figure 4. Rubbery modulus comparison from DMA of blends of PMA with PEGDA 258 irradiated at 50 kGy.

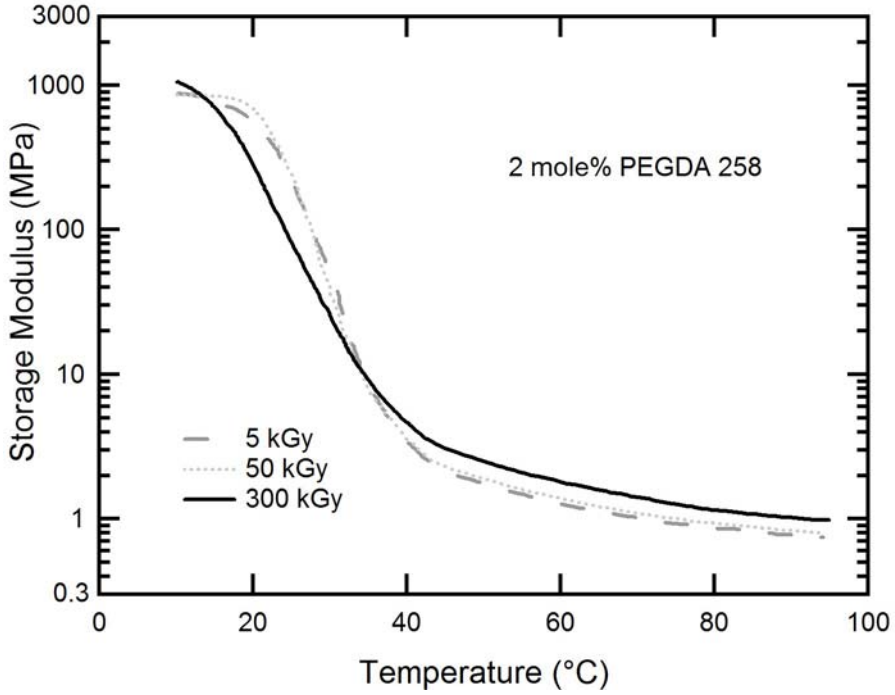

Figure 5. Dynamic mechanical response of blends of PMA with 2 mole% PEGDA 258 at 5, 50 and 300 kGy.

5.3.2 Increasing PEGDA Length

The next figures show equal molar ratios of PEGDA to PMA, and thus contain equal numbers of reactive acrylate ends. This is accomplished in each blend by *altering the weight ratio* of PEGDA to PMA across different length sensitizers. Figures 6b through 9b show equal blended weight ratios of the differing length PEGDA by *altering the molar ratio* of PEDGA to PMA and have different numbers of reactive acrylate ends.

In **Figure 6a**, the gel fractions of 2.00 mole% PEGDA of three molecular weights 258, 575, 700 are displayed across nine radiation doses between 5 and 300 kGy. Below 200 kGy, a trend between increasing PEGDA length and increasing gel fraction can be observed. In **Figure 6b**, the weight ratio of PEGDA to PMA is held constant at 13.63 wt% PEGDA for three molecular weights 258, 575, 700. It should be noted that a trend between increasing PEGDA length and decreasing gel fraction can be observed.

In **Figure 7a**, $s+s^{1/2}$ is plotted against $1/d$ for four samples of a constant 2.00 mole% PEGDA 258, 575 and 700 and for the PMA control. In **Figure 7b**, $s+s^{1/2}$ is plotted against $1/d$ for four other samples of a constant 13.63 wt% PEGDA 258, 575 and 700 and for the PMA control. Table 1 contains d_o, p_o/q_o and R^2 values for each of the Charlesby-Pinner analyses from Figure 7. It should be noted, from Figure 7a and **Table 2** that d_o decreases with increased PEGDA length for blends with 2 mole% PEGDA. Furthermore, p_o/q_o decreases between PEGDA 258 and PEGDA 575, but remains steady between PEGDA 575 and 700. It is shown in Figure 7b and Table 2 that d_o increases between PEGDA 258 and PEGDA 575, but decreases between PEGDA 575 and PEGDA 700. With increasing PEGDA length, p_o/q_o increases for samples at a constant 13.63 wt% PEGDA. R^2 values are above 0.8 for all samples assessing linear fit to Equation 1.

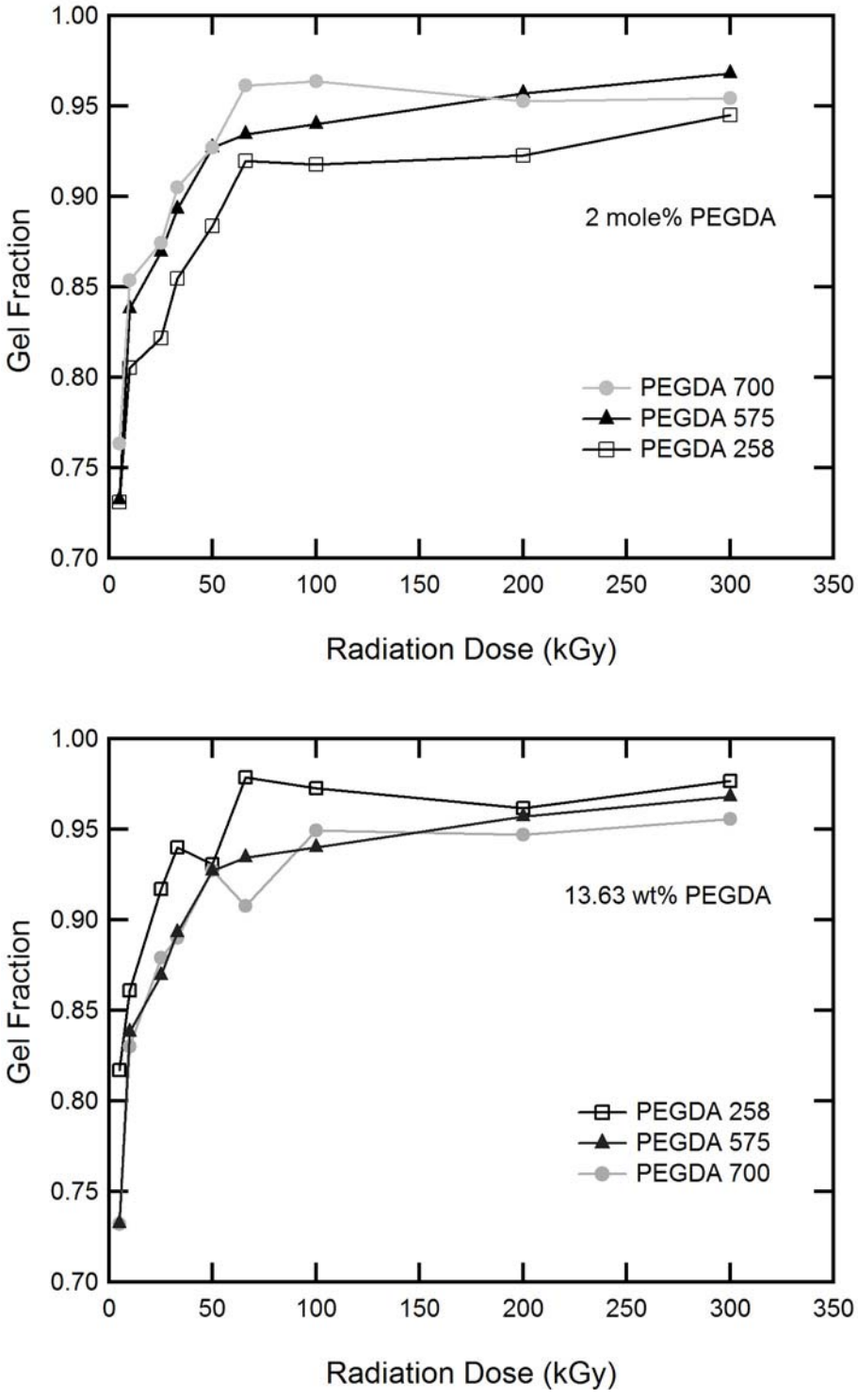

Figure 6. Gel Fraction for irradiated blends of PMA with a) 2 mole% PEGDA and b) 13.63 wt% PEGDA.

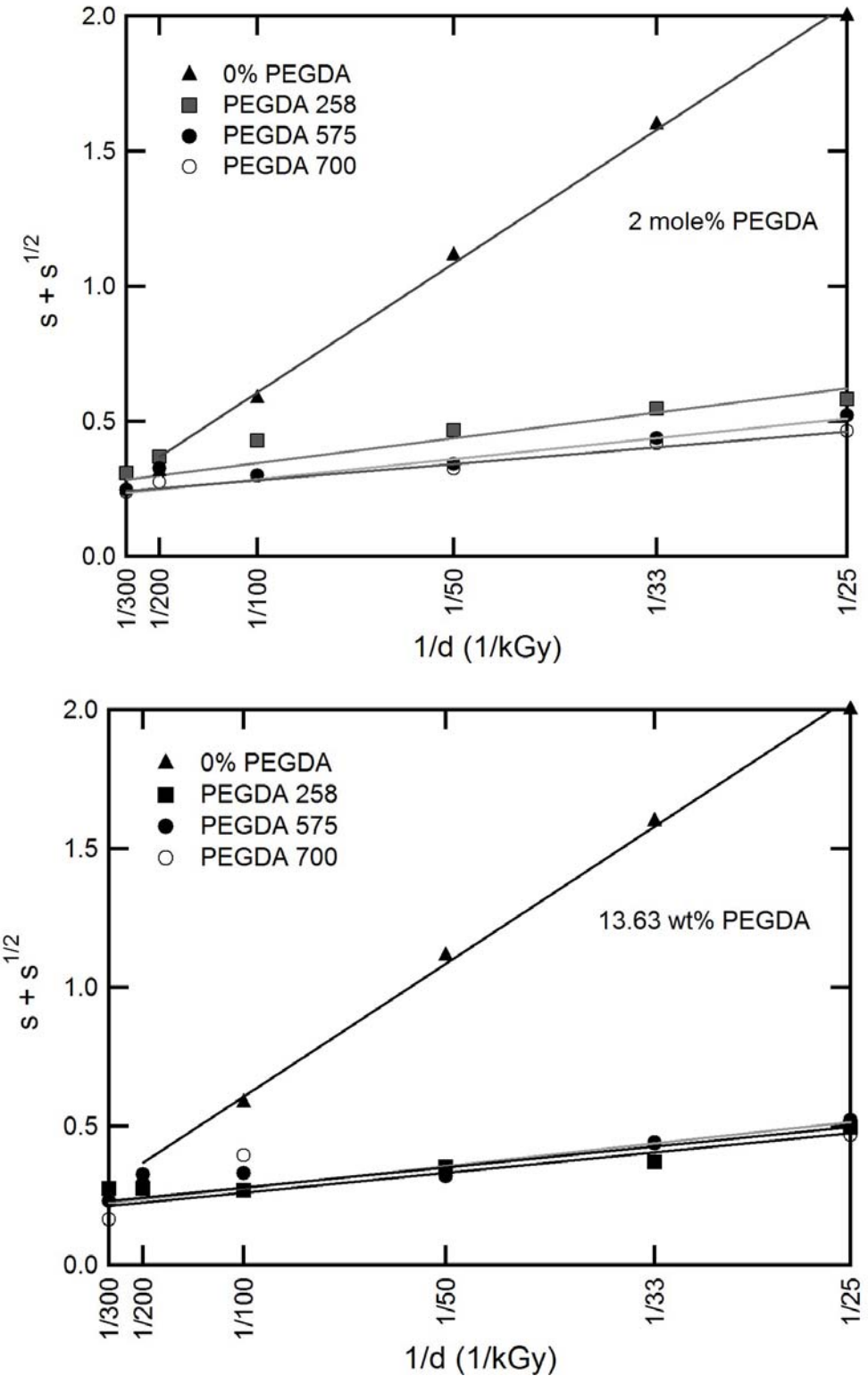

Figure 7. Relationship of $s + s^{1/2}$ and the 1/d for blends of PMA with a) 2 mole% PEGDA and b) 13.63 wt% PEGDA.

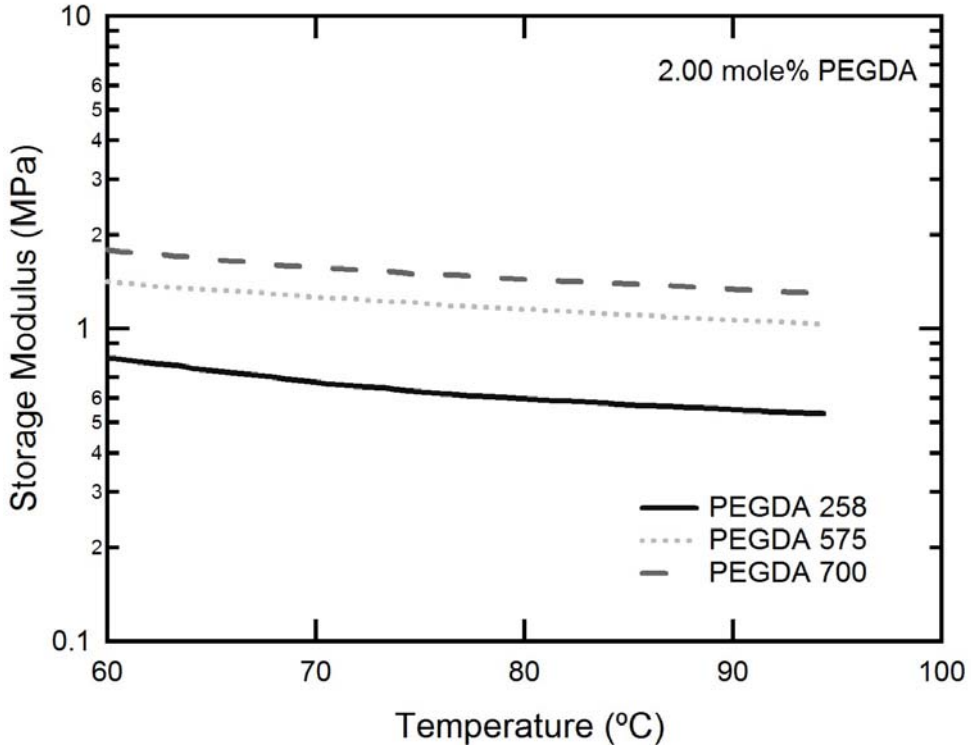

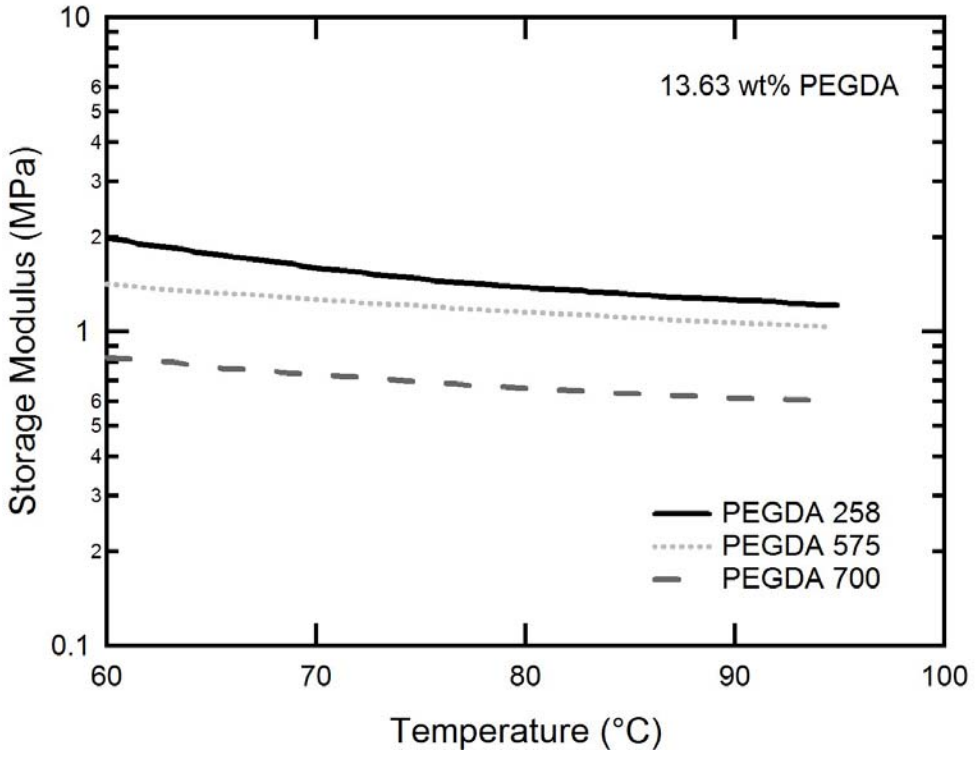

Figure 8. Rubbery modulus comparison from DMA of blends, irradiated at 50kGy, of PMA with a) 2 mole% PEGDA and b) 13.63 wt% PEGDA.

Table 2. Radiation crosslinking parameters of blends of PMA with PEGDA

Crosslinker	p_0/q_0	d_0 (kGy)	R^2
2% PEGDA 258	.294	4.56	.964
2% PEGDA 575	.209	4.21	.927
2% PEGDA 700	.212	3.62	.963
13.63 wt% PEGDA 258	.190	3.92	.885
13.63 wt% PEGDA 575	.198	4.41	.940
13.63 wt% PEGDA 700	.207	4.06	.802

Figure 8a plots storage modulus in the rubbery regime for blends of PMA and 2 mole% PEGDA 258, 575 and 700, irradiated at 50 kGy. **Figure 8b** plots storage modulus in the rubbery regime for blends of PMA and 13.63 wt% PEGDA 258, 575 and 700, irradiated at 50 kGy. The rubbery modulus increases with increased PEGDA length at a constant 2 mole% PEGDA, but decreases with increasing PEGDA length at a constant 13.63 wt% PEGDA.

Consistent with the results at a single dose, samples blended with 2 mole% PEGDA 258, 575 and 700, the rubbery modulus increases as both a function of dose and PEGDA length as shown in **Figure 9a**. **Figure 9b** shows blends with 13.63 wt% PEGDA 258, 575 and 700. These blends show an increase in rubbery modulus with dose, but a decrease in rubbery modulus with increasing PEGDA length.

5.3.3 Shape-Memory Behavior

Three samples blended with 0.50%, 2.00% and 5.00% PEGDA 258 and irradiated at 50 kGy were subjected to a single shape-memory cycle. **Figure 10** shows the shape-memory cycle for each of these materials in the a) stress-temperature, b) stress-strain and

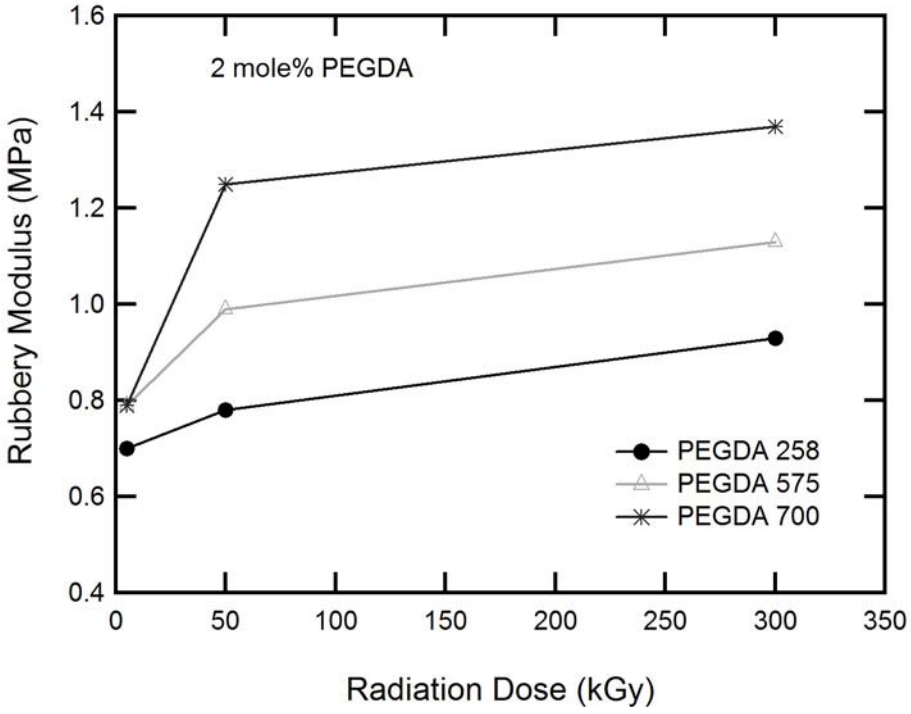

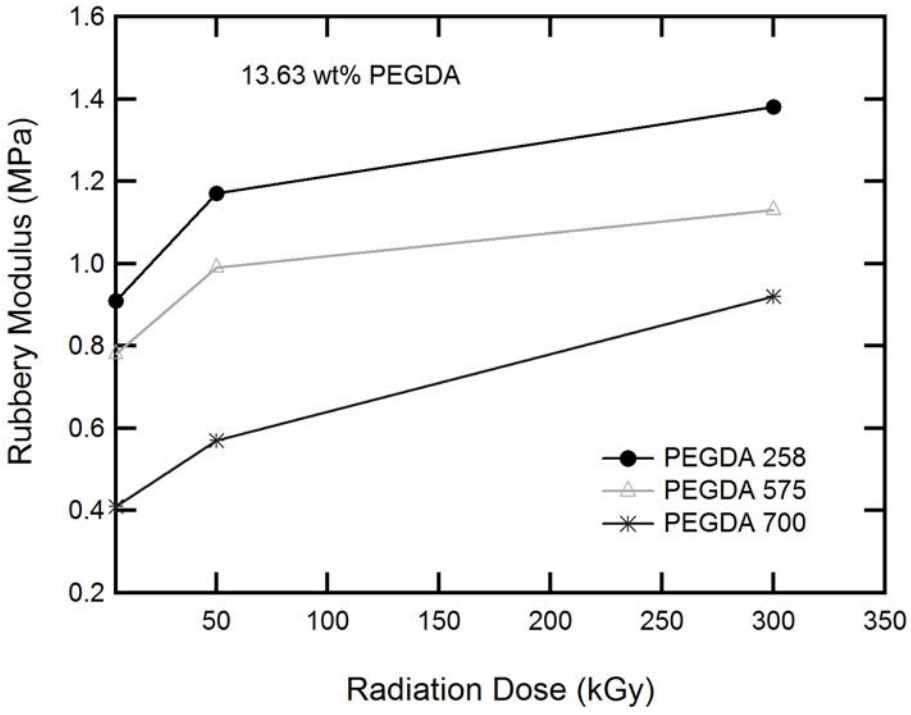

Figure 9. Rubbery modulus as a function of radiation dose from DMA of blends of PMA with a) 2 mole% PEGDA and b) 13.63 wt% PEGDA.

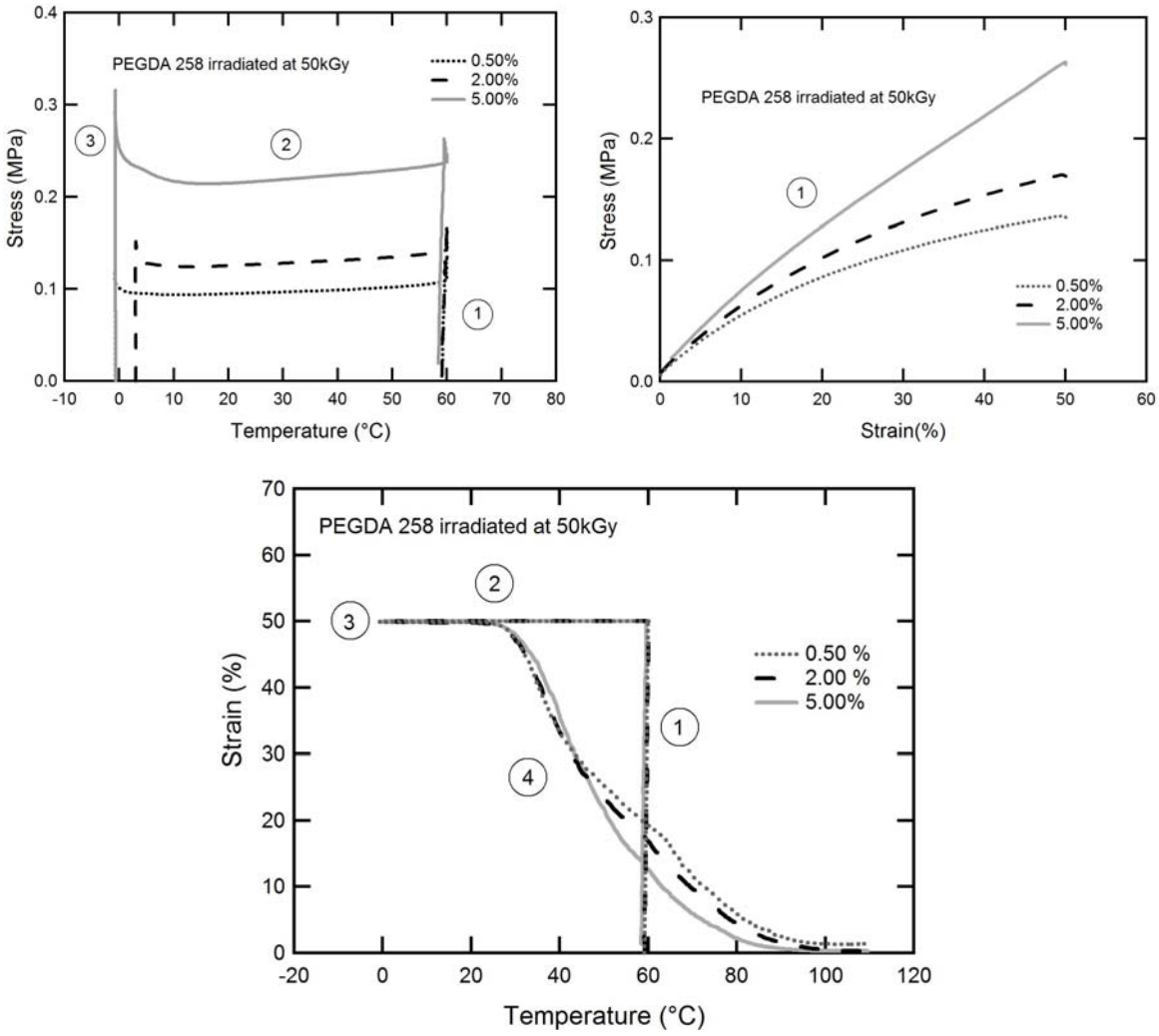

Figure 10. Shape-memory cycle of blends of PMA and PEGDA 258, irradiated at 50kGy, as a) a stress - temperature relationship, b) a stress - strain relationship and c) a strain-temperature relationship. Step 1 is isothermal loading. Step 2 is cooling at constant load. Step 3 is isothermal unloading. Step 4 is shape recovery upon heating.

c) strain-temperature planes. The cycle composed of experimental data mimics the theoretical shape-memory cycle presented in Figure 1. An increase in the stress at 50% strain, and stress at unloading, can be observed with increased PEGDA 258. All three samples showed strain fixity greater than 99%. Residual strain after one cycle decreased from 1.34% residual strain for 0.50 mole% PEGDA 258 to 0.34% residual strain for 5.00 mole% PEGDA 258.

5.4. Discussion

The ability to control and utilize the shape-memory properties of radiation crosslinked polyacrylates may enable their use in commodity devices with specific thermomechanical needs. Enhanced crosslinking, obtained by blending radiation sensitizers into thermoplastic polymers, is required to demonstrate precise control over network properties. The goal of this study is to understand the effect of PEGDA structure and concentration on the radiation crosslinking of PMA. Specifically the study assesses the effect of sensitizer length on gel fraction and thermomechanical properties of PMA blended with PEGDA.

5.4.1 Increasing Concentration of PEGDA 258

PEGDA sensitizes the radiation crosslinking of PMA. Increasing the concentration of PEGDA 258 is shown to increase the extent of network formation in Figure 2. This result is confirmed by the accompanying trend of decreasing minimum dose for gelation with increased PEGDA 258, as can be seen in Figure 3 and Table 1. Increased gel fraction, Figure 2, can be attributed to a much larger quantity of total scission and crosslinking events due to the effects of the radiation sensitizer. More total radiation-induced events leads to larger gel fractions since p_o/q_o, which is less than 1 in all tested samples, favors crosslinking, despite the fact that the ratio of scission to crosslinking increases. Above 2.00 mole% PEGDA, p_o/q_o decreases with increasing PEGDA—thus there is more crosslinking relative to scission. This can be attributed to the relatively large volume fraction of the network that has access to an unincorporated acrylate group. Deviation from the Charlesby–Pinner equation increases with increasing

concentration of radiation sensitizer and can be attributed to rapid conversion of double bonds at low doses. Gel fractions at extremely high doses, 200 and 300 kGy, reflect fully formed networks for all samples regardless of sensitizer length or concentration. In Figure 4, the increase in rubbery modulus with increasing PEGDA 258 also demonstrates additional crosslinking due to the sensitization effects of PEGDA 258. Increased radiation dose also leads to increased crosslinking as demonstrated in Figure 5.

5.4.2.1 Increasing PEGDA Length at Constant Molar Ratio

The radiation sensitization of different length PEGDA molecules at equivalent mole percentages was evaluated. At higher M_n of PEGDA, more repeat ethylene glycol units add chain mobility and increase the probability that the acrylate ends will participate in crosslinking events. Although the number of reactive acrylate ends remains unchanged, the efficacy of each PEDGA molecule as a crosslinker is statistically higher as evidenced in Figures 6a through 9a. Increased sensitizer length increases crosslinking on a per mole basis. To the authors' knowledge this effect has not before been demonstrated in the existing literature in radiation crosslinked thermosets.

Enhanced crosslinking with longer PEGDA sensitizer can be observed through increased gel fractions in Figure 6a and in a reduction in the minimum dose for gelation (the intercept where $s+s^{1/2}=2$) in Figure 7a and in Table 1. Mechanical tests also confirm enhanced crosslinking effectiveness of longer PEGDA blends at a single dose of 50 kGy as observed through the increase in rubbery modulus in Figure 8a. Across multiple doses, this trend is confirmed by Figure 9a. Figure 9a additionally shows a second mechanism

for increasing rubbery modulus: increasing the radiation dose which is consistent with results shown in Figure 5.

5.4.2.2 Increasing PEGDA Length at Constant Weight Ratio

At constant weight ratios of PEDGA to PMA, the trends are significantly different. Blends of equal *weight ratios* of PEGDA 258, 575 and 700 with PMA were characterized in order to compare the trend in increasing *molar ratio* of PEGDA to PMA to the trend in increasing PEGDA length. Within the bounds assessed, increasing molar ratio is relatively more effective than increasing PEGDA length. PEGDA 258 has more functional ends than PEGDA 700 of the same weight ratio. The larger molar ratio of PEGDA 258 to PMA sensitizes more crosslinking than the smaller molar ratio of PEGDA 700 to PMA at the same weight ratio, despite the increased efficacy of longer PEGDA molecules on a per mole basis. In essence, increasing molar ratio is more effective than increasing PEGDA length.

The resultant properties of simultaneously altering the molar ratio and the length of PEGDA are the combination of two competing trends. These competing effects are evident in the gel fraction in Figure 6b and in the Charlesby-Pinner analysis in Figure 7b. The gel fraction decreases slightly with increasing PEGDA length. The minimum dose for gelation increases between PEGDA 258 and PEGDA 575, but decreases between PEGDA 575 and PEGDA 700. This is evidence of the increased efficacy of PEGDA 700 as a radiation sensitizer. The ratio p_o/q_o increases slightly with increasing crosslinker length. This can be attributed to the increased probability of scission events occurring in the ethylene glycol chain of the long PEGDA molecules.

Sol-gel analysis of networks that are fully formed, but only differ in the extent of crosslinking will not illuminate this difference in crosslinking. For 13.63 wt% PEGDA, near complete network formation is achieved at doses above 25 kGy. Thermomechanical tests are required to evaluate the efficacy of the radiation sensitizer. Figures 8b and 9b demonstrate an *increase* in rubbery modulus with a *decrease* in PEGDA length, at constant weight fraction. Across multiple doses, this trend is confirmed by Figure 9b. Mechanical tests confirm that increasing PEDGA length is less effective than increasing molar ratios of PEGDA, but nonetheless does have an influence on the final thermomechanical properties.

5.4.3 Shape-Memory Behavior

Figure 10 demonstrates the shape-memory properties of three PMA and PEGDA 258 blends. Each sample shows excellent shape fixity and recovery over one cycle. An increased molar ratio of PEGDA leads to a greater increases in stress in *Steps 1* and *2* and leads to lower residual strains after a full shape-memory cycle. Blends with an increased molar ratio of PEGDA to PMA experience more rapid recovery and are less affected by packaging as evidenced by a more uniform recovery during *Step 4*. Control of rubbery modulus achieved by varying radiation dose, sensitizer concentration or sensitizer length has been demonstrated. Altering these parameters within the bounds considered here does not alter the T_g by more than 5 ˚C resulting in independent control of rubbery modulus from T_g. A polymer from this system could be used in "smart" devices which are stored at temperatures below 20 ˚C and recover at near ambient temperatures.

5.4. Conclusions

Blends of PMA and PEGDA of three molecular weights were radiation crosslinked at doses between 5 and 300 kGy. The resulting networks were characterized through Charlesby-Pinner analyses and dynamic mechanical analyses. PEGDA successfully sensitized the radiation crosslinking of PMA. The extent of crosslinking was greater with increasing molar concentration of PEGDA of a single M_n. Longer PEGDA molecules were found to be more effective at sensitizing crosslinking at a given molar ratio of sensitizer to PMA. At a given weight ratio, shorter PEGDA molecules were found to be more effective at sensitizing crosslinking because there are more reactive acrylate ends. The shape-memory properties of three blends crosslinked at 50 kGy were evaluated. Shape fixity was above 99% for all three materials. Shape recovery over one cycle was between 97% and 99% and increased with increasing molar ratio of PEGDA. Control of rubbery modulus, independent from T_g, was achieved for shape-memory polymers which are stored at temperatures below 20 ˚C and recover at ambient temperatures.

5.6. References

1. Banik, I., Bhowmick, A.K., 2000. Effect of electron beam irradiation on the properties of crosslinked rubbers. Radiation Physics and Chemistry 58 (3), 293-298.
2. Bellin, I., Kelch,S., Langer,R., and A. Lendlein, 2006. Polymeric triple-shape materials. PNAS 103 (48), 18043–18047.
3. Burlant, W., Hinsch, J., Taylor, C., 1964. Crosslinking and Degradation in Gamma-Irradiated Poly-n-alkyl Acrylates. Polymer Science 2, 56-57.
4. Charlesby, A., Pinner, S.H., 1959. Analysis of the Solubility Behaviour of Irradiated Polyethylene and Other Polymers. Proceedings of the Royal Society of London. Series A, Mathematical and Physical Sciences 249 (1258), 367-386.
5. Dworjanyn, P.A., Garner, J.A., Khan, M.A., Maojun, X.Y., Ring, M.G., Nho, C.Y., 1993. Novel additives for accelerating radiation grafting and curing reactions. Radiation Physics and Chemistry 42, 31-40.
6. Feninat, F.E., G. Laroche, M. Fiset, and D. Mantovani, 2002. Shape Memory Materials for Biomedical Applications. Advanced Engineering Materials 4 (3), 91-104.
7. Gall, K., Kreiner, P., Turner, D., Hulse, M., 2004. Shape-memory polymers for microelectromechanical systems. Microelectromechanical Systems, Journal of 13 (3), 472-483.
8. Gall, K., Yakacki, C.M., Liu, Y., Shandas, R., Willett, N., Anseth, K.S., 2005. Thermomechanics of the shape memory effect in polymers for biomedical applications. Journal of Biomedical Materials Research, Part A 73A (3), 339-348.
9. Haque, M.E., N. C. Dafader, F. Akhtar, and M. U. Ahmad, 1996. Radiation Dose Required for the Vulcanization of Natural Rubber Latex. Radiat. Phys. Chem. 48 (4), 505-510.
10. James, H.M., Guth, E., 1943. Theory of the Elastic Properties of Rubber. The Journal of Chemical Physics 11 (10), 455-481.
11. Kurtz, S.M., Muratoglu, O.K., Evans, M., Edidin, A.A., 1999. Advances in the processing, sterilization, and crosslinking of ultra-high molecular weight polyethylene for total joint arthroplasty. Biomaterials 20 (18), 1659-1688.
12. Langer, R., Tirrell, D.A., 2004. Designing materials for biology and medicine. Nature 428 (6982), 487-492.
13. Lendlein, A., Langer, R., 2002. Biodegradable, Elastic Shape-Memory Polymers for Potential Biomedical Applications. Science 296 (5573), 1673-1676.
14. Liu, C., Qin,H., and P. T. Mather, 2007. Review of progress in shape-memory polymers. Journal of Materials Chemistry 17, 1543–1558.
15. Liu, Y., Gall, K., Dunn, M.L., Greenberg, A.R., Diani, J., 2006. Thermomechanics of shape memory polymers: Uniaxial experiments and constitutive modeling. International Journal of Plasticity 22 (2), 279-313.
16. Safranski, D.L., Gall, K., 2008. Effect of chemical structure and crosslinking density on the thermo-mechanical properties and toughness of (meth)acrylate shape memory polymer networks. Polymer 49 (20), 4446-4455.
17. Sharma, V.K., J. Mahajan, and P. K. Bhattacharyyali, 1995. Electron Beam (Eb) Crosslinking of PVC Insulation in Presence of Sensitiser Additives. Radiat. Phys. Chem. 45 (5), 695 701.
18. Shultz, A.R., 1959. High-Energy Radiation Effects on Polyacrylates and Polymethacrylates. Journal of Polymer Science: XXXV, 369-380.
19. Tobushi, H., Hara, H., Yamada, E., Hayashi, S., 1996. Thermomechanical Properties in a Thin Film of Shape Memory Polymer of Polyurethane Series. Smart Materials and Structures 5, 483-491.
20. Vijayabaskar, V., Bhattacharya, S., Tikku, V.K., Bhowmick, A.K., 2004. Electron beam initiated modification of acrylic elastomer in presence of polyfunctional monomers. Radiation Physics and Chemistry 71 (5), 1045-1058.

21. Voit, W., Ware, T., Dasari, R.R., Smith, P., Danz, L., Simon, D., et al., 2009a. High Strain Shape Memory Polymers. Advanced Functional Materials submitted.
22. Yakacki, C.M., Shandas, R., Lanning, C., Rech, B., Eckstein, A., Gall, K., 2007. Unconstrained recovery characterization of shape-memory polymer networks for cardiovascular applications. Biomaterials 28 (14), 2255-2263.
23. Yakacki, C.M., Shandas, R., Safranski, D., Ortega, A.M., Sassaman, K., Gall, K., 2008. Strong, Tailored, Biocompatible Shape-Memory Polymer Networks**. Advanced Functional Materials 18, 1-8.
24. Zhu, G., Liang, G., Xu, Q., Yu, Q., 2003. Shape-memory effects of radiation crosslinked poly(ε-caprolactone). Journal of Applied Polymer Science 90 (6), 1589-1595.
25. Zhu, G., Shuogui Xu, Jinhua Wang, and Longbin Zhang, 2006. Shape memory behaviour of radiation-crosslinked PCL/PMVS blends. Radiation Physics and Chemistry 75, 443–448.

CHAPTER 6

SMP-FIBER COMPOSITES

6.1 Problem

Cast immobilization of a surgically repaired injury site remains a critical medical procedure, particularly in adolescent medicine. After traumatic injury, increased blood flow and the immune response cause affected injured areas to undergo dramatic shape changes. Often casts that are applied to swollen limbs do not fit well after short periods of time and the need for expensive and tedious recasts arises. This work lays the groundwork to investigate dynamic fiber-reinforced shape-memory polymer casting sleeves that can be adjusted to account for post-operative edema and swelling by reshaping the cast upon the immobilization site without the need for recasting. A shape-memory polymer (SMP) is a smart material that "remembers" its original shape after deformation at temperature and returns to that state upon future reheating to a set temperature. The proposed casting sleeve design is a two-layer fiber-reinforced copolymer. The rigid inner layer provides stability and necessary compression while the softer outer layer protects the inner layer from brittle failure. The multi-actuated polymer system would soften upon a determined temperature increase allowing for increased malleability and ease in application to the affected body part. Fundamental research is necessary to find an appropriate polymer system and manufacturing technique. Further research is required to explore the effects of polymer-fiber interfaces in composites materials. Strain capacity, crosslinker density, glass transition temperature (T_g), rubbery modulus (E_R), fiber type, fiber weave, fiber orientation and volume fraction of polymer to fiber can all be adjusted. The work presented in this Chapter is a preliminary effort

towards establishing and solving a host of underlying technical challenges necessary before commercialization of a fiber-reinforced SMP cast can be undertaken.

6.2 Background

The idea to use shape-memory polymers for orthopedic casts is not new. Patent literature dating back more than 20 years demonstrates then novel proposals to design self-adjusting orthopedic casts with shape memory properties *[1-7]*. However, no fiber-reinforced SMP commercial solution exists today in the mass market. To gain acceptance, the Class I biomedical devices must be constructed in a cost-comparable fashion to existing market solutions such as 3M's *Scotchcast[8]* and Smith and Nephew's *Dynacast[9]* and meet stringent mechanical property specifications to be efficacious. Some potential manufacturing techniques to meet cost requirements are e-beam curing, which Lopata et al. described for epoxy composites*[10]* or a vacuum-bag resin transfer process*[11]*.

Fiber-reinforced shape-memory polymer casts present a potential solution with which to meet these cost and mechanical property specifications. However, in the past, the paradigm for composite manufacture has been to combine materials to increase the strength of the composite. To meet the requirements of a self-adjusting casting sleeve, the polymer-composite must meet a certain *stress threshold*, but more importantly, must have a much higher strain capacity than existing fiber composites. This chapter explores a new paradigm in SMP composite manufacture: combining fibers and SMPs to increase the *strain capacity* of the underlying composite material.

Abrahamson et al. have shown that stiffness and recovery force of SMP-composites can be dramatically improved using Elastic Memory Composite (EMC) materials*[12]*. They further showed that materials can be activated through a temperature change but only observed strains up to 30%. Other papers employ SMP composites to improve strength but also do not characterize strains in the regime necessary for this application. Gall et al. describe the fabrication and characterization of composites with an SMP matrix and SiC nanoparticulate reinforcements. Composites based on a SMP matrix are active materials capable of recovering mechanical strains of approx. 22% due to the application of heat *[13, 14]*. SMP composites are also used for intracranial aneurysm coils*[15]*, while SMP polyurethane composite systems have been proposed for other applications *[16]*.

High strength SMP composites have received considerable attention. Nielson outlines fundamental thermomechanical responses of polymer composites*[17]* and Ohki describes creep and the mechanical properties of SMP composites*[18]*, but no mention of large strain enhancements is made as the focus remains on enhancing strength and toughness. Ratna et al. present an overview of SMPs and SMP composites focused on improving strength*[19]*, while Wei et al. compare SMPs, SMAs and shape-memory ceramics, but without a push for developing high strain memory materials *[20]*. From building fiber reinforced polymer concretes*[21]* to developing high strength SMP nanocomposites with carbon nanotubes *[22]* to studying the effects of moisture on the strength of SMPs with nanocomposites*[23]* to creating high strength SMA alloy composites*[24]*, shape memory materials have been popular composites components for many applications. However the author is not aware of SMP composite studies with a

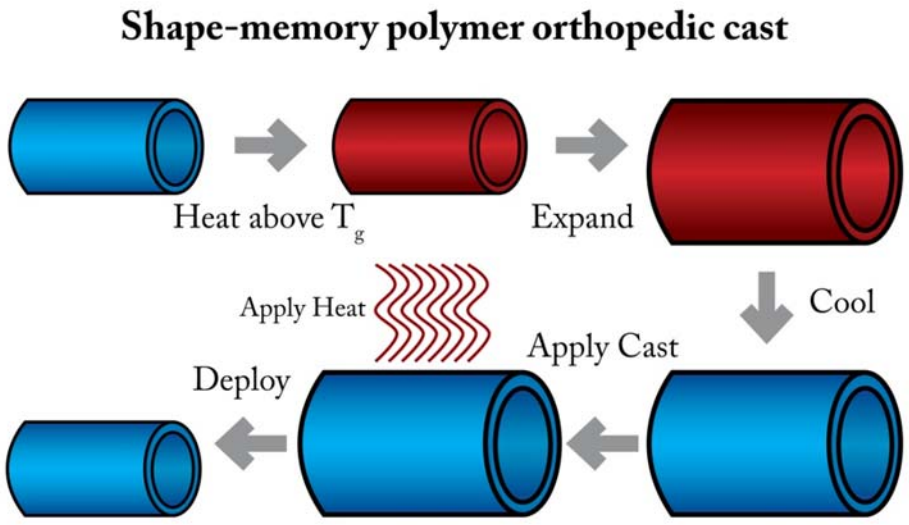

Figure 1. Schematic for shape storage and deployment of a shape-memory polymer orthopedic cast. The cast is manufactured in a set shape. Upon heating above T_g, the cast is stretched and stored in a temporary shape. The cast is applied, reheated and deployed.

target goal of developing fully recoverable large strain, moderate stress materials with shape memory. The majority of prior studies just increase stiffness without regard for strain capacity under tension (several studies look at strain capacity under bending).

6.3 Road Map

The research will address fundamental technical hurdles necessary to improve cast immobilization using novel shape-memory polymer (SMP) systems to build adjustable, multi-actuated, fiber-reinforced casting sleeves that shrink wrap over an affected limb and can be readjusted to account for post operative edema and swelling after the initial trauma. The schematic overview for the SMP cast application can be seen in **Figure 1**. A casting sleeve is synthesized, heated and deformed, and cooled in its

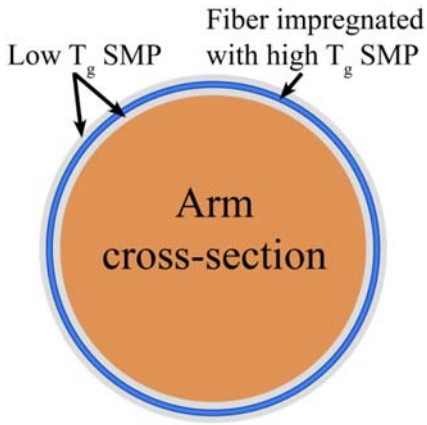

Figure 2. Cross section of the proposed shape-memory polymer orthopedic cast. A rigid inner layer is a woven fiber impregnated with a high T_g polymer. A softer outer layer consists of a low T_g shape-memory polymer while helps prevent brittle failure. The cast is affixed arbitrarily about an arm.

expanded shape. After deployment, the cast is reheated and compressed about the affected extremity. The research will examine different techniques used to synthesize the cast system that will allow for all three layers (soft outer SMP layer, hard inner SMP layer, innermost fiber layer) to be synthesized together as one unit which will be in the shape of a cylindrical tube. These layers are presented in **Figure 2**. In the past, there has been only limited research performed in this area due to the difficulty of manufacturing and layering thermoset materials such as the polymers being used in this proposed cast system. However, combining advances in high strain acrylate synthesis from Chapter 3, with *Mnemosynation* from Chapter 4 and the optimization of radiation sensitization from Chapter 5, the difficult technical challenges and cost boundaries do not seem insurmountable.

Multiple design decisions depend on understanding fundamentally how the polymer will interact with different fibers in different weave and geometries. For the purpose of the casting sleeve, the fiber weave must be rigid enough to toughen the core

polymer layer and flexible enough to accommodate the high strains associated with clinical application. Antares nylon lycra has been selected for the fiber's high tensile stress and strain, its breathability, and desirable interface with polymerized acrylate copolymers. The thermo-mechanical properties of the antares-nylon lycra-SMP composite were measured to determine the mechanical properties of the casting material in activated and non-activate states and to assure activation and use loads would not cause failure. If the research can address the outstanding technical problems and devise clever manufacturing solutions, multi-actuated fiber-reinforced shape memory polymer casting sleeve prototypes may emerge to enable products that improve post-operative care.

To begin explorations, a well-characterized model polymer system was required. Yakacki et al. have described in detail the thermomechanical responses of various tBA-PEGDA systems *[25, 26]*, which provided a starting point for the research. As the choice of fiber was refined, fiber orientation and weave geometry were also investigated. Once a fiber had been chosen, the polymer system was then refined to move the T_g and E_R to meets the needs of this application. Tests helped refine the target T_g range in the design of the final polymers. Preliminary results have shown that there exists a toughness peak or deformability peak and a maximum in the strain-to-failure of systems when the testing temperature is near (within approximately 15 °C) the T_g. These tests allow for a minimal final geometry to meet a specific engineering need and therefore reduce the volume and the final cost of material needed to solve a particular problem.

Expanding upon this idea of reducing the final volume of the polymer, the research began to examine shape-memory polymer composites. The composite material imparts increased fracture toughness onto the final device and imparts other increased mechanical properties above and beyond the pure polymer at a reduced cost. Within this realm, several issues were investigated. The volume fraction of polymer to composite was hypothesized to dictate the overall mechanical properties of the device and is the factor that determines the raw materials price point. To conduct this research, a vacuum bagging resin transfer system was developed to precisely control the ratio of polymer to fiber. Acrylates were infused across different fiber weaves and an assessment of the emerging properties was made. In addition, the effect of crosslinker density within composite shape memory polymers had not been assessed in the literature. Assessing the effect of crosslinker density on SMP-composites sets a point of comparison to allow an extrapolation from initial crosslinker density results within pure polymer systems. Tests were conducted using a tight weave polyester fiber in the 0 degree orientation. Other fibers (Kevlar, spandex, cotton, fiberglass, nylon) have been studied in an effort to generalize many of these results across shape memory polymer composite systems.

In the manufacturing realm, *Mnemosynation*, the post-processing method to crosslink thermoplastics with high-energy radiation to induce crosslinking was explored. This procedure allows a thermoplastic to be synthesized, melted and molded into a final shape. This final shape, the orthopedic cast in this case, can be exposed to the high-energy radiation and crosslinked to fix that shape as the permanent shape in the shape memory cycle. Building SMP-fiber composites combines the interesting properties of both the polymer and reinforcement material allowing shape fixation and material

memory at increased levels of fracture toughness and tensile strength without relying on exotic high-cost chemistries. However few studies have fundamentally addressed the effects of varying crosslinker densities and polymer-to-fiber volume fractions in SMP composites. Furthermore, the literature lacks thorough assessments of the whole spectrum of mechanical properties of SMP composites beyond tensile strength and fracture toughness. Controlling the effects of gamma radiation on thermoplastic SMP precursors enables the crosslinking of these materials after they undergo low cost thermoplastic polymer processing which molds them into a desired shape. This post-synthesis crosslinking step triggers the emergence of polymer memory and bestows enhanced mechanical properties upon the polymers.

One task of this work has been to develop a method to mold and subsequently crosslink a polymer-fiber system to create a prototype of the casting sleeve. Vacuum-assisted resin transfer molding (VARTM) has been proposed as an improved method to impregnate the fiber core with resin while maintaining control of the overall cast thickness. The VARTM mold would securely house the fiber while the vacuum draws across the heated, blended thermoplastic resin. Upon cooling the cast will be exposed to high energy radiation to activate crosslinking.

Another task of the ongoing research is to test the thermo-mechanical properties of the prototyped casting sleeve. Initial tests on flat samples have been previously performed to test the SMP-fiber composites for strength and toughness. These tests will be repeated on the cylindrical prototypes in ensure appropriate toughness and rigidity of the casting material in a prototype-like geometry. It is imperative that the casting sleeve provides rigid stability to the affected limb while maintaining structural comfort. Yet

another task of the research is to meld an outer, softer SMP layer that protects the casting sleeve from brittle failure with a sturdier, higher T_g inner layer, which, without cushioning, is prone to brittle failure. This layered approach will allow for small shape adjustments to account for swelling while keeping the body part stable and immobilized. The inner SMP must be stiffer than the outer cushion in order to maintain proper compression upon the affected limb. This multi-actuated polymer system will soften when heated in order to expand the sleeve over the limb. This allows for easy application and removal while stabilizing the body part.

Furthermore, to enable prototype creation, the inner fiber core must be impregnated with an optimized polymer system. The fiber will provide the cast system will the toughness and rigidity needed to maintain enough stiffness for the cast, which will provide the requisite stability and compression for the limb to ensure bone fusion over the lifetime of the cast.

6.4 Initial Results

In order to accomplish this novel SMP system casting design solution, many different facets of research, completed and proposed, must be amalgamated. The research requires a further the investigation into the thermo-mechanical properties of the multi-actuated polymer system in order to develop proper geometric and layering designs for the SMP cast system. Future research will include the manufacturing and testing of the design solution prototypes on a limb system that imitates the swelling response.

During the course of the initial explorations presented in this Chapter, several high-strain SMPs were synthesized and characterized. These copolymers were composed

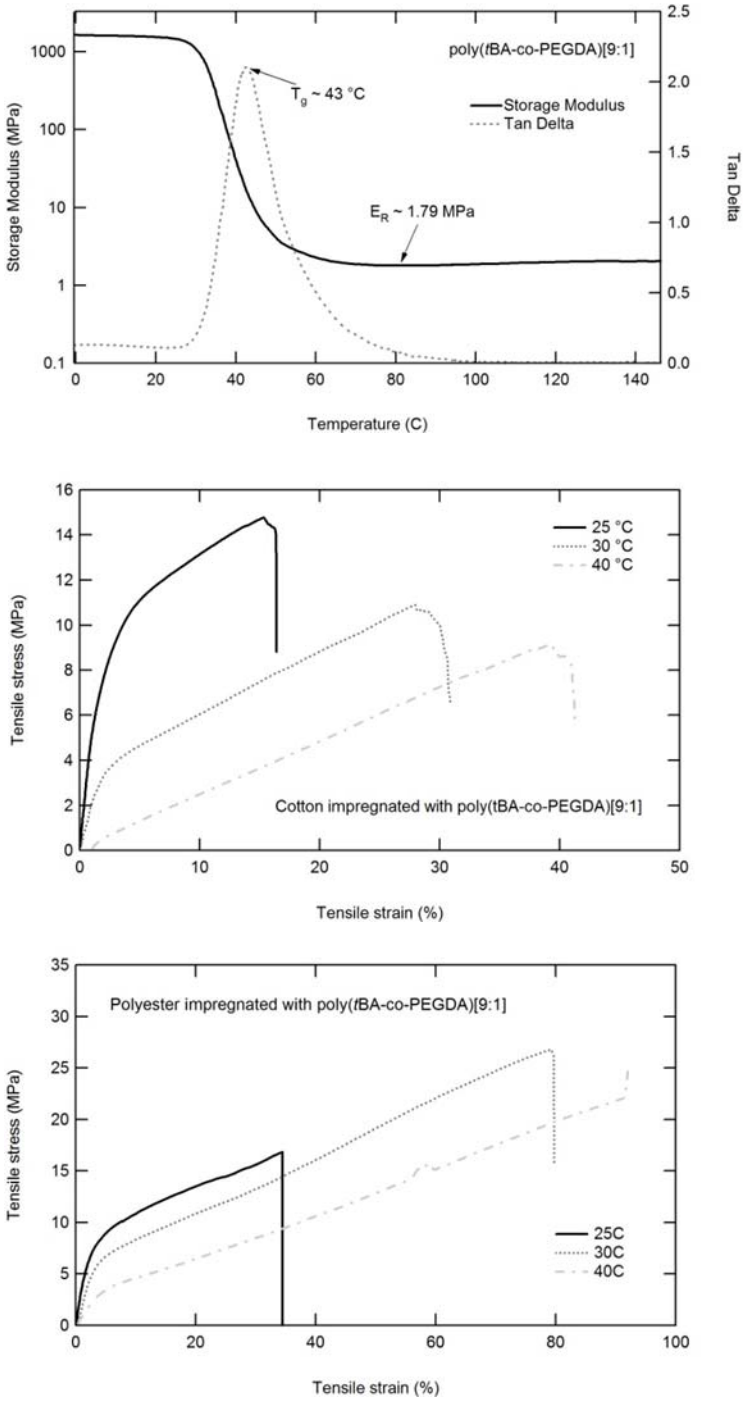

Figure 3. a) *tert*-butyl acrylate and poly(ethylene glycol) diacrylate are copolymerized in a 9 to 1 ratio yielding the resulting thermomechanical response. This 10% crosslinked systems has a rubbery modulus below 2 MPa and a T_g several degrees above body temperature as measured by the peak of tan delta. This polymer is impregnated into b) cotton and c) polyester and the stress-strain response is characterized at 25°C, 30°C and 40°C, temperatures that an orthopedic cast would experience during use.

of either linear monomer *tert*-butyl acrylate (tBA) and poly(ethylene glycol) diacrylate (PEGDA) or linear monomers methyl acrylate (MA), butyl acrylate (BA) and methyl methacrylate (MMA) and crosslinker bisphenol A ethoxylate dimethacrylate (BPAEDMA). Within this system, the concentrations of MA and MMA were varied by increments of 10.0 wt% while fixing the BA and BPAEDMA at 15.0 wt% and 2.50 wt%, respectively. The first series of high strain polymers that were synthesized and characterized were control samples: they consisted only of the chosen polymer itself. The second series of polymers that were synthesized were polymerized around a fiber core. The mechanical properties of these two sets were compared by various techniques. Over the course of the research the impregnated fiber of choice changed to accommodate new design parameters that emerged during the research and development. So too was the polymer system refined.

The first mock polymer system characterized was a copolymer of tBA and PEGDA in a 9:1 ratio. **Figure 3a** shows the DMA curve of poly(tBA-co-PEGDA) with the tan delta peaking at 43 °C and the E_R at about 1.79 MPa. This figure served as a control without fiber reinforcement from which to compare successive thermomechanical tests. **Figure 3b** shows the thermomechanical effects of impregnating a cotton fiber with poly(tBA-co-PEGDA) [9:1] and observing the stress-strain response at three different temperatures that a casting sleeve may experience during normal use: 25 °C, 30°C and 40°C. **Figure 3c** presents a similar plot for a polyester reinforced polymer. In **Table 1** and **Table 2**, six fibers from the initial screening round are assessed under these same conditions. Table 1 presents the maximum strains experienced by each fiber-polymer composite while Table 2 depicts the toughness of each composite.

Table 1. Max strains (%) of polymer-impregnated fibers at different temperatures

Temp (°C)	Cotton	Fiberglass(LW)	Nylon	Polyester	Spandex	Fiberglass (TW)
25	15.5	2.1	43.5	34.5	80	4.4
30	28	2.5	45	80	100	5
40	39	3.6	-	90	86	5.5

Table 2. Toughness (MJ/m^3) of polymer-impregnated fibers at different temperatures

Temp (°C)	Cotton	Fiberglass(LW)	Nylon	Polyester	Spandex	Fiberglass (TW)
25	1.89	0.71	11.94	-	8.44	6.35
30	2.25	0.93	13.84	12.89	5.52	7.32
40	2.03	1.21	-	11.22	2.44	5.38

The data is these tables are not rigorous. Each test in the initial screen was only run once because of the large number of samples that needed to be made and tested. So while the values may not be statistically significant at each temperature, the combination of all tests presents a broad approach across many fibers to develop intuitions as to how the polymer interacts with each different fiber. Since this was a general screen to test a wide variety of fibers, breadth over precision was preferred when given limited time and resources. As the material choices mature, data collection will begin to be extremely precise for the chosen polymer and fiber, characterizing the potential casting components across temperature regimes multiple times to ensure inter sample variability is minimized. Given this caveat, strains were generally highest nearer to the T_g of the polymer while toughness was maximized near the onset of T_g. This behavior follows trends observed by Smith et al. for pure polymer systems*[27]*.

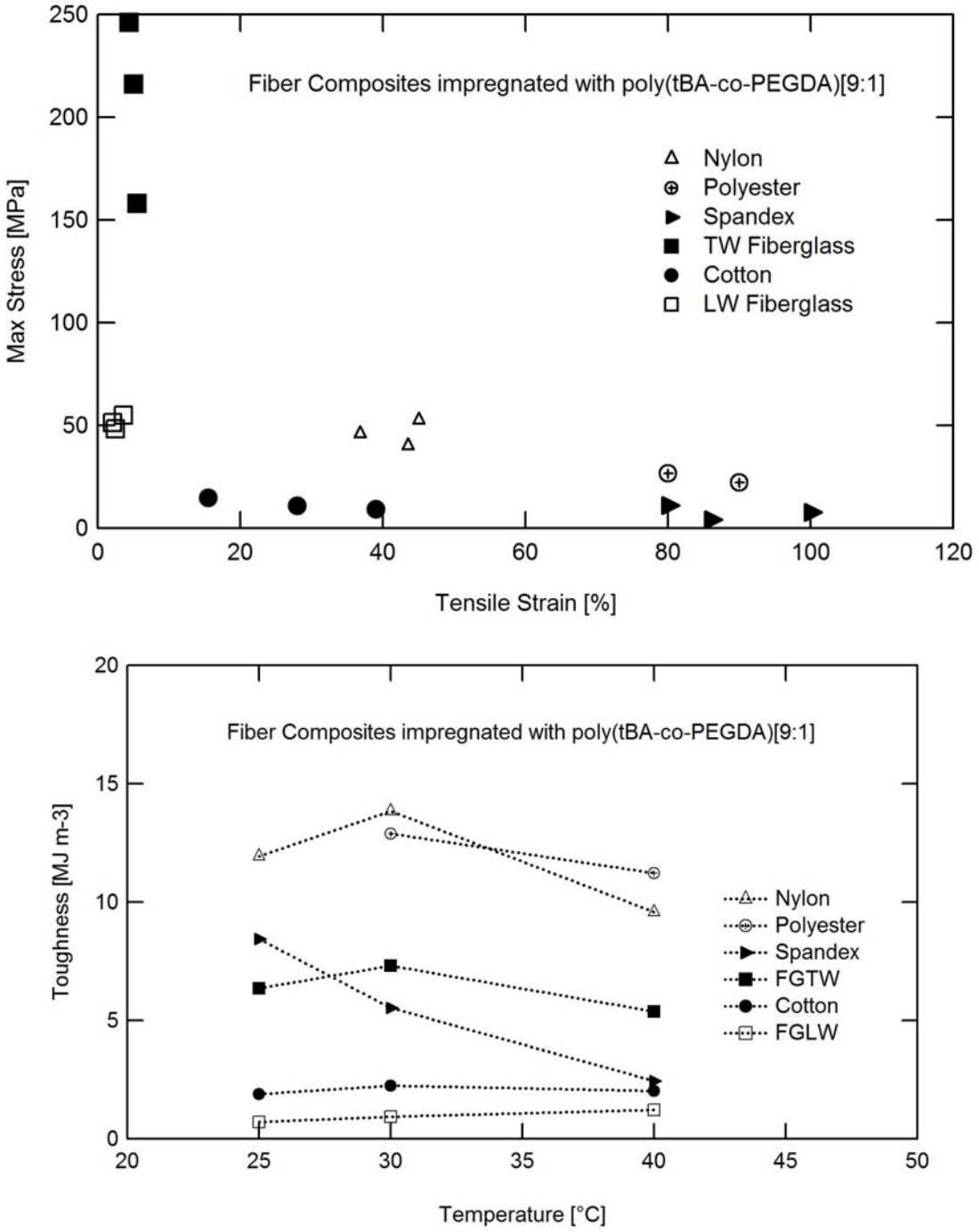

Figure 4. a) The stress-strain endpoints for polymer-impregnated fibers highlight the tradeoff in properties between strain capacity and device strength. b) Toughness as a function of temperature is compared among the different polymer-impregnated fibers. Nylon and Polyester were the most promising casting fiber candidates.

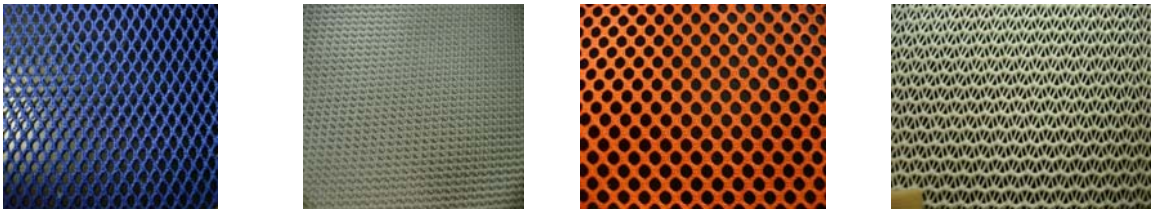

a) b) c) d)

Figure 5. The thermomechanical properties, notably the strain capacity limited device design of a shape-memory polymer orthopedic cast. In the first round of polymers, the polyester fiber provided the best balance of stress, strain and toughness. A new round of fiber selection* including different weave patterns included a) loose-weave navy polyester b) tight-weave white polyester c) loose-weave orange polyester and d) directional weave opaque polyester.

* Kevlar was selected as a candidate but could not be impregnated with the chosen polymers

Figure 4a plots the stress-strain endpoints for each of the aforementioned six composites. Although each stress-strain analysis was conducted at a different temperature (25, 30 and 40 °C), the figure demonstrates that the choice of fiber reinforcement plays a much larger role than a 15 °C temperature shift in the thermomechanical behavior of the polymer composite. Materials are clumped together in clusters based on the underlying fiber in the composite, not on the testing temperature. **Figure 4b** shows toughness as a function of temperature for each of the polymer composites and gives credence for choosing polyester or nylon as a candidate for moving forward and undertaking additional targeted tests. Thus for the second screening round, four new polyester fibers in different weave patterns were selected to continue testing to assess the effect of weave pattern on the composite. The different weave patterns included a) loose-weave navy polyester, b) tight-weave white polyester, c) loose-weave orange polyester, and d) directional weave opaque polyester as pictured in **Figure 5**. Each of these fibers was

pulled in tension until failure both as a fiber and then as a fiber-polymer composite with the same poly(tBA-co-PEGDA) system.

Figure 6 compares the fiber meshes by themselves to the polymer composites. Figure 6a shows the stress-strain response of the fibers alone while Figure 6b shows the stress-strain response of the fiber-polymer composites. What is important to notice is the scale of the y-axis on both figures. The polymer composites are nearly half as strong as the fibers alone, but strain nearly 20% more across the board. The composites strain farther than either the underlying fiber alone or the control polymer system alone in all cases except the opaque polyester. These graphs are representative plots of three duplicate tests run for each system. The other plots can be found in the Appendix. These plots give the first indication that through proper polymer and fiber selection, composites may be manufactured with enhanced *strain capacity.* Combining two materials with lower strain capacities at a certain temperature yields a new material with enhanced strain capacity at that temperature.

The next step is to deduce what effect the crosslinker density of the underlying polymer system has on the ultimate thermomechanical properties of the composite. **Figure 7a** shows two DMA runs of the same material to assess inter sample variability. As the research hones in on a suitable candidate casting material, testing rigor increases with increased number of test samples. The T_g does not move by more than 1 °C and the rubbery modulus varies less than 0.5 MPa. **Figure 7b** demonstrates the effect that the fiber has on the DMA curve. The entire elastic modulus curve is shifted upwards. As the rubbery modulus is proportional to the recoverable force the SMP can exert during

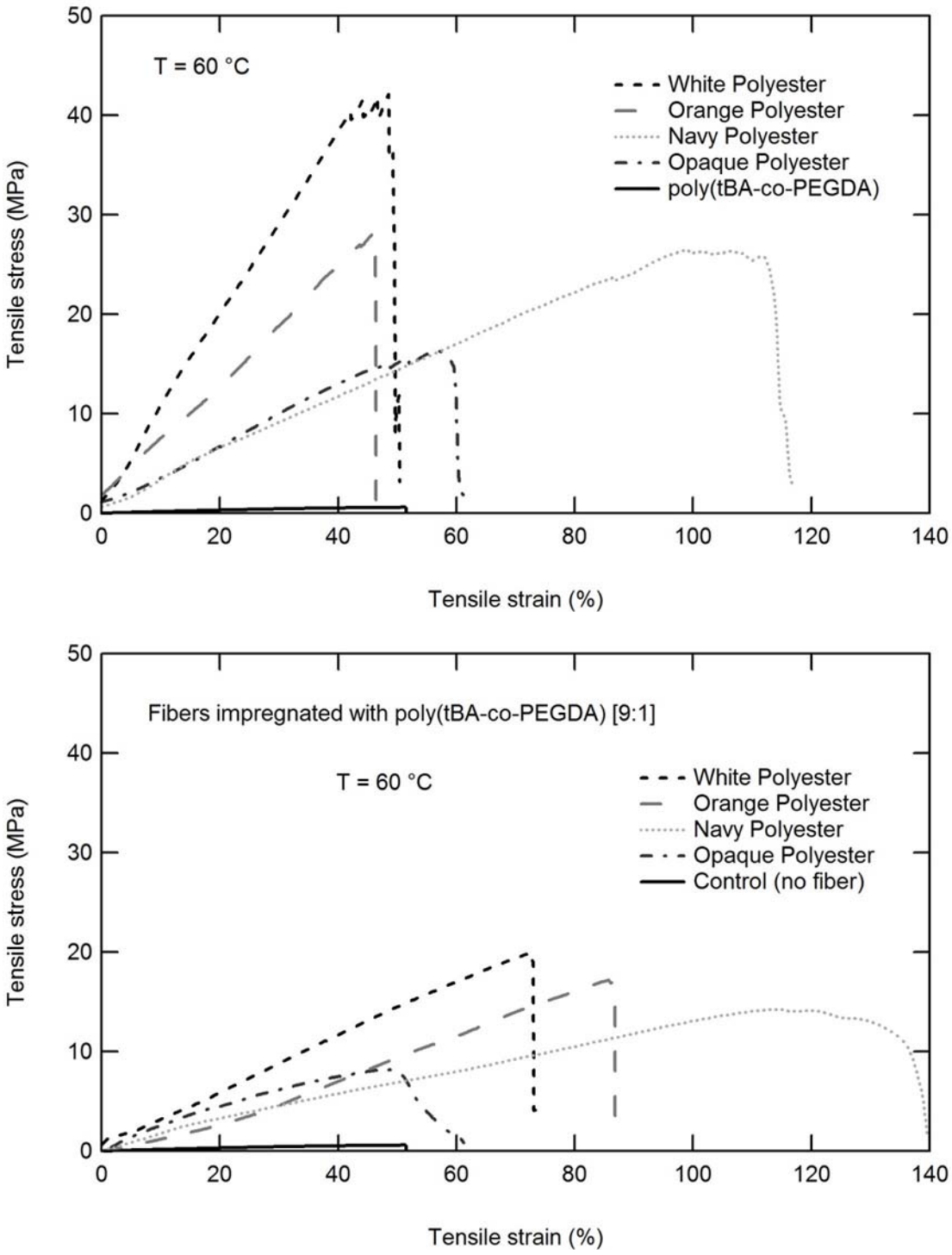

Figure 6. The stress strain response for the a) pure fibers and pure polymer is compared to the b) polymer-impregnated fibers above T_g. Impregnation enhances the strain capacity by roughly 20 to 40% at the cost of reducing tensile stress by a factor of roughly 2.

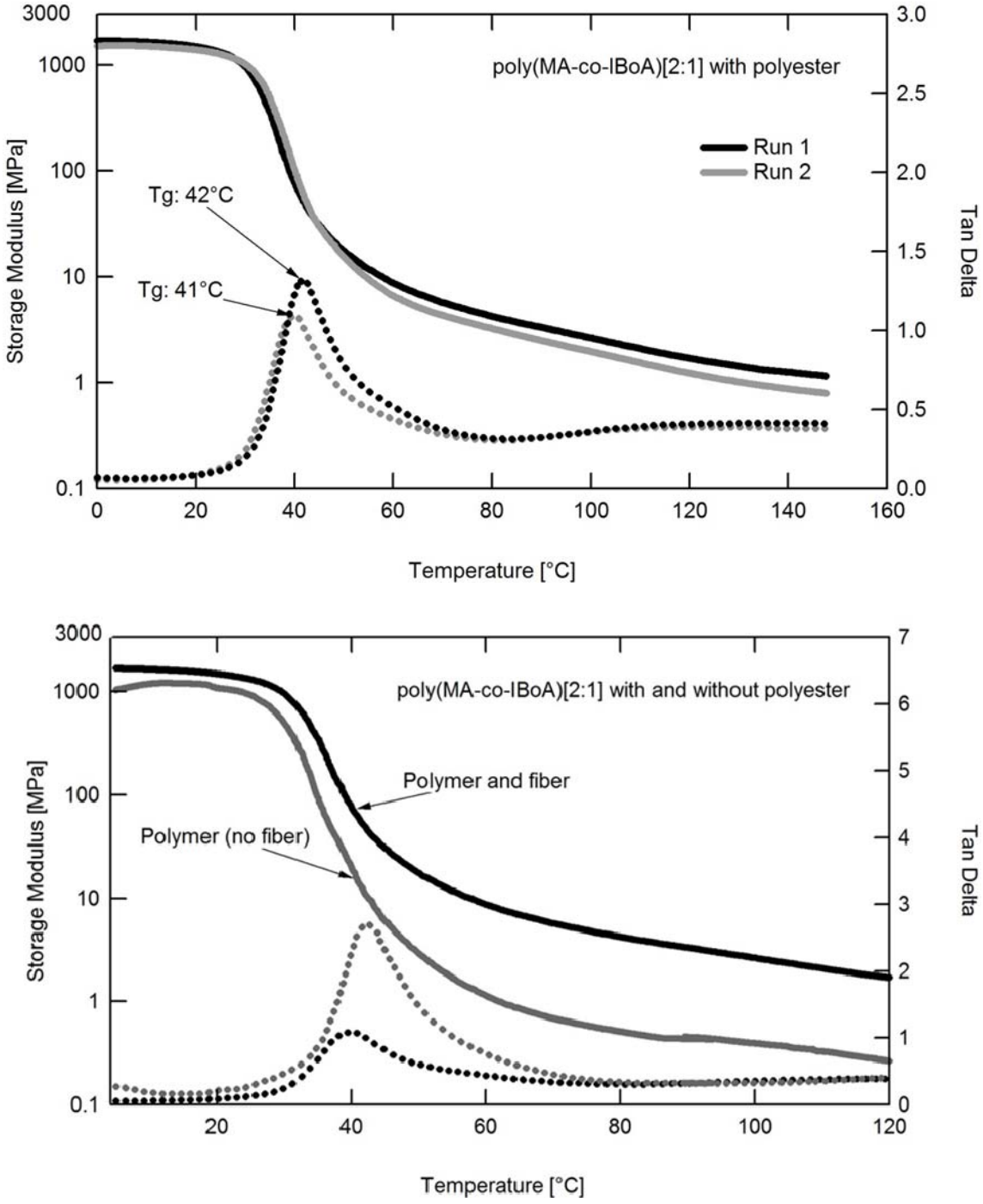

Figure 7. a) A sample size of two for the DMA data gives insight into the variability between samples. The T_g is shifted by less than a degree and the rubbery modulus is different by less than 1 MPa. However, the effect of reinforcing the polymer with a white polyester fiber moves the rubbery modulus by more than 2 MPa.

Table 3. Changing T_g and Onset in Fiber-reinforced SMP samples with 15 wt% BA

#	Wt% of MA	Wt% of MMA	Onset (°C)	DSC T_{trans} (°C)	Tan δ Peak (°C)
1	85	0	4	11	16
2	75	10	9	14	22
3	65	20	10	15	22
4	55	30	14	17	26
5	45	40	18	22	40
6	35	50	35	30	48
7	25	60	42	35	68

deployment, the fiber shows to be superior to the pure polymer in this regard. As the fiber selection progresses, this phenomenon will be quantified in more detail. **Figure 8** explains the effect of altering the ratio of linear monomers MA and MMA in a pure SMP system without fiber reinforcement. The rubbery modulus does not change much while the T_g moves almost 13 °C according to the shift in the peak of the tan delta. The DSC plot also confirms the shift in T_g although the DSC T_{trans} which is derived from a change in heat flow and not a change in chain mobility occurs between onset and T_g as measured by the DMA. **Table 3** presents seven different copolymer systems that were synthesized and assesses the experimental effect on T_g both with the DMA and DSC. As before in the initial screen for a fiber candidate, the initial screens for a suitable polymer system does not involve multiple tests for each different sample, but monitors trends across the sample preparation spectrum. To have firm numbers for each system, multiple tests of each sample would have to be made and compared and this will be done as the soft and

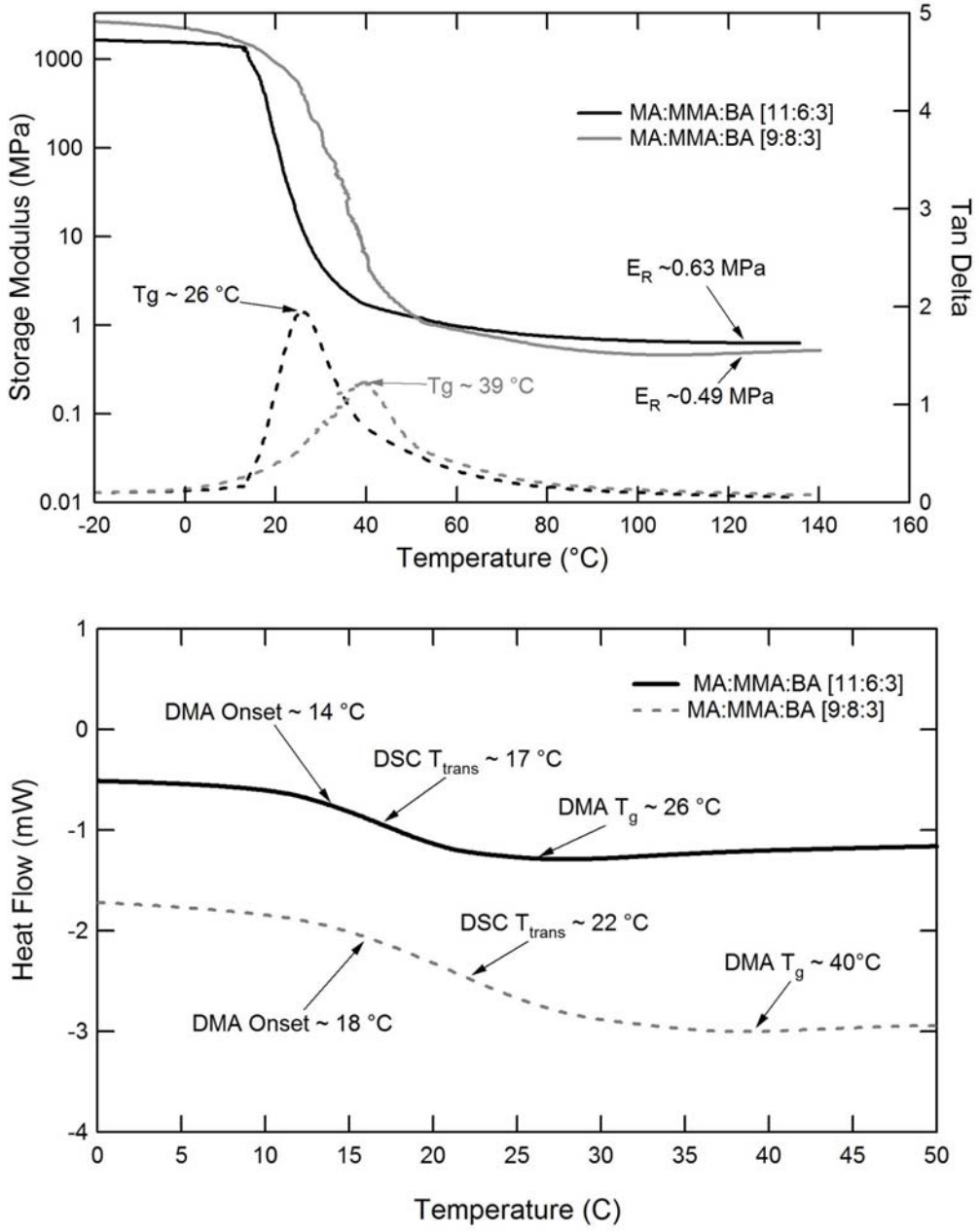

Figure 8. Moving away from the poly(tBA-co-PEGDA) system, a new system that provides independent control over the rubbery modulus and the T_g of the underlying polymer system was chosen. All systems were crosslinked with 2.5 wt% BPAEDMA 1700. a) By altering the ratio of MA and MMA the Tg is shifted by 15 degrees without significantly affecting the rubbery modulus as determined by DMA. b) A similar although smaller shift is observable for the same samples in a plot of Heat Flow and Temperature as determined by DSC.

hard layer SMPs are chosen for the cast. What is important at this point however is the macro scale ability to move T_g by altering the ratios of the chosen linear monomers. This trend is confirmed with both DSC and DMA measurements. As the concentration of MMA to MA increases so too does the T_g. This matches theoretical assumptions for pure polymer systems but had to be confirmed for fiber-composites. The DSC transition falls between the onset and T_g for each sample characterized in the DMA.

Following an assessment of T_g and rubbery modulus, each of the characterized system controls (only polymer) was strained at 22 °C. **Figure 9a** demonstrates the strain-to-failure of different polymer systems (without fibers) with differing T_gs. The maximum strains-to-failure at 22 °C occur in polymer systems whose underlying T_g is near that temperature. However, when composites are tested at T_g, the stress-strain response is very similar for different composites systems as evidenced in **Figure 9b**. Thus the polymer dominates when observing the stiffness of the material while the fiber dominates when assessing the maximum strain-to-failure.

The effect of crosslinker density on solid SMPs is well-known and well-characterized in the literature *[25, 26, 28, 29]*. However the effects of crosslinker density on fiber-composites are much less discussed. Initial results in this study show that when combining a small portion of crosslinker into the underlying polymer system, the effects on the strain-to-failure curve are dominated by the behavior of the fiber, when tested at the T_g of the polymer. These results were observed when impregnating a medium density polyester weave and have not been verified across other fibers. Although many more curves would need to be tested to find a trend here (if it existed), even such a trend would be insignificant in comparison to the effect of the fiber. The fiber plays a larger role in

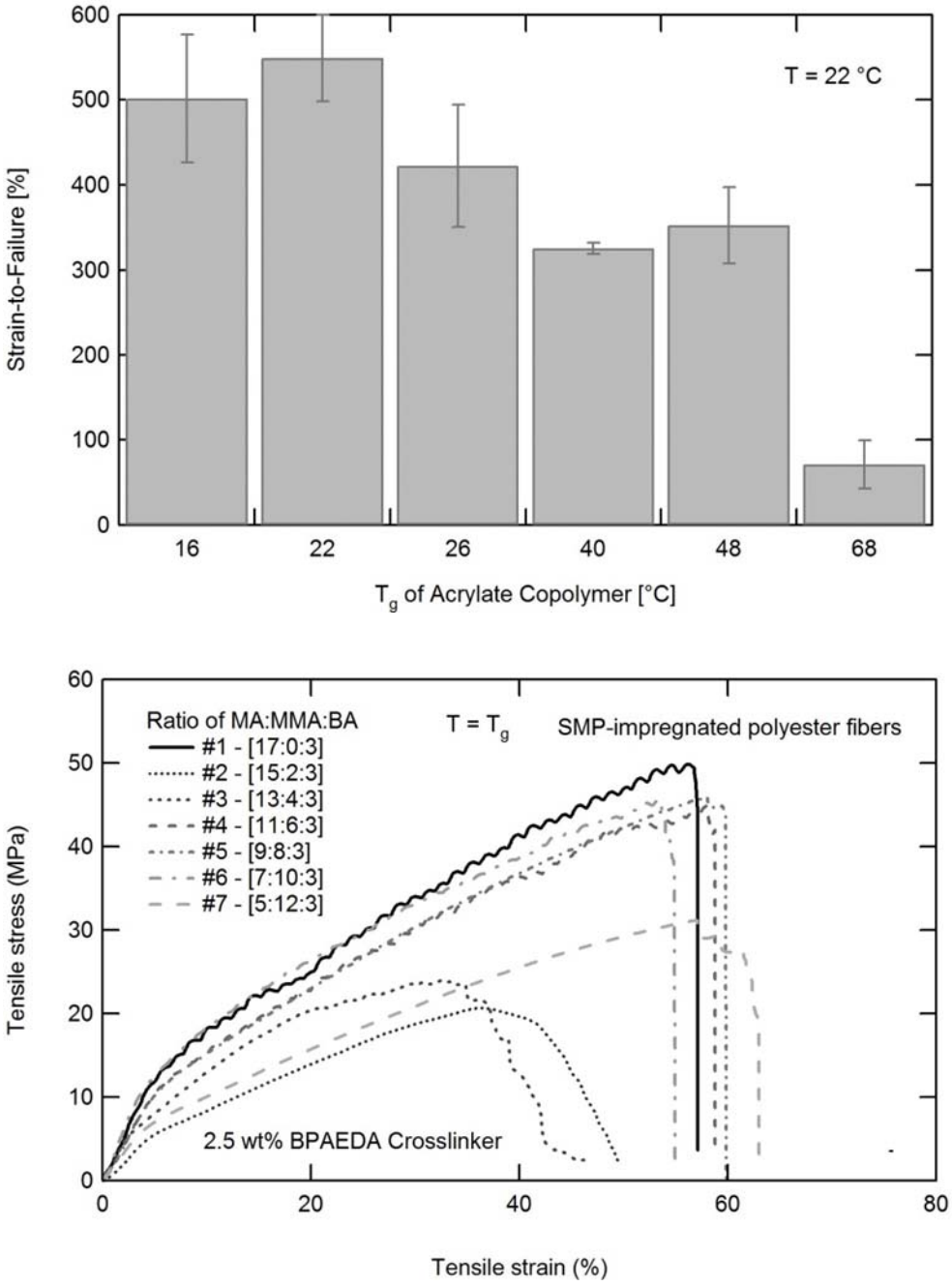

Figure 9. a) When tested at 22 °C, the strain-to-failure of the acrylate copolymers with 2.5 wt% crosslinker is greatest when $T = T_g$. b) However, the stress-strain response of polyester fibers impregnated with various acrylate copolymers is similar when tested at the T_g of the underlying polymer.

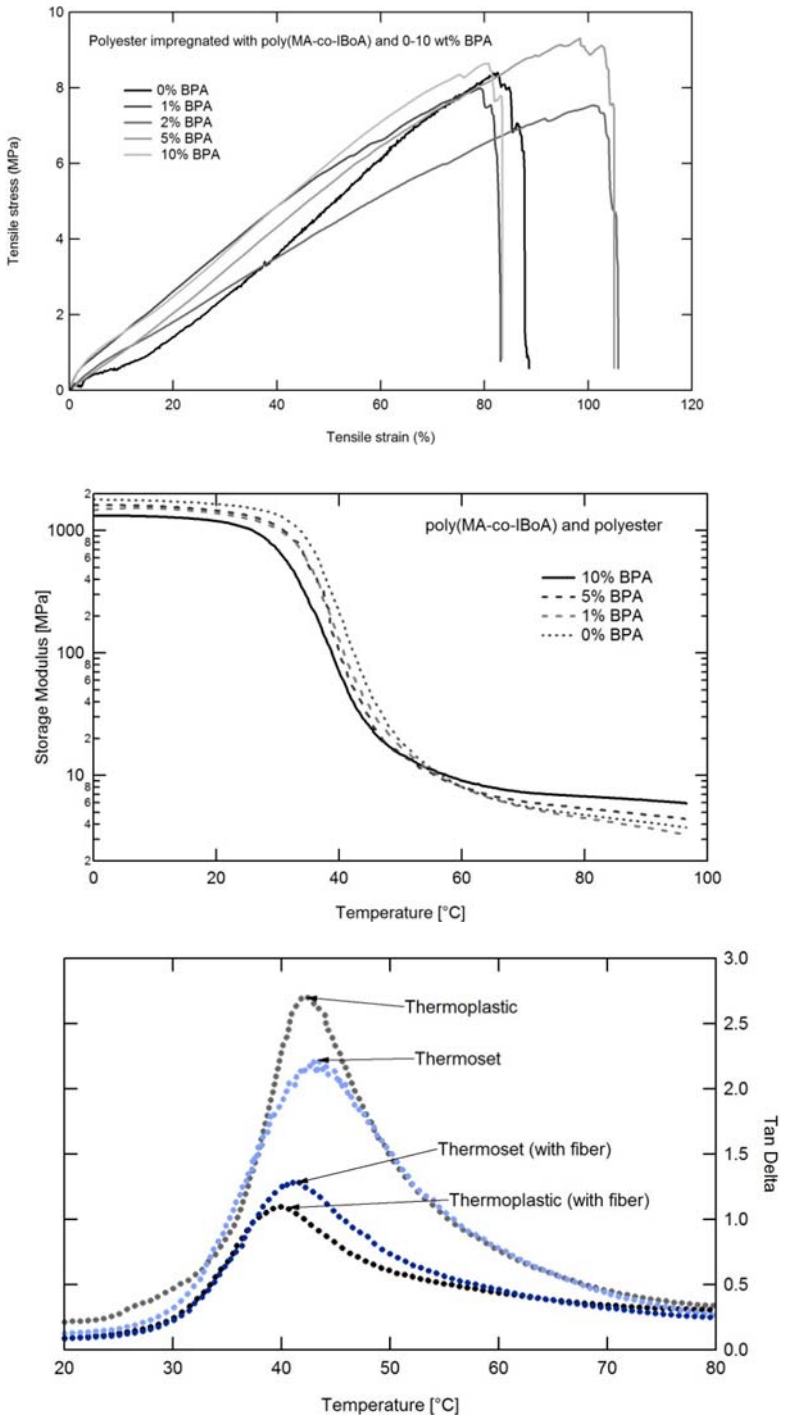

Figure 10. a) Altering the crosslinker concentration between 0 wt% and 10 wt% has a limited effect on the stress-strain response of fiber composites when strained at the Tg of the underlying polymer systems. However, in the rubbery regime b) the effect of increasing crosslinker concentration has a significant effect on the E_R shifting it by more than 3 MPa and c) a significant effect on the shape and peak of the tan delta.

determining the E_R when the concentration of BPAEDMA 1700 in the chosen acrylate copolymer remains below 10 wt% as in **Figure 10a**. However in **Figure 10b** the trend in increasing rubbery modulus is apparent even in fiber composites. Crosslinker density does have an effect, a tunable effect, but an effect that is dominated by the presence of the fiber. Increasing the concentration of BPAEDMA 1700 yields an increasing E_R. **Figure 10c** shows the difference in shapes of tan delta curves for pure polymers and fiber-reinforced polymers with 0 and 1.00 wt% crosslinker and also the difference between pure polymers and fiber-reinforced polymers. The highest tan delta peak is the thermoplastic material with no fiber and no crosslinker because the transition at T_g is the narrowest. Adding copolymers or fibers increases the broadness of the transition and drops the peak of tan delta.

Figure 11a and **11b** are the takeaway analysis from the initial work presented in this Chapter. Figure 11a shows the stress-strain endpoints of a wide variety of new fibers selected for their potential to experience large strains. The supporting stress-strain curves from which these points were generated are shown in the Appendix. Figure 11b repeats the stress-strain endpoints for one particular fiber from Figure 11a—the antares nylon lycra—and shows the stress-strain endpoints for a selected poly(MA-co-IBoA-co-BPAEDA) SMP. It also shows the properties of the polymer-fiber composites. These materials experience enormous strain near 400% but at stresses on the order of casting tapes on the market today. The anteres nylon lycra composites have toughness metrics around 36 mJ cm^{-3}.

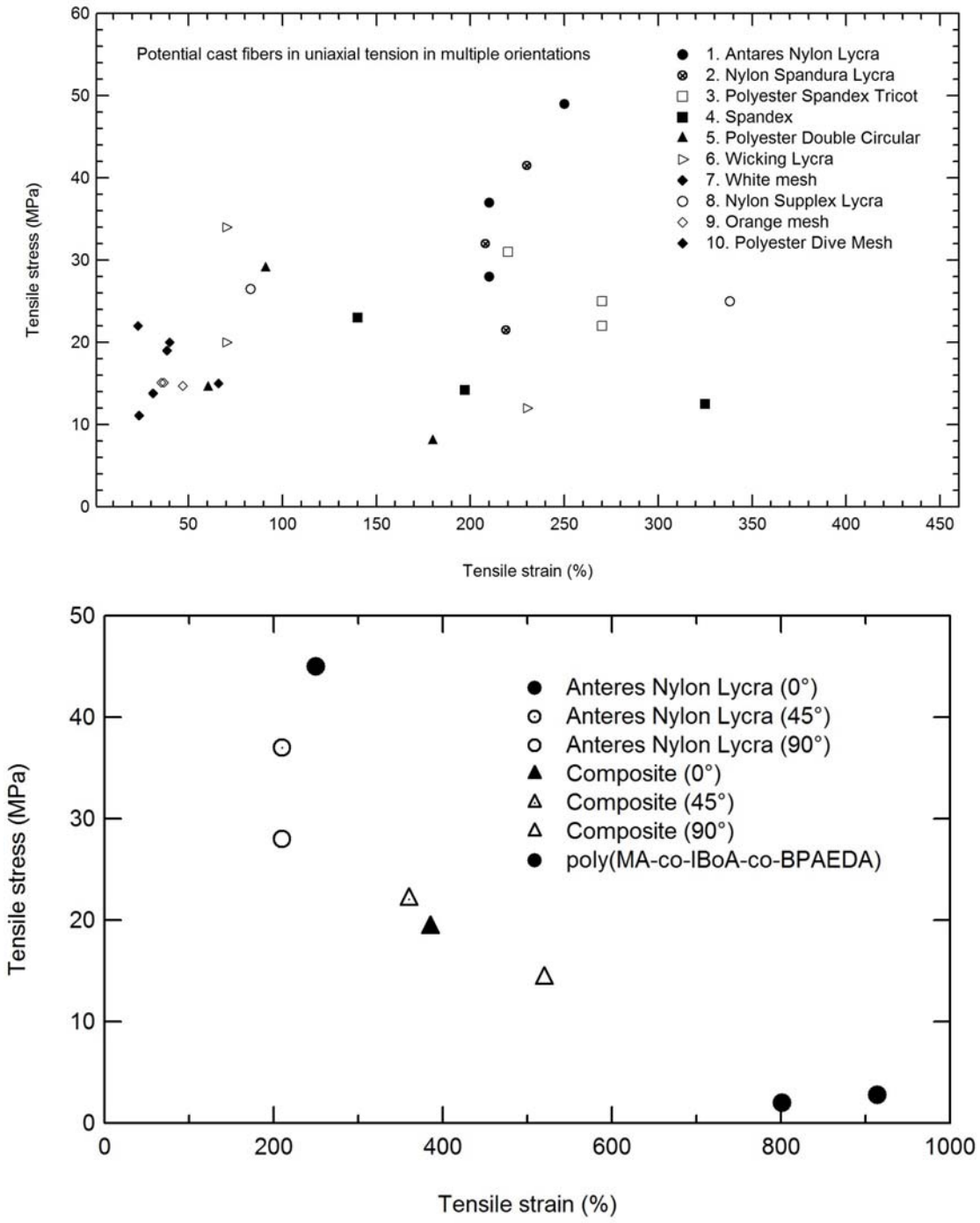

Figure 11. a) The stress strain endpoints of a multiple potential cast fibers each tested in three different orientations. The Anteres Nylon Lycra showed the best combination of strain capacity and strength. b) The anteres nylon lycra is impregnated with a poly(MA-co-IBoA-co-BPAEDA) and compared against the pure polymer sample. The composite yields thermomechanical properties in the range for a potential shape-memory polymer orthopedic cast, with strains upwards of 400% and strength near 20 MPa.

Thus after a pseudo rigorous materials selection process, several new technical drivers were established and utilized to create a new material with unique properties. The effect of crosslinker density on various fibers with various polymers is an open technical problem. It is unclear whether other fibers beyond the nylon and polyester in this study will behave similarly. It is also impossible to draw conclusions about the effect of larger concentrations of crosslinker on the fiber composites. As this research sought to derive methods to explore the new paradigm in enhancing strain capacity, necessary limits were placed on the maximum crosslinker concentration mixed into the underlying polymer. All of the presented stress-strain tests were also performed at a constant rate. One batch of variable rate tests showed dramatically different properties (toughness and max strains) when the fibers were stretched more quickly. This deserves additional attention and scrutiny.

6.5 Material Selection

The takeaway result from the previous section was that anteres nylon lycra impregnated with an acrylate copolymer system in which the T_g and E_R can be tuned, that also yields a large toughness, could be a suitable candidate for an orthopedic shape-memory polymer cast. The next step would be to assess mass-manufacture of the anteres nylon lycra composites. This necessitates an exploration into crosslinkers such as TMPTA instead of BPAEDA or PEGDA that lend themselves well to the *Mnemosynation* process and compare these samples to polymers crosslinked with BPAEDA. **Figure 12** compares the poly(MA-co-IBoA)-anteres nylon lycra composites that are crosslinked with TMPTA with poly(MA-co-IBoA)-anteres nylon lycra composites crosslinked with

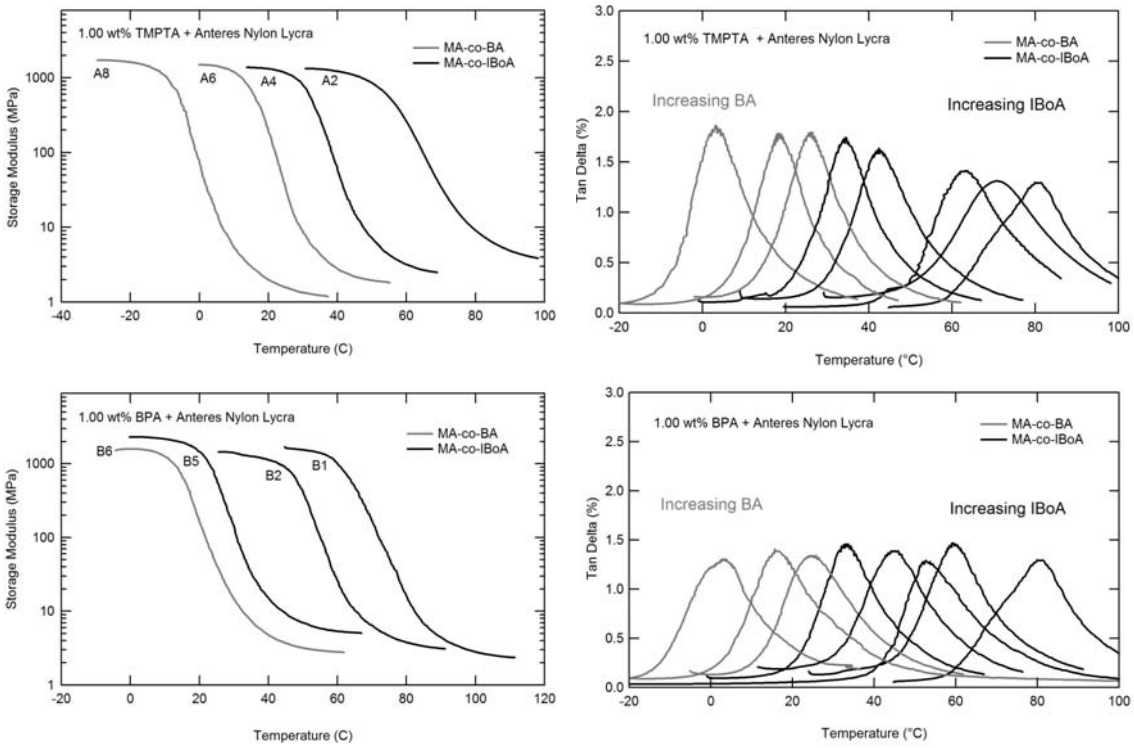

Figure 12. TMPTA is used as a crosslinker and different acrylate copolymers with fiber reinforcement are seen in a) elastic modulus curves and a function of temperature and b) peaks of tan delta as a function of temperature. Similarly, BPAEDA is used a s a crosslinker and different acrylate copolymers with fiber reinforcement are seen in c) elastic modulus curves and a function of temperature and d) peaks of tan delta as a function of temperature.

BPAEDA. Figure 12 demonstrates the ability to move T_g in both systems by presenting the change in elastic modulus as a function of temperature and the peaks of tan delta for the different systems. A shift was also made to use the linear monomer IBoA instead of MMA for the same reasons described in Chapter 4. For the materials to be mass manufactured, the Mnemosynation process will be employed. This necessitates post-curing the composite with e-beam radiation to crosslink the material. Since PMMA derivatives will undergo chain scission and ruin the mechanical integrity of the cast, IBoA was chosen as a replacement ingredient because it lacks a ternary carbon in the

Table 4 – Thermomechanical properties of various fiber-reinforced acrylate copolymers

Acrylate Copolymer Compositions				
#	**MA**	**IBoA**	**BA**	**XL**
A1	25	75	0	TMPTA
A2	45	55	0	TMPTA
A3	60	40	0	TMPTA
A4	75	25	0	TMPTA
A5	95	5	0	TMPTA
A6	90	0	10	TMPTA
A7	70	0	30	TMPTA
A8	50	0	50	TMPTA
B1	25	75	0	BPA
B2	45	55	0	BPA
B3	60	40	0	BPA
B4	75	25	0	BPA
B5	95	5	0	BPA
B6	90	0	10	BPA
B7	70	0	30	BPA
B8	50	0	50	BPA

	Control Samples				Fiber-Reinforced			
#	T_g (°C) (Tan δ)	T_g (°C) (DSC)	Onset (°C)	E_R (MPa)	T_g (°C) (Tan δ)	T_g (°C) (DSC)	Onset (°C)	E_R (MPa)
A1	75	53.2	58.9	0.62	75.3	59.2	61.9	2.97
A2	60	36.0	46.5	0.69	70.8	41.66	54.4	3.88
A3	50	28.5	36.8	0.90	63.3	33.1	50	3.72
A4	39	22.9	29.1	0.70	42.4	23.8	31.7	2.35
A5	31	13.5	21.2	0.97	34.4	15.2	24.2	4.03
A6	24	6.3	13.1	0.98	26.0	7.3	15.6	1.50
A7	13	-6.1	2.0	0.97	18.3	-6.1	8.0	1.40
A8	0	-19.5	-10.9	0.84	3.3	-19.9	-7.0	1.20
B1	75	62.2	57	0.58	80.7	-	64.6	2.36
B2	55	42.0	57.1	0.61	59.6	-	48.7	3.12
B3	49	28.2	37.9	0.40	49.7	-	38.2	4.75
B4	37	21.1	25.9	0.79	44.6	-	34.1	3.98
B5	31	12.9	20.9	1.14	33.1	-	24.3	4.03
B6	26	6.2	15.5	1.10	25.2	-	13.6	2.79
B7	12	-6.4	1.3	0.86	22.2	-	10	5.30
B8	0	-19.5	-11.2	0.69	2.9	-	-6.4	1.6

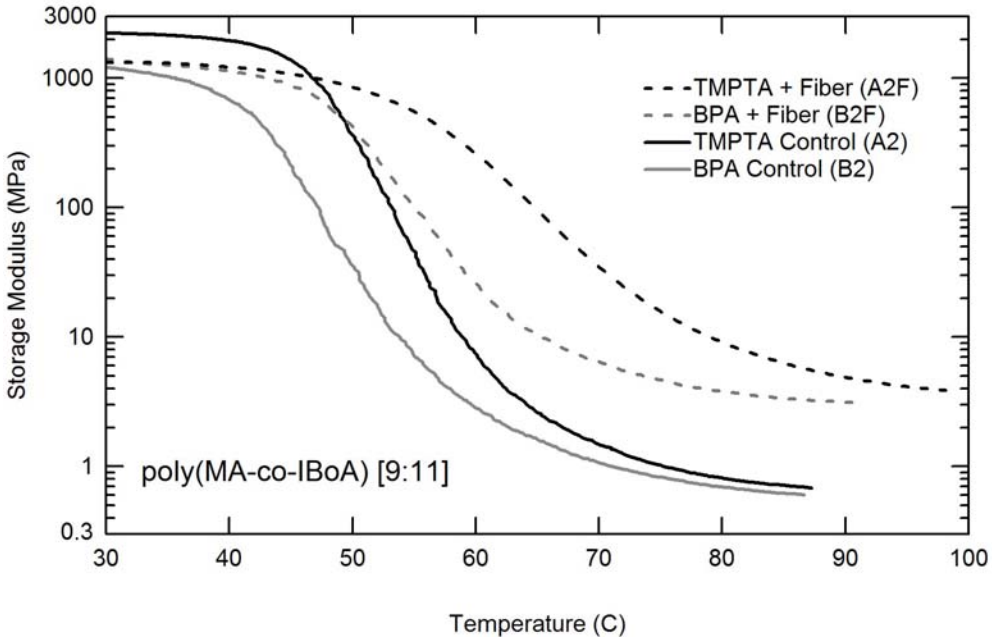

Figure 13. The DMA curves for the hard inner layer of the cast. The elastic modulus as a function of temperature of poly(MA-co-IBoA) in a 9:11 ratio with 1.00 wt% crosslinker (TMPTA and BPAEDA) both with and without anteres nylon lycra reinforcement.

backbone after it has been polymerized. The specific systems studied are labeled A1 to A8 (with TMPTA) and B1 to B8 (with BPAEDA) and the compositions are presented in **Table 4**. Table 4 further shows the T_g (both as determined by the DMA and DSC) and the E_R as a function of changing the underlying ratio of MA to IBoA or BA.

Figure 13 shows the effect of fiber-reinforcement on the chosen poly(MA-co-IBoA) polymer systems. When compared with controls which are pure polymers of the same compositions, the impregnated fibers show higher E_R by an order of magnitude. In this figure, the underlying polymers are the A2 and B2 polymers which consist of MA and IBoA in a 9 to 11 ratio with 1.00 wt% of TMPTA and BPAEDA respectively. This polymer has been selected with a T_g near 60 °C to serve as the candidate for the hard inner layer of the cast.

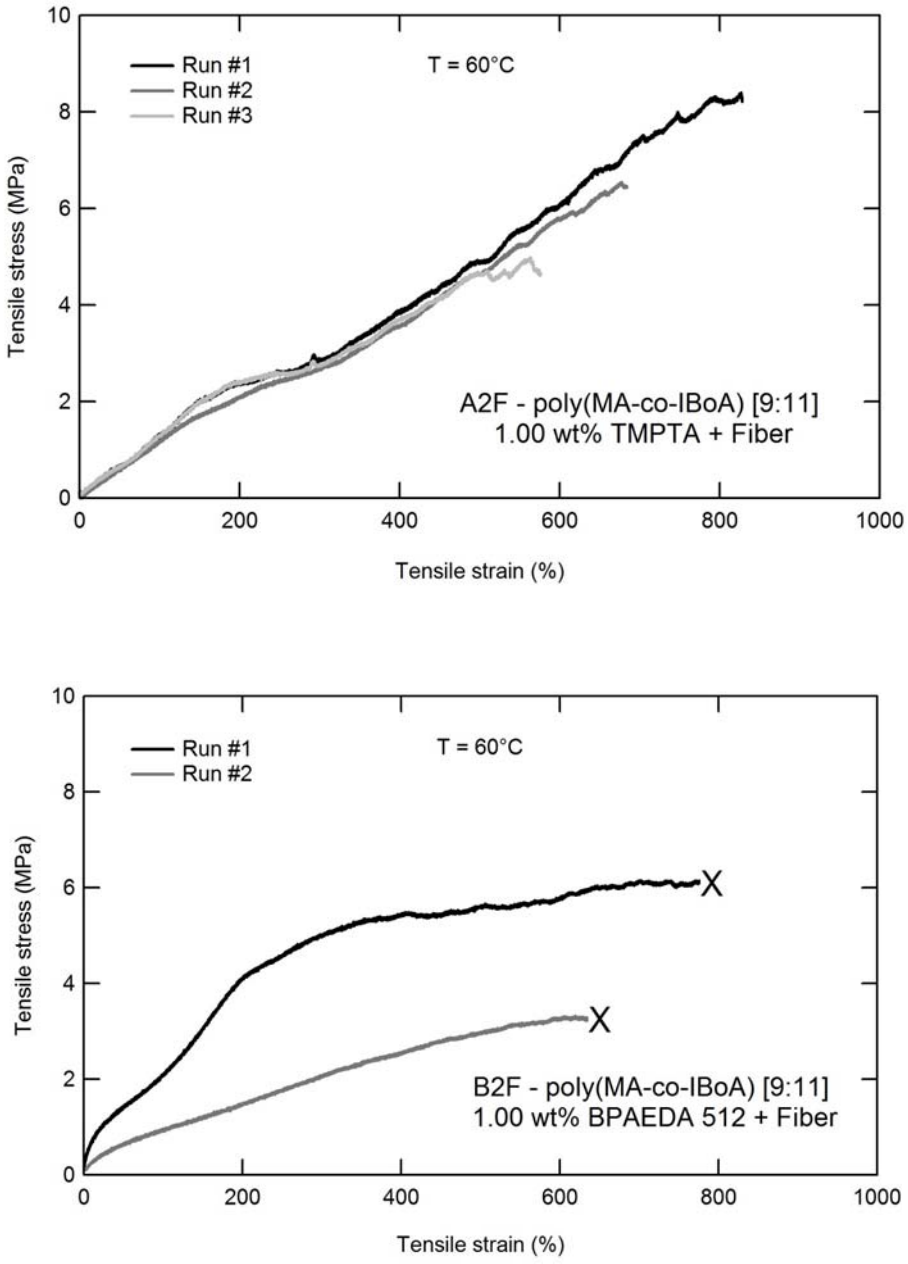

Figure 14. The stress-strain response (sample size of 3) of poly(MA-co-IBoA) in a 9:11 ratio with 1.00 wt% a) TMPTA crosslinker and b) BPAEDA 512 crosslinker when tested near Tg at 60 °C. The absolute strains are inaccurate although the order of magnitude is correct due to contributions from the grips sections because strain was measured with crosshead displacement. Special methods developed in Chapter 3 estimate actual strains to be roughly 1/3 the value of the collected data.

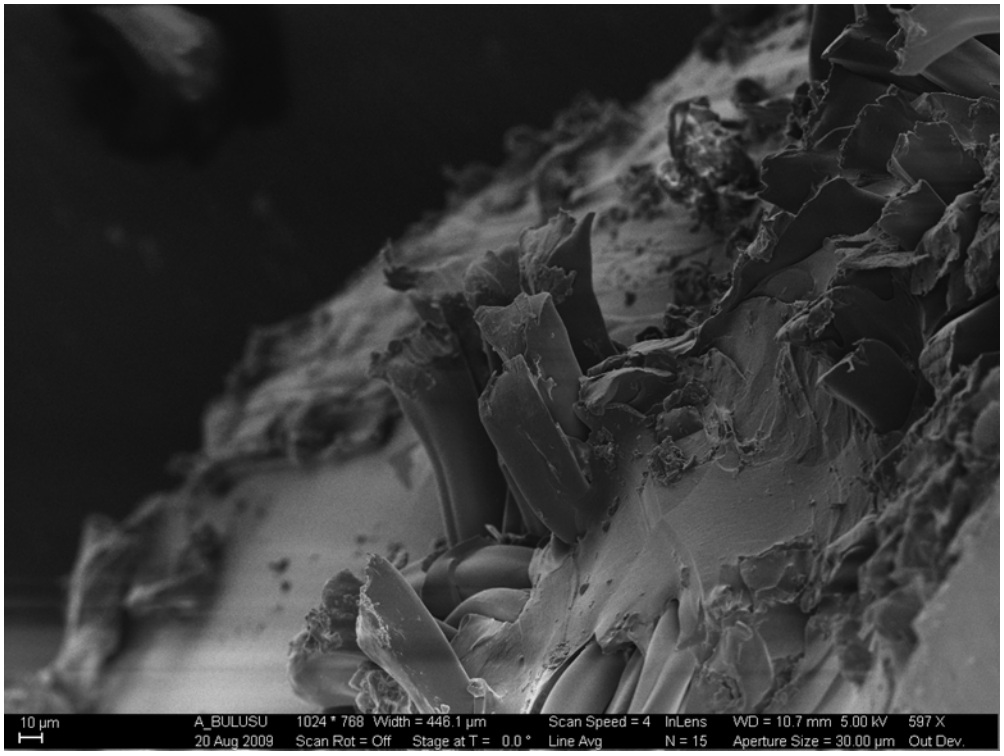
10 µm
A_BULUSU 1024 * 768 Width = 446.1 µm Scan Speed = 4 InLens WD = 10.7 mm 5.00 kV 597 X
20 Aug 2009 Scan Rot = Off Stage at T = 0.0 ° Line Avg N = 15 Aperture Size = 30.00 µm Out Dev.

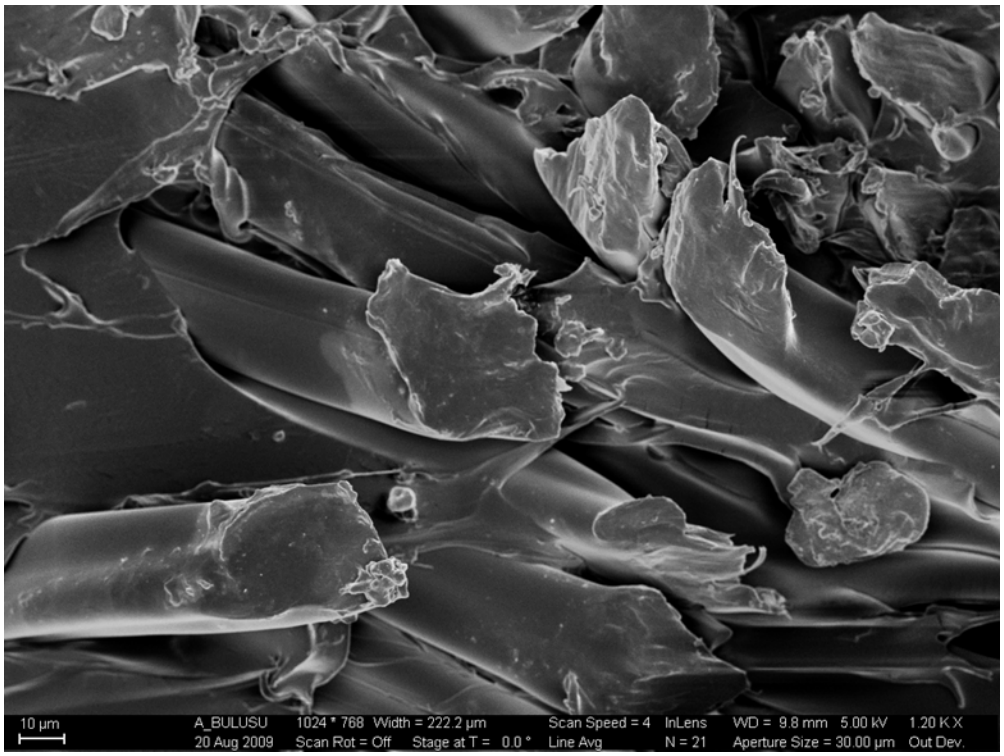
10 µm
A_BULUSU 1024 * 768 Width = 222.2 µm Scan Speed = 4 InLens WD = 9.8 mm 5.00 kV 1.20 K X
20 Aug 2009 Scan Rot = Off Stage at T = 0.0 ° Line Avg N = 21 Aperture Size = 30.00 µm Out Dev.

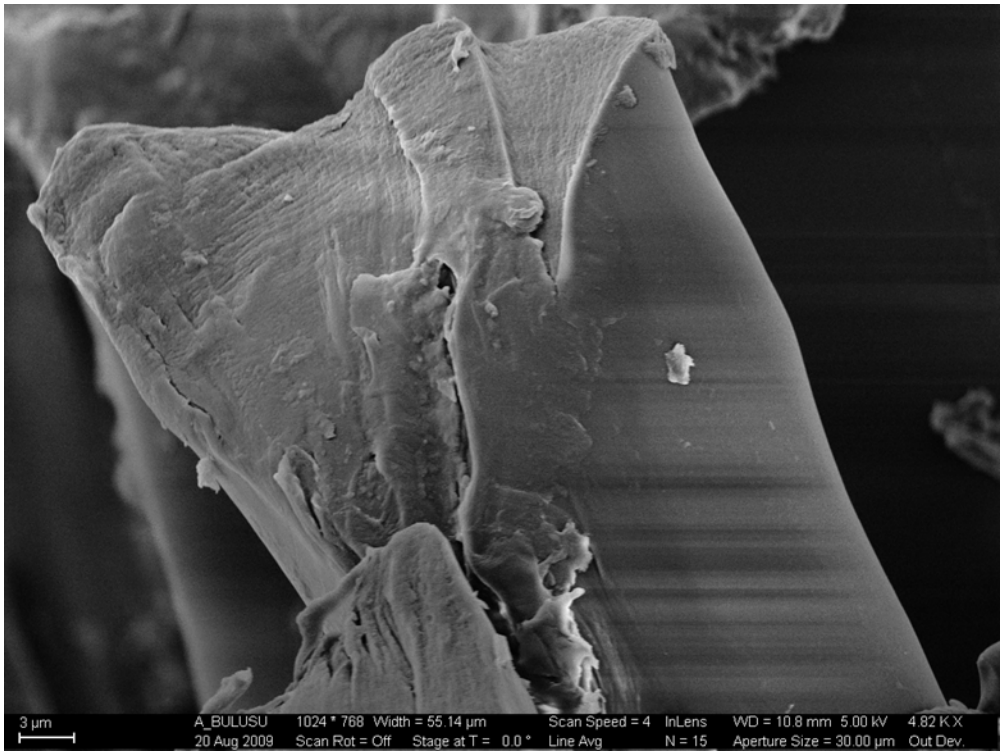

Figure 15. SEM images at increasing magnification of poly(MA-co-IBoA) in a 9:11 ratio with 1.00 wt% TMPTA crosslinker.

Figure 14a shows the stress-strain response of three runs of the A2F material when tested at 60 °C which is near the T_g of the poly(MA-co-IBoA) in the 9 to 11 ratio. Some sample variability, especially in the strain-to-failure metric is observed.

Figure 14b shows the stress-strain response of three runs of the B2F material when tested at 60 °C which is also near the T_g of the underlying polymer. The shapes of these curves are different than those crosslinked with TMPTA due to the different functionalities and molecular weights of the crosslinkers. The TMPTA system is more heavily crosslinked as it is a trifunctional acrylate.

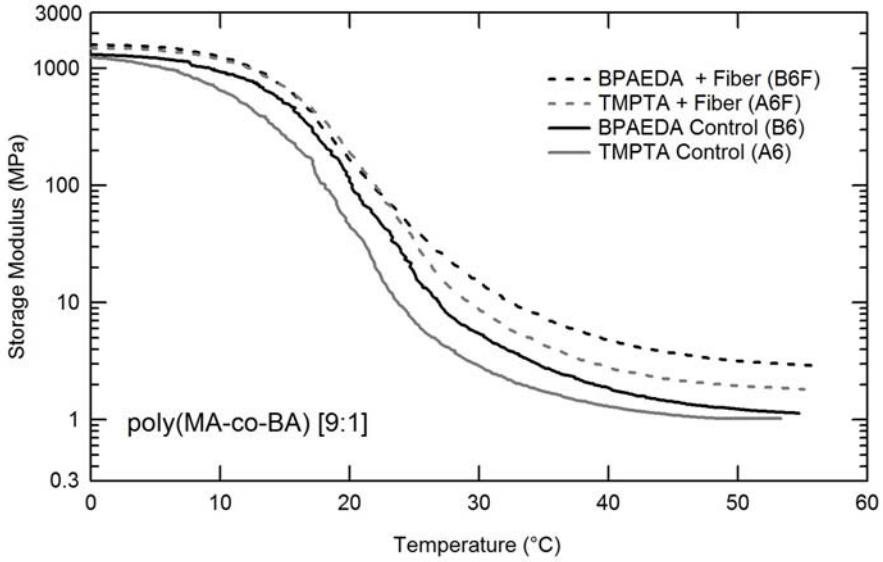

Figure 16. The DMA curves for the soft outer cast layers that are viscoelastic at room temperature.

Figure 15 shows SEM images at increasing magnification of the polymer-fiber interaction. Part (a) is magnified nearly 600x while part (b) is magnified 1.2kX and part (c) is magnified 4.8kX. The images were taken on a cut edge of the composite. The interaction of the polymer and fiber is best observed in the 1.2kX magnified image as the fibers appear to emerge from a polymer casing.

Figure 16 is similar to Figure 13 in that it presents a comparison of elastic modulus as a function of temperature of a chosen fiber-reinforced acrylate copolymer. However the samples represented in this curve are the polymers that would comprise the soft outer layer of the casting sleeve with a T_g near room temperature. Thus the materials are viscoelastic and least likely to tear or suffer brittle fracture during normal operating temperatures. The response of the hard and soft layers is confirmed by the DSC in **Figure 17**. Two distinct transitions in heat flow are observed between 0 and 50 °C representing

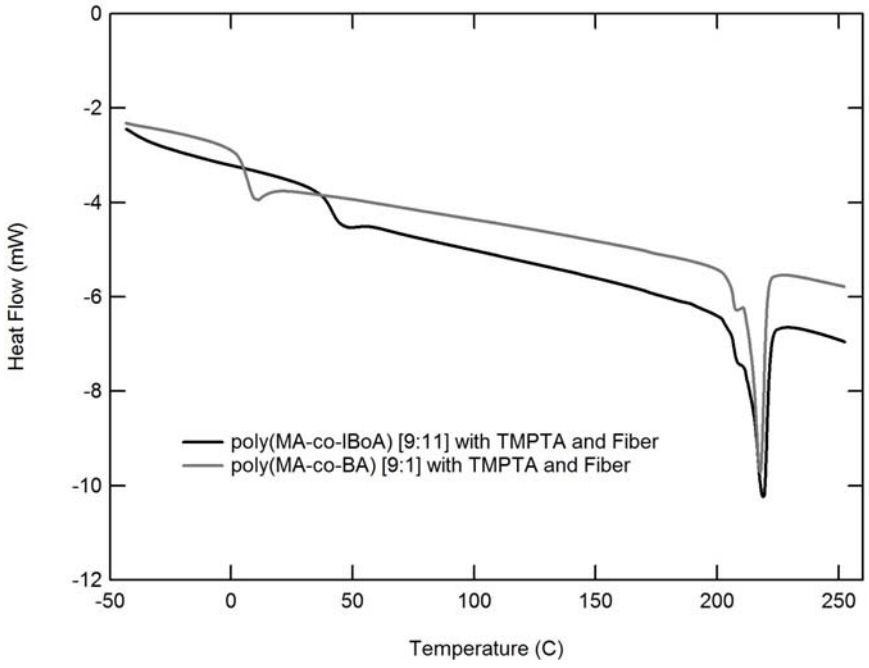

Figure 17. The DSC response of the two selected cast layers, the soft outer layer and the hard inner layer. The dips near room temperature and near 50 °C represent the change in heat flow during the Tg phase change while the large exotherm at 210°C represents the melt peak of the nylon fiber.

the two casting layers. Both composites show the large melting exotherm as the nylon interior of the samples melts near 225 °C.

Figure 18 examines the behavior of the hard inner layer polymer both with and without fiber at room temperature. Strains are extremely low (around 2-3%) and the stresses are consistently above 20 MPa. However the soft outer layer when strained at room temperature which is close to its T_g shows large strains and low stresses as seen in the three repeat runs of **Figure 19**. Thus combining these two polymer layers into a single casting device yields optimum properties in several different temperature scenarios: during use the outer layer will be soft and accommodating and the hard inner layer will maintain the rigidity necessary for compression; during shape fixing the hard inner layer

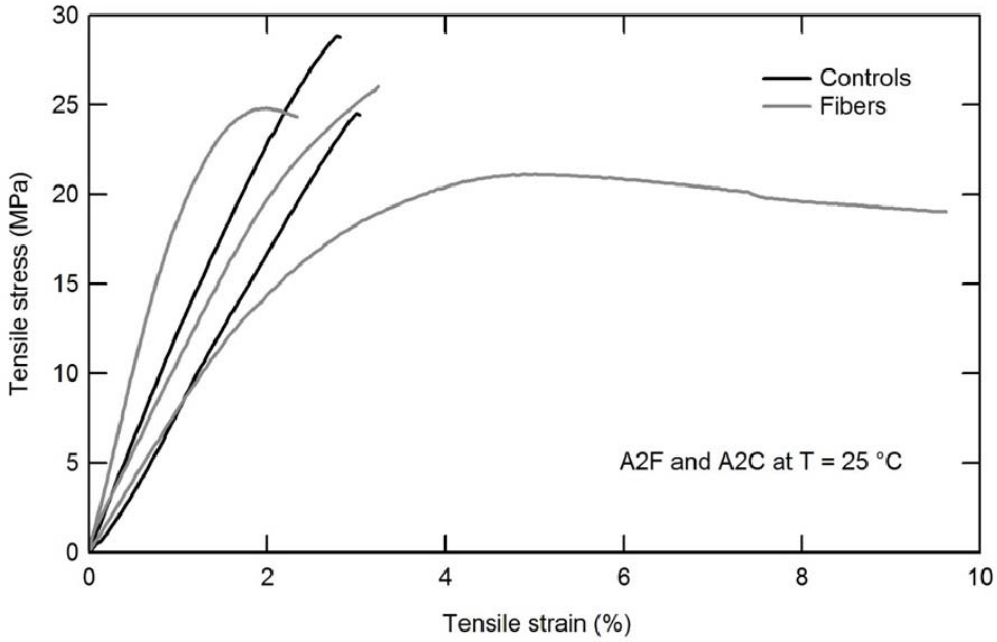

Figure 18. The stress-strain behavior of the hard inner layer as a polymer and a composite at room temperature .

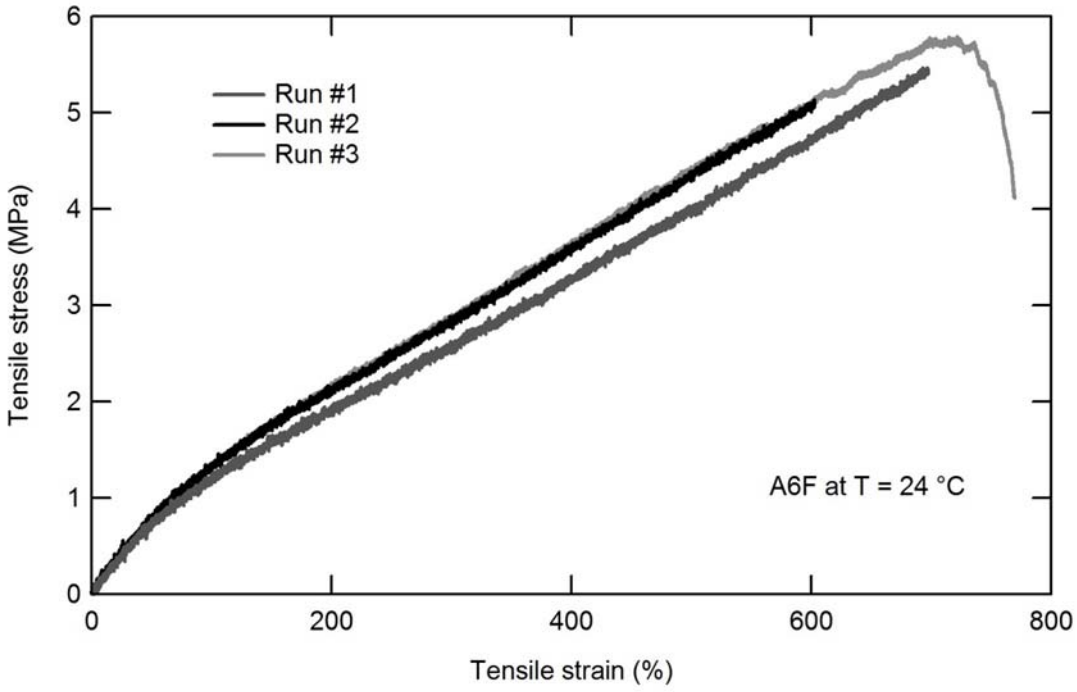

Figure 19. The stress-strain behavior of the soft outer layer at room temperature.

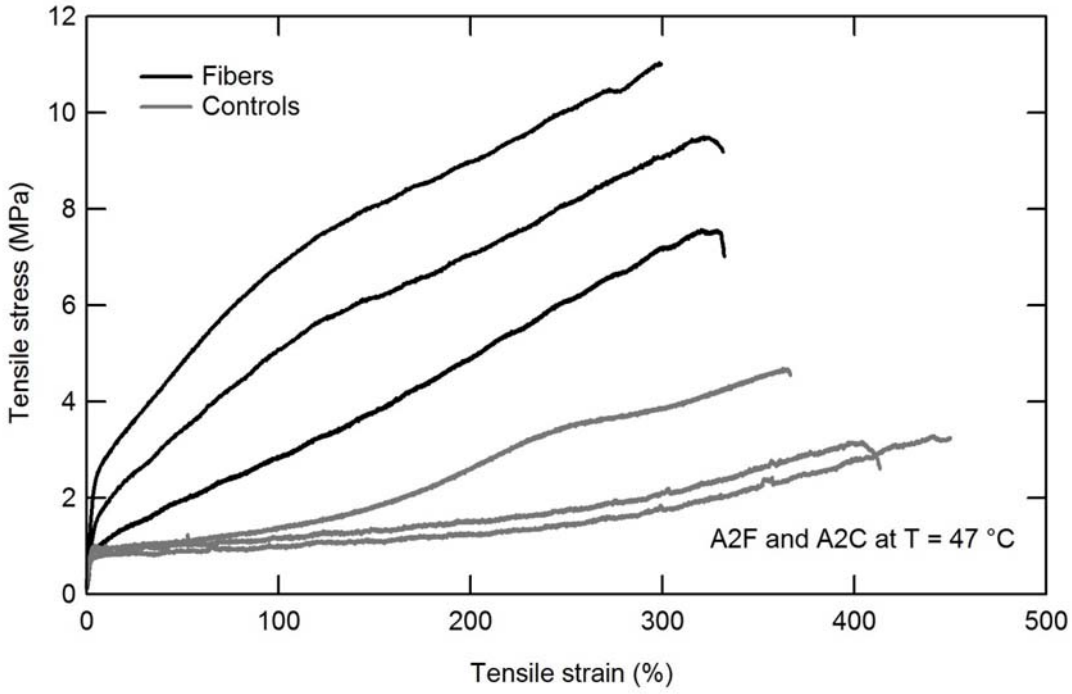

Figure 20. The behavior of the hard inner layer with and without fiber at 47 °C.

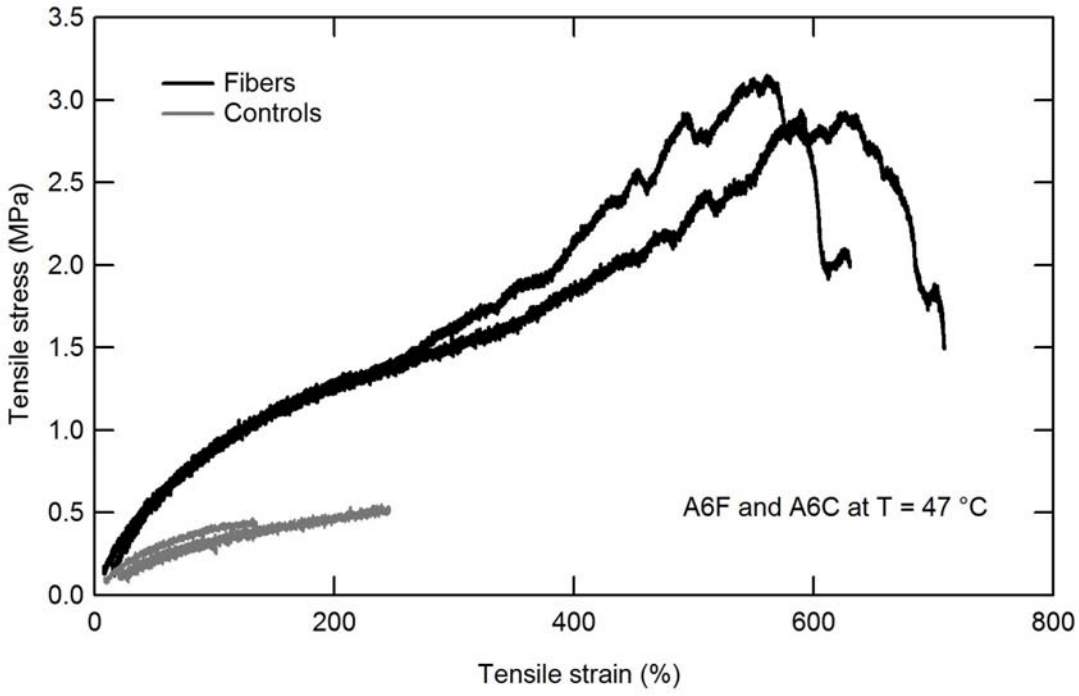

Figure 21. The behavior of the soft outer layer with and without fibers at 47 °C.

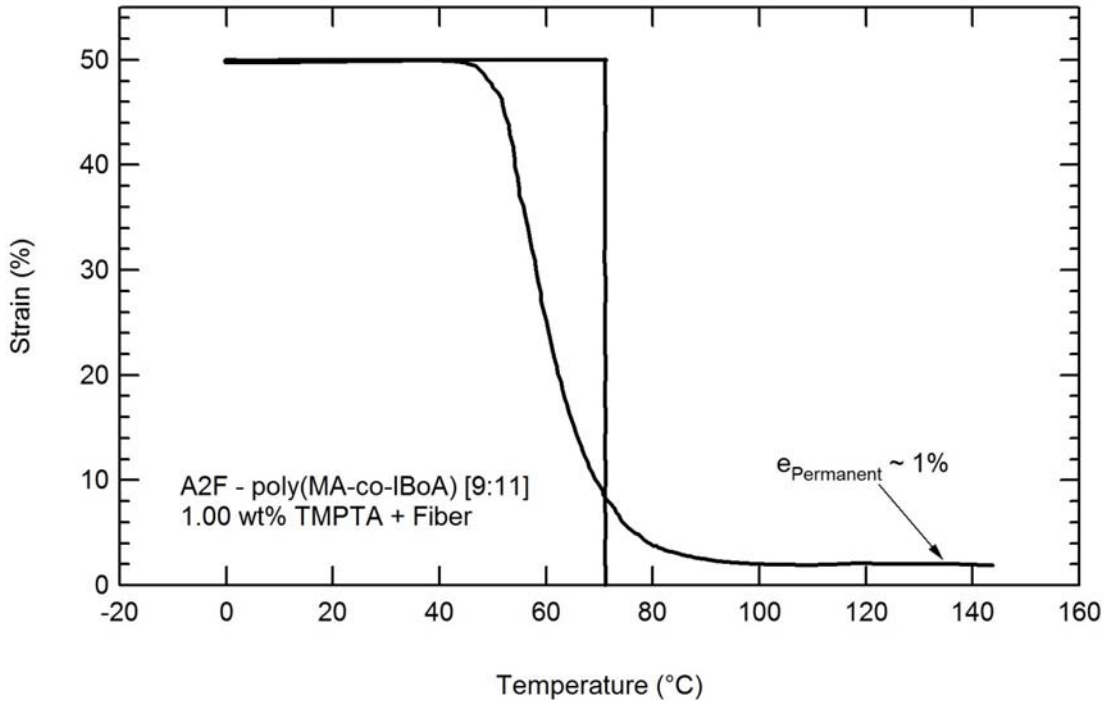

Figure 22. The free strain recovery plot of the hard inner layer with fiber. Shape fixity is near 100% while the residual strain after a full shape-memory cycle is roughly 1% when strained to 50%.

will soften and allow the large strain shape change necessary for the casting sleeve. **Figure 20** shows the stress-strain response of the hard inner layer, both with and without fiber at the predicted training temperature or the temperature at which the sleeve will be deformed into its temporary shape. All materials show large strains with and without the fiber reinforcements. **Figure 21** shows the stress-strain response of the soft outer layer at 47 °C. The control samples (polymer only) fail at much lower strains than do the composites. **Figure 22** presents evidence that the hard inner layer chosen is indeed a shape memory polymer. The temporary shape can be well fixed (shape fixity is near 100%) while the residual strain upon recovery is low.

6.5 Conclusion

Although further studies are necessary to utilize the *Mnemosynation* manufacturing technique to synthesize and crosslink new cast sleeve prototypes, proof of concept has been developed in this initial exploration. Many fundamental technical problems have been unearthed and limited direction toward solutions to these problems has been established within this initial data. However, much work remains. With the high sample variability in composites, a greater sample size is needed in several of the presented figures before accurate values for strain-to-failure can be established. While the data as collected serves to establish relative trends among polymer systems, the lack of sophisticated methods to measure accurate strains hampers the analysis and conclusions. A large swath of fibers was characterized. Each fiber was tested alone and in conjunction with different SMP networks. This research ushers in a new paradigm in SMP composites manufacture—namely that materials can be designed to enhance the strain capacity rather than the maximum strength. Anteres nylon lycra was chosen as a potential candidate to serve as the central fiber layer in an SMP casting device. An SMP with a high T_g was chosen to surround this fiber and serve as the shape fixing component in the cast. A softer, lower T_g polymer was selected as a potential outer layer for the casting device. Both layers, with and without fiber-reinforcement were characterized at different temperatures. Remaining work is required to build and test a two layer composite material. Remaining work also remains to integrate the *Mnemosynation* manufacturing technique into the large strain composite application to enable low-cost scale up to compete with current market solutions. Once this is complete, cylindrical fiber weaves must be made and VARTM techniques employed to evenly distribute thermoplastic resin

across the fiber in the correct ratios. This must be accomplished with both layers. Devices made with VARTM must then also be subjected to e-beam radiation for the post-crosslinking during the last step of Mnemosynation. Additional studies concerning breathability and aesthetics would also need to be undertaken, as would the effects of moisture and an aqueous environment on the casting sleeve. Thus the research presented has made significant progress toward a functioning shape-memory polymer cast. However numerous technical and market challenges remain before such a device can gain widespread acceptance.

6.7 References

[1] C. F. Quick, *3314419*, 1963 (Nov 15).
[2] W. A. Gruber, *4193395*, 1978 (Aug 24).
[3] L. H. Wartman, *4483333*, 1982 (Jun 1).
[4] P. L. Massey, *4704129*, 1984 (Jul 10).
[5] M. J. Borroff, D. A. Willstead, *4661535*, 1985 (Jul 9).
[6] A. J. Campagna, T. C. Sandvig, D. A. Ersfeld, M. T. Scholz, *4989593*, 1988 (Jul 22).
[7] R. J. Gorka, E. R. Dan, *4951656*, 1988 (Nov 9).
[8] 2008.
[9] 2008.
[10] V. J. Lopata, C. B. Saunders, A. Singh, C. J. Janke, G. E. Wrenn, S. J. Havens, *Radiation Physics and Chemistry* 1999, *56*, 405.
[11] W. L. MK Kang, HT Hahn, *Composites Part A, Applied science and manufacturing* 2001.
[12] E. R. Abrahamson, M. S. Lake, N. A. Munshi, K. Gall, *Journal of Intelligent Material Systems and Structures* 2003, *14*, 623.
[13] K. Gall, M. L. Dunn, Y. Liu, D. Finch, M. Lake, N. A. Munshi, *Acta Materialia* 2002, *50*, 5115.
[14] Y. Liu, K. Gall, M. L. Dunn, P. McCluskey, *Mechanics of Materials* 2004, *36*, 929.
[15] J. M. Hampikian, B. C. Heaton, F. C. Tong, Z. Q. Zhang, C. P. Wong, *Materials Science & Engineering C-Biomimetic and Supramolecular Systems* 2006, *26*, 1373.
[16] C. Liang, C. A. Rogers, E. Malafeew, *Journal of Intelligent Material Systems and Structures* 1997, *8*, 380.
[17] L. E. Nielson, R. F. Landel, *Mechanical Properties of Polymers and Composites*, Marcel Dekker, Columbus, OH 1994.
[18] T. Ohki, Q. Q. Ni, M. Iwamoto, *Science and Engineering of Composite Materials* 2004, *11*, 137.
[19] D. Ratna, J. Karger-Kocsis, *Journal of Materials Science* 2008, *43*, 254.
[20] Z. G. Wei, R. Sandstroröm, S. Miyazaki, *Journal of Materials Science* 1998, *33*, 3743.
[21] M. Muthukumar, D. Mohan, M. Rajendran, *Cement and Concrete Composites* 2003, *25*, 751.
[22] Q.-Q. Ni, C.-s. Zhang, Y. Fu, G. Dai, T. Kimura, *Composite Structures* 2007, *81*, 176.
[23] B. Yang, W. Min Huang, C. Li, J. Hoe Chor, *European Polymer Journal* 2005, *41*, 1123.
[24] Y. C. Park, J. K. Lee, G. C. Lee, *Composite Structures* 2007, *77*, 241.
[25] C. M. Yakacki, R. Shandas, D. Safranski, A. M. Ortega, K. Sassaman, K. Gall, *Advanced Functional Materials* 2008, *18*, 1.
[26] C. M. Yakacki, S. Willis, C. Luders, K. Gall, *Advanced Engineering Materials* 2008, *10*, 112.
[27] K. E. Smith, J. S. Temenoff, K. Gall, *Journal of Applied Polymer Science* 2009, *In Press.* .
[28] K. Gall, C. M. Yakacki, Y. Liu, R. Shandas, N. Willett, K. S. Anseth, *Journal of Biomedical Materials Research, Part A* 2005, *73A*, 339.
[29] A. M. Ortega, S. E. Kasprzak, C. M. Yakacki, J. Diani, A. R. Greenberg, K. Gall, *Journal of Applied Polymer Science* 2008, *9999*, NA.

CHAPTER 7

CONCLUSIONS

Much work has been done to characterize and improve the strain capacity and toughness of shape memory polymers and shape-memory polymer composites. It was demonstrated that tailored shape-memory polymer networks could be photopolymerized from methyl acrylate and isobornyl acrylate (or methyl methacrylate) with an optimized amount of crosslinker such as bisphenol A ethoxylate di(meth)acrylate to achieve large recoverable strains. Linear monomers can be combined in the appropriate ratios to tailor the base glass transition temperature, while photoinitiator and crosslinker are minimized to ensure a crosslinked network with fully recoverable strains. Recoverable strains of above 800%, twice the previously published value, can be obtained for materials with a T_g of 28 ˚C, while fully recoverable strains above 550% can be achieved for materials with a T_g of 55 ˚C. In the quest to maximize fully recoverable strains in shape-memory polymers, a new hybrid molecule, Xini, was theorized, synthesized, polymerized into SMP networks and characterized. Although Xini-based systems do not stretch as far as traditionally crosslinked, optimized systems, Xini may be used as both a crosslinker and initiator combined into a single molecule and exhibits novel properties including large strains.

Progress has also been made towards developing a new manufacturing paradigm for shape-memory polymers. In the past, thermoset SMPs were made into complex shapes using expensive top-down techniques. A block of polymer was made and custom machining was required to craft complex parts. This process is okay for advanced

biomedical applications where the manufacturing cost per device is essentially irrelevant and the difference between dollars and cents in manufacturing is indistinguishable. However in cost-competitive commodity applications, this simply is not the case. Thus, a new method has been proposed and validated for accurately tuning the thermomechanical properties of network acrylates with shape-memory properties. The proposed method, *Mnemosynation*, enables low cost mass-manufactured devices in complex shapes with tunable thermomechanical and shape-memory properties. Adjustment of rubbery modulus in the range from below 1 MPa to above 13 MPa has been demonstrated. Rubbery moduli were tailored by varying both radiation dosage between 5 and 300 kGy and crosslinker concentration between 1.00 and 25.0 wt%. T_g manipulation was independently shown between 23 ˚C and 70 ˚C in copolymers of MA and various other linear acrylates and acrylamides. Shape memory behavior was shown by free strain recovery tests with recovered strains above 90%.

Injection molding, blow molding, VARTM and other modern plastics processing techniques enable cheap mass production of polymers. These techniques are only possible using thermoplastic resins, which can be melted and reshaped after initial polymerization. Fully recoverable, durable SMPs rely on chemical crosslinks (thermoset) to maintain device shape over multiple strain cycles. Desired are materials with the properties of thermosets that can be mass-manufactured like thermoplastics. In this vein, targeted irradiation of thermoplastic precursors leads to grafting and the creation of a network polymer structure through the union of generated macromolecules. *Mnemosynation*, named for the Greek goddess of memory, Mnemosyne, is the manufacturing process developed that is the controlled imparting of memory on an

otherwise amorphous thermoplastic material utilizing radiation-induced covalent crosslinking, much like *vulcanization* of rubber is the controlled imparting of strength on a rubber using sulfur crosslinks. *Mnemosynation* combines advances in radiation grafting and advances in simultaneously tuning the mechanical properties of acrylic SMPs to enable traditional plastics processing (blow molding, injection molding, etc.) that allows complex geometries and also thermosetting shape memory properties.

An overview of the five necessary steps of *Mnemosynation* are as follows:

1. Combine linear acrylic monomers and photo-initiator in optimum ratios to tailor T_g, and M_w (thus viscosity) of the thermoplastic precursor
2. Cure with ultraviolet (UV) light based on the photo-initiator used (e.g. long wave UV at 365nm for 2,2 dimethoxy-2-phenylacetophenone) for a specified time and intensity (both polymer system dependent)
3. Melt the thermoplastic precursor and blend in an optimized amount of crosslinking agent (e.g. TMPTA) at an optimized temperature and torque (both polymer system dependent)
4. Injection mold a device in a custom mold using the polymer system resulting from *Step 3*
5. Cure molded part with e-beam (or γ-) radiation at a specified dosage (polymer system dependent) to covalently crosslink and obtain desired mechanical/acoustic properties

The novelty in this process lies in the ability to finely tune the end mechanical properties through modifications at each step in the process. The correct ratio and type of linear monomers must be combined with the proper ratio of photo-initiator to tailor the

thermoplastic precursor. The correct ratio of crosslinking agent blend must be mixed in at the correct temperature and torque to facilitate homogeneity in the mixing process and ensure proper dispersion of the agent throughout the polymer. The blended system must be exposed to proper dosage of high-energy radiation to target specific crosslink densities and ensure control of the end thermo-mechanical and acoustic properties.

Numerous studies were undertaken to enhance the effectiveness and control the effects of *Mnemosynation*. Blends of PMA and PEGDA of three molecular weights were radiation crosslinked at dosages between 5 and 300 kGy. The resulting networks were characterized through Charlesby-Pinner analyses and dynamic mechanical analyses. PEGDA successfully sensitized the radiation crosslinking of PMA. The extent of crosslinking was greater with increasing molar concentration of PEGDA of a single M_n. Longer PEGDA molecules were found to be more effective at sensitizing crosslinking at a given molar ratio of sensitizer to PMA. At a given weight ratio, shorter PEGDA molecules were found to be more effective at sensitizing crosslinking because there are more reactive acrylate ends. The shape-memory properties of three blends crosslinked at 50 kGy were evaluated. Shape fixity was above 99% for all three materials. Shape recovery over one cycle was between 97% and 99% and increased with increasing molar ratio of PEGDA. Control of rubbery modulus, independent from T_g, was achieved for shape-memory polymers, which are stored at temperatures below 20 ˚C and recover at ambient temperatures.

Putting together advances in high-strain SMP synthesis and *Mnemosynation*, the idea to develop, test and ultimately prototype a multi-layer, multi-actuated shape-memory polymer orthopedic cast became tenable. A new paradigm in SMP composite

manufacture—namely that materials can be designed to enhance *strain capacity* at moderate stress rather than maximum strength—was established. However several basic materials studies were missing regarding the effects of fiber-reinforcement on shape memory polymers that would meet the stringent strain requirements for such an application. A large array of fiber candidates was characterized. Each fiber was tested alone and in conjunction with different SMP networks. Ultimately, anteres nylon lycra was chosen as a potential candidate to serve as the central inner fiber layer in an SMP casting device. An SMP with a high T_g, poly(MA-co-IBoA) in a 9 to 11 ratio with 1.00 wt% TMPTA crosslinker, was chosen as the inner polymer layer to surround this fiber and serve as the shape fixing component in the cast. A softer, lower T_g polymer, poly(MA-co-BA) in a 9 to 1 ratio with 1.00 wt% TMPTA crosslinker, was selected as a potential outer layer for the casting device to help mitigate brittle failures. Both layers, with and without fiber-reinforcement were characterized at different temperatures.

Future work centers on building and testing a two layer composite material. Future work also remains to integrate the *Mnemosynation* manufacturing technique into the large strain composite casting application to enable low-cost scale up to compete with current market solutions. Once this is complete, cylindrical fiber weaves must be made and VARTM techniques employed to evenly distribute thermoplastic resin across the fiber in the correct ratios. This must be accomplished with both layers. Devices made with VARTM must then also be subjected to e-beam radiation for the post-crosslinking during the last step of *Mnemosynation*. Additional studies concerning breathability and aesthetics would also need to be undertaken, as would the effects of moisture and an aqueous environment on the casting sleeve. Thus the research presented has made

significant progress toward a functioning shape-memory polymer cast. However numerous technical and market challenges remain before such a device can gain widespread acceptance.

Ultimately using *Mnemosynation* and the possessing ability to enhance the strain capacity of shape memory polymers have many benefits in both commercial markets and academia. The taxing scientific problems that are entwined with the application of these technical advances to new fields and new ideas can sustain a career in academia into the next decade. The commercial benefits of brining such technologies to the mass market can sustain innovation and the ability to raise money and interest in commercial spheres.

I look forward to the challenges and frustrations that the future holds and will eagerly and persistently pursue these problems in both academic and commercial settings until the day when I can take one of my grandchildren aside and tell him one word—if he is listening. Plastics. I will tell him that there's *still* a great future in plastics.

APPENDIX

A.1. Supplementary Figures

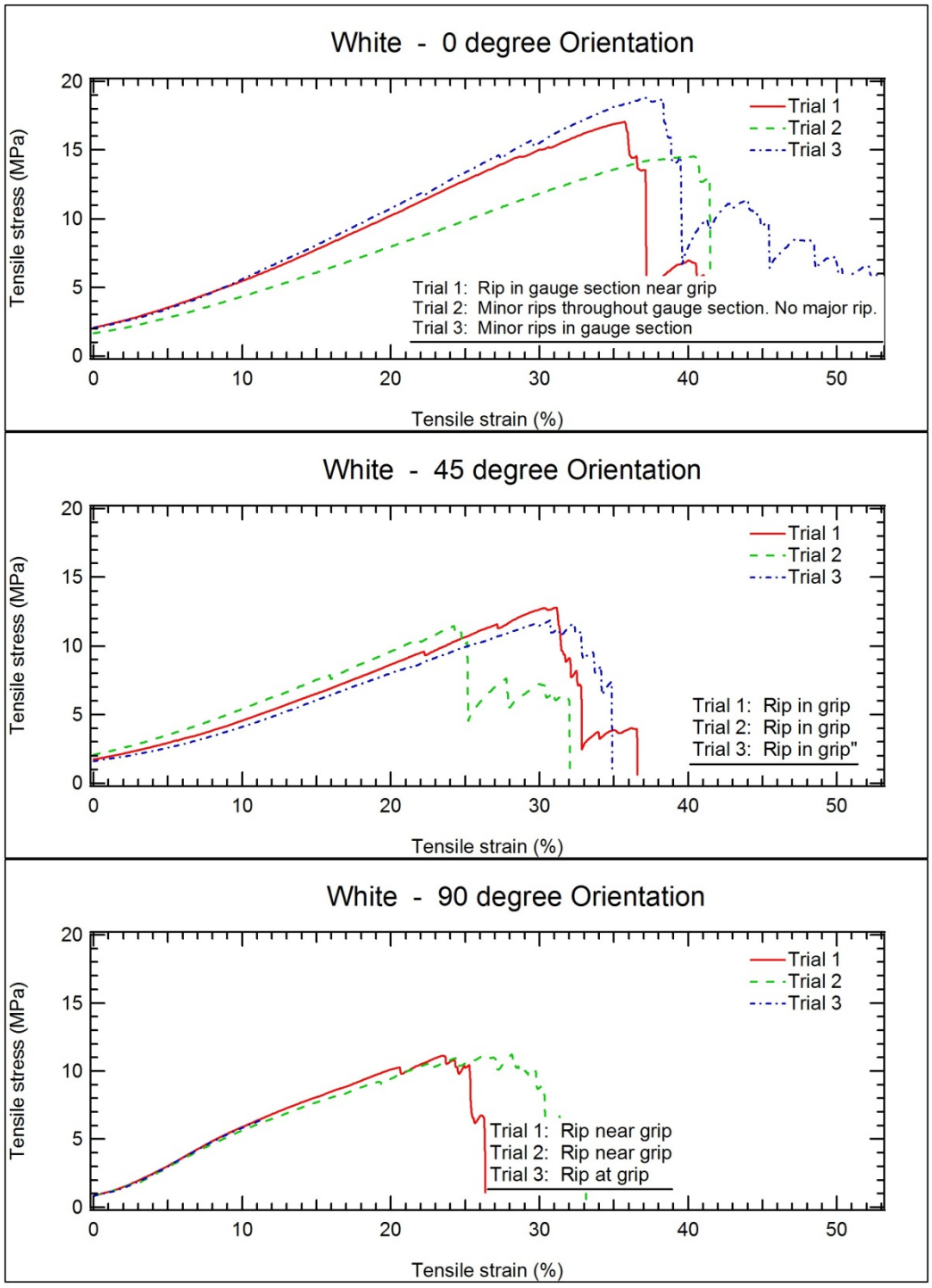

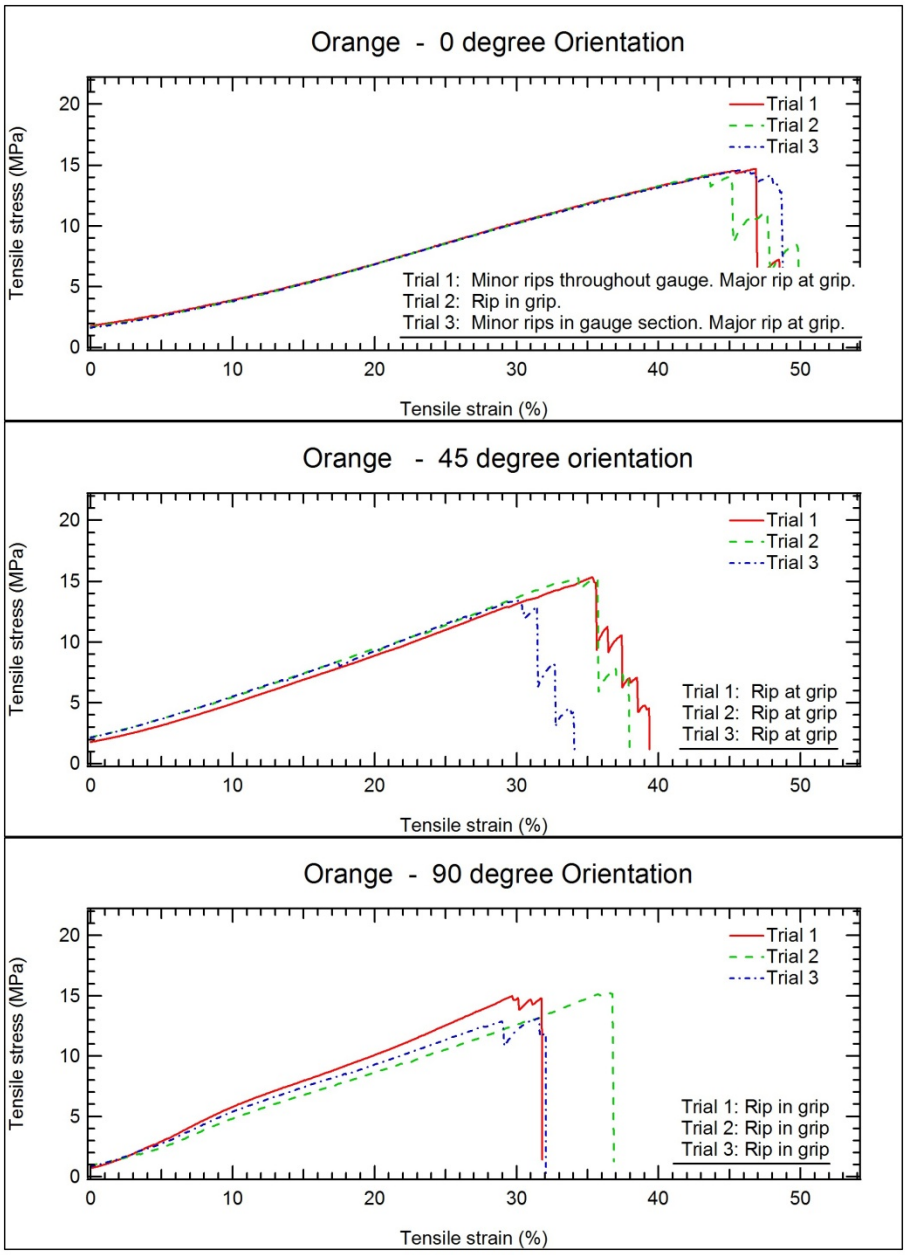
Orange - 0 degree Orientation
Tensile stress (MPa)
Tensile strain (%)
Trial 1
Trial 2
Trial 3
Trial 1: Minor rips throughout gauge. Major rip at grip.
Trial 2: Rip in grip.
Trial 3: Minor rips in gauge section. Major rip at grip.
Orange - 45 degree orientation
Tensile stress (MPa)
Tensile strain (%)
Trial 1
Trial 2
Trial 3
Trial 1: Rip at grip
Trial 2: Rip at grip
Trial 3: Rip at grip
Orange - 90 degree Orientation
Tensile stress (MPa)
Tensile strain (%)
Trial 1
Trial 2
Trial 3
Trial 1: Rip in grip
Trial 2: Rip in grip
Trial 3: Rip in grip

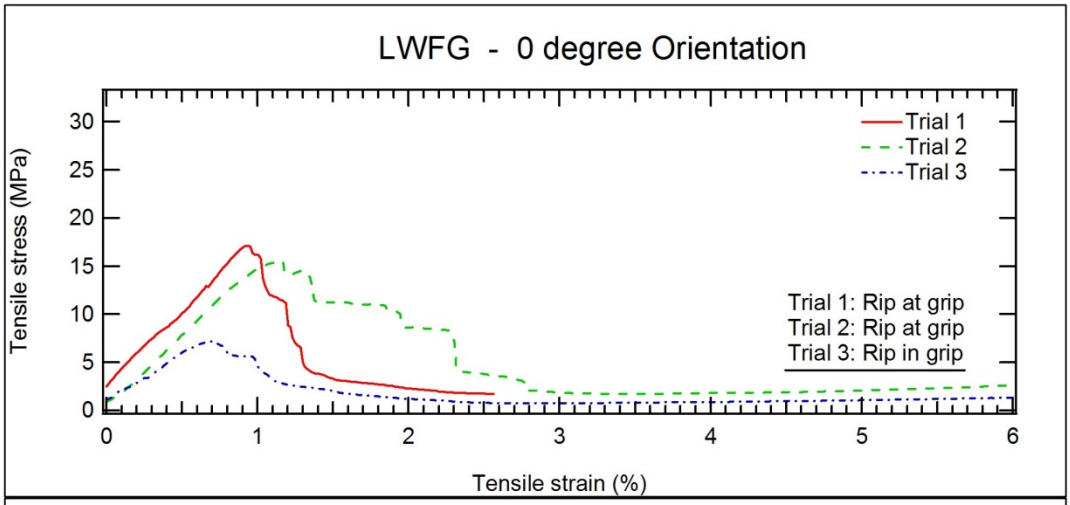
LWFG - 0 degree Orientation
Tensile stress (MPa)
Tensile strain (%)
Trial 1
Trial 2
Trial 3
Trial 1: Rip at grip
Trial 2: Rip at grip
Trial 3: Rip in grip

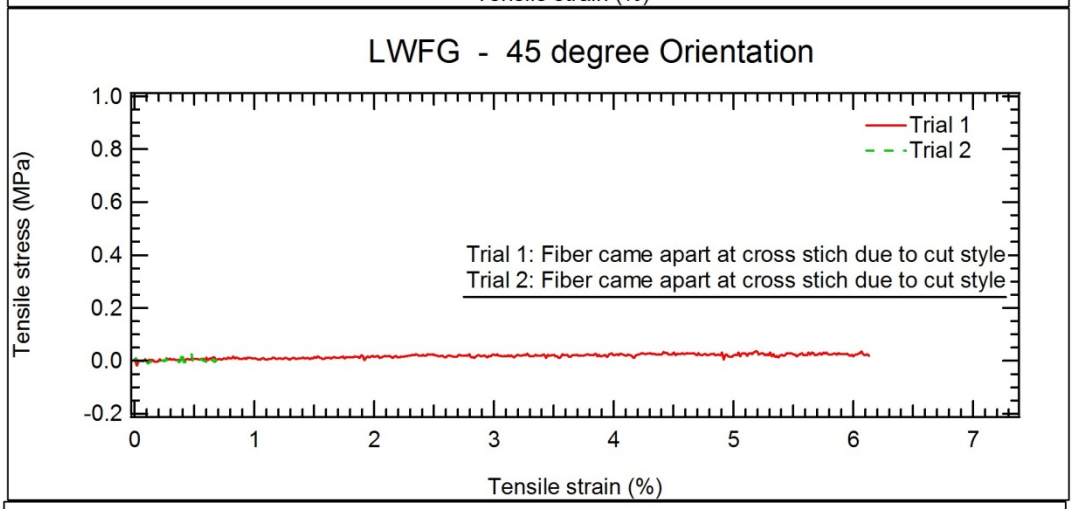
LWFG - 45 degree Orientation
Tensile stress (MPa)
Tensile strain (%)
Trial 1
Trial 2
Trial 1: Fiber came apart at cross stich due to cut style
Trial 2: Fiber came apart at cross stich due to cut style

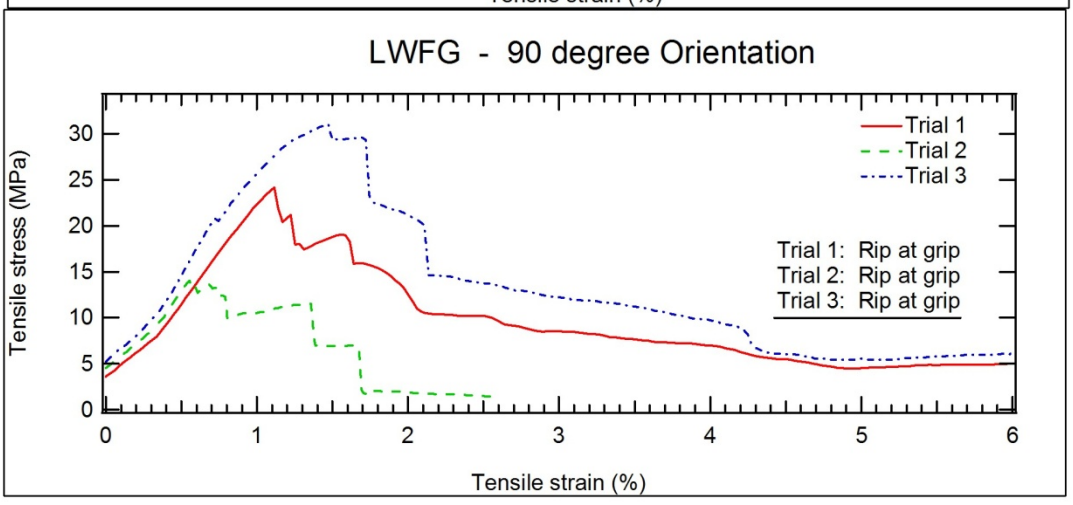
LWFG - 90 degree Orientation
Tensile stress (MPa)
Tensile strain (%)
Trial 1
Trial 2
Trial 3
Trial 1: Rip at grip
Trial 2: Rip at grip
Trial 3: Rip at grip

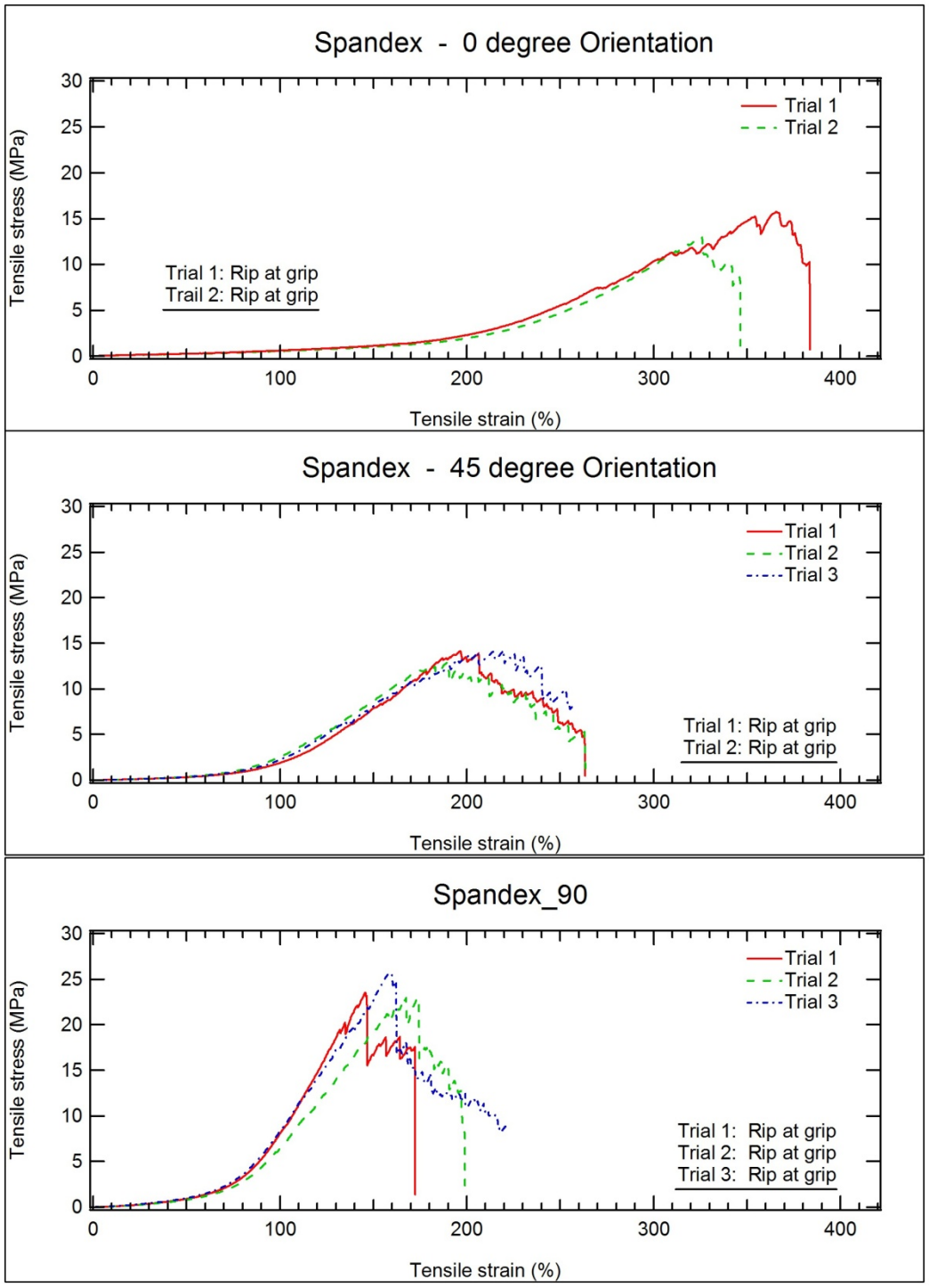
Spandex - 0 degree Orientation
Tensile stress (MPa)
Tensile strain (%)
Trial 1
Trial 2
Trial 1: Rip at grip
Trail 2: Rip at grip
Spandex - 45 degree Orientation
Tensile stress (MPa)
Tensile strain (%)
Trial 1
Trial 2
Trial 3
Trial 1: Rip at grip
Trial 2: Rip at grip
Spandex_90
Tensile stress (MPa)
Tensile strain (%)
Trial 1
Trial 2
Trial 3
Trial 1: Rip at grip
Trial 2: Rip at grip
Trial 3: Rip at grip

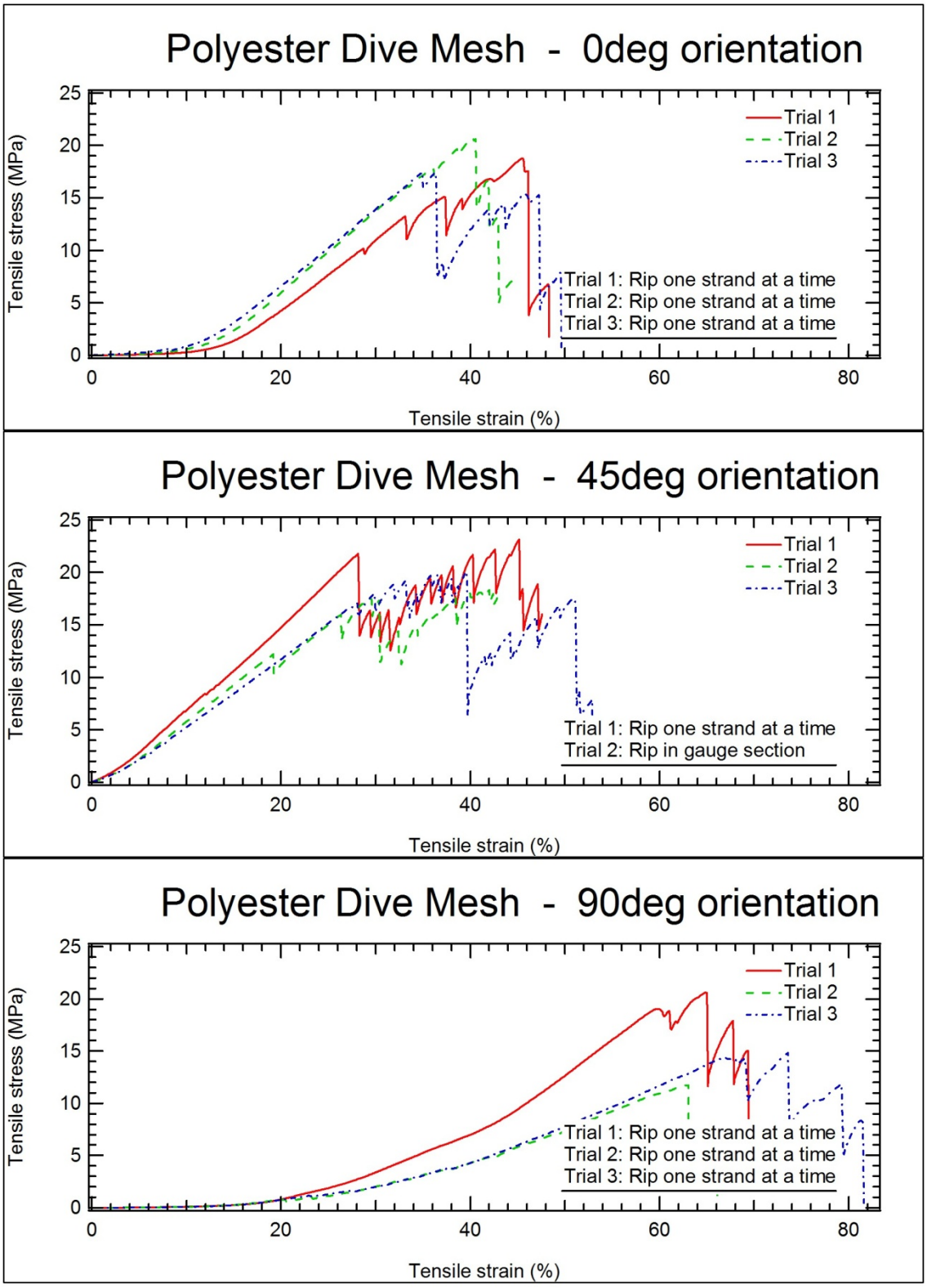
Polyester Dive Mesh - 0deg orientation
Tensile stress (MPa)
Tensile strain (%)
Trial 1
Trial 2
Trial 3
Trial 1: Rip one strand at a time
Trial 2: Rip one strand at a time
Trial 3: Rip one strand at a time
Polyester Dive Mesh - 45deg orientation
Tensile stress (MPa)
Tensile strain (%)
Trial 1
Trial 2
Trial 3
Trial 1: Rip one strand at a time
Trial 2: Rip in gauge section
Polyester Dive Mesh - 90deg orientation
Tensile stress (MPa)
Tensile strain (%)
Trial 1
Trial 2
Trial 3
Trial 1: Rip one strand at a time
Trial 2: Rip one strand at a time
Trial 3: Rip one strand at a time

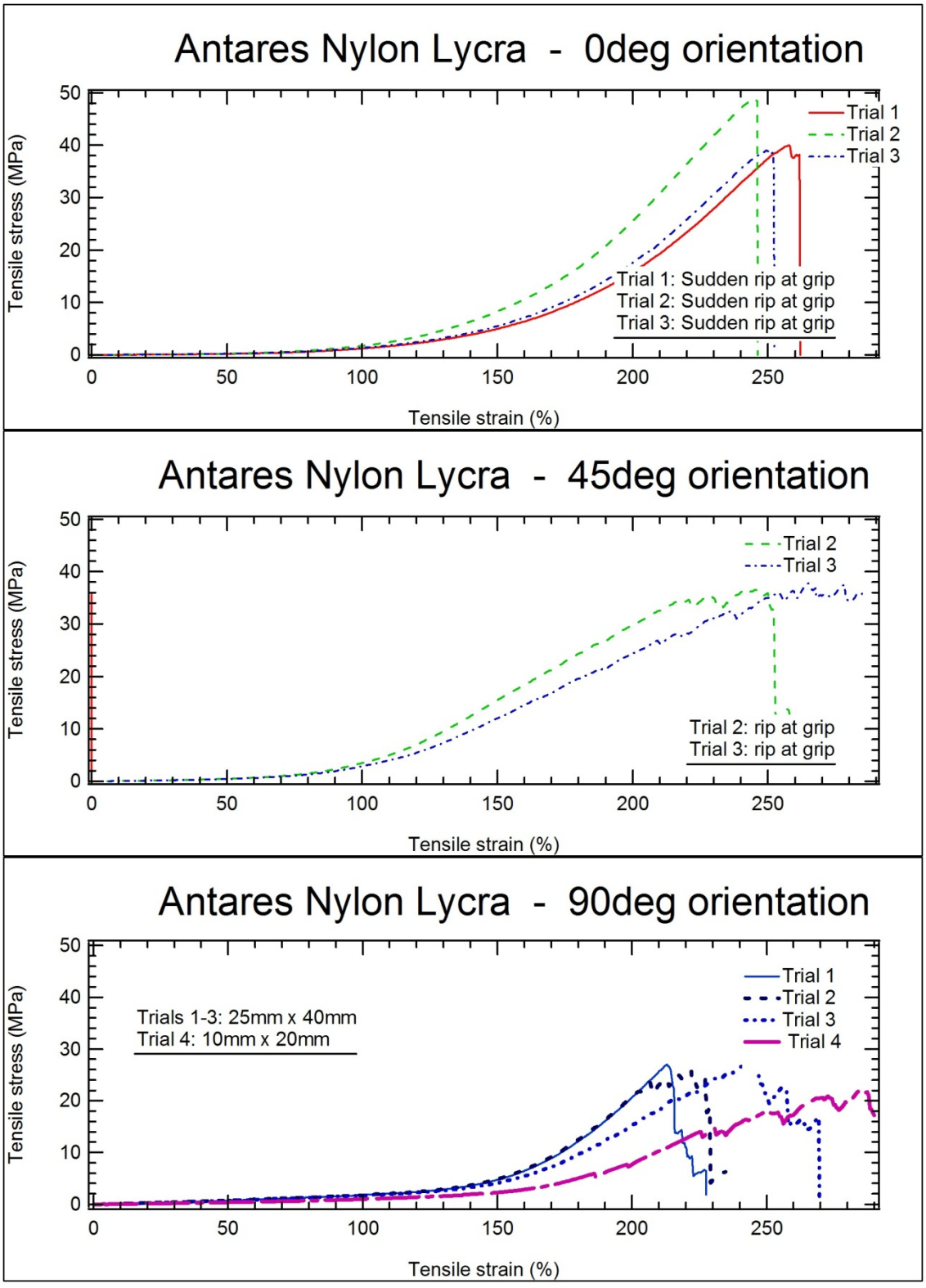
Antares Nylon Lycra - 0deg orientation
Tensile stress (MPa)
Tensile strain (%)
Trial 1
Trial 2
Trial 3
Trial 1: Sudden rip at grip
Trial 2: Sudden rip at grip
Trial 3: Sudden rip at grip
Antares Nylon Lycra - 45deg orientation
Tensile stress (MPa)
Tensile strain (%)
Trial 2
Trial 3
Trial 2: rip at grip
Trial 3: rip at grip
Antares Nylon Lycra - 90deg orientation
Tensile stress (MPa)
Tensile strain (%)
Trials 1-3: 25mm x 40mm
Trial 4: 10mm x 20mm
Trial 1
Trial 2
Trial 3
Trial 4

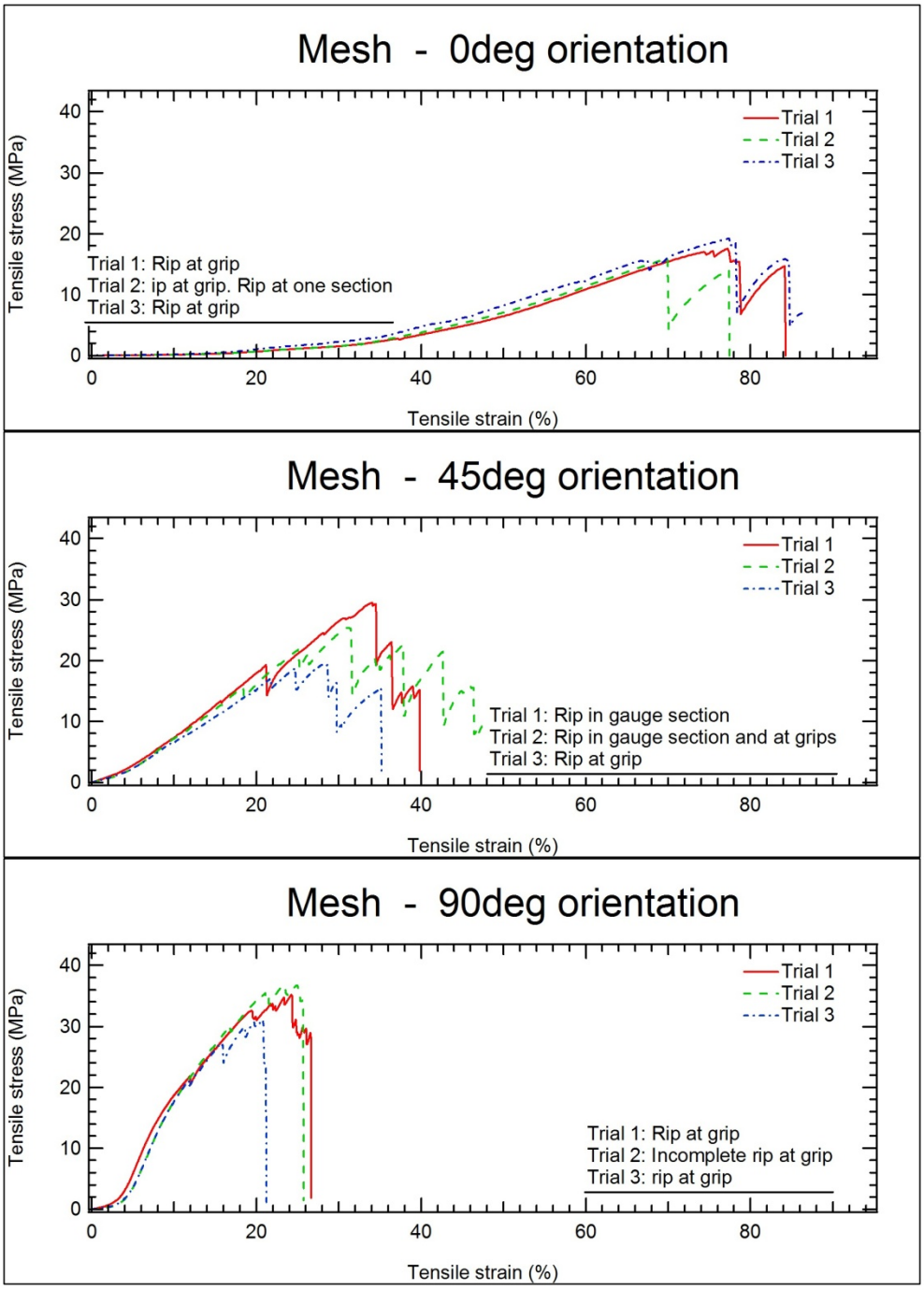
Mesh - 0deg orientation
Tensile stress (MPa)
Tensile strain (%)
Trial 1
Trial 2
Trial 3
Trial 1: Rip at grip
Trial 2: ip at grip. Rip at one section
Trial 3: Rip at grip
Mesh - 45deg orientation
Tensile stress (MPa)
Tensile strain (%)
Trial 1
Trial 2
Trial 3
Trial 1: Rip in gauge section
Trial 2: Rip in gauge section and at grips
Trial 3: Rip at grip
Mesh - 90deg orientation
Tensile stress (MPa)
Tensile strain (%)
Trial 1
Trial 2
Trial 3
Trial 1: Rip at grip
Trial 2: Incomplete rip at grip
Trial 3: rip at grip

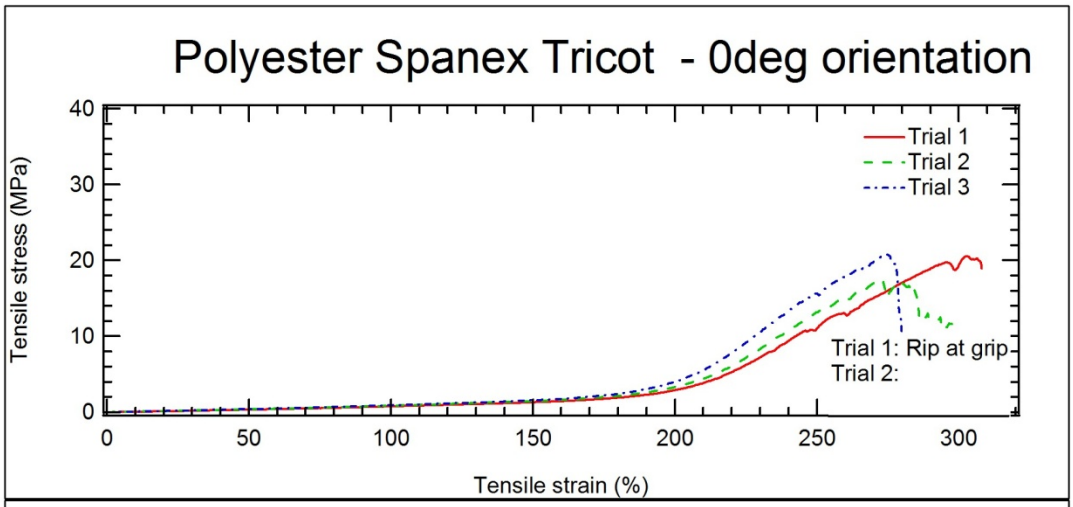
Polyester Spanex Tricot - 0deg orientation
Tensile stress (MPa)
Tensile strain (%)
Trial 1
Trial 2
Trial 3
Trial 1: Rip at grip
Trial 2:

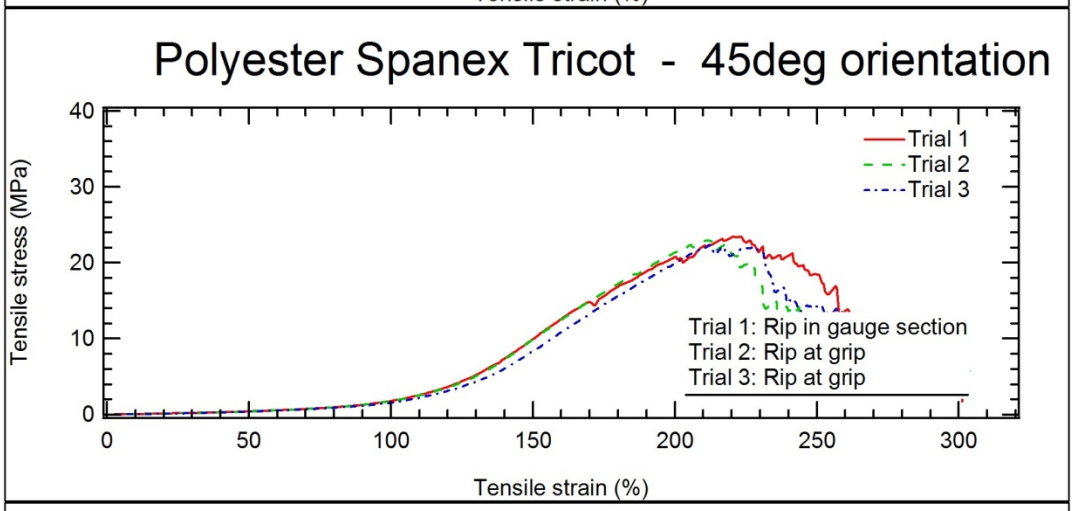
Polyester Spanex Tricot - 45deg orientation
Tensile stress (MPa)
Tensile strain (%)
Trial 1
Trial 2
Trial 3
Trial 1: Rip in gauge section
Trial 2: Rip at grip
Trial 3: Rip at grip

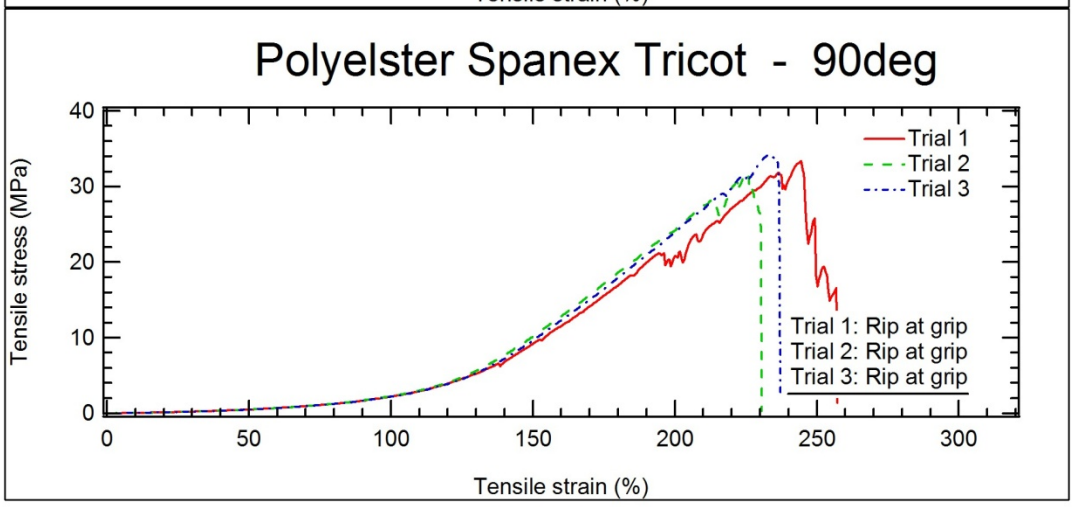
Polyelster Spanex Tricot - 90deg
Tensile stress (MPa)
Tensile strain (%)
Trial 1
Trial 2
Trial 3
Trial 1: Rip at grip
Trial 2: Rip at grip
Trial 3: Rip at grip

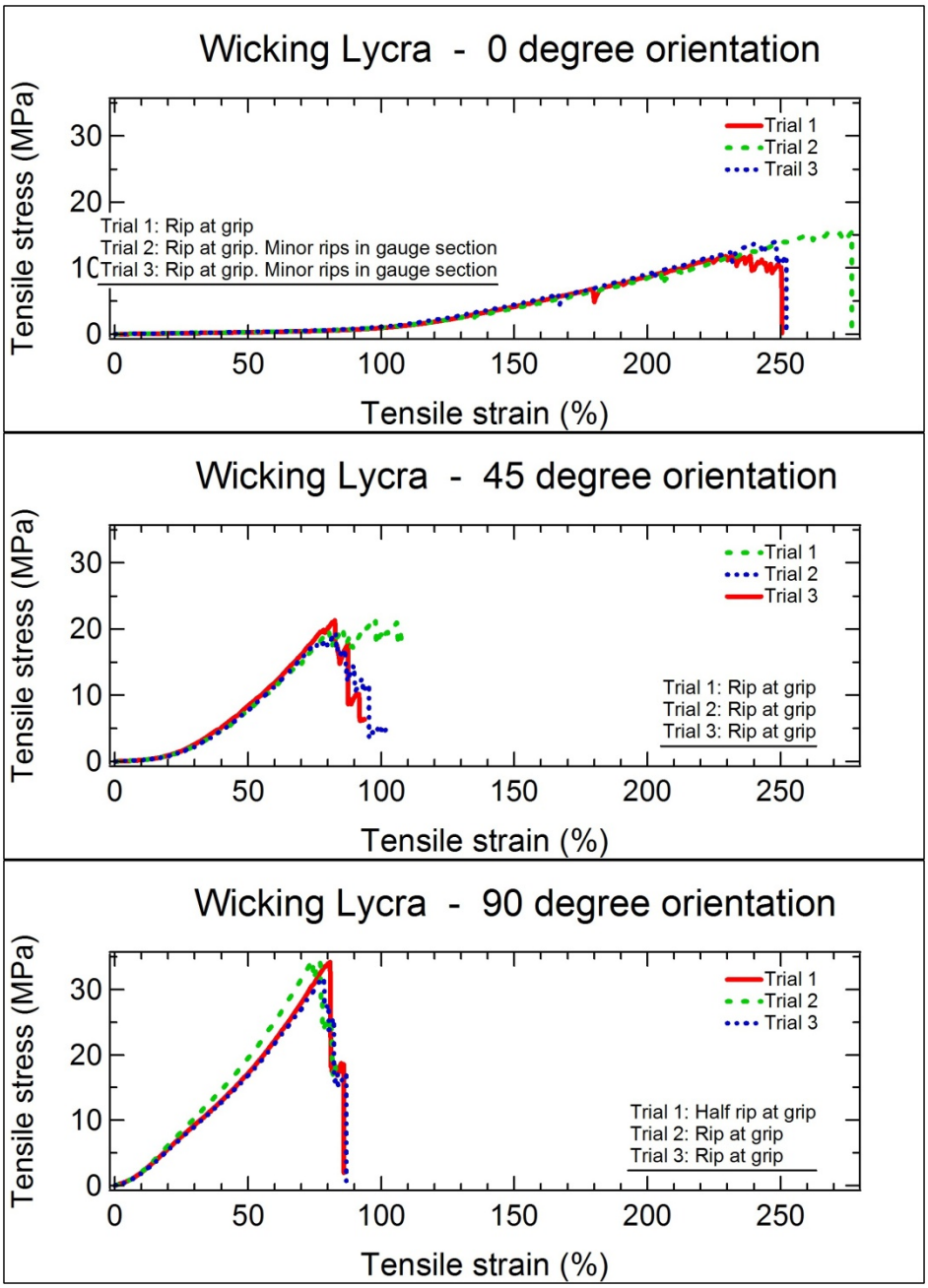
Wicking Lycra - 0 degree orientation
Tensile stress (MPa)
Tensile strain (%)
Trial 1
Trial 2
Trail 3
Trial 1: Rip at grip
Trial 2: Rip at grip. Minor rips in gauge section
Trial 3: Rip at grip. Minor rips in gauge section
Wicking Lycra - 45 degree orientation
Tensile stress (MPa)
Tensile strain (%)
Trial 1
Trial 2
Trial 3
Trial 1: Rip at grip
Trial 2: Rip at grip
Trial 3: Rip at grip
Wicking Lycra - 90 degree orientation
Tensile stress (MPa)
Tensile strain (%)
Trial 1
Trial 2
Trial 3
Trial 1: Half rip at grip
Trial 2: Rip at grip
Trial 3: Rip at grip

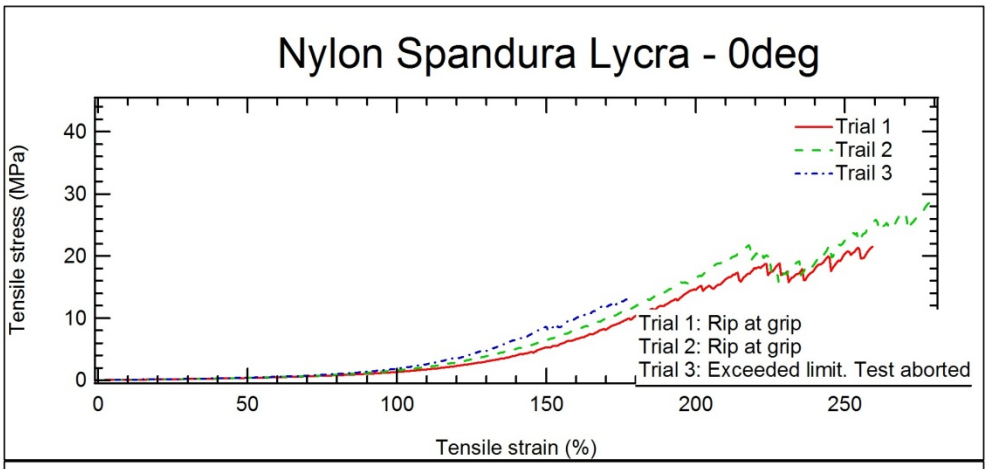
Nylon Spandura Lycra - 0deg
Tensile stress (MPa)
Tensile strain (%)
Trial 1
Trail 2
Trail 3
Trial 1: Rip at grip
Trial 2: Rip at grip
Trial 3: Exceeded limit. Test aborted

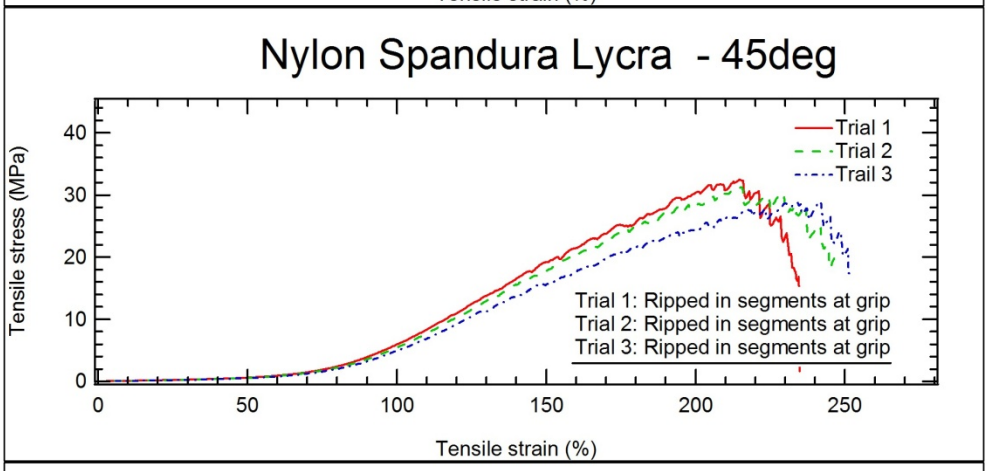
Nylon Spandura Lycra - 45deg
Tensile stress (MPa)
Tensile strain (%)
Trial 1
Trial 2
Trail 3
Trial 1: Ripped in segments at grip
Trial 2: Ripped in segments at grip
Trial 3: Ripped in segments at grip

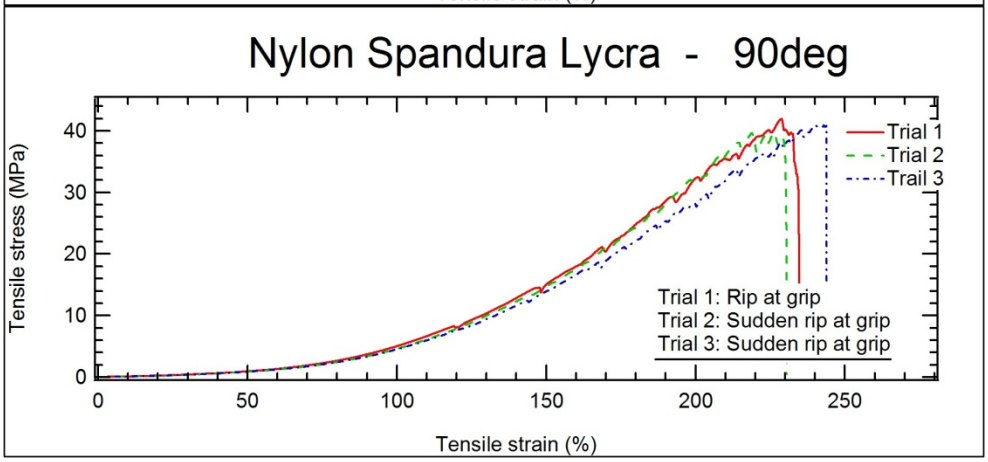
Nylon Spandura Lycra - 90deg
Tensile stress (MPa)
Tensile strain (%)
Trial 1
Trial 2
Trail 3
Trial 1: Rip at grip
Trial 2: Sudden rip at grip
Trial 3: Sudden rip at grip

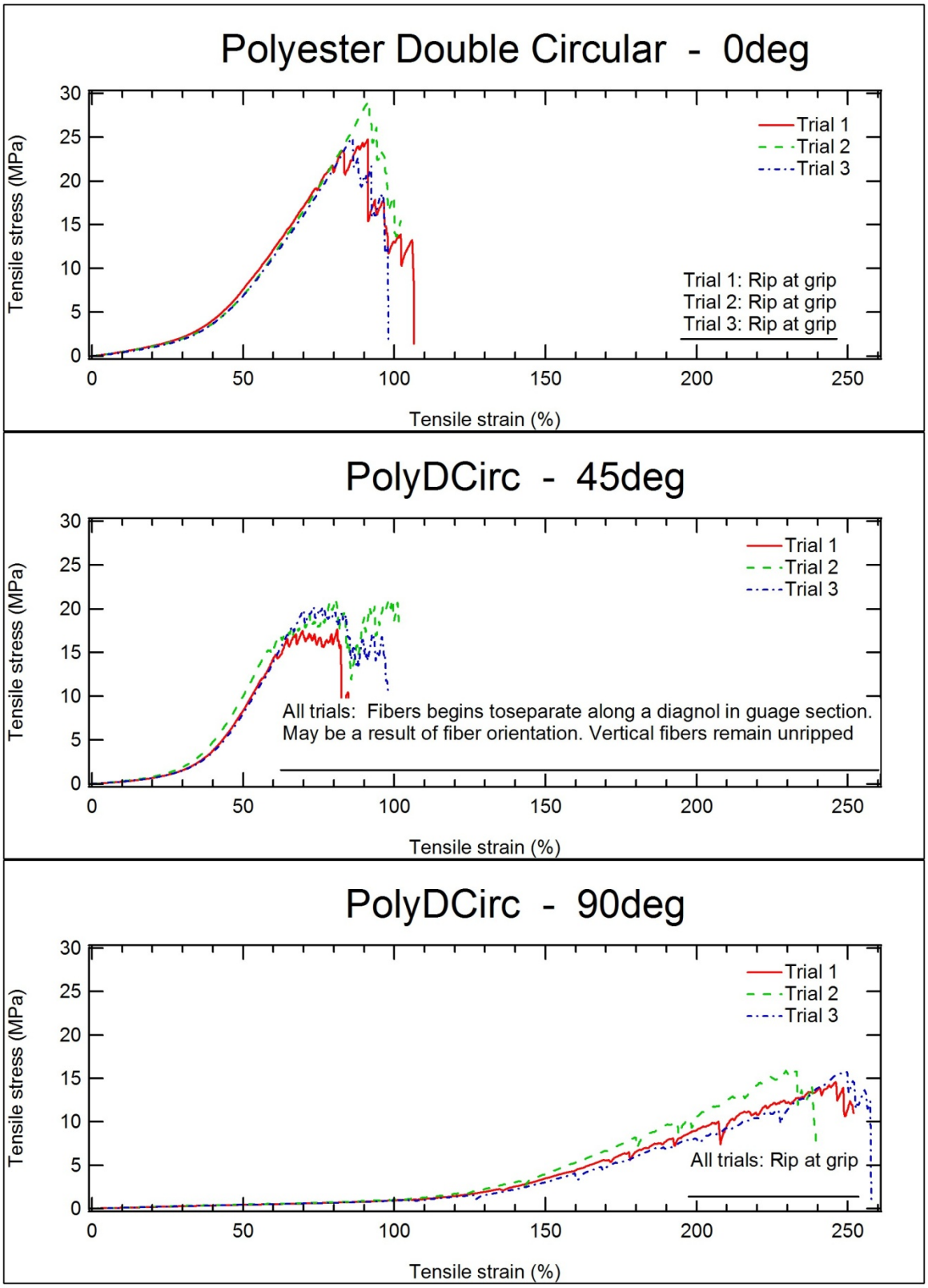
Polyester Double Circular - 0deg
Tensile stress (MPa)
Tensile strain (%)
Trial 1
Trial 2
Trial 3
Trial 1: Rip at grip
Trial 2: Rip at grip
Trial 3: Rip at grip
PolyDCirc - 45deg
Tensile stress (MPa)
Tensile strain (%)
Trial 1
Trial 2
Trial 3
All trials: Fibers begins toseparate along a diagnol in guage section.
May be a result of fiber orientation. Vertical fibers remain unripped
PolyDCirc - 90deg
Tensile stress (MPa)
Tensile strain (%)
Trial 1
Trial 2
Trial 3
All trials: Rip at grip

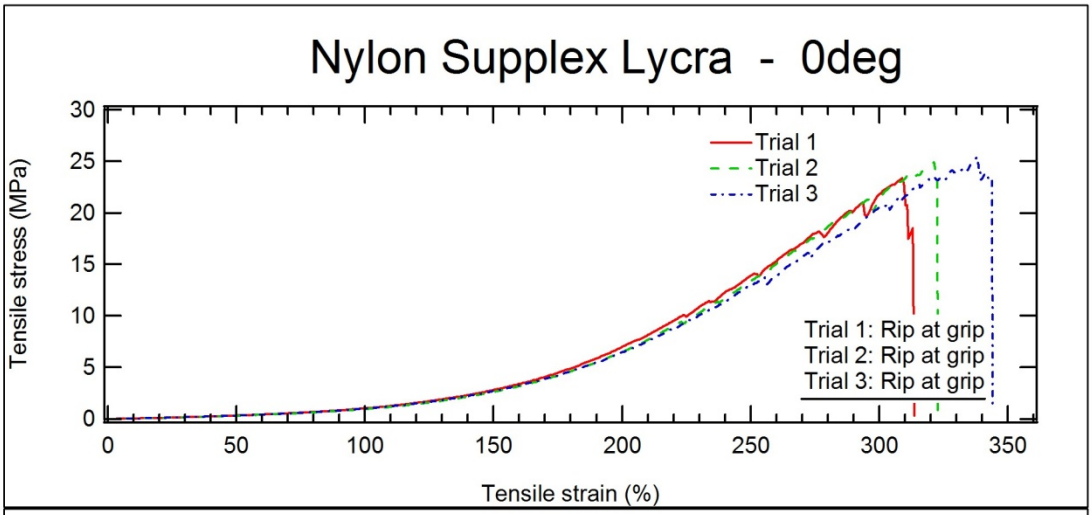
Nylon Supplex Lycra - 0deg
Tensile stress (MPa)
Tensile strain (%)
Trial 1
Trial 2
Trial 3
Trial 1: Rip at grip
Trial 2: Rip at grip
Trial 3: Rip at grip

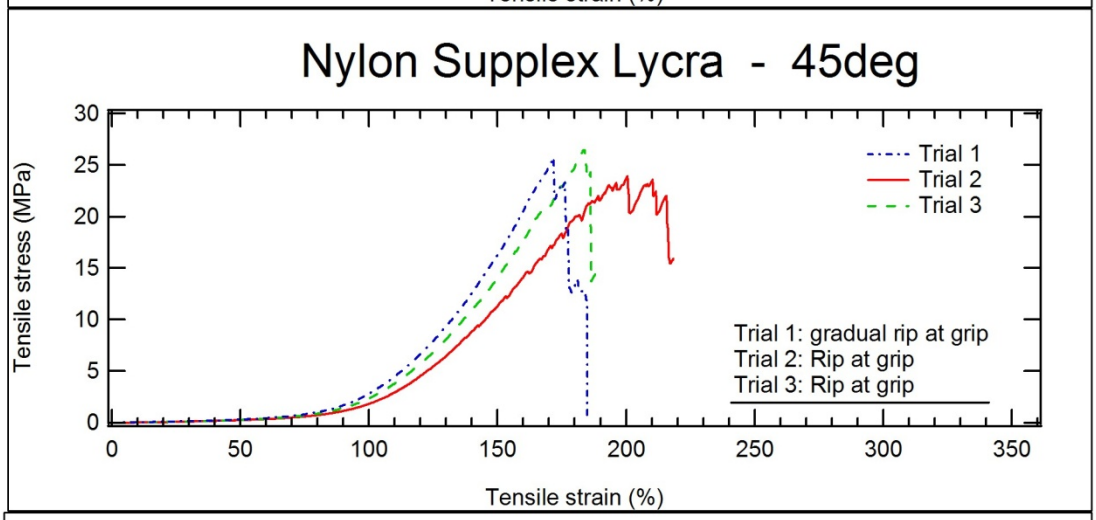
Nylon Supplex Lycra - 45deg
Tensile stress (MPa)
Tensile strain (%)
Trial 1
Trial 2
Trial 3
Trial 1: gradual rip at grip
Trial 2: Rip at grip
Trial 3: Rip at grip

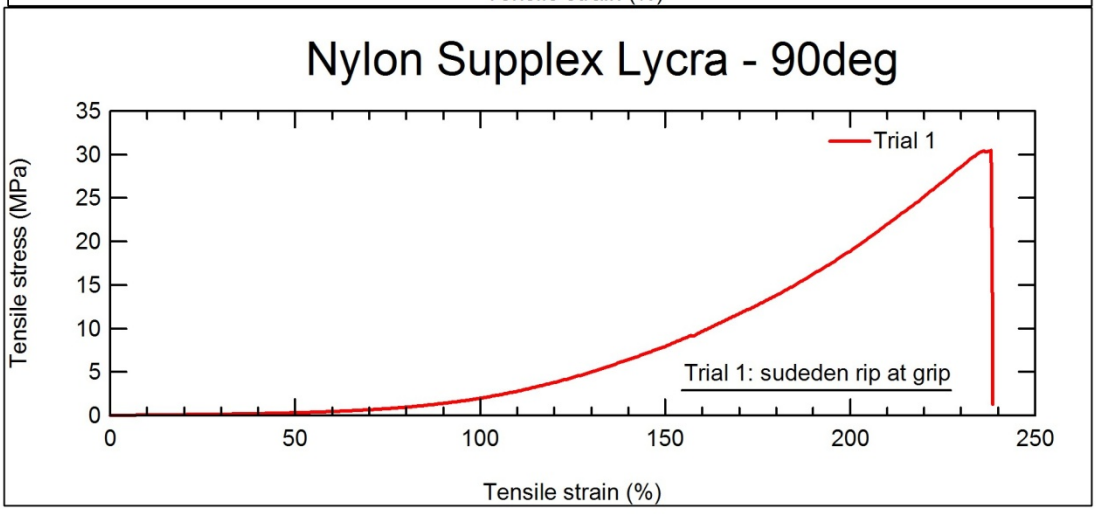
Nylon Supplex Lycra - 90deg
Tensile stress (MPa)
Tensile strain (%)
Trial 1
Trial 1: sudeden rip at grip

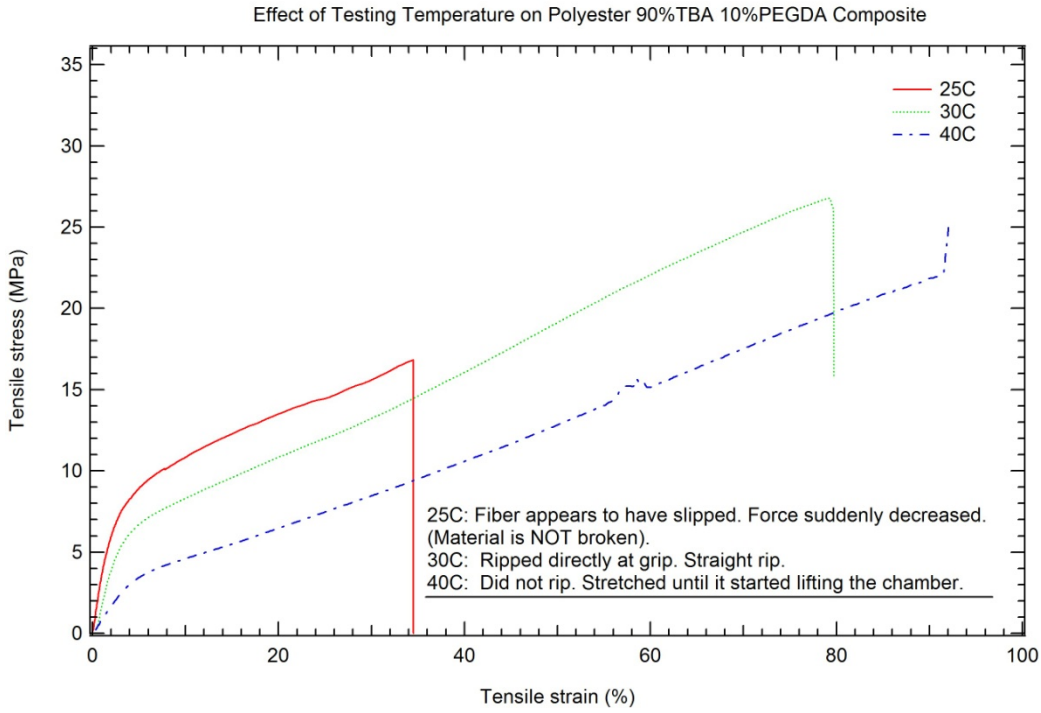
Effect of Testing Temperature on Polyester 90%TBA 10%PEGDA Composite
Tensile stress (MPa)
Tensile strain (%)
25C
30C
40C
25C: Fiber appears to have slipped. Force suddenly decreased.
(Material is NOT broken).
30C: Ripped directly at grip. Straight rip.
40C: Did not rip. Stretched until it started lifting the chamber.

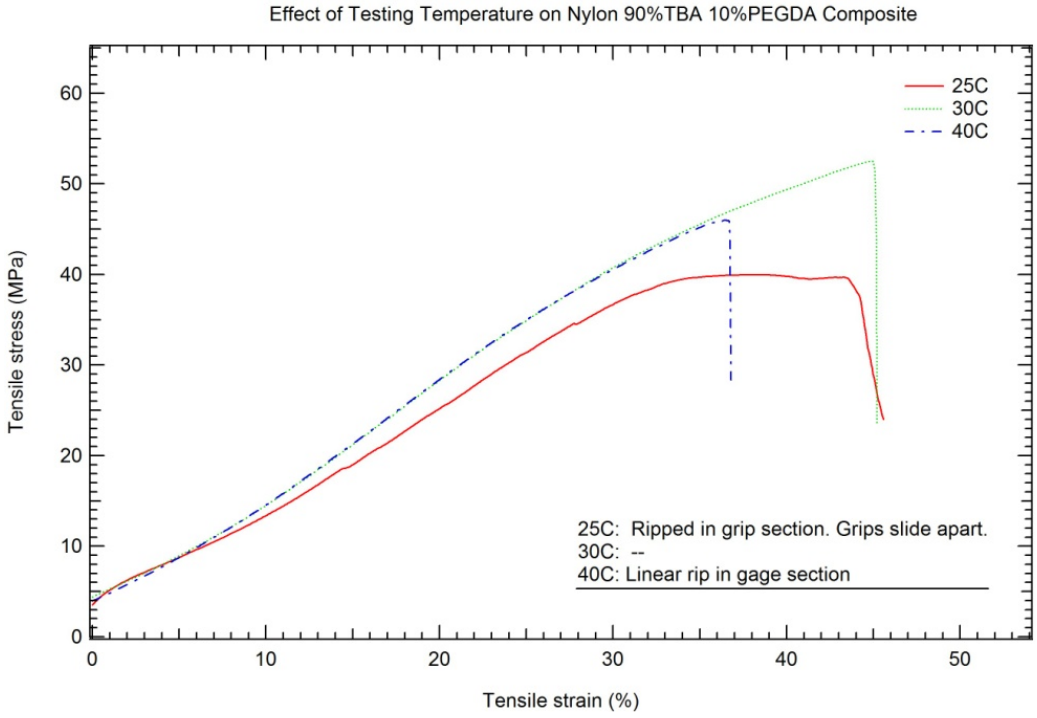
Effect of Testing Temperature on Nylon 90%TBA 10%PEGDA Composite
Tensile stress (MPa)
Tensile strain (%)
25C
30C
40C
25C: Ripped in grip section. Grips slide apart.
30C: --
40C: Linear rip in gage section

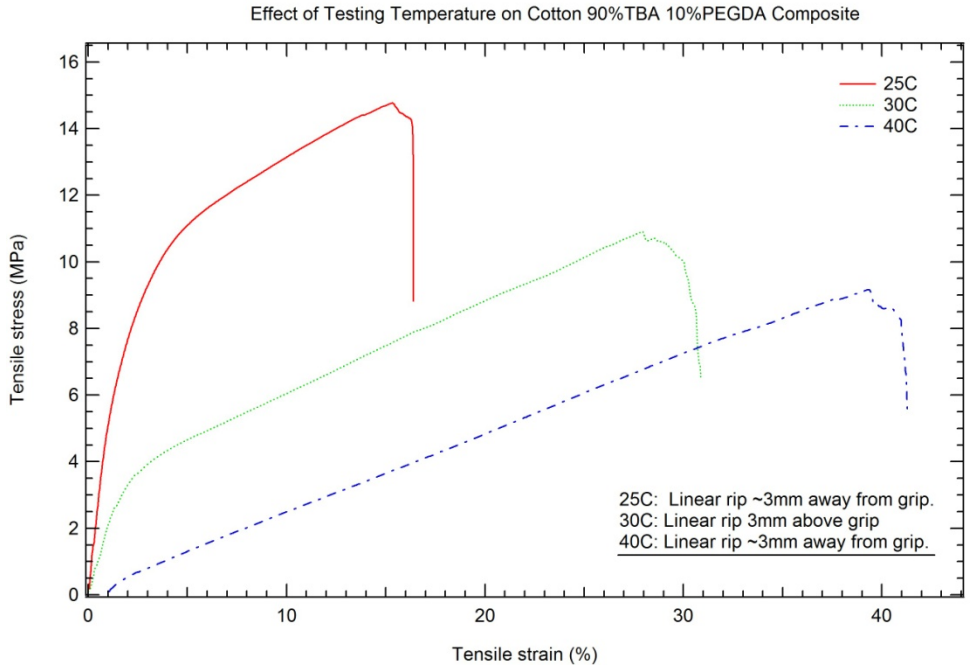
Effect of Testing Temperature on Cotton 90%TBA 10%PEGDA Composite
Tensile stress (MPa)
Tensile strain (%)
25C
30C
40C
25C: Linear rip ~3mm away from grip.
30C: Linear rip 3mm above grip
40C: Linear rip ~3mm away from grip.

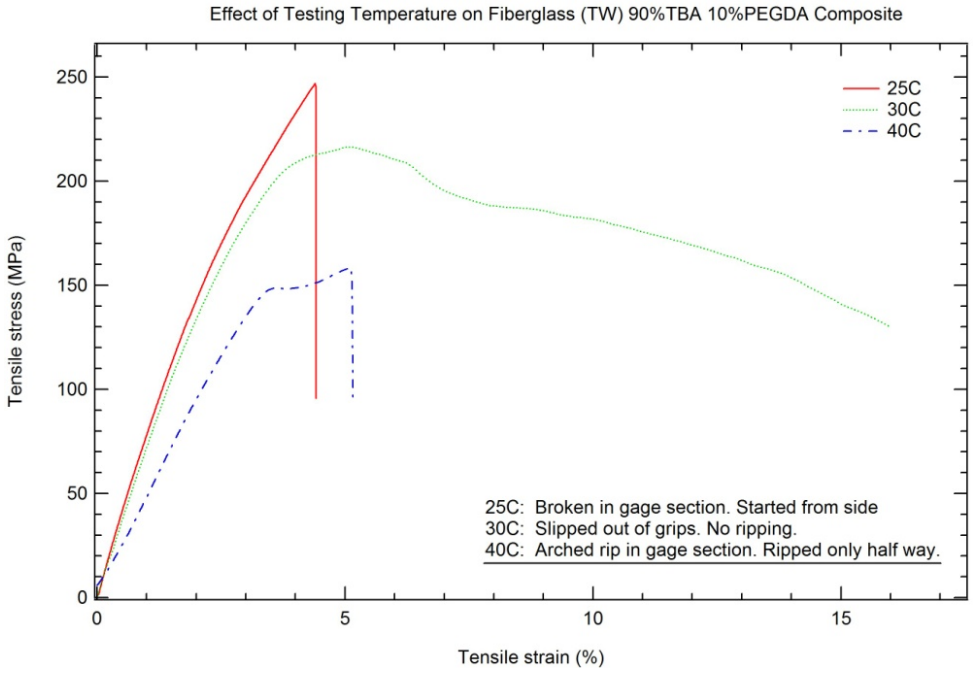
Effect of Testing Temperature on Fiberglass (TW) 90%TBA 10%PEGDA Composite
Tensile stress (MPa)
Tensile strain (%)
25C
30C
40C
25C: Broken in gage section. Started from side
30C: Slipped out of grips. No ripping.
40C: Arched rip in gage section. Ripped only half way.

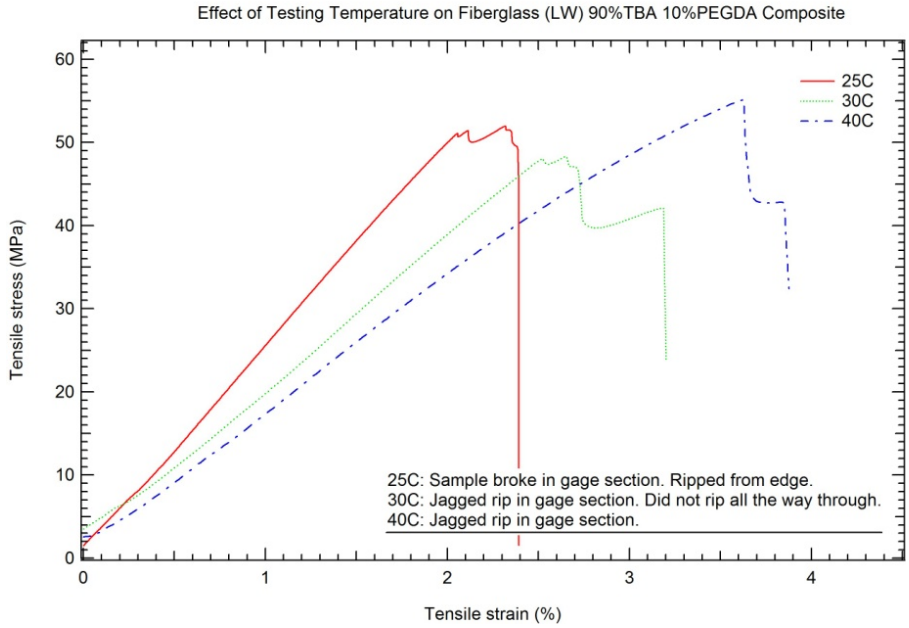
Effect of Testing Temperature on Fiberglass (LW) 90%TBA 10%PEGDA Composite
Tensile stress (MPa)
Tensile strain (%)
25C
30C
40C
25C: Sample broke in gage section. Ripped from edge.
30C: Jagged rip in gage section. Did not rip all the way through.
40C: Jagged rip in gage section.

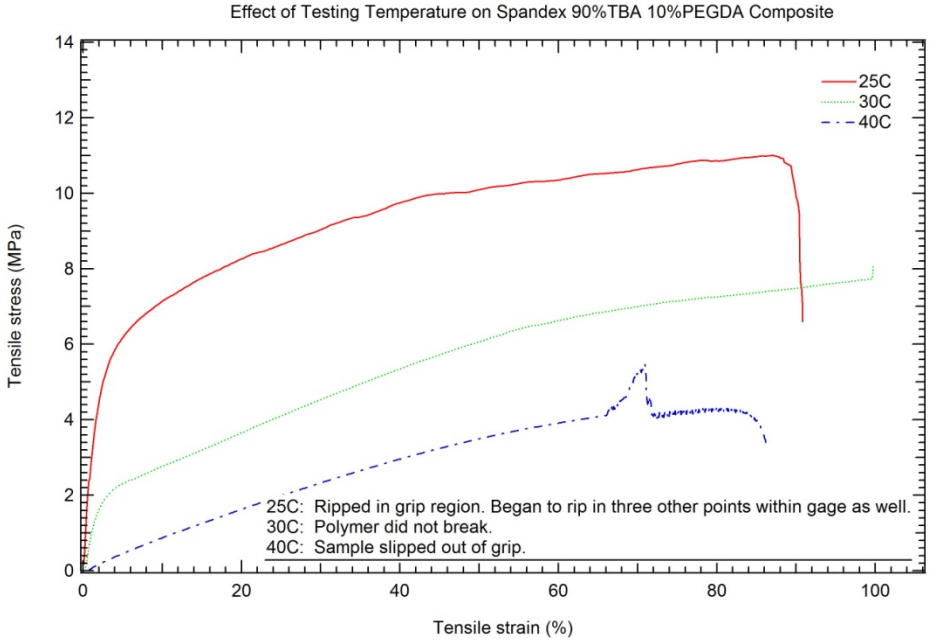
Effect of Testing Temperature on Spandex 90%TBA 10%PEGDA Composite
Tensile stress (MPa)
Tensile strain (%)
25C
30C
40C
25C: Ripped in grip region. Began to rip in three other points within gage as well.
30C: Polymer did not break.
40C: Sample slipped out of grip.

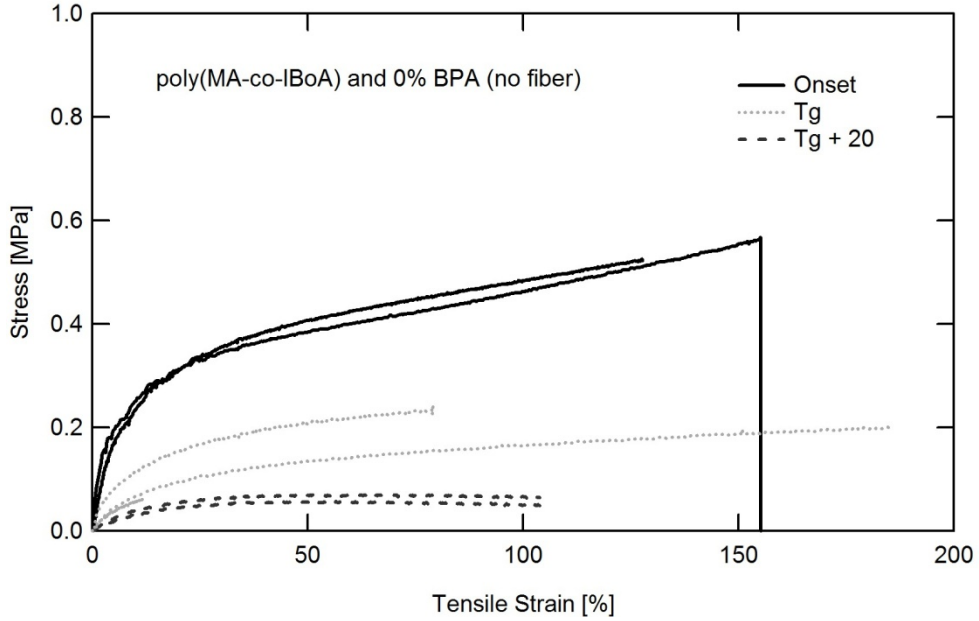
poly(MA-co-IBoA) and 0% BPA (no fiber)
Onset
Tg
Tg + 20
Stress [MPa]
Tensile Strain [%]
0.0
0.2
0.4
0.6
0.8
1.0
0
50
100
150
200

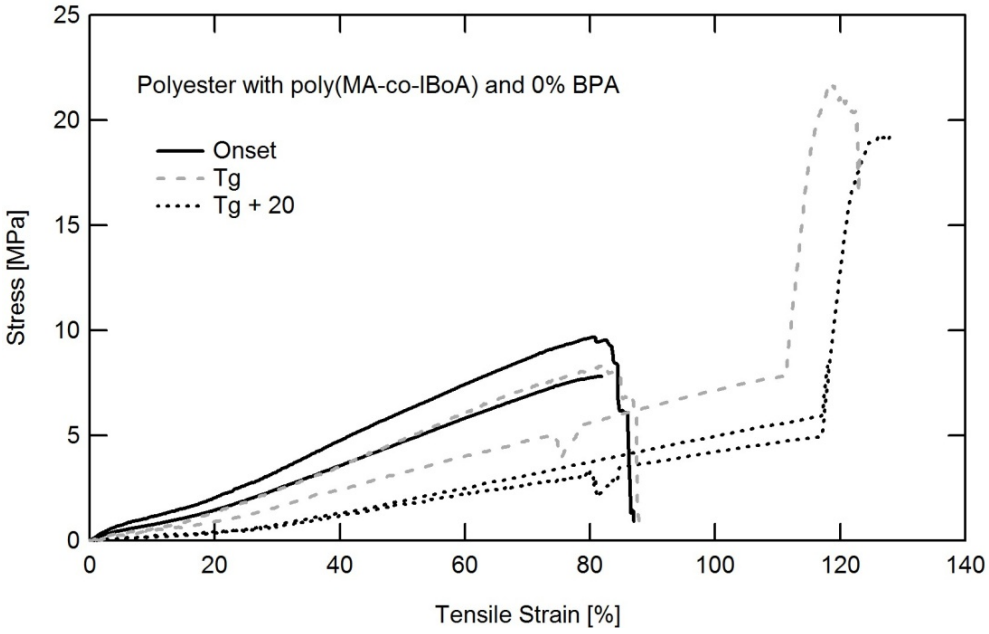
Polyester with poly(MA-co-IBoA) and 0% BPA
Onset
Tg
Tg + 20
Stress [MPa]
Tensile Strain [%]
0
5
10
15
20
25
0
20
40
60
80
100
120
140

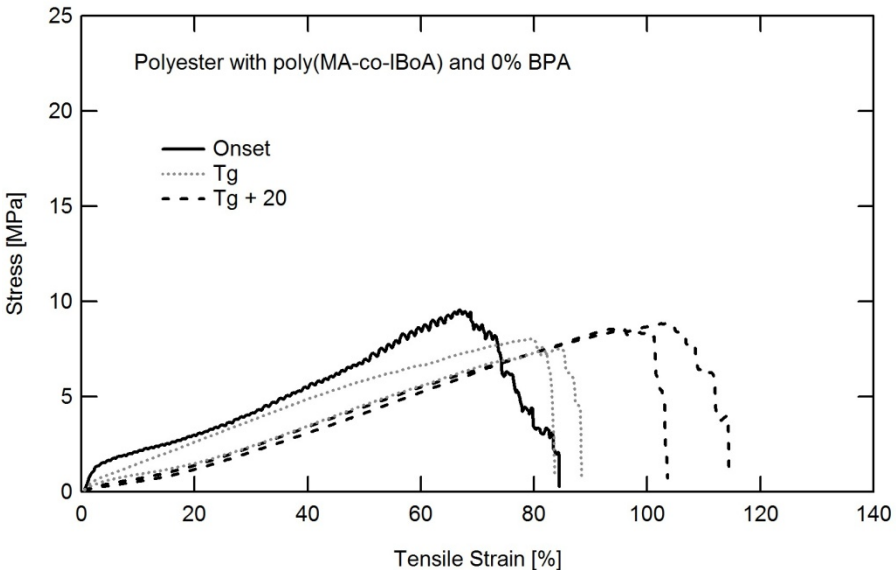
Polyester with poly(MA-co-IBoA) and 0% BPA
Onset
Tg
Tg + 20
Stress [MPa]
Tensile Strain [%]
0
5
10
15
20
25
0
20
40
60
80
100
120
140

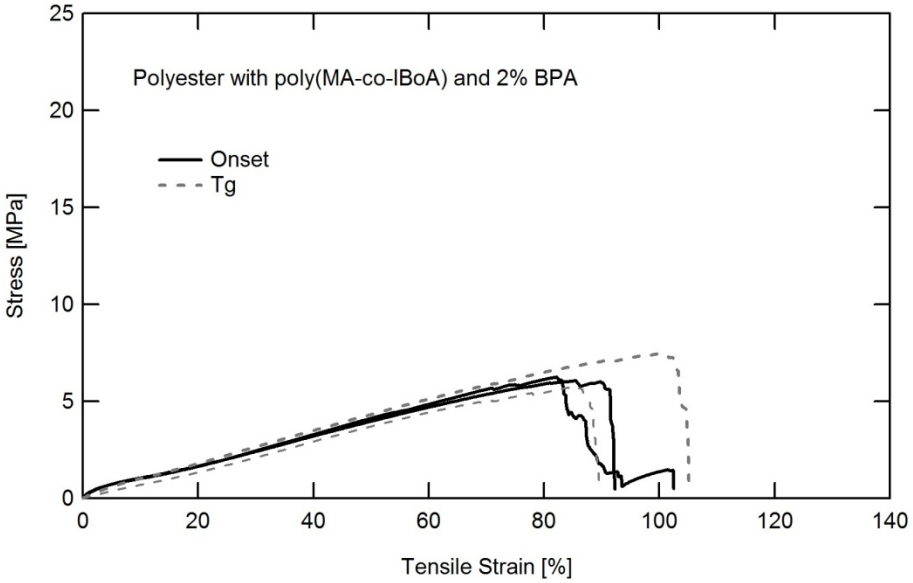
Polyester with poly(MA-co-IBoA) and 2% BPA
Onset
Tg
Stress [MPa]
Tensile Strain [%]
0
5
10
15
20
25
0
20
40
60
80
100
120
140

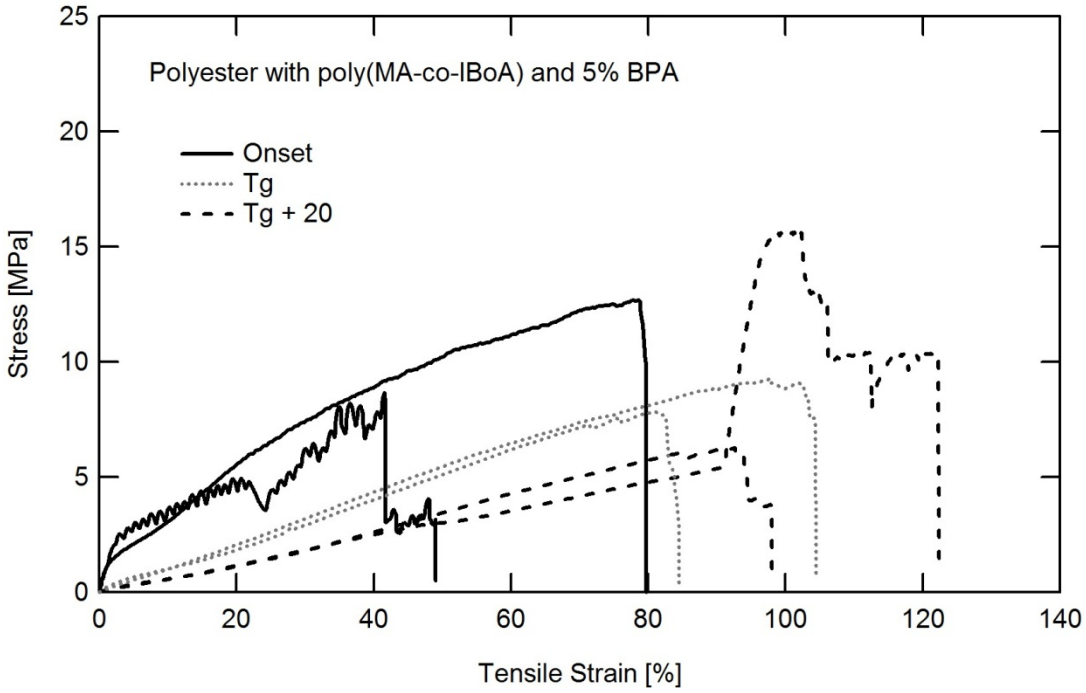
Polyester with poly(MA-co-IBoA) and 5% BPA
Onset
Tg
Tg + 20
Stress [MPa]
Tensile Strain [%]
0
5
10
15
20
25
0
20
40
60
80
100
120
140

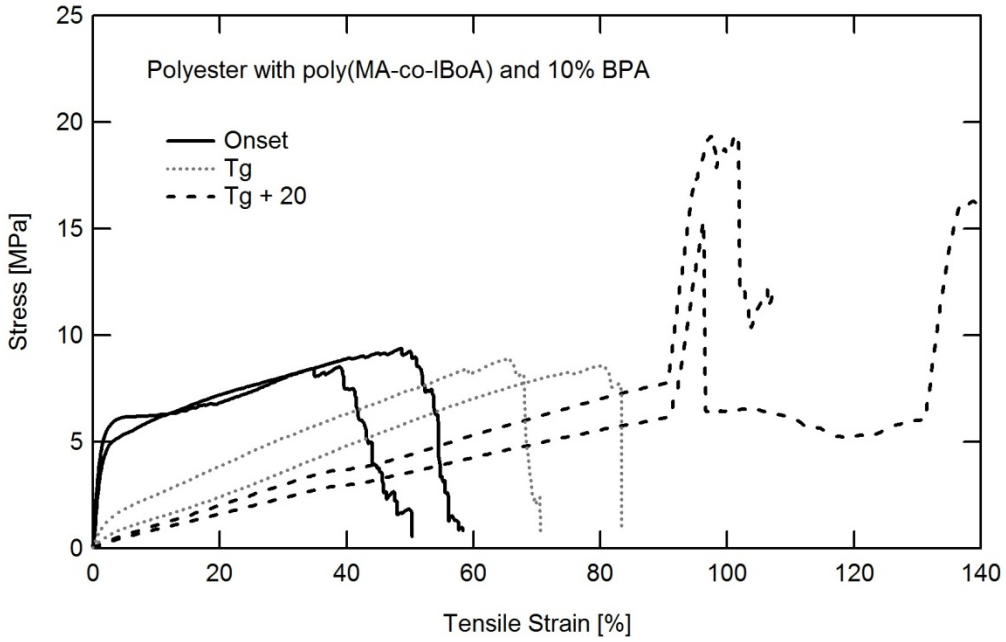
Polyester with poly(MA-co-IBoA) and 10% BPA
Onset
Tg
Tg + 20
Stress [MPa]
Tensile Strain [%]
0
5
10
15
20
25
0
20
40
60
80
100
120
140

A.2 Supplementary Code

```
/*************************************************************************
*
*  Walter Voit
*  16 April 2007
*  Modified: 18 September 2008
*  Georgia Institute of Technology
*
*  Purpose: This user procedure is designed to load waves exported from
*    Universal Analysis generated by the AutoQ C# application. This Igor
*    procedure will facilitate data manipulation and formatting for DMA plots.
*
*    This program also works for the DSC and the Instron.
*    Type UA( printSetting, InstrumentName) where print setting 1 means that
*    each graph will be sent straight to the office printer. Any other number will
*    create the table and graphs but not print them.
*
*    The instrument name should be in quotes and be "DMA", "DSC", or "Instron"*
*
*
*************************************************************************/

#pragma rtGlobals=1    // Use modern global access method.

//These are some of the shortcuts you can call for quick use
Function DMA()
UA(0,"DMA", "temp")
End
Function DSC()
UA(0,"DSC", "temp")
End
Function Instron()
UA(0,"Instron", "strain ")
End
Function Insight()
UA(0,"Insight", "strain ")
End

//This is the main function that is used to access raw data from the various instruments
Function UA(pprint, instrument, xAxis)

Variable pprint
String instrument
String xAxis
String pathName // Name of symbolic path or "" to get dialog
String fileName
String graphName
Variable index=0
```

```
NewPath/O temporaryPath // This will put up a dialog
if (V_flag != 0)
return -1 // User cancelled
endif
pathName = "temporaryPath"

Variable result
do // Loop through each file in folder
if (stringmatch(instrument,"Instron")==1)
fileName = IndexedFile($pathName, index, ".txt")
endif
if (stringmatch(instrument,"DSC")==1)
fileName = IndexedFile($pathName, index, ".txt")
endif
if (stringmatch(instrument,"DMA")==1)
fileName = IndexedFile($pathName, index, ".txt")
endif
if (stringmatch(instrument,"Insight")==1)
fileName = IndexedFile($pathName, index, ".txt")
endif

if ( stringmatch(fileName,"") )// No more files?
print "Index: ", index
return 0 // Break out of loop
endif
result = LoadAndGraph(fileName, pathName, index, instrument, xAxis)
if (result == 0) // Did LoadAndGraph succeed?
// Print the graph.
graphName = WinName(0, 1) // Get the name of the top graph
if (pprint == 1)
PrintSettings /W=$graphName orientation=1
String cmd
sprintf cmd, "PrintGraphs/I %s(1,1,10,7.5)", graphName
Execute cmd // Explained below.
endif
//DoWindow/K $graphName // Kill the graph
KillWaves/A/Z // Kill all unused waves


endif
index += 1
while (1)

if (Exists("temporaryPath")) // Kill temp path if it exists
KillPath temporaryPath
endif



return 0 // Signifies success.
End
```

```
Function LoadUAWaves(input)
String input
LoadWave/J/D/W/N/O/E=1/K=0/V={"\t"," $",0,1}/L={0,1,0,0,0} input
End

Function UAGUI()
LoadWave/J/D/W/N/O/E=1/K=0/V={"\t"," $",0,1}/L={0,1,0,0,0}
UAGraph()

End

Function UAGraph()
Display Storage_Modulus__MPa_, Tan_Delta vs Temperature___C_
ModifyGraph axisOnTop=1, log(left)=1, mirror=1, minor=1, tick=2
Label left, "Storage Modulus (MPa)"
Label bottom, "Temperature (C)"
End

Function LoadAndGraph(fileName, pathName, index, instrument, xAxis)
String fileName // Name of file to load or "" to get dialog
String pathName // Name of path or "" to get dialog
Variable index
String instrument
String xAxis
// load the waves, overwriting existing waves
print "LG Index: ", index
Wave myWave
if (stringmatch(instrument, "DMA")==1)
LoadWave/J/D/W/O/N/E=1/K=0/V={"\t"," $",0,1}/L={0,1,0,0,0}/P=$pathName fileName
endif

if (stringmatch(instrument, "DSC")==1)
LoadWave/J/D/W/O/N/E=1/K=0/V={"\t"," $",0,1}/L={0,1,0,0,0}/P=$pathName fileName
endif

if (stringmatch(instrument, "Instron")==1)
LoadWave/J/D/W/O/N/E=1/K=0/V={"\t"," $",0,1}/L={0,1,0,0,0}/P=$pathName fileName
endif

if (stringmatch(instrument, "Insight")==1)
LoadWave/J/D/W/O/N/E=1/K=0/V={"\t"," $",0,1}/L={0,1,0,0,0}/P=$pathName fileName
endif

if (V_flag==0) // No waves loaded. Perhaps user canceled.
return -1
endif

//Declare all of the variables to use in the funcitons
String graphTitle, timeOrTemp, stress, strain, modulus, tanDelta, heatFlow, load, comment,
toughness, newname

if (stringmatch(instrument, "DMA")==1)
```

```
	//get the graph title from the filename
	splitString/E=("([[:ascii:]]+).AutoQ.txt") fileName, graphTitle


	//various data to collect from file
	modulus = StringFromList(0,WaveList("Storage_Modulus*",";","WIN:") )
	tanDelta = StringFromList(0,WaveList("Tan_Delta*",";","WIN:") )
	if (stringmatch(xAxis,"time")==1)
	timeOrTemp = StringFromList(0,WaveList("Time__min_*",";","WIN:") )
	else
	timeOrTemp = StringFromList(0,WaveList("Temperature___C_*",";","WIN:") )
	endif

	//ensure that wavenames are not more than 31 characters

	//for strain waves
	newname  = "E" + num2str(index) + "_"+graphTitle[0,(min(strlen(graphTitle),10))] + "_" + modulus
	newname = newname[0,30]
	//Duplicate/O $strain, $newname; KillWaves/Z $strain
	Rename $modulus, $newname
	modulus = newname

	//and for stress waves
	newname  = "td" + num2str(index) + "_"+graphTitle[0,(min(strlen(graphTitle),10))] + "_" + tanDelta
	newname = newname[0,30]
	//Duplicate/O $stress, $newname; KillWaves/Z $stress
	Rename $tanDelta, $newname
	tanDelta = newname

	//and for timeTemp waves
	newname  = "t" + num2str(index) + "_"+graphTitle[0,(min(strlen(graphTitle),10))] + "_" +
timeOrTemp
	newname = newname[0,30]
	//Duplicate/O $stress, $newname; KillWaves/Z $stress
	Rename $timeOrTemp, $newname
	timeOrTemp = newname


	//two axes to plot
	//modulus = "Storage_Modulus__MPa_" + num2str(index)
	//tanDelta = "Tan_Delta" + num2str(index)

	//different curves labeled successively with index
	//Duplicate/O Storage_Modulus__MPa_, $modulus
	//Duplicate/O Tan_Delta, $tanDelta

	//if (stringmatch(xAxis,"time")==1)
	// Duplicate/O Time__min_, $timeOrTemp
	//else
	// Duplicate/O Temperature___C_, $timeOrTemp
	//endif
```

```
//set up and display the graph
Display $modulus vs $timeOrTemp as graphTitle
AppendToGraph/R $tanDelta vs $timeOrTemp
ModifyGraph axisOnTop(left)=1, log(left)=1, minor(left)=1, tick(left)=2
ModifyGraph axisOnTop(right)=1, minor(right)=1, tick(right)=2
ModifyGraph axisOnTop(bottom)=1, mirror(bottom)=1, minor(bottom)=1, tick(bottom)=2
ModifyGraph rgb($tanDelta)=(32000,65535,0), lStyle($tanDelta)=2
SetAxis/A/N=1/E=1 right
GetAxis left
SetAxis left, .1, V_max*2
Label left, "Storage Modulus (MPa)"
if (stringmatch(xAxis,"time")==1)
Label bottom, "Time (Min)"
else
Label bottom, "Temperature (C)"
endif
Label right, "Tan Delta"
Legend/C/N=text0/F=0/A=RT "\\s("+modulus+")Storage Modulus\r\\s("+tanDelta+")Tan Delta"
Textbox/F=0/E/C/N=TBFileName/A=MT "\\Z20" + graphTitle

endif

if (stringmatch(instrument,"DSC")==1)

//get the graph title from the filename
splitString/E=("([[:ascii:]]+).AutoQ.txt") fileName, graphTitle

//axis to plot
heatFlow = "Heat_Flow__mW_" + num2str(index)

//different curves labeled successively with index
Duplicate/O Heat_Flow__mW_, $heatFlow
//if (stringmatch(xAxis,"time")==1)
// Duplicate/O Time__min_, $timeOrTemp
//else
// Duplicate/O Temperature___C_, $timeOrTemp
//endif
if (stringmatch(xAxis,"time")==1)
timeOrTemp = StringFromList(0,WaveList("Time__min_*",";","WIN:") )
else
timeOrTemp = StringFromList(0,WaveList("Temperature___C_*",";","WIN:") )
endif



//set up and display the graph
Display $heatFlow vs $timeOrTemp as graphTitle
ModifyGraph axisOnTop(left)=1, log(left)=0, minor(left)=1, tick(left)=2, mirror(left)=1
ModifyGraph axisOnTop(bottom)=1, mirror(bottom)=1, minor(bottom)=1, tick(bottom)=2
ModifyGraph rgb($heatFlow)=(65535,0, 65535)
GetAxis left
```

```
if ((V_min <0)&&(V_max >0))
SetAxis left, V_min - (V_max - V_min)/10, V_max + (V_max - V_min)/10
else
SetAxis/A/N=2 left
endif
GetAxis bottom
if ((V_min <0)&&(V_max >0))
SetAxis bottom, V_min - (V_max - V_min)/10, V_max + (V_max - V_min)/10
else
SetAxis/A/N=2 bottom
endif
Label left, "Heat Flow (mW)"
if (stringmatch(xAxis,"time")==1)
Label bottom, "Time (Min)"
else
Label bottom, "Temperature (C)"
endif
Legend/C/N=text0/F=0/A=RT "\\s("+heatFlow+")HeatFlow"
Textbox/F=0/E/C/N=TBFileName/A=MT "\\Z20" + graphTitle

endif

if (stringmatch(instrument,"Instron")==1)

//get the graph title from the filename
splitString/E=("([[:ascii:]]+).txt") fileName, graphTitle

//two axes to plot
strain = "Tensile strain %" + num2str(index)
stress = "Tensile Stress MPa" + num2str(index)
load = "Load N" + num2str(index)

//different curves labeled successively with index
Duplicate/O Tensile_strain__, $strain
Duplicate/O Tensile_stress_MPa, $stress

//set up and display the graph
Display $stress vs $strain as graphTitle
ModifyGraph axisOnTop(left)=1, mirror(left)=1, minor(left)=1, tick(left)=2
ModifyGraph axisOnTop(bottom)=1, mirror(bottom)=1, minor(bottom)=1, tick(bottom)=2
ModifyGraph rgb($stress)=(65535,0, 0) //red
//ModifyGraph rgb($stress)=(65535,0, 65535) //purple
ModifyGraph lStyle($stress)=0
GetAxis left
SetAxis left, 0, V_max*1.5
GetAxis bottom
SetAxis bottom, 0, V_max*1.2
Label left, "Tensile stress (MPa)"
Label bottom, "Tensile strain (%)"
Legend/C/N=text0/F=0/A=RT "\\s("+stress+")Tensile Stress\r"
Textbox/F=0/E/C/N=TBFileName/A=MT "\\Z20" + num2str(index+1) + ". " + graphTitle
```

```
endif

if (stringmatch(instrument,"Insight")==1)

//get the graph title from the filename
splitString/E=("([[:ascii:]]+).AutoQ.txt") fileName, graphTitle

//various data to collect from file
stress = StringFromList(0,WaveList("Stress*",";","WIN:") )
strain = StringFromList(0,WaveList("Strain*",";","WIN:") )
toughness = StringFromList(0,WaveList("Tough*",";","WIN:"))
comment = StringFromList(0,WaveList("Comment*",";","WIN:,TEXT:1") )
Wave /T commentWave = $comment

//ensure that wavenames are not more than 31 characters


//for strain waves
if (strlen(strain) >=25)
newname  = "e" + num2str(index) + "_"+strain[0,24]
else
newname  = "e" + num2str(index) + "_"+strain
endif
//Duplicate/O $strain, $newname; KillWaves/Z $strain
Rename $strain, $newname
strain = newname

//and for stress waves
if (strlen(stress) >=25)
newname  = "o" + num2str(index) + "_"+stress[0,24]
else
newname  = "o" + num2str(index) + "_"+stress
endif
//Duplicate/O $stress, $newname; KillWaves/Z $stress
Rename $stress, $newname
stress = newname

//and for toughness waves
if (strlen(toughness) >=25)
newname  = "t" + num2str(index) + "_"+toughness[0,24]
else
newname  = "t" + num2str(index) + "_"+toughness
endif
//Duplicate/O $toughenss, $newname; KillWaves/Z $toughness
Rename $toughness, $newname
toughness = newname

//and for comments
if (strlen(comment) >=25)
newname  = "x" + num2str(index) + "_"+comment[0,24]
else
newname  = "x" + num2str(index) + "_"+comment
```

```
    endif
    //Duplicate/O $comment, $newname; KillWaves/Z $comment
    Rename $comment, $newname
    comment = newname


    //set up and display the graph
    Display $stress vs $strain as graphTitle
    ModifyGraph axisOnTop(left)=1, mirror(left)=1, minor(left)=1, tick(left)=2
    ModifyGraph axisOnTop(bottom)=1, mirror(bottom)=1, minor(bottom)=1, tick(bottom)=2
    ModifyGraph rgb($stress)=(65535,0, 0) //red
    ModifyGraph lStyle($stress)=0
    //print "Strain is: ", strain
    GetAxis left
    SetAxis left, 0, V_max*1.5
    GetAxis bottom
    SetAxis bottom, 0, V_max*1.2
    Label left, "Tensile stress (MPa)"
    Label bottom, "Tensile strain (%)"
    Legend/C/N=text0/F=0/A=RT "\\s("+stress+")Tensile Stress\r"
    Textbox/F=0/E/C/N=TBFileName/A=MT "\\Z20" + num2str(index+1) + ". " + graphTitle
    if (waveexists(commentWave))
    Textbox/F=1/E=0/A=RB commentWave [0]
    endif

    endif

    return 0 // Signifies success.
    End

    /*******************************End of Load
Waves*************************************/
```

```
/************  Program.cs ***************************

Walter Voit
Advanced Materials Lab

*****************************************************/

using System;
using System.Collections.Generic;
using System.Windows.Forms;

namespace AutoQ
{
static class Program
{
/// <summary>
/// The main entry point for the application.
/// </summary>
[STAThread]
static void Main()
{
Application.EnableVisualStyles();
Application.SetCompatibleTextRenderingDefault(false);
Application.Run(new AutoQGen());
}
}
   }

/***************End of
Program.cs************************************/



/************  RecursiveFileProcessor.cs ***************************

Walter Voit
Advanced Materials Lab

*****************************************************/


// For Directory.GetFiles and Directory.GetDirectories
// For File.Exists, Directory.Exists
using System;
using System.IO;
using System.Collections;

namespace AutoQ
{
public class RecursiveFileProcessor
{
public static void Main(string[] args)
{
foreach (string path in args)
{
if (File.Exists(path))
```

```
{
// This path is a file
ProcessFile(path);
}
else if (Directory.Exists(path))
{
// This path is a directory
ProcessDirectory(path);
}
else
{
Console.WriteLine("{0} is not a valid file or directory.", path);
}
}
}


// Process all files in the directory passed in, recurse on any
directories
// that are found, and process the files they contain.
public static void ProcessDirectory(string targetDirectory)
{
// Process the list of files found in the directory.
string[] fileEntries = Directory.GetFiles(targetDirectory);
foreach (string fileName in fileEntries)
ProcessFile(fileName);

// Recurse into subdirectories of this directory.
string[] subdirectoryEntries =
Directory.GetDirectories(targetDirectory);
foreach (string subdirectory in subdirectoryEntries)
ProcessDirectory(subdirectory);
}

// Insert logic for processing found files here.
public static void ProcessFile(string path)
{
Console.WriteLine("Processed file '{0}'.", path);
}
}
}

/************  End of RecursiveFileProcessor.cs
*************************/
```

```
/************  Form1.Designer.cs ***************************/


namespace AutoQ
{
partial class AutoQGen
{
/// <summary>
/// Required designer variable.
/// </summary>
private System.ComponentModel.IContainer components = null;

/// <summary>
/// Clean up any resources being used.
/// </summary>
/// <param name="disposing">true if managed resources should be
disposed; otherwise, false.</param>
protected override void Dispose(bool disposing)
{
if (disposing && (components != null))
{
components.Dispose();
}
base.Dispose(disposing);
}

#region Windows Form Designer generated code

/// <summary>
/// Required method for Designer support - do not modify
/// the contents of this method with the code editor.
/// </summary>
private void InitializeComponent()
{
this.components = new System.ComponentModel.Container();
System.ComponentModel.ComponentResourceManager resources = new
System.ComponentModel.ComponentResourceManager(typeof(AutoQGen));
this.dataPath = new System.Windows.Forms.TextBox();
this.browseData = new System.Windows.Forms.Button();
this.buildAQ = new System.Windows.Forms.Button();
this.label1 = new System.Windows.Forms.Label();
this.checkBox_txt = new System.Windows.Forms.CheckBox();
this.checkBox_001 = new System.Windows.Forms.CheckBox();
this.dataFolderDialog = new System.Windows.Forms.FolderBrowserDialog();
this.macroPath = new System.Windows.Forms.TextBox();
this.label2 = new System.Windows.Forms.Label();
this.label3 = new System.Windows.Forms.Label();
this.browseMacro = new System.Windows.Forms.Button();
this.openFileDialog1 = new System.Windows.Forms.OpenFileDialog();
this.label4 = new System.Windows.Forms.Label();
this.checkBox_AQ = new System.Windows.Forms.CheckBox();
this.toolTip1 = new System.Windows.Forms.ToolTip(this.components);
this.downloadButton = new System.Windows.Forms.Button();
this.downloadButton2 = new System.Windows.Forms.Button();
this.backgroundWorker1 = new System.ComponentModel.BackgroundWorker();
this.dowloadButton = new System.Windows.Forms.Button();
```

```
this.downloadFolderDialog = new
System.Windows.Forms.FolderBrowserDialog();
this.macroName = new System.Windows.Forms.ComboBox();
this.label5 = new System.Windows.Forms.Label();
this.label6 = new System.Windows.Forms.Label();
this.label7 = new System.Windows.Forms.Label();
this.label8 = new System.Windows.Forms.Label();
this.label9 = new System.Windows.Forms.Label();
this.label10 = new System.Windows.Forms.Label();
this.label11 = new System.Windows.Forms.Label();
this.label12 = new System.Windows.Forms.Label();
this.AutoQTxtLoc = new System.Windows.Forms.TextBox();
this.label13 = new System.Windows.Forms.Label();
this.label14 = new System.Windows.Forms.Label();
this.label15 = new System.Windows.Forms.Label();
this.procedureFile = new System.Windows.Forms.TextBox();
this.label16 = new System.Windows.Forms.Label();
this.IgorFolder = new System.Windows.Forms.TextBox();
this.label17 = new System.Windows.Forms.Label();
this.backgroundWorker2 = new System.ComponentModel.BackgroundWorker();
this.openFileDialog2 = new System.Windows.Forms.OpenFileDialog();
this.UAdownloaded = new System.Windows.Forms.CheckBox();
this.IgorDownloaded = new System.Windows.Forms.CheckBox();
this.tabInstruments = new System.Windows.Forms.TabControl();
this.tabDownload = new System.Windows.Forms.TabPage();
this.have64bits = new System.Windows.Forms.CheckBox();
this.LoadDefaults = new System.Windows.Forms.Button();
this.label27 = new System.Windows.Forms.Label();
this.tabTA = new System.Windows.Forms.TabPage();
this.tabInsight = new System.Windows.Forms.TabPage();
this.groupBox1 = new System.Windows.Forms.GroupBox();
this.commentBox = new System.Windows.Forms.CheckBox();
this.toughnessBox = new System.Windows.Forms.CheckBox();
this.label28 = new System.Windows.Forms.Label();
this.comboBox2 = new System.Windows.Forms.ComboBox();
this.label18 = new System.Windows.Forms.Label();
this.label19 = new System.Windows.Forms.Label();
this.IgorFolder2 = new System.Windows.Forms.TextBox();
this.label20 = new System.Windows.Forms.Label();
this.label21 = new System.Windows.Forms.Label();
this.procedureFile2 = new System.Windows.Forms.TextBox();
this.comboBox1 = new System.Windows.Forms.ComboBox();
this.tabInstron = new System.Windows.Forms.TabPage();
this.label22 = new System.Windows.Forms.Label();
this.label23 = new System.Windows.Forms.Label();
this.IgorFolder3 = new System.Windows.Forms.TextBox();
this.label24 = new System.Windows.Forms.Label();
this.label25 = new System.Windows.Forms.Label();
this.procedureFile3 = new System.Windows.Forms.TextBox();
this.tabData = new System.Windows.Forms.TabPage();
this.label29 = new System.Windows.Forms.Label();
this.decadeShift = new System.Windows.Forms.TextBox();
this.button2 = new System.Windows.Forms.Button();
this.MovingAverageFile = new System.Windows.Forms.TextBox();
this.button1 = new System.Windows.Forms.Button();
this.dataGridView = new System.Windows.Forms.DataGridView();
```

```
this.label26 = new System.Windows.Forms.Label();
this.openFileDialog3 = new System.Windows.Forms.OpenFileDialog();
this.label30 = new System.Windows.Forms.Label();
this.freqPtsBox = new System.Windows.Forms.TextBox();
this.tabInstruments.SuspendLayout();
this.tabDownload.SuspendLayout();
this.tabTA.SuspendLayout();
this.tabInsight.SuspendLayout();
this.groupBox1.SuspendLayout();
this.tabInstron.SuspendLayout();
this.tabData.SuspendLayout();
((System.ComponentModel.ISupportInitialize)(this.dataGridView)).BeginIn
it();
this.SuspendLayout();
//
// dataPath
//
this.dataPath.Location = new System.Drawing.Point(11, 41);
this.dataPath.Name = "dataPath";
this.dataPath.Size = new System.Drawing.Size(696, 20);
this.dataPath.TabIndex = 1;
this.dataPath.Text = "C:\\";
this.dataPath.TextChanged += new
System.EventHandler(this.dataPath_TextChanged);
//
// browseData
//
this.browseData.Location = new System.Drawing.Point(632, 7);
this.browseData.Name = "browseData";
this.browseData.Size = new System.Drawing.Size(75, 23);
this.browseData.TabIndex = 2;
this.browseData.Text = "Browse";
this.browseData.UseVisualStyleBackColor = true;
this.browseData.Click += new System.EventHandler(this.button1_Click);
//
// buildAQ
//
this.buildAQ.Font = new System.Drawing.Font("Microsoft Sans Serif",
16F, System.Drawing.FontStyle.Regular,
System.Drawing.GraphicsUnit.Point, ((byte)(0)));
this.buildAQ.Location = new System.Drawing.Point(434, 108);
this.buildAQ.Name = "buildAQ";
this.buildAQ.Size = new System.Drawing.Size(283, 44);
this.buildAQ.TabIndex = 7;
this.buildAQ.Text = "Build AutoQ";
this.buildAQ.UseVisualStyleBackColor = true;
this.buildAQ.Click += new System.EventHandler(this.button2_Click);
//
// label1
//
this.label1.AutoSize = true;
this.label1.Location = new System.Drawing.Point(19, 274);
this.label1.Name = "label1";
this.label1.Size = new System.Drawing.Size(119, 13);
this.label1.TabIndex = 0;
this.label1.Text = "File Extensions to Parse";
```

```
//
// checkBox_txt
//
this.checkBox_txt.AutoSize = true;
this.checkBox_txt.Location = new System.Drawing.Point(153, 272);
this.checkBox_txt.Name = "checkBox_txt";
this.checkBox_txt.Size = new System.Drawing.Size(40, 17);
this.checkBox_txt.TabIndex = 5;
this.checkBox_txt.Text = ".txt";
this.checkBox_txt.UseVisualStyleBackColor = true;
this.checkBox_txt.CheckedChanged += new
System.EventHandler(this.checkBox_txt_CheckedChanged);
//
// checkBox_001
//
this.checkBox_001.AutoSize = true;
this.checkBox_001.Checked = true;
this.checkBox_001.CheckState = System.Windows.Forms.CheckState.Checked;
this.checkBox_001.Location = new System.Drawing.Point(208, 272);
this.checkBox_001.Name = "checkBox_001";
this.checkBox_001.Size = new System.Drawing.Size(89, 17);
this.checkBox_001.TabIndex = 6;
this.checkBox_001.Text = ".001, .002, ...";
this.checkBox_001.UseVisualStyleBackColor = true;
//
// macroPath
//
this.macroPath.Location = new System.Drawing.Point(19, 204);
this.macroPath.Name = "macroPath";
this.macroPath.Size = new System.Drawing.Size(603, 20);
this.macroPath.TabIndex = 3;
this.macroPath.Text = "G:\\TA\\macros\\AutoQ.mac";
this.macroPath.TextChanged += new
System.EventHandler(this.macroPath_TextChanged);
//
// label2
//
this.label2.AutoSize = true;
this.label2.Location = new System.Drawing.Point(12, 108);
this.label2.Name = "label2";
this.label2.Size = new System.Drawing.Size(0, 13);
this.label2.TabIndex = 0;
//
// label3
//
this.label3.AutoSize = true;
this.label3.Location = new System.Drawing.Point(12, 244);
this.label3.Name = "label3";
this.label3.Size = new System.Drawing.Size(0, 13);
this.label3.TabIndex = 0;
this.label3.Click += new System.EventHandler(this.label3_Click);
//
// browseMacro
//
this.browseMacro.Location = new System.Drawing.Point(623, 204);
this.browseMacro.Name = "browseMacro";
```

```
this.browseMacro.Size = new System.Drawing.Size(75, 21);
this.browseMacro.TabIndex = 4;
this.browseMacro.Text = "Browse";
this.browseMacro.UseVisualStyleBackColor = true;
this.browseMacro.Click += new System.EventHandler(this.button3_Click);
//
// openFileDialog1
//
this.openFileDialog1.FileName = "openFileDialog1";
//
// label4
//
this.label4.AutoSize = true;
this.label4.Location = new System.Drawing.Point(12, 227);
this.label4.Name = "label4";
this.label4.Size = new System.Drawing.Size(0, 13);
this.label4.TabIndex = 8;
//
// checkBox_AQ
//
this.checkBox_AQ.AutoSize = true;
this.checkBox_AQ.Location = new System.Drawing.Point(302, 273);
this.checkBox_AQ.Name = "checkBox_AQ";
this.checkBox_AQ.Size = new System.Drawing.Size(63, 17);
this.checkBox_AQ.TabIndex = 10;
this.checkBox_AQ.Text = ".AutoQ*";
this.toolTip1.SetToolTip(this.checkBox_AQ, "Exclusive comparison. When
unchecked, old AutoQ files are avoided. Checking this " +
"will trump all other extensions and only search for old AutoQ files.
");
this.checkBox_AQ.UseVisualStyleBackColor = true;
this.checkBox_AQ.CheckedChanged += new
System.EventHandler(this.checkBox_AQ_CheckedChanged);
//
// toolTip1
//
this.toolTip1.Popup += new
System.Windows.Forms.PopupEventHandler(this.toolTip1_Popup);
//
// downloadButton
//
this.downloadButton.Location = new System.Drawing.Point(76, 114);
this.downloadButton.Name = "downloadButton";
this.downloadButton.Size = new System.Drawing.Size(160, 25);
this.downloadButton.TabIndex = 11;
this.downloadButton.Text = "UA Macro download\r\n";
this.toolTip1.SetToolTip(this.downloadButton, "This button will
download Igor.mac and LoadUAWaves.ipf for use in Universal Analy" +
"sis and Igor. A prompt will allow you to specify the download
folder.");
this.downloadButton.UseVisualStyleBackColor = true;
this.downloadButton.Click += new
System.EventHandler(this.downloadButton_Click);
//
// downloadButton2
//
```

```
this.downloadButton2.Location = new System.Drawing.Point(332, 114);
this.downloadButton2.Name = "downloadButton2";
this.downloadButton2.Size = new System.Drawing.Size(160, 25);
this.downloadButton2.TabIndex = 30;
this.downloadButton2.Text = "Igor Prodecure Download";
this.toolTip1.SetToolTip(this.downloadButton2, "This button will
download Igor.mac and LoadUAWaves.ipf for use in Universal Analy" +
"sis and Igor. A prompt will allow you to specify the download
folder.");
this.downloadButton2.UseVisualStyleBackColor = true;
this.downloadButton2.Click += new
System.EventHandler(this.downloadButton2_Click);
//
// backgroundWorker1
//
this.backgroundWorker1.DoWork += new
System.ComponentModel.DoWorkEventHandler(this.backgroundWorker1_DoWork)
;
this.backgroundWorker1.RunWorkerCompleted += new
System.ComponentModel.RunWorkerCompletedEventHandler(this.backgroundWor
ker1_RunWorkerCompleted);
//
// dowloadButton
//
this.dowloadButton.Location = new System.Drawing.Point(0, 0);
this.dowloadButton.Name = "dowloadButton";
this.dowloadButton.Size = new System.Drawing.Size(75, 23);
this.dowloadButton.TabIndex = 0;
//
// macroName
//
this.macroName.BackColor = System.Drawing.Color.LightSkyBlue;
this.macroName.FormattingEnabled = true;
this.macroName.Items.AddRange(new object[] {
"DMA",
"DSC",
"Instron",
"Insight"});
this.macroName.Location = new System.Drawing.Point(368, 71);
this.macroName.Name = "macroName";
this.macroName.Size = new System.Drawing.Size(339, 21);
this.macroName.TabIndex = 13;
this.macroName.Text = "Instron";
this.macroName.SelectedIndexChanged += new
System.EventHandler(this.macroName_SelectedIndexChanged);
//
// label5
//
this.label5.AutoSize = true;
this.label5.Font = new System.Drawing.Font("Microsoft Sans Serif", 12F,
System.Drawing.FontStyle.Regular, System.Drawing.GraphicsUnit.Point,
((byte)(0)));
this.label5.Location = new System.Drawing.Point(19, 54);
this.label5.Name = "label5";
this.label5.Size = new System.Drawing.Size(538, 20);
this.label5.TabIndex = 14;
```

```
this.label5.Text = "Step A: Download the Universal Analysis Macro and
the Igor Procedure file.";
this.label5.Click += new System.EventHandler(this.label5_Click);
//
// label6
//
this.label6.AutoSize = true;
this.label6.Font = new System.Drawing.Font("Microsoft Sans Serif", 12F,
System.Drawing.FontStyle.Regular, System.Drawing.GraphicsUnit.Point,
((byte)(0)));
this.label6.Location = new System.Drawing.Point(19, 181);
this.label6.Name = "label6";
this.label6.Size = new System.Drawing.Size(439, 20);
this.label6.TabIndex = 15;
this.label6.Text = "Step B: Tell us where the Universal Analysis macro
is located.\r\n";
//
// label7
//
this.label7.AutoSize = true;
this.label7.Font = new System.Drawing.Font("Microsoft Sans Serif", 12F,
System.Drawing.FontStyle.Regular, System.Drawing.GraphicsUnit.Point,
((byte)(0)));
this.label7.Location = new System.Drawing.Point(11, 72);
this.label7.Name = "label7";
this.label7.Size = new System.Drawing.Size(350, 20);
this.label7.TabIndex = 16;
this.label7.Text = "Step 2: Tell us which instrument the data is
from.";
//
// label8
//
this.label8.AutoSize = true;
this.label8.Font = new System.Drawing.Font("Microsoft Sans Serif", 12F,
System.Drawing.FontStyle.Regular, System.Drawing.GraphicsUnit.Point,
((byte)(0)));
this.label8.Location = new System.Drawing.Point(11, 7);
this.label8.Name = "label8";
this.label8.Size = new System.Drawing.Size(561, 20);
this.label8.TabIndex = 17;
this.label8.Text = "Step 1: Pick any file in the raw data folder. We
will process all files in that f" +
"older.\r\n";
this.label8.Click += new System.EventHandler(this.label8_Click);
//
// label9
//
this.label9.AutoSize = true;
this.label9.Location = new System.Drawing.Point(19, 81);
this.label9.Name = "label9";
this.label9.Size = new System.Drawing.Size(538, 13);
this.label9.TabIndex = 18;
this.label9.Text = "These are typically saved in C:\\TA\\Macros and
C:\\Program Files\\WaveMetrics\\Igor P" +
"ro Folder\\User Procedures\r\n";
//
```

```
// label10
//
this.label10.AutoSize = true;
this.label10.Font = new System.Drawing.Font("Microsoft Sans Serif",
12F, System.Drawing.FontStyle.Regular,
System.Drawing.GraphicsUnit.Point, ((byte)(0)));
this.label10.Location = new System.Drawing.Point(19, 243);
this.label10.Name = "label10";
this.label10.Size = new System.Drawing.Size(396, 20);
this.label10.TabIndex = 19;
this.label10.Text = "Step C: Select advanced options and build your
AutoQ.";
//
// label11
//
this.label11.AutoSize = true;
this.label11.Font = new System.Drawing.Font("Microsoft Sans Serif",
12F, System.Drawing.FontStyle.Regular,
System.Drawing.GraphicsUnit.Point, ((byte)(0)));
this.label11.Location = new System.Drawing.Point(13, 12);
this.label11.Name = "label11";
this.label11.Size = new System.Drawing.Size(409, 20);
this.label11.TabIndex = 20;
this.label11.Text = "Step 4: Open Universal Analysis and run the
AutoQueue.\r\n";
//
// label12
//
this.label12.AutoSize = true;
this.label12.Font = new System.Drawing.Font("Microsoft Sans Serif",
10F, System.Drawing.FontStyle.Regular,
System.Drawing.GraphicsUnit.Point, ((byte)(0)));
this.label12.Location = new System.Drawing.Point(13, 38);
this.label12.Name = "label12";
this.label12.Size = new System.Drawing.Size(565, 51);
this.label12.TabIndex = 21;
this.label12.Text = resources.GetString("label12.Text");
//
// AutoQTxtLoc
//
this.AutoQTxtLoc.Location = new System.Drawing.Point(31, 97);
this.AutoQTxtLoc.Name = "AutoQTxtLoc";
this.AutoQTxtLoc.Size = new System.Drawing.Size(662, 20);
this.AutoQTxtLoc.TabIndex = 22;
//
// label13
//
this.label13.AutoSize = true;
this.label13.Font = new System.Drawing.Font("Microsoft Sans Serif",
10F, System.Drawing.FontStyle.Regular,
System.Drawing.GraphicsUnit.Point, ((byte)(0)));
this.label13.Location = new System.Drawing.Point(13, 124);
this.label13.Name = "label13";
this.label13.Size = new System.Drawing.Size(676, 51);
this.label13.TabIndex = 23;
```

```
this.label13.Text = "d.) Click Run\r\ne.) Now you will have to click
save for each graph once.  (Sorry b" +
"ut there is no good way to automate this!)\r\nf.) Now your data is
formatted and r" +
"eady for Igor.";
//
// label14
//
this.label14.AutoSize = true;
this.label14.Font = new System.Drawing.Font("Microsoft Sans Serif",
12F, System.Drawing.FontStyle.Regular,
System.Drawing.GraphicsUnit.Point, ((byte)(0)));
this.label14.Location = new System.Drawing.Point(13, 191);
this.label14.Name = "label14";
this.label14.Size = new System.Drawing.Size(360, 20);
this.label14.TabIndex = 24;
this.label14.Text = "Step 5: Open Igor and see your formatted
graphs.\r\n";
//
// label15
//
this.label15.AutoSize = true;
this.label15.Font = new System.Drawing.Font("Microsoft Sans Serif",
10F, System.Drawing.FontStyle.Regular,
System.Drawing.GraphicsUnit.Point, ((byte)(0)));
this.label15.Location = new System.Drawing.Point(13, 217);
this.label15.Name = "label15";
this.label15.Size = new System.Drawing.Size(581, 17);
this.label15.TabIndex = 25;
this.label15.Text = "a.) Make sure you open the Correct Prodecure file
called LoadWaves.ipf. It should" +
" be here:";
//
// procedureFile
//
this.procedureFile.Location = new System.Drawing.Point(31, 237);
this.procedureFile.Name = "procedureFile";
this.procedureFile.Size = new System.Drawing.Size(662, 20);
this.procedureFile.TabIndex = 26;
//
// label16
//
this.label16.AutoSize = true;
this.label16.Font = new System.Drawing.Font("Microsoft Sans Serif",
10F, System.Drawing.FontStyle.Regular,
System.Drawing.GraphicsUnit.Point, ((byte)(0)));
this.label16.Location = new System.Drawing.Point(13, 267);
this.label16.Name = "label16";
this.label16.Size = new System.Drawing.Size(512, 119);
this.label16.TabIndex = 27;
this.label16.Text = resources.GetString("label16.Text");
//
// IgorFolder
//
this.IgorFolder.Location = new System.Drawing.Point(31, 391);
this.IgorFolder.Name = "IgorFolder";
```

```
this.IgorFolder.Size = new System.Drawing.Size(662, 20);
this.IgorFolder.TabIndex = 28;
this.IgorFolder.TextChanged += new
System.EventHandler(this.IgorFolder_TextChanged);
//
// label17
//
this.label17.AutoSize = true;
this.label17.Font = new System.Drawing.Font("Microsoft Sans Serif",
10F, System.Drawing.FontStyle.Regular,
System.Drawing.GraphicsUnit.Point, ((byte)(0)));
this.label17.Location = new System.Drawing.Point(13, 416);
this.label17.Name = "label17";
this.label17.Size = new System.Drawing.Size(294, 17);
this.label17.TabIndex = 29;
this.label17.Text = "d.) Click Ok and have fun tweaking your
data.\r\n";
//
// backgroundWorker2
//
this.backgroundWorker2.DoWork += new
System.ComponentModel.DoWorkEventHandler(this.backgroundWorker2_DoWork)
;
this.backgroundWorker2.RunWorkerCompleted += new
System.ComponentModel.RunWorkerCompletedEventHandler(this.backgroundWor
ker2_RunWorkerCompleted);
//
// openFileDialog2
//
this.openFileDialog2.FileName = "openFileDialog1";
//
// UAdownloaded
//
this.UAdownloaded.AutoSize = true;
this.UAdownloaded.Location = new System.Drawing.Point(242, 120);
this.UAdownloaded.Name = "UAdownloaded";
this.UAdownloaded.Size = new System.Drawing.Size(15, 14);
this.UAdownloaded.TabIndex = 31;
this.UAdownloaded.UseVisualStyleBackColor = true;
//
// IgorDownloaded
//
this.IgorDownloaded.AutoSize = true;
this.IgorDownloaded.Location = new System.Drawing.Point(498, 120);
this.IgorDownloaded.Name = "IgorDownloaded";
this.IgorDownloaded.Size = new System.Drawing.Size(15, 14);
this.IgorDownloaded.TabIndex = 32;
this.IgorDownloaded.UseVisualStyleBackColor = true;
//
// tabInstruments
//
this.tabInstruments.Controls.Add(this.tabDownload);
this.tabInstruments.Controls.Add(this.tabTA);
this.tabInstruments.Controls.Add(this.tabInsight);
this.tabInstruments.Controls.Add(this.tabInstron);
this.tabInstruments.Controls.Add(this.tabData);
```

```
this.tabInstruments.Location = new System.Drawing.Point(52, 158);
this.tabInstruments.Name = "tabInstruments";
this.tabInstruments.SelectedIndex = 0;
this.tabInstruments.Size = new System.Drawing.Size(721, 465);
this.tabInstruments.TabIndex = 33;
this.tabInstruments.TabIndexChanged += new
System.EventHandler(this.tabInstruments_TabIndexChanged);
//
// tabDownload
//
this.tabDownload.BackColor = System.Drawing.Color.LightGray;
this.tabDownload.Controls.Add(this.have64bits);
this.tabDownload.Controls.Add(this.LoadDefaults);
this.tabDownload.Controls.Add(this.label27);
this.tabDownload.Controls.Add(this.label5);
this.tabDownload.Controls.Add(this.label10);
this.tabDownload.Controls.Add(this.IgorDownloaded);
this.tabDownload.Controls.Add(this.label9);
this.tabDownload.Controls.Add(this.macroPath);
this.tabDownload.Controls.Add(this.checkBox_AQ);
this.tabDownload.Controls.Add(this.UAdownloaded);
this.tabDownload.Controls.Add(this.browseMacro);
this.tabDownload.Controls.Add(this.downloadButton2);
this.tabDownload.Controls.Add(this.downloadButton);
this.tabDownload.Controls.Add(this.checkBox_001);
this.tabDownload.Controls.Add(this.label6);
this.tabDownload.Controls.Add(this.checkBox_txt);
this.tabDownload.Controls.Add(this.label1);
this.tabDownload.Location = new System.Drawing.Point(4, 22);
this.tabDownload.Name = "tabDownload";
this.tabDownload.Size = new System.Drawing.Size(713, 439);
this.tabDownload.TabIndex = 3;
this.tabDownload.Text = "Downloads";
this.tabDownload.UseVisualStyleBackColor = true;
this.tabDownload.Click += new
System.EventHandler(this.tabDownload_Click);
//
// have64bits
//
this.have64bits.AutoSize = true;
this.have64bits.Checked = true;
this.have64bits.CheckState = System.Windows.Forms.CheckState.Checked;
this.have64bits.Location = new System.Drawing.Point(153, 307);
this.have64bits.Name = "have64bits";
this.have64bits.Size = new System.Drawing.Size(87, 17);
this.have64bits.TabIndex = 35;
this.have64bits.Text = "64-bit system";
this.have64bits.UseVisualStyleBackColor = true;
//
// LoadDefaults
//
this.LoadDefaults.Location = new System.Drawing.Point(570, 243);
this.LoadDefaults.Name = "LoadDefaults";
this.LoadDefaults.Size = new System.Drawing.Size(128, 23);
this.LoadDefaults.TabIndex = 34;
this.LoadDefaults.Text = "Load Defaults";
```

```
this.LoadDefaults.UseVisualStyleBackColor = true;
this.LoadDefaults.Click += new
System.EventHandler(this.LoadDefaults_Click);
//
// label27
//
this.label27.AutoSize = true;
this.label27.Font = new System.Drawing.Font("Microsoft Sans Serif",
14F, System.Drawing.FontStyle.Regular,
System.Drawing.GraphicsUnit.Point, ((byte)(0)));
this.label27.Location = new System.Drawing.Point(124, 8);
this.label27.Name = "label27";
this.label27.Size = new System.Drawing.Size(472, 24);
this.label27.TabIndex = 33;
this.label27.Text = "Download these files the first time you use this
program.";
//
// tabTA
//
this.tabTA.BackColor = System.Drawing.Color.LightSkyBlue;
this.tabTA.Controls.Add(this.label11);
this.tabTA.Controls.Add(this.label12);
this.tabTA.Controls.Add(this.AutoQTxtLoc);
this.tabTA.Controls.Add(this.label13);
this.tabTA.Controls.Add(this.label17);
this.tabTA.Controls.Add(this.label14);
this.tabTA.Controls.Add(this.IgorFolder);
this.tabTA.Controls.Add(this.label15);
this.tabTA.Controls.Add(this.label16);
this.tabTA.Controls.Add(this.procedureFile);
this.tabTA.Location = new System.Drawing.Point(4, 22);
this.tabTA.Name = "tabTA";
this.tabTA.Padding = new System.Windows.Forms.Padding(3);
this.tabTA.Size = new System.Drawing.Size(713, 439);
this.tabTA.TabIndex = 0;
this.tabTA.Text = "TA Instruments";
this.tabTA.UseVisualStyleBackColor = true;
//
// tabInsight
//
this.tabInsight.BackColor = System.Drawing.Color.Plum;
this.tabInsight.Controls.Add(this.groupBox1);
this.tabInsight.Controls.Add(this.label28);
this.tabInsight.Controls.Add(this.comboBox2);
this.tabInsight.Controls.Add(this.label18);
this.tabInsight.Controls.Add(this.label19);
this.tabInsight.Controls.Add(this.IgorFolder2);
this.tabInsight.Controls.Add(this.label20);
this.tabInsight.Controls.Add(this.label21);
this.tabInsight.Controls.Add(this.procedureFile2);
this.tabInsight.Controls.Add(this.comboBox1);
this.tabInsight.Location = new System.Drawing.Point(4, 22);
this.tabInsight.Name = "tabInsight";
this.tabInsight.Padding = new System.Windows.Forms.Padding(3);
this.tabInsight.Size = new System.Drawing.Size(713, 439);
this.tabInsight.TabIndex = 1;
```

```
this.tabInsight.Text = "Insight";
this.tabInsight.UseVisualStyleBackColor = true;
//
// groupBox1
//
this.groupBox1.Controls.Add(this.commentBox);
this.groupBox1.Controls.Add(this.toughnessBox);
this.groupBox1.Location = new System.Drawing.Point(6, 6);
this.groupBox1.Name = "groupBox1";
this.groupBox1.Size = new System.Drawing.Size(418, 119);
this.groupBox1.TabIndex = 40;
this.groupBox1.TabStop = false;
this.groupBox1.Text = "Formatting Options";
//
// commentBox
//
this.commentBox.AutoSize = true;
this.commentBox.Checked = true;
this.commentBox.CheckState = System.Windows.Forms.CheckState.Checked;
this.commentBox.Location = new System.Drawing.Point(13, 19);
this.commentBox.Name = "commentBox";
this.commentBox.Size = new System.Drawing.Size(218, 17);
this.commentBox.TabIndex = 36;
this.commentBox.Text = "Include Comments as Annotations in Igor";
this.commentBox.UseVisualStyleBackColor = true;
this.commentBox.CheckedChanged += new
System.EventHandler(this.checkBox1_CheckedChanged);
//
// toughnessBox
//
this.toughnessBox.AutoSize = true;
this.toughnessBox.Checked = true;
this.toughnessBox.CheckState = System.Windows.Forms.CheckState.Checked;
this.toughnessBox.Location = new System.Drawing.Point(13, 42);
this.toughnessBox.Name = "toughnessBox";
this.toughnessBox.Size = new System.Drawing.Size(177, 17);
this.toughnessBox.TabIndex = 39;
this.toughnessBox.Text = "Add Toughness Column to Data";
this.toughnessBox.UseVisualStyleBackColor = true;
this.toughnessBox.CheckedChanged += new
System.EventHandler(this.toughnessBox_CheckedChanged);
//
// label28
//
this.label28.AutoSize = true;
this.label28.Location = new System.Drawing.Point(468, 26);
this.label28.Name = "label28";
this.label28.Size = new System.Drawing.Size(75, 13);
this.label28.TabIndex = 38;
this.label28.Text = "X-axis variable";
//
// comboBox2
//
this.comboBox2.FormattingEnabled = true;
this.comboBox2.Items.AddRange(new object[] {
"Strain",
```

```
"Toughness"});
this.comboBox2.Location = new System.Drawing.Point(559, 23);
this.comboBox2.Name = "comboBox2";
this.comboBox2.Size = new System.Drawing.Size(121, 21);
this.comboBox2.TabIndex = 37;
this.comboBox2.Text = "Strain";
//
// label18
//
this.label18.AutoSize = true;
this.label18.Font = new System.Drawing.Font("Microsoft Sans Serif",
10F, System.Drawing.FontStyle.Regular,
System.Drawing.GraphicsUnit.Point, ((byte)(0)));
this.label18.Location = new System.Drawing.Point(15, 385);
this.label18.Name = "label18";
this.label18.Size = new System.Drawing.Size(294, 17);
this.label18.TabIndex = 35;
this.label18.Text = "d.) Click Ok and have fun tweaking your
data.\r\n";
//
// label19
//
this.label19.AutoSize = true;
this.label19.Font = new System.Drawing.Font("Microsoft Sans Serif",
12F, System.Drawing.FontStyle.Regular,
System.Drawing.GraphicsUnit.Point, ((byte)(0)));
this.label19.Location = new System.Drawing.Point(15, 155);
this.label19.Name = "label19";
this.label19.Size = new System.Drawing.Size(360, 20);
this.label19.TabIndex = 30;
this.label19.Text = "Step 4: Open Igor and see your formatted
graphs.\r\n";
//
// IgorFolder2
//
this.IgorFolder2.Location = new System.Drawing.Point(32, 360);
this.IgorFolder2.Name = "IgorFolder2";
this.IgorFolder2.Size = new System.Drawing.Size(648, 20);
this.IgorFolder2.TabIndex = 34;
this.IgorFolder2.TextChanged += new
System.EventHandler(this.IgorFolder2_TextChanged);
//
// label20
//
this.label20.AutoSize = true;
this.label20.Font = new System.Drawing.Font("Microsoft Sans Serif",
10F, System.Drawing.FontStyle.Regular,
System.Drawing.GraphicsUnit.Point, ((byte)(0)));
this.label20.Location = new System.Drawing.Point(15, 182);
this.label20.Name = "label20";
this.label20.Size = new System.Drawing.Size(581, 17);
this.label20.TabIndex = 31;
this.label20.Text = "a.) Make sure you open the Correct Prodecure file
called LoadWaves.ipf. It should" +
" be here:";
//
```

```
// label21
//
this.label21.AutoSize = true;
this.label21.Font = new System.Drawing.Font("Microsoft Sans Serif",
10F, System.Drawing.FontStyle.Regular,
System.Drawing.GraphicsUnit.Point, ((byte)(0)));
this.label21.Location = new System.Drawing.Point(14, 234);
this.label21.Name = "label21";
this.label21.Size = new System.Drawing.Size(512, 119);
this.label21.TabIndex = 33;
this.label21.Text = resources.GetString("label21.Text");
//
// procedureFile2
//
this.procedureFile2.Location = new System.Drawing.Point(32, 207);
this.procedureFile2.Name = "procedureFile2";
this.procedureFile2.Size = new System.Drawing.Size(648, 20);
this.procedureFile2.TabIndex = 32;
//
// comboBox1
//
this.comboBox1.FormattingEnabled = true;
this.comboBox1.Items.AddRange(new object[] {
"Tension",
"Compression"});
this.comboBox1.Location = new System.Drawing.Point(559, 54);
this.comboBox1.Name = "comboBox1";
this.comboBox1.Size = new System.Drawing.Size(121, 21);
this.comboBox1.TabIndex = 0;
this.comboBox1.Text = "Tension";
//
// tabInstron
//
this.tabInstron.BackColor = System.Drawing.Color.PaleGreen;
this.tabInstron.Controls.Add(this.label22);
this.tabInstron.Controls.Add(this.label23);
this.tabInstron.Controls.Add(this.IgorFolder3);
this.tabInstron.Controls.Add(this.label24);
this.tabInstron.Controls.Add(this.label25);
this.tabInstron.Controls.Add(this.procedureFile3);
this.tabInstron.Location = new System.Drawing.Point(4, 22);
this.tabInstron.Name = "tabInstron";
this.tabInstron.Size = new System.Drawing.Size(713, 439);
this.tabInstron.TabIndex = 2;
this.tabInstron.Text = "Instron";
this.tabInstron.UseVisualStyleBackColor = true;
//
// label22
//
this.label22.AutoSize = true;
this.label22.Font = new System.Drawing.Font("Microsoft Sans Serif",
10F, System.Drawing.FontStyle.Regular,
System.Drawing.GraphicsUnit.Point, ((byte)(0)));
this.label22.Location = new System.Drawing.Point(19, 259);
this.label22.Name = "label22";
this.label22.Size = new System.Drawing.Size(294, 17);
```

```
this.label22.TabIndex = 41;
this.label22.Text = "d.) Click Ok and have fun tweaking your
data.\r\n";
//
// label23
//
this.label23.AutoSize = true;
this.label23.Font = new System.Drawing.Font("Microsoft Sans Serif",
12F, System.Drawing.FontStyle.Regular,
System.Drawing.GraphicsUnit.Point, ((byte)(0)));
this.label23.Location = new System.Drawing.Point(19, 29);
this.label23.Name = "label23";
this.label23.Size = new System.Drawing.Size(360, 20);
this.label23.TabIndex = 36;
this.label23.Text = "Step 4: Open Igor and see your formatted
graphs.\r\n";
//
// IgorFolder3
//
this.IgorFolder3.Location = new System.Drawing.Point(36, 234);
this.IgorFolder3.Name = "IgorFolder3";
this.IgorFolder3.Size = new System.Drawing.Size(648, 20);
this.IgorFolder3.TabIndex = 40;
this.IgorFolder3.TextChanged += new
System.EventHandler(this.IgorFolder3_TextChanged);
//
// label24
//
this.label24.AutoSize = true;
this.label24.Font = new System.Drawing.Font("Microsoft Sans Serif",
10F, System.Drawing.FontStyle.Regular,
System.Drawing.GraphicsUnit.Point, ((byte)(0)));
this.label24.Location = new System.Drawing.Point(19, 56);
this.label24.Name = "label24";
this.label24.Size = new System.Drawing.Size(581, 17);
this.label24.TabIndex = 37;
this.label24.Text = "a.) Make sure you open the Correct Prodecure file
called LoadWaves.ipf. It should" +
" be here:";
//
// label25
//
this.label25.AutoSize = true;
this.label25.Font = new System.Drawing.Font("Microsoft Sans Serif",
10F, System.Drawing.FontStyle.Regular,
System.Drawing.GraphicsUnit.Point, ((byte)(0)));
this.label25.Location = new System.Drawing.Point(18, 108);
this.label25.Name = "label25";
this.label25.Size = new System.Drawing.Size(512, 119);
this.label25.TabIndex = 39;
this.label25.Text = resources.GetString("label25.Text");
//
// procedureFile3
//
this.procedureFile3.Location = new System.Drawing.Point(36, 81);
this.procedureFile3.Name = "procedureFile3";
```

```
this.procedureFile3.Size = new System.Drawing.Size(648, 20);
this.procedureFile3.TabIndex = 38;
//
// tabData
//
this.tabData.Controls.Add(this.label30);
this.tabData.Controls.Add(this.freqPtsBox);
this.tabData.Controls.Add(this.label29);
this.tabData.Controls.Add(this.decadeShift);
this.tabData.Controls.Add(this.button2);
this.tabData.Controls.Add(this.MovingAverageFile);
this.tabData.Controls.Add(this.button1);
this.tabData.Controls.Add(this.dataGridView);
this.tabData.Location = new System.Drawing.Point(4, 22);
this.tabData.Name = "tabData";
this.tabData.Size = new System.Drawing.Size(713, 439);
this.tabData.TabIndex = 4;
this.tabData.Text = "Data Review";
this.tabData.UseVisualStyleBackColor = true;
//
// label29
//
this.label29.AutoSize = true;
this.label29.Location = new System.Drawing.Point(341, 16);
this.label29.Name = "label29";
this.label29.Size = new System.Drawing.Size(69, 13);
this.label29.TabIndex = 38;
this.label29.Text = "Decade Shift";
//
// decadeShift
//
this.decadeShift.Location = new System.Drawing.Point(416, 13);
this.decadeShift.Name = "decadeShift";
this.decadeShift.Size = new System.Drawing.Size(44, 20);
this.decadeShift.TabIndex = 37;
this.decadeShift.Text = "6";
//
// button2
//
this.button2.Location = new System.Drawing.Point(158, 11);
this.button2.Name = "button2";
this.button2.Size = new System.Drawing.Size(147, 23);
this.button2.TabIndex = 36;
this.button2.Text = "3D Absorption Map";
this.button2.UseVisualStyleBackColor = true;
this.button2.Click += new System.EventHandler(this.button2_Click_1);
//
// MovingAverageFile
//
this.MovingAverageFile.Location = new System.Drawing.Point(13, 57);
this.MovingAverageFile.Name = "MovingAverageFile";
this.MovingAverageFile.Size = new System.Drawing.Size(307, 20);
this.MovingAverageFile.TabIndex = 35;
//
// button1
//
```

```
this.button1.Location = new System.Drawing.Point(13, 11);
this.button1.Name = "button1";
this.button1.Size = new System.Drawing.Size(128, 23);
this.button1.TabIndex = 1;
this.button1.Text = "Moving Average";
this.button1.UseVisualStyleBackColor = true;
this.button1.Click += new System.EventHandler(this.button1_Click_2);
//
// dataGridView
//
this.dataGridView.ColumnHeadersHeightSizeMode =
System.Windows.Forms.DataGridViewColumnHeadersHeightSizeMode.AutoSize;
this.dataGridView.Location = new System.Drawing.Point(3, 40);
this.dataGridView.Name = "dataGridView";
this.dataGridView.Size = new System.Drawing.Size(707, 396);
this.dataGridView.TabIndex = 0;
//
// label26
//
this.label26.AutoSize = true;
this.label26.Font = new System.Drawing.Font("Microsoft Sans Serif",
12F, System.Drawing.FontStyle.Regular,
System.Drawing.GraphicsUnit.Point, ((byte)(0)));
this.label26.Location = new System.Drawing.Point(11, 113);
this.label26.Name = "label26";
this.label26.Size = new System.Drawing.Size(394, 20);
this.label26.TabIndex = 34;
this.label26.Text = "Step 3: Process raw data for Universal Analysis or
Igor.";
//
// openFileDialog3
//
this.openFileDialog3.FileName = "openFileDialog3";
//
// label30
//
this.label30.AutoSize = true;
this.label30.Location = new System.Drawing.Point(501, 16);
this.label30.Name = "label30";
this.label30.Size = new System.Drawing.Size(71, 13);
this.label30.TabIndex = 40;
this.label30.Text = "# of Freq. Pts";
//
// freqPtsBox
//
this.freqPtsBox.Location = new System.Drawing.Point(576, 13);
this.freqPtsBox.Name = "freqPtsBox";
this.freqPtsBox.Size = new System.Drawing.Size(44, 20);
this.freqPtsBox.TabIndex = 39;
this.freqPtsBox.Text = "50";
this.freqPtsBox.TextChanged += new
System.EventHandler(this.textBox1_TextChanged);
//
// AutoQGen
//
this.AutoScaleDimensions = new System.Drawing.SizeF(6F, 13F);
```

```
this.AutoScaleMode = System.Windows.Forms.AutoScaleMode.Font;
this.AutoScroll = true;
this.BackColor = System.Drawing.Color.Khaki;
this.ClientSize = new System.Drawing.Size(914, 669);
this.Controls.Add(this.label26);
this.Controls.Add(this.buildAQ);
this.Controls.Add(this.tabInstruments);
this.Controls.Add(this.label8);
this.Controls.Add(this.label7);
this.Controls.Add(this.label4);
this.Controls.Add(this.label3);
this.Controls.Add(this.macroName);
this.Controls.Add(this.label2);
this.Controls.Add(this.browseData);
this.Controls.Add(this.dataPath);
this.Name = "AutoQGen";
this.Text = "AutoQ Generator";
this.Load += new System.EventHandler(this.AutoQGen_Load);
this.FormClosed += new
System.Windows.Forms.FormClosedEventHandler(this.AutoQGen_FormClosed);
this.tabInstruments.ResumeLayout(false);
this.tabDownload.ResumeLayout(false);
this.tabDownload.PerformLayout();
this.tabTA.ResumeLayout(false);
this.tabTA.PerformLayout();
this.tabInsight.ResumeLayout(false);
this.tabInsight.PerformLayout();
this.groupBox1.ResumeLayout(false);
this.groupBox1.PerformLayout();
this.tabInstron.ResumeLayout(false);
this.tabInstron.PerformLayout();
this.tabData.ResumeLayout(false);
this.tabData.PerformLayout();
((System.ComponentModel.ISupportInitialize)(this.dataGridView)).EndInit
();
this.ResumeLayout(false);
this.PerformLayout();

}

#endregion

private System.Windows.Forms.TextBox dataPath;
private System.Windows.Forms.Button browseData;
private System.Windows.Forms.Button buildAQ;
private System.Windows.Forms.Label label1;
private System.Windows.Forms.CheckBox checkBox_txt;
private System.Windows.Forms.CheckBox checkBox_001;
private System.Windows.Forms.FolderBrowserDialog dataFolderDialog;
private System.Windows.Forms.TextBox macroPath;
private System.Windows.Forms.Label label2;
private System.Windows.Forms.Label label3;
private System.Windows.Forms.Button browseMacro;
private System.Windows.Forms.OpenFileDialog openFileDialog1;
private System.Windows.Forms.Label label4;
private System.Windows.Forms.CheckBox checkBox_AQ;
```

```
private System.Windows.Forms.ToolTip toolTip1;
private System.Windows.Forms.Button downloadButton;
private System.Windows.Forms.FolderBrowserDialog downloadFolderDialog;
private System.Windows.Forms.ComboBox macroName;
private System.Windows.Forms.Label label5;
private System.Windows.Forms.Label label6;
private System.Windows.Forms.Label label7;
private System.Windows.Forms.Label label8;
private System.Windows.Forms.Label label9;
private System.Windows.Forms.Label label10;
private System.Windows.Forms.Label label11;
private System.Windows.Forms.Label label12;
private System.Windows.Forms.TextBox AutoQTxtLoc;
private System.Windows.Forms.Label label13;
private System.Windows.Forms.Label label14;
private System.Windows.Forms.Label label15;
private System.Windows.Forms.TextBox procedureFile;
private System.Windows.Forms.Label label16;
private System.Windows.Forms.TextBox IgorFolder;
private System.Windows.Forms.Label label17;
private System.Windows.Forms.Button downloadButton2;
private System.ComponentModel.BackgroundWorker backgroundWorker2;
private System.Windows.Forms.OpenFileDialog openFileDialog2;
private System.Windows.Forms.CheckBox UAdownloaded;
private System.Windows.Forms.CheckBox IgorDownloaded;
private System.Windows.Forms.TabControl tabInstruments;
private System.Windows.Forms.TabPage tabTA;
private System.Windows.Forms.TabPage tabInsight;
private System.Windows.Forms.TabPage tabInstron;
private System.Windows.Forms.ComboBox comboBox1;
private System.Windows.Forms.Label label18;
private System.Windows.Forms.Label label19;
private System.Windows.Forms.TextBox IgorFolder2;
private System.Windows.Forms.Label label20;
private System.Windows.Forms.Label label21;
private System.Windows.Forms.TextBox procedureFile2;
private System.Windows.Forms.Label label22;
private System.Windows.Forms.Label label23;
private System.Windows.Forms.TextBox IgorFolder3;
private System.Windows.Forms.Label label24;
private System.Windows.Forms.Label label25;
private System.Windows.Forms.TextBox procedureFile3;
private System.Windows.Forms.TabPage tabDownload;
private System.Windows.Forms.Label label26;
private System.Windows.Forms.Label label27;
private System.Windows.Forms.Button LoadDefaults;
private System.Windows.Forms.CheckBox commentBox;
private System.Windows.Forms.Label label28;
private System.Windows.Forms.ComboBox comboBox2;
private System.Windows.Forms.GroupBox groupBox1;
private System.Windows.Forms.CheckBox toughnessBox;
private System.Windows.Forms.CheckBox have64bits;
private System.Windows.Forms.TabPage tabData;
private System.Windows.Forms.DataGridView dataGridView;
private System.Windows.Forms.Button button1;
private System.Windows.Forms.OpenFileDialog openFileDialog3;
```

```
private System.Windows.Forms.TextBox MovingAverageFile;
private System.Windows.Forms.Button button2;
private System.Windows.Forms.Label label29;
private System.Windows.Forms.TextBox decadeShift;
private System.Windows.Forms.Label label30;
private System.Windows.Forms.TextBox freqPtsBox;
}
}


/************  End of Form1.Designer.cs **************************/
```

```
/*****************************************************
*
* Walter Voit
* 9 October 2007
* Georgia Institute of Technology
* AutoQ
*
* Purpose: This program analyses a selected folder and attempts to
determine
* which files are Universal Analysis data files. The program goes on to
* rename the files and move them into a folder to prepare them for data
* analysis in Igor.
*
*****************************************************/

using System;
using System.Collections.Generic;
using System.ComponentModel;
using System.Data;
using System.Drawing;
using System.Text;
using System.Windows.Forms;
using System.IO;
using System.Threading;
using System.Net;
using System.Reflection;
using Microsoft.Office.Interop.Excel;
using Microsoft.Win32;
using Utility.ModifyRegistry;



namespace AutoQ
{
public partial class AutoQGen : Form
{
private BackgroundWorker backgroundWorker1;
private System.Windows.Forms.Button dowloadButton;
ModifyRegistry myRegistry = new ModifyRegistry();
String lastUpdate = "June 24, 2008";


public AutoQGen()
{
InitializeComponent();
loadSettings();

}

private void button1_Click(object sender, EventArgs e)
{

this.openFileDialog2.InitialDirectory = this.dataPath.Text;
this.openFileDialog2 = new OpenFileDialog();
this.openFileDialog2.ShowDialog();
```

```
try
{
this.dataPath.Text = this.openFileDialog2.FileName.ToString();
this.dataPath.Text = this.dataPath.Text.Substring(0,
(this.dataPath.Text.LastIndexOf('\\')));
saveSettings();
}
catch
{ }
}

private void button2_Click(object sender, EventArgs e)
{

//make sure the program is up to date before building the autoQ
this.tabInstruments.SelectedTab = this.tabDownload;
if (!this.have64bits.Checked)
{
if (this.lastUpdate != this.myRegistry.ReadReg("Last AutoQ update"))
{
this.promptDownloadAutoQ();
}
if (this.lastUpdate != this.myRegistry.ReadReg("Last Igor update"))
{
this.promptDownloadIgor();
}
this.saveSettings();
this.loadSettings();
}

CopyDirectory(this.dataPath.Text, this.dataPath.Text + "-AutoQ");
this.dataPath.Text = this.dataPath.Text + "-AutoQ";

if ((this.macroName.Text == "Instron")||(this.macroName.Text ==
"Insight"))
{
RecursiveFileProcessor rfp = new
RecursiveFileProcessor(this.dataPath.Text, this.macroName.Text,
this.checkBox_001.Checked, this.toughnessBox.Checked,
this.dataGridView);
}
else
{
using (StreamWriter sw = new StreamWriter(this.dataPath.Text +
"\\AutoQ.txt", false))
{
// Add some text to the file.
sw.WriteLine("[AQV1] Autoqueue File. Created " + GetTADate1() + ".");

foreach (string fn in Directory.GetFiles(this.dataPath.Text))
{

if (((fn.Contains(".0") == (this.checkBox_001.Checked) == true) ||
//Rule 1: allows file with .0 in name except by R3
(fn.Contains(".txt") == (this.checkBox_txt.Checked) == true)) && //Rule
2: allows files with .txt in name except by R3
```

```
(fn.Contains(".AutoQ") == (this.checkBox_AQ.Checked)))     //Rule 3:
excludes files already processed unless checked
{
sw.Write('"' + copyFile(fn) + '"');
//sw.WriteLine(" \"G:\\TA\\Macros\\Gall.mac\" \"ExportToIgor2\" {" +
GetTADate()+ "}");
sw.WriteLine("\"" + this.macroPath.Text + "\" \"" + this.macroName.Text
+ "\" {" + GetTADate() + "}");
}
}
sw.Close();
}
}
saveSettings();
this.AutoQTxtLoc.Text = this.dataPath.Text + "\\AutoQ.txt";
this.IgorFolder.Text = this.dataPath.Text + "\\Igor";

}

private string copyFile(string path)
{
string path2 = path + ".AutoQ.001";
path2 = path2.Insert(path2.LastIndexOf('\\') + 1, "Igor\\");
try
{
if (!Directory.Exists(path2.Substring(0, (path2.LastIndexOf('\\') +
1))))
Directory.CreateDirectory(path2.Substring(0, (path2.LastIndexOf('\\') +
1)));
// Only do the Copy operation if the first file exists
// and the second file does not.
if (File.Exists(path))
{
if (File.Exists(path2))
{
Console.WriteLine("The target already exists");
}
else
{
// Try to copy the file.
File.Move(path, path2);
Console.WriteLine("{0} was copied to {1}.", path, path2);
}
}
else
{
Console.WriteLine("The source file does not exist.");
}
}
catch
{
Console.WriteLine("Double copying is not allowed, as expected.");
}
return path2;
}
```

```
private void CopyDirectory(string source, string destination)
{
try
{

if (destination[destination.Length - 1] != Path.DirectorySeparatorChar)
{
destination += Path.DirectorySeparatorChar;
}

if (!Directory.Exists(destination))
{
Directory.CreateDirectory(destination);
}

string[] fileSystemEntries = Directory.GetFileSystemEntries(source);
foreach (string entry in fileSystemEntries)
{
if (Directory.Exists(entry))
{
// It's a subdirectory so recurse
CopyDirectory(entry, destination + Path.GetFileName(entry));
}
else
{
// It's a file so copy it
File.Copy(entry, destination + Path.GetFileName(entry), true);
}
}
}
catch
{


}

}




private string GetTADate()
{
string myDate = DateTime.Now.ToString("dd-MMM-yyyy hh:mm");
return myDate;
}

private string GetTADate1()
{
string myDate = DateTime.Now.ToString("d-MMM-yyyy hh:mm");
return myDate;
}

private void button3_Click(object sender, EventArgs e)
{
this.openFileDialog1.InitialDirectory = this.macroPath.Text;
```

```
this.openFileDialog1 = new OpenFileDialog();
this.openFileDialog1.ShowDialog();
this.macroPath.Text = this.openFileDialog1.FileName.ToString();
saveSettings();
}



private void backgroundWorker1_DoWork(
object sender,
DoWorkEventArgs e)
{
try
{
WebClient download = new WebClient();
download.DownloadFile(@"http://www.advancedmaterialslab.com/programs/Au
toQ/AutoQ.mac", this.downloadFolderDialog.SelectedPath +
"\\AutoQ.mac");
}
catch { }
}
private void backgroundWorker2_DoWork(
object sender,
DoWorkEventArgs e)
{
try
{
WebClient download = new WebClient();
//this.downloadFolderDialog.RootFolder = this.myRegistry.ReadReg("Igor
Procedure folder");
download.DownloadFile(@"http://www.advancedmaterialslab.com/programs/Au
toQ/LoadUAWaves.ipf", this.downloadFolderDialog.SelectedPath +
"\\LoadUAWaves.ipf");
}
catch { }
}

private void backgroundWorker1_RunWorkerCompleted(
object sender,
RunWorkerCompletedEventArgs e)
{
if (e.Error == null)
{
MessageBox.Show("Download of AutoQ.mac complete");
//this.macroPath.Text = Directory.GetCurrentDirectory().ToString() +
"\\Igor.mac";
//this.macroPath.Text = Directory.GetCurrentDirectory().ToString() +
"\\poop";
}
else
{
MessageBox.Show(
"Failed to download file",
"Download failed",
```

```
MessageBoxButtons.OK,
MessageBoxIcon.Error);
}
}

private void backgroundWorker2_RunWorkerCompleted(
object sender,
RunWorkerCompletedEventArgs e)
{
if (e.Error == null)
{
MessageBox.Show("Download of LoadUAWaves.ipf complete");
//this.macroPath.Text = Directory.GetCurrentDirectory().ToString() +
"\\Igor.mac";
//this.macroPath.Text = Directory.GetCurrentDirectory().ToString() +
"\\poop1";
}
else
{
MessageBox.Show(
"Failed to download file",
"Download failed",
MessageBoxButtons.OK,
MessageBoxIcon.Error);
}
}

private void saveSettings()
{
try
{

this.myRegistry.WriteReg("Data folder", this.dataPath.Text);
this.myRegistry.WriteReg("UA Macro folder", this.macroPath.Text);
this.myRegistry.WriteReg("UA Macro name", this.macroName.Text);
this.myRegistry.WriteReg("Igor Procedure folder",
this.procedureFile.Text);
if (this.myRegistry.WriteReg("Window Size", this.Height + ":" +
this.Width))
this.have64bits.Checked = false;
this.procedureFile2.Text = this.procedureFile.Text;
this.procedureFile3.Text = this.procedureFile.Text;

}


catch { }



}

private void LoadDefaults_Click(object sender, EventArgs e)
{
DialogResult answer = MessageBox.Show(
"Are you sure you want to resest all parameters to their defaults",
```

```
"Loading Default Settings",
MessageBoxButtons.YesNo,
MessageBoxIcon.Exclamation);
if (answer == DialogResult.Yes)
{
this.dataPath.Text = null;
this.macroPath.Text = null;
this.macroName.Text = null;
this.procedureFile.Text = null;
this.Height = 555;
this.Width = 777;
this.IgorDownloaded.Checked = false;
this.UAdownloaded.Checked = false;
saveSettings();
this.tabInstruments.SelectTab(this.tabDownload);
}


}
private void promptDownloadAutoQ()
{
DialogResult answer = MessageBox.Show(
"Press OK to download newest version",
"AutoQ macro out of date",
MessageBoxButtons.OKCancel,
MessageBoxIcon.Warning);
if (answer == DialogResult.OK)
{
this.downloadAutoQ();
}

}

private void promptDownloadIgor()
{
DialogResult answer = MessageBox.Show(
"Press OK to download newest version",
"Igor macro out of date",
MessageBoxButtons.OKCancel,
MessageBoxIcon.Warning);

if (answer == DialogResult.OK)
{
this.downloadIgor();
}


}


private void loadSettings()
{
try
{
if (this.have64bits.Checked)
```

```
this.myRegistry.SubKey = "SOFTWARE\\Wow6432Node\\" +
System.Windows.Forms.Application.ProductName.ToUpper();
this.dataPath.Text = this.myRegistry.ReadReg("Data folder");
this.macroPath.Text = this.myRegistry.ReadReg("UA Macro folder");
this.macroName.Text = this.myRegistry.ReadReg("UA Macro name");
this.procedureFile.Text = this.myRegistry.ReadReg("Igor Procedure
folder");

//if ((this.dataPath.Text != null) || (this.macroPath.Text != null) ||
//   (this.macroName.Text != null) || (this.procedureFile.Text !=
null))
//{
//    this.noRegistry.Checked = false;
//}

//test to see if Registry is working
//if (this.myRegistry.WriteReg("Data folder", this.dataPath.Text))
//    this.have64bits.Checked = false;


this.procedureFile2.Text = this.procedureFile.Text;
this.procedureFile3.Text = this.procedureFile.Text;



if ((this.procedureFile.Text != null) && (this.procedureFile.Text !=
""))
{
this.IgorDownloaded.Checked = true;
this.macroName_SelectedIndexChanged(null, null);
}
else
this.tabInstruments.SelectTab(this.tabInstron);
if ((this.macroPath.Text != null) && (this.macroPath.Text != ""))
{
this.UAdownloaded.Checked = true;
this.macroName_SelectedIndexChanged(null, null);
}
else
this.tabInstruments.SelectTab(this.tabInstron);

String[] sep = { ":" };
string mySize = this.myRegistry.ReadReg("Window Size");
this.Height = int.Parse(mySize.Split(sep, StringSplitOptions.None)[0]);
this.Width = int.Parse(mySize.Split(sep, StringSplitOptions.None)[1]);

}
catch
{
//saveSettings();
}



}
```

```
private void checkBox_txt_CheckedChanged(object sender, EventArgs e)
{

}

private void toolTip1_Popup(object sender, PopupEventArgs e)
{

}

private void button1_Click_1(object sender, EventArgs e)
{


}

private void macroName_SelectedIndexChanged(object sender, EventArgs e)
{
if (this.macroName.Text == "Instron")
{
this.tabInstruments.SelectTab(this.tabInstron);
this.macroName.BackColor = Color.PaleGreen;

}
else if (this.macroName.Text == "Insight")
{
this.tabInstruments.SelectTab(this.tabInsight);
this.macroName.BackColor = Color.Plum;
}
else
{
this.tabInstruments.SelectTab(this.tabTA);
this.macroName.BackColor = Color.LightBlue;
}
}

private void macroPath_TextChanged(object sender, EventArgs e)
{

}

private void label3_Click(object sender, EventArgs e)
{

}

private void label8_Click(object sender, EventArgs e)
{

}

private void checkBox_AQ_CheckedChanged(object sender, EventArgs e)
{

}
```

```
private void dataPath_TextChanged(object sender, EventArgs e)
{

}

private void downloadButton_Click(object sender, EventArgs e)
{
this.downloadAutoQ();
}

private void downloadAutoQ()
{
this.downloadFolderDialog = new FolderBrowserDialog();
this.downloadFolderDialog.Description = "Choose the location to save
the Igor Procedure" +
"This is typically saved in C:\\TA\\Macros.";

this.downloadFolderDialog.SelectedPath = this.myRegistry.ReadReg("UA
Macro folder");
if ((this.downloadFolderDialog.SelectedPath ==
null)||(this.downloadFolderDialog.SelectedPath == ""))
{
this.downloadFolderDialog.RootFolder =
Environment.SpecialFolder.MyComputer;
DialogResult answer = this.downloadFolderDialog.ShowDialog();
if (answer == DialogResult.Cancel)
return;
}

this.macroPath.Text = this.downloadFolderDialog.SelectedPath +
"\\AutoQ.mac";
// Start the download operation in the background.
this.backgroundWorker1.RunWorkerAsync();

// Disable the button for the duration of the download.
this.dowloadButton.Enabled = false;

// Wait for the BackgroundWorker to finish the download.
while (this.backgroundWorker1.IsBusy)
{
// Keep UI messages moving, so the form remains
// responsive during the asynchronous operation.
System.Windows.Forms.Application.DoEvents();
}

// The download is done, so enable the button.
this.dowloadButton.Enabled = true;
saveSettings();
this.myRegistry.WriteReg("Last AutoQ update", this.lastUpdate);
this.UAdownloaded.Checked = true;
}

private void downloadButton2_Click(object sender, EventArgs e)
{
this.downloadIgor();
}
```

```
private void downloadIgor()
{
this.downloadFolderDialog = new FolderBrowserDialog();
this.downloadFolderDialog.Description = "Choose the location to save
the AutoQ Macro.\nClick cancel if not" +
"in Program Files.\nTypically saved in C:\\Program
Files\\WaveMetrics\\Igor Pro Folder\\User Procedures\r\n";



this.downloadFolderDialog.SelectedPath = this.myRegistry.ReadReg("Igor
Procedure folder");
if ((this.downloadFolderDialog.SelectedPath == null) ||
(this.downloadFolderDialog.SelectedPath == ""))
{
this.downloadFolderDialog.RootFolder =
Environment.SpecialFolder.ProgramFiles;
DialogResult answer = this.downloadFolderDialog.ShowDialog();
if (answer == DialogResult.Cancel)
{
this.downloadFolderDialog.RootFolder =
Environment.SpecialFolder.MyComputer;
answer = this.downloadFolderDialog.ShowDialog();
if (answer == DialogResult.Cancel)
{
return;
}


}
}
this.procedureFile.Text = this.downloadFolderDialog.SelectedPath +
"\\LoadUAWaves.ipf";
this.procedureFile2.Text = this.procedureFile.Text;
this.procedureFile3.Text = this.procedureFile.Text;


// Start the download operation in the background.
this.backgroundWorker2.RunWorkerAsync();

// Disable the button for the duration of the download.
this.dowloadButton.Enabled = false;

// Wait for the BackgroundWorker to finish the download.
while (this.backgroundWorker2.IsBusy)
{
// Keep UI messages moving, so the form remains
// responsive during the asynchronous operation.
System.Windows.Forms.Application.DoEvents();
}

// The download is done, so enable the button.
this.dowloadButton.Enabled = true;
saveSettings();
this.myRegistry.WriteReg("Last Igor update", this.lastUpdate);
```

```
this.IgorDownloaded.Checked = true;
}

private void progressBar1_Click(object sender, EventArgs e)
{

}

private void label5_Click(object sender, EventArgs e)
{

}

private void tabDownload_Click(object sender, EventArgs e)
{

}

private void tabInstruments_TabIndexChanged(object sender, EventArgs e)
{

}

private void IgorFolder_TextChanged(object sender, EventArgs e)
{
this.IgorFolder2.Text = this.IgorFolder.Text;
this.IgorFolder3.Text = this.IgorFolder.Text;
}

private void IgorFolder2_TextChanged(object sender, EventArgs e)
{

}

private void IgorFolder3_TextChanged(object sender, EventArgs e)
{

}

private void checkBox1_CheckedChanged(object sender, EventArgs e)
{
//this.checkBox_001.Checked
}

private void toughnessBox_CheckedChanged(object sender, EventArgs e)
{

}

private void AutoQGen_Load(object sender, EventArgs e)
{

}

private void AutoQGen_FormClosed(object sender, FormClosedEventArgs e)
{
```

```
this.saveSettings();
}

private void button1_Click_2(object sender, EventArgs e)
{
String dir = "";
String newfilename = "";

try
{
this.openFileDialog3.InitialDirectory = this.MovingAverageFile.Text;
this.openFileDialog3 = new OpenFileDialog();
this.openFileDialog3.ShowDialog();

this.MovingAverageFile.Text = this.openFileDialog3.FileName.ToString();
dir = this.MovingAverageFile.Text.Substring(0,
(this.MovingAverageFile.Text.LastIndexOf('\\')));
newfilename = this.MovingAverageFile.Text.Substring(0,
this.MovingAverageFile.Text.LastIndexOf(".xls")) + "MovingAverage.xls";

}
catch (Exception except)
{ }


//this.dataPath.Text is where the file to open is
Microsoft.Office.Interop.Excel.Application app = null;
Workbook book = null;
Worksheet sheet = null;
Range range = null;


try
{
// -- Now write the next file

app = new Microsoft.Office.Interop.Excel.Application();
book = app.Workbooks.Open(this.MovingAverageFile.Text, Missing.Value,
Missing.Value, Missing.Value, Missing.Value, Missing.Value,
Missing.Value, Missing.Value, Missing.Value, Missing.Value,
Missing.Value, Missing.Value, Missing.Value, Missing.Value,
Missing.Value);  //<--Error here
sheet =
(Microsoft.Office.Interop.Excel.Worksheet)book.Sheets.get_Item(1);

app.DisplayAlerts = false;

sheet.Activate();



range = sheet.UsedRange;
object[,] values = (object[,])range.Value2;

Console.WriteLine("Row Count: " + values.GetLength(0).ToString());
Console.WriteLine("Col Count: " + values.GetLength(1).ToString());
```

```
//bool write = false;
int i = 1;

using (StreamWriter sw = new StreamWriter(newfilename, false))
{
sw.WriteLine("Temp\tRun 1\tRun2\tRun3\tRun4\tRun5\tAverage\tStd.
Dev.");
int x = 0; int y = 19; //this is where the first set of data would go
int[] compRows = { 10, 11, 12, 13, 14 };
int[] modRows = { 1, 2, 3, 4,5 };
double[] compSums = { 0, 0, 0, 0,0 };
double[] compCounts = { 0, 0, 0, 0,0 };
double RowAverage = 0;
double RowSTD = 0;
int valueCount = 0;
int compNum = 0;

for (x = 3; x <= values.GetLength(0); x++)
{

for (i = 2; i <= values.GetLength(0); i++)
{
if ((values[x - 1, y - 1] != null) &&
(values[x + 1, y - 1] != null))
{
for (compNum = 0; compNum < compRows.Length ; compNum++)
{
if ((values[i, compRows[compNum]] != null) &&
(double.Parse(values[i, compRows[compNum]].ToString()) >
double.Parse(values[x - 1, y - 1].ToString())) &&
(double.Parse(values[i, compRows[compNum]].ToString()) <
double.Parse(values[x + 1, y - 1].ToString())))
{
if (values[i, modRows[compNum]] != null)
{
compSums[compNum] += double.Parse(values[i,
modRows[compNum]].ToString());
compCounts[compNum]++;
}
}


}


}
}

if (values[x, y - 1] == null)
{
//this means we do not need data at this temp
}
```

```
else
{
sw.Write(values[x, y - 1]);
RowAverage = 0; RowSTD = 0; valueCount = 0;
for (compNum = 0; compNum < compRows.Length ; compNum++)
{
values[x, y +compNum] = compSums[compNum] / compCounts[compNum];
if (compCounts[compNum] == 0)
values[x, y +compNum] = null;

compSums[compNum] = 0;
compCounts[compNum] = 0;

sw.Write("\t" + values[x, y+compNum]);
if (values[x, y + compNum] != null)
{
RowAverage += double.Parse(values[x, y + compNum].ToString());
valueCount++;
}
}

if (valueCount == 0)
{
RowAverage = 0;
RowSTD = 0;
sw.WriteLine();
}
else
{
RowAverage /= valueCount;


for (compNum = 0; compNum < compRows.Length; compNum++)
{
if (values[x, y + compNum] != null)
{
RowSTD += Math.Pow((double.Parse(values[x, y + compNum].ToString()) -
RowAverage), 2);
//valueCount++;
}
}
RowSTD /= (valueCount - 1);
RowSTD = Math.Sqrt(RowSTD);

sw.WriteLine("\t" + RowAverage + "\t" + RowSTD);
}
}

}

sw.Close();
}
```

```
//for (i=1; i <= values.GetLength(0); i++)
//{
//    if (values[i, 1].ToString().Contains("Time"))
//    {
//   break;
//    }
//}
//for (; i <= values.GetLength(0); i++)
//{
//    if (values[i, 1].ToString().Contains("Specimen"))
//    {
//   break;
//    }
//    else
//    {
//   for (int j = 1; j <= values.GetLength(1); j++)
//   {
//    if (values[i, j] != null)
//    sw.Write(values[i, j] + "\t");
//   }
//   sw.Write("\n");
//    }

//}



range = null;
sheet = null;
if (book != null)
book.Close(false, Type.Missing, Type.Missing);
book = null;
if (app != null)
app.Quit();
app = null;
}

catch (Exception exception)
{

range = null;
sheet = null;
if (book != null)
book.Close(false, Type.Missing, Type.Missing);
book = null;
if (app != null)
app.Quit();
app = null;

MessageBox.Show(
"Error Message: " + e.ToString(),
"Problem with Excel Reformatting",
MessageBoxButtons.OK,
MessageBoxIcon.Error);
```

```
}


}

private void button2_Click_1(object sender, EventArgs e)
{

String dir = "";
String newfilename = "";

try
{
this.openFileDialog3.InitialDirectory = this.MovingAverageFile.Text;
this.openFileDialog3 = new OpenFileDialog();
this.openFileDialog3.ShowDialog();

this.MovingAverageFile.Text = this.openFileDialog3.FileName.ToString();
dir = this.MovingAverageFile.Text.Substring(0,
(this.MovingAverageFile.Text.LastIndexOf('\\')));
newfilename = this.MovingAverageFile.Text.Substring(0,
this.MovingAverageFile.Text.LastIndexOf(".xls")) + "3DTanDelta.xlsx";

}
catch (Exception except)
{ }


//this.dataPath.Text is where the file to open is
Microsoft.Office.Interop.Excel.Application app = null;
Workbook book = null;
Worksheet sheet = null;
Range range = null;


try
{
// -- Now write the next file

app = new Microsoft.Office.Interop.Excel.Application();
book = app.Workbooks.Open(this.MovingAverageFile.Text, Missing.Value,
Missing.Value, Missing.Value, Missing.Value, Missing.Value,
Missing.Value, Missing.Value, Missing.Value, Missing.Value,
Missing.Value, Missing.Value, Missing.Value, Missing.Value,
Missing.Value);  //<--Error here
sheet =
(Microsoft.Office.Interop.Excel.Worksheet)book.Sheets.get_Item(1);

app.DisplayAlerts = false;

sheet.Activate();



range = sheet.UsedRange;
```

```
object[,] values = (object[,])range.Value2;

Console.WriteLine("Row Count: " + values.GetLength(0).ToString());
Console.WriteLine("Col Count: " + values.GetLength(1).ToString());



//bool write = false;
int i = 1;

using (StreamWriter sw = new StreamWriter(newfilename, false))
{



//sw.WriteLine("Test");
sw.Close();

}



//{
//    sw.WriteLine("Temp\tRun 1\tRun2\tRun3\tRun4\tRun5\tAverage\tStd.
Dev.");
//    int x = 0; int y = 19; //this is where the first set of data
would go
//    int[] compRows = { 10, 11, 12, 13, 14 };
//    int[] modRows = { 1, 2, 3, 4, 5 };
//    double[] compSums = { 0, 0, 0, 0, 0 };
//    double[] compCounts = { 0, 0, 0, 0, 0 };
//    double RowAverage = 0;
//    double RowSTD = 0;
//    int valueCount = 0;
//    int compNum = 0;

//    for (x = 3; x <= values.GetLength(0); x++)
//    {

//   for (i = 2; i <= values.GetLength(0); i++)
//    {
//    if ((values[x - 1, y - 1] != null) &&
//    (values[x + 1, y - 1] != null))
//    {
//    for (compNum = 0; compNum < compRows.Length; compNum++)
//    {
//    if ((values[i, compRows[compNum]] != null) &&
//    (double.Parse(values[i, compRows[compNum]].ToString()) >
double.Parse(values[x - 1, y - 1].ToString())) &&
//    (double.Parse(values[i, compRows[compNum]].ToString()) <
double.Parse(values[x + 1, y - 1].ToString())))
//    {
//        if (values[i, modRows[compNum]] != null)
//        {
```

```
//         compSums[compNum] += double.Parse(values[i,
modRows[compNum]].ToString());
//         compCounts[compNum]++;
//         }
//     }


//     }


//     }
//     }

//     if (values[x, y - 1] == null)
//     {
//     //this means we do not need data at this temp
//     }
//     else
//     {
//     sw.Write(values[x, y - 1]);
//     RowAverage = 0; RowSTD = 0; valueCount = 0;
//     for (compNum = 0; compNum < compRows.Length; compNum++)
//     {
//     values[x, y + compNum] = compSums[compNum] / compCounts[compNum];
//     if (compCounts[compNum] == 0)
//     values[x, y + compNum] = null;

//     compSums[compNum] = 0;
//     compCounts[compNum] = 0;

//     sw.Write("\t" + values[x, y + compNum]);
//     if (values[x, y + compNum] != null)
//     {
//     RowAverage += double.Parse(values[x, y + compNum].ToString());
//     valueCount++;
//     }
//     }

//     if (valueCount == 0)
//     {
//     RowAverage = 0;
//     RowSTD = 0;
//     sw.WriteLine();
//     }
//     else
//     {
//     RowAverage /= valueCount;


//     for (compNum = 0; compNum < compRows.Length; compNum++)
//     {
//     if (values[x, y + compNum] != null)
//     {
//         RowSTD += Math.Pow((double.Parse(values[x, y +
compNum].ToString()) - RowAverage), 2);
//         //valueCount++;
```

```
//     }
//     }
//     RowSTD /= (valueCount - 1);
//     RowSTD = Math.Sqrt(RowSTD);

//     sw.WriteLine("\t" + RowAverage + "\t" + RowSTD);
//     }
//     }

//     }

//     sw.Close();
//}







//for (i=1; i <= values.GetLength(0); i++)
//{
//     if (values[i, 1].ToString().Contains("Time"))
//     {
//    break;
//     }
//}
//for (; i <= values.GetLength(0); i++)
//{
//     if (values[i, 1].ToString().Contains("Specimen"))
//     {
//    break;
//     }
//     else
//     {
//    for (int j = 1; j <= values.GetLength(1); j++)
//    {
//    if (values[i, j] != null)
//     sw.Write(values[i, j] + "\t");
//    }
//    sw.Write("\n");
//     }

//sw.Close();
//}



range = null;
sheet = null;
if (book != null)
book.Close(false, Type.Missing, Type.Missing);
book = null;
if (app != null)
app.Quit();
app = null;
}
```

```
catch (Exception exception)
{

range = null;
sheet = null;
if (book != null)
book.Close(false, Type.Missing, Type.Missing);
book = null;
if (app != null)
app.Quit();
app = null;

MessageBox.Show(
"Error Message: " + e.ToString(),
"Problem with Excel Reformatting",
MessageBoxButtons.OK,
MessageBoxIcon.Error);

}









}


}
public class RecursiveFileProcessor
{
public DataGridView myGrid;

public RecursiveFileProcessor(string path, string instrument, bool
comment, bool tough, DataGridView gridView)
{
//myGrid=gridView;

// Create an unbound DataGridView by declaring a column count.
// gridView.ColumnCount = 5;
// gridView.ColumnHeadersVisible = true;

// // Set the column header style.
// DataGridViewCellStyle columnHeaderStyle = new
DataGridViewCellStyle();

// columnHeaderStyle.BackColor = Color.Beige;
// columnHeaderStyle.Font = new System.Drawing.Font("Verdana", 10,
FontStyle.Bold);
// gridView.ColumnHeadersDefaultCellStyle = columnHeaderStyle;

// // Set the column header names.
// gridView.Columns[0].Name = "Sample";
// gridView.Columns[1].Name = "Onset";
// gridView.Columns[2].Name = "Glass Transition";
```

```
// gridView.Columns[3].Name = "Glassy Modulus";
// gridView.Columns[4].Name = "Rubbery Modulus";

// // Populate the rows.
// string[] row1 = new string[] { "Meatloaf", "Main Dish", "ground
beef",
//"**","6" };
// string[] row2 = new string[] { "Key Lime Pie", "Dessert",
//"lime juice, evaporated milk", "****","8" };
// string[] row3 = new string[] { "Orange-Salsa Pork Chops", "Main
Dish",
//"pork chops, salsa, orange juice", "****","6" };
// string[] row4 = new string[] { "Black Bean and Rice Salad", "Salad",
//"black beans, brown rice", "****","3" };
// string[] row5 = new string[] { "Chocolate Cheesecake", "Dessert",
//"cream cheese", "***","2" };
// string[] row6 = new string[] { "Black Bean Dip", "Appetizer",
//"black beans, sour cream", "***","1" };
// object[] rows = new object[] { row1, row2, row3, row4, row5, row6 };

// foreach (string[] rowArray in rows)
// {
//     gridView.Rows.Add(rowArray);
// }



if (File.Exists(path))
{
// This path is a file
if (!path.Contains("AutoQ.txt"))
ProcessFile(path, instrument, comment, tough);
}
else if (Directory.Exists(path))
{
// This path is a directory
ProcessDirectory(path, instrument, comment, tough);
}
else
{
Console.WriteLine("{0} is not a valid file or directory.", path);
}

}


// Process all files in the directory passed in, recurse on any
directories
// that are found, and process the files they contain.
public static void ProcessDirectory(string targetDirectory, string
instrument, bool comment, bool tough)
{
// Process the list of files found in the directory.
string[] fileEntries = Directory.GetFiles(targetDirectory);
foreach (string fileName in fileEntries)
if (!fileName.Contains("AutoQ.txt"))
```

```
ProcessFile(fileName, instrument, comment, tough);

// Recurse into subdirectories of this directory.
string[] subdirectoryEntries =
Directory.GetDirectories(targetDirectory);
foreach (string subdirectory in subdirectoryEntries)
ProcessDirectory(subdirectory, instrument, comment, tough);
}

//public string myReadLine(StreamReader sr)
//{
//    string ln, ch;
//    while ((ch = sr.Read().ToString()) >= 0)
//    {
//    if ((ch != "\0")||(ch!="\n"))
//    ln += ch;
//    else
//    return ln;
//    }


//}

// Insert logic for processing found files here.
public static void ProcessFile(string path, string instrument, bool
comment, bool tough)
{
Microsoft.Office.Interop.Excel.Application app = null;
Workbook book = null;
Worksheet sheet = null;
Range range = null;



try
{

app = new Microsoft.Office.Interop.Excel.Application();
book = app.Workbooks.Open(path, Missing.Value, Missing.Value,
Missing.Value, Missing.Value, Missing.Value, Missing.Value,
Missing.Value, Missing.Value, Missing.Value, Missing.Value,
Missing.Value, Missing.Value, Missing.Value, Missing.Value);  //<--
Error here
sheet =
(Microsoft.Office.Interop.Excel.Worksheet)book.Sheets.get_Item(1);

app.DisplayAlerts = false;

sheet.Activate();



//range = sheet.get_Range("A1", Missing.Value);

//range = range.get_End(XlDirection.xlDown);
```

```
//if (instrument == "Instron")
//range = range.get_End(XlDirection.xlToRight);
//else
//range = range.get_End((XlDirection)4);

//string downAddress = range.get_Address(
//false, false, XlReferenceStyle.xlA1,
//Type.Missing, Type.Missing);
//range = sheet.get_Range("A1", downAddress.Replace("A","D"));

range = sheet.UsedRange;
object[,] values = (object[,])range.Value2;

Console.WriteLine("Row Count: " + values.GetLength(0).ToString());
Console.WriteLine("Col Count: " + values.GetLength(1).ToString());

// -- Now write the next file
String dir = Directory.GetParent(path).FullName;
Directory.CreateDirectory(dir + "\\Igor");
//String doc;
//String[] seps1 = { ",", "\t", "\0" };
//String[] seps2 = { "\0", "\n", "\n\r" };
//String[] seps3 = { "Specimen label" };
String newfilename;
//bool write = false;

if (instrument == "Instron")
{

if (values[1, 2] != null)
{









//}
//else
//{


int i = 1, count = 1;

for (; i <= values.GetLength(0); i++)
{

if (values[i, 1].ToString().Contains("Specimen label"))
{
if (values[i, 2] == null)
{
values[i, 2] = "Specimen " + count;
}
count++;
newfilename = dir + "\\Igor\\" + values[i, 2] + ".AutoQ.txt";
```

```
using (StreamWriter sw = new StreamWriter(newfilename, false))
{
for (; i <= values.GetLength(0); i++)
{
if (values[i, 1].ToString().Contains("Time sec"))
{
break;
}
}
for (; i <= values.GetLength(0); i++)
{
if (values[i, 1].ToString().Contains("Specimen"))
{
break;
}
else
{
for (int j = 1; j <= values.GetLength(1); j++)
{
if (values[i, j] != null)
sw.Write(values[i, j] + "\t");
}
sw.Write("\n");
}

}
sw.Close();


}
}
}
}
}
else if (instrument == "Insight")
{
int i = 1, count = 1;
string samplename = "", tempname = "";
string commentIn = "";
double toughness = 0;
String[] seps = { ",",".mss"};
String[] data;
int stressIndex = 0, strainIndex = 0;
double lastStrain = 0;

for (; i <= values.GetLength(0); i++)
{

if ((values[i,1] != null )&&(values[i,1].ToString().StartsWith("Test
Method")))
{


}
else
{
```

```
if (values[i, 3] != null)
{
if (values[i, 3].ToString().Contains("BeginData"))
{
tempname = samplename + "-" +count++;
newfilename = dir + "\\Igor\\" + tempname + ".AutoQ.txt";
using (StreamWriter sw = new StreamWriter(newfilename, false))
{
String[] columns = values[++i, 4].ToString().Split(seps,
StringSplitOptions.RemoveEmptyEntries);
//labelling the wave names with the columns and the specimen ID
sw.Write(values[i, 4].ToString().Replace(",", "(" + tempname + ")\t") +
"(" + tempname + ")");
if (tough)
{
sw.Write("\t" + "Tough(" + tempname + ")");
}
if (comment)
{
sw.Write("\t" + "Comment(" + tempname + ")");
}
sw.WriteLine();

//sw.WriteLine(values[i, 4].ToString().Replace(",", "\t"));
String[] units = values[++i, 4].ToString().Split(seps,
StringSplitOptions.RemoveEmptyEntries);

if (tough)
{
for (int j = 0; j < columns.Length; j++)
{
if (columns[j].Contains("Stress"))
{
stressIndex = j;
}
if (columns[j].Contains("Strain"))
{
strainIndex = j;
}
}
}


bool first = true;
for (i=i+1; i <= values.GetLength(0); i++)
{
if ((values[i, 3] != null) && (values[i,
3].ToString().Contains("EndData")))
{
break;
}
else
{
if (first)
{
if (tough)
```

```
{
lastStrain = Double.Parse(values[i, 4].ToString().Split(seps,
StringSplitOptions.None)[strainIndex]);
toughness = 0;
values[i, 4] = values[i, 4] + "," + toughness;
}
sw.WriteLine(values[i, 4].ToString().Replace(",", "\t") + "\t" +
commentIn);
first = false;


}

else if (tough)
{
//stores each of the data points in 0 indexed array
data = values[i, 4].ToString().Split(seps, StringSplitOptions.None);

//data[stressIndex] contains stress pt.
//data[strainIndex] contains strain pt.
//lastStrain contains the last strain value
toughness += Math.Abs((Double.Parse(data[strainIndex]) - lastStrain) *
Double.Parse(data[stressIndex]));
values[i, 4] = values[i, 4] + "," + toughness;
lastStrain = Double.Parse(data[strainIndex]);
sw.WriteLine(values[i, 4].ToString().Replace(",", "\t"));

}


else
{
sw.WriteLine(values[i, 4].ToString().Replace(",", "\t"));

}

}
}
sw.Close();
commentIn = "";

}

}
else if (values[i, 3].ToString().Contains("Comment"))
{
if (comment)
{
String[] sepsLocal = { "omment," };
commentIn += values[i, 3].ToString().Split(sepsLocal,
StringSplitOptions.RemoveEmptyEntries)[1];
while (values[++i, 3] == null)
{
commentIn += values[i, 1].ToString();

}
```

```
commentIn = commentIn.Replace("\n", " ");
commentIn = commentIn.Replace("\t", " ");
}

}
}
else if (values[i, 2] != null)
{
if (values[i, 2].ToString().Contains("_SampleName"))
{
String[] seps2 = { ",",".mss","\\","\""};
samplename = values[i, 2].ToString().Split(seps2,
StringSplitOptions.RemoveEmptyEntries)[2];


}
else if (values[i, 2].ToString().StartsWith("Comment"))
{


}

else if (values[i, 2].ToString().StartsWith("Where's Wal"))
{
/// people people people people people people
/// people people people people people people
/// people people w  do people people people
/// people people people people people people
/// people people people people people people
}



}
else if (values[i, 1] != null)
{
if (values[i, 1].ToString().Contains("EndSample"))
break;
}

}
}




}

range = null;
sheet = null;
if (book != null)
book.Close(false, Type.Missing, Type.Missing);
book = null;
if (app != null)
app.Quit();
app = null;
```

```
}



catch (Exception e)
{

range = null;
sheet = null;
if (book != null)
book.Close(false, Type.Missing, Type.Missing);
book = null;
if (app != null)
app.Quit();
app = null;

MessageBox.Show(
"Error Message: " + e.ToString(),
"Problem with Excel Reformatting",
MessageBoxButtons.OK,
MessageBoxIcon.Error);

}

}
}

}

namespace Utility.ModifyRegistry
{
/// <summary>
/// An useful class to read/write/delete/count registry keys
/// </summary>
public class ModifyRegistry
{
private bool showError = false;
/// <summary>
/// A property to show or hide error messages
/// (default = false)
/// </summary>
public bool ShowError
{
get { return showError; }
set { showError = value; }
}
private string subKey = "SOFTWARE\\" +
System.Windows.Forms.Application.ProductName.ToUpper();
/// <summary>
/// A property to set the SubKey value
/// (default = "SOFTWARE\\" + Application.ProductName.ToUpper())
/// </summary>

public string SubKey
{
```

```
get { return subKey; }
set { subKey = value; }
}
private RegistryKey baseRegistryKey = Registry.LocalMachine;
/// <summary>
/// A property to set the BaseRegistryKey value.
/// (default = Registry.LocalMachine)
/// </summary>
public RegistryKey BaseRegistryKey
{
get { return baseRegistryKey; }
set { baseRegistryKey = value; }
}


/*
*********************************************************************
***
*
*********************************************************************
***/



public string ReadReg(string KeyName)
{
// Opening the registry key
RegistryKey rk = baseRegistryKey;
// Open a subKey as read-only
RegistryKey sk1 = rk.OpenSubKey(subKey);
// If the RegistrySubKey doesn't exist -> (null)
if (sk1 == null)
{
return null;
}
else
{
try
{
// If the RegistryKey exists I get its value
// or null is returned.
return (string)sk1.GetValue(KeyName.ToUpper());
}
catch (Exception e)
{
ShowErrorMessage(e, "Reading registry " + KeyName.ToUpper());
return null;
}
}
}

public bool WriteReg(string KeyName, object Value)
{
try
{
```

```
// Setting
RegistryKey rk = baseRegistryKey;
// I have to use CreateSubKey
// (create or open it if already exits),
// 'cause OpenSubKey open a subKey as read-only
RegistryKey sk1 = rk.CreateSubKey(subKey);
// Save the value
sk1.SetValue(KeyName.ToUpper(), Value);

return true;
}
catch (Exception e)
{
ShowErrorMessage(e, "Writing registry " + KeyName.ToUpper());
return false;
}
}

public bool DeleteKey(string KeyName)
{
try
{
// Setting
RegistryKey rk = baseRegistryKey;
RegistryKey sk1 = rk.CreateSubKey(subKey);
// If the RegistrySubKey doesn't exists -> (true)
if (sk1 == null)
return true;
else
sk1.DeleteValue(KeyName);

return true;
}
catch (Exception e)
{
ShowErrorMessage(e, "Deleting SubKey " + subKey);
return false;
}
}

public bool DeleteSubKeyTree()
{
try
{
// Setting
RegistryKey rk = baseRegistryKey;
RegistryKey sk1 = rk.OpenSubKey(subKey);
// If the RegistryKey exists, I delete it
if (sk1 != null)
rk.DeleteSubKeyTree(subKey);

return true;
}
catch (Exception e)
{
ShowErrorMessage(e, "Deleting SubKey " + subKey);
```

```
return false;
}
}

public int SubKeyCount()
{
try
{
// Setting
RegistryKey rk = baseRegistryKey;
RegistryKey sk1 = rk.OpenSubKey(subKey);
// If the RegistryKey exists...
if (sk1 != null)
return sk1.SubKeyCount;
else
return 0;
}
catch (Exception e)
{
ShowErrorMessage(e, "Retriving subkeys of " + subKey);
return 0;
}
}

public int ValueCount()
{
try
{
// Setting
RegistryKey rk = baseRegistryKey;
RegistryKey sk1 = rk.OpenSubKey(subKey);
// If the RegistryKey exists...
if (sk1 != null)
return sk1.ValueCount;
else
return 0;
}
catch (Exception e)
{
ShowErrorMessage(e, "Retriving keys of " + subKey);
return 0;
}
}

private void ShowErrorMessage(Exception e, string Title)
{
if (showError == true)
MessageBox.Show(e.Message,
Title
, MessageBoxButtons.OK
, MessageBoxIcon.Error);
}

}
}
```

VITA

Walter Everett Voit was born in Cologne, Germany on August 26, 1982. He grew up in Ann Arbor, MI and Mt. Pleasant, SC. He also spent a year in Hobart, Tasmania. Voit attended Wando High School where he lettered in soccer and captained the Quiz Bowl team. He graduated valedictorian and attended the University of Texas at Dallas as a Eugene McDermott Scholar. Voit has traveled extensively, having visited more than 35 countries, and spent his junior year studying abroad in Munich and in Cologne. Voit spent two summers as an intern at Los Alamos National Labs as a computer scientist performing research in global grid computing for ocean modeling applications and bandwidth monitoring of the Linux kernel. Voit also worked for two and half years with Dallas nanotechnology startup company Zyvex. Voit helped build custom scripts in python, C++, OpenGL, html and other languages and toolkits to manipulate precision instruments and visualize 3D MEMS constructions. Voit received a B.S. in Computer Science in May 2005 and a Masters in Artificial Intelligence from UT Dallas in August 2006. Voit's Master's thesis work was conducted under the mentorship of I. Hal Sudborough where their team helped improve the upper bound of the pancake problem: a theoretical inquiry into sorting by prefix reversals. Voit was named a Presidential Scholar at Georgia Tech and was selected to the prestigious TI:GER program, which is a partnership with the College of Management and Emory Law School. Voit performed his doctoral work under the guidance of Ken Gall. Voit cofounded Syzygy Memory Plastics in December 2007.